UTS UNIVERSITY OF TECHNOLOGY SYDNEY

# Microbial community analysis using next-generation sequencing and bioinformatics tools to better understand biological waste and wastewater treatment

**by Quynh Anh Nguyen**

Thesis submitted in fulfilment of the requirements for the degree of

**Doctor of Philosophy**

under the supervision of Professor Duc Long Nghiem & Professor Huu Hao Ngo

University of Technology Sydney
Faculty of Engineering and Information Technology

Aug 2022

## CERTIFICATE OF ORIGINAL AUTHORSHIP

I, **Quynh Anh Nguyen** declare that this thesis, is submitted in fulfilment of the requirements for the award of **Doctor of Philosophy**, in the **School of Civil and Environmental Engineering** at the University of Technology Sydney.

This thesis is wholly my own work unless otherwise referenced or acknowledged. In addition, I certify that all information sources and literature used are indicated in the thesis.

This document has not been submitted for qualifications at any other academic institution.

This research is supported by the Australian Government Research Training Program.

Production Note:
Signature: Signature removed prior to publication.

Date: 28/8/2022

## ACKNOWLEDGEMENT

Every journey has to come to an end, but I could not believe that it was already the end of my PhD. It has been a long journey, and there were many ups and downs on the way, but finally, I am here. I was lucky enough to receive the kind support from many wonderful people throughout my journey. Without them, I would not be where I am today, and it is time for me to express my sincere gratitude to them.

First and foremost, I would like to send my deepest thank to my principal supervisor, Professor Long Nghiem. He has been more than a supervisor to me. I am grateful for his understanding and support throughout my journey, both in my professional and personal lives. He always believed in me, even when I did not believe in myself. He has given me valuable learning opportunities and advice that I will carry with me for the rest of my life.

I also want to thank my co-supervisor, Professor Huu Hao Ngo, for his tremendous encouragement and insightful advice on my research. I am grateful for his kindness and genuine care, and his sense of humour has brightened up my PhD days.

I truly appreciate Dr Luong Ngoc Nguyen's constructive comments on different aspects of my study. His critical questions always got me thinking out of the box and helped me to improve my work's quality.

I am also thankful to work in a harmonious and productive research group full of motivated, helpful, and friendly colleagues. They have been a source of my motivation and facilitated me in their ways. Here, great gratitude is expressed to Lei Zheng, Minh Vu, Chelsey Vu, and Jamshed Ali Khan. Technical staffs of the Faculty of Engineering and Information Technology, Dr Md Johir and Dr Niren Pathak, are also thanked for their assistance in multiple aspects of my experiments.

Special thanks go to my husband, Thien Bui, and my best friend, Chi Nguyen. There were so many times that I wanted to give up, but they have given me the strength to hold on and keep moving forward.

My UTS friends are thanked for their empathy, encouragement, and all the happy memories that I will forever cherish. Finally, I would like to thank my family and other friends in Vietnam and Australia for their unconditional love and support and making my life richer and more meaningful.

## LIST OF PUBLICATIONS

1. **Nguyen QA**, Vu HP, McDonald JA, Nguyen LN, Leusch FDL, Neale PA, et al. Chiral Inversion of 2-Arylpropionic Acid Enantiomers under Anaerobic Conditions. Environmental Science & Technology. 2022;56(12):8197-208.
2. **Nguyen AQ**, Nguyen LN, Johir MAH, Ngo HH, Nghiem LD. Linking endogenous decay and sludge bulking in the microbial community to membrane fouling at sub-critical flux. Journal of Membrane Science Letters. 2022;2(1):100023.
3. **Nguyen AQ**, Nguyen LN, Xu Z, Luo W, Nghiem LD. New insights to the difference in microbial composition and interspecies interactions between fouling layer and mixed liquor in a membrane bioreactor. Journal of Membrane Science. 2022;643:120034.
4. **Nguyen AQ**, Nguyen LN, McDonald JA, Nghiem LD, Leusch FDL, Neale PA, et al. Chiral inversion of 2-arylpropionic acid (2-APA) enantiomers during simulated biological wastewater treatment. Water Research. 2021:117871.
5. **Nguyen AQ**, Vu HP, Nguyen LN, Wang Q, Djordjevic SP, Donner E, et al. Monitoring antibiotic resistance genes in wastewater treatment: Current strategies and future challenges. Science of The Total Environment. 2021;783:146964.
6. Cheng D, Ngo HH, Guo W, Chang SW, Nguyen DD, **Nguyen QA**, et al. Improving sulfonamide antibiotics removal from swine wastewater by supplying a new pomelo peel derived biochar in an anaerobic membrane bioreactor. Bioresource Technology. 2021;319:124160.
7. **Nguyen AQ**, Nguyen LN, Johir MAH, Ngo H-H, Chaves AV, Nghiem LD. Derivation of volatile fatty acid from crop residues digestion using a rumen membrane bioreactor: A feasibility study. Bioresource Technology. 2020;312:123571.
8. Nguyen LN, Truong MV, **Nguyen AQ**, Johir MAH, Commault AS, Ralph PJ, et al. A sequential membrane bioreactor followed by a membrane microalgal reactor for nutrient removal and algal biomass production. Environmental Science: Water Research & Technology. 2020;6(1):189-96.
9. Nguyen LN, **Nguyen AQ**, Johir MAH, Guo W, Ngo HH, Chaves AV, et al. Application of rumen and anaerobic sludge microbes for bio harvesting from lignocellulosic biomass. Chemosphere. 2019;228:702-8.
10. **Nguyen AQ**, Nguyen LN, Phan HV, Galway B, Bustamante H, Nghiem LD. Effects of operational disturbance and subsequent recovery process on microbial community during a pilot-scale anaerobic co-digestion. International Biodeterioration & Biodegradation. 2019;138:70-7.
11. Nguyen LN, **Nguyen AQ**, Nghiem LD. Microbial Community in Anaerobic Digestion System: Progression in Microbial Ecology. In: Bui X-T, Chiemchaisri C, Fujioka T,

Varjani S, editors. Water and Wastewater Treatment Technologies. Singapore: Springer Singapore; 2019. p. 331-55.

12. **Nguyen AQ**, Wickham R, Nguyen LN, Phan HV, Galway B, Bustamante H, et al. Impact of anaerobic co-digestion between sewage sludge and carbon-rich organic waste on microbial community resilience. Environmental Science: Water Research & Technology. 2018;4(12):1956-65.

## LIST OF ACHIEVEMENTS

1. Winner of 2021 Women in Engineering and IT HDR Award.
2. UTS Vice-Chancellor's Conference Fund 2021.
3. Honourable Mention in *National Innovation Game – Northern Territory Series – Territorians discovering opportunity in Renewable Energy* - team effort (2021).
4. Polish NAWA PROM International Scholarship exchange of PhD candidates (2020).
5. Research Training Program and UTS Faculty of Engineering and IT Scholarship (2018 – current).
6. 1st prize poster presentation at *2nd International Conference on Green Technologies for Sustainable Water* (2019).
7. Polish NAWA PROM PhD students exchange scholarship recipient (2019).
8. Best oral presentation award at *Technology and Innovation Research Showcase* (2018).
9. Awarded travel bursary at the Winter School in Mathematical and Computational Biology (2018).

# TABLE OF CONTENTS

## LIST OF FIGURES

## LIST OF TABLES

## LIST OF ABBREVIATIONS

| | |
|---|---|
| 2-APA | 2-arylpropionic acid |
| ACN | Acetonitrile |
| AD | Anaerobic digestion |
| ANCOM | Analysis of composition of microbiomes |
| ASV | Amplicon sequent variant |
| BMP | Biochemical methane potential |
| BOD | Biological oxygen demand |
| CAS | Conventional activated sludge |
| CEs | Collision energies |
| COD | Chemical oxygen demand |
| CS | Corn silage |
| DCM | Dichloromethane |
| DO | Dissolved oxygen |
| EF | Enantiomeric fraction |
| EPS | Extracellular polymeric substance |
| EROD | Ethoxyresorufin-O-deethylase |
| F/M | Food-to-microorganism |
| FISH | Fluorescence in situ hybridization |
| GH | Glycoside hydrolase |
| HLB | Hydrophilic/lipophilic balance |
| HRT | Hydraulic retention time |

| | |
|---|---|
| ISTD | Internal standard |
| LCBM | Lignocellulosic biomass |
| LH | Lucerne hay |
| LOQ | Limits of quantification |
| LR | Loading rate |
| MBR | Membrane bioreactor |
| MENA | Molecular ecological network analysis |
| MLSS | Mixed liquor suspended solids |
| MLVSS | Mixed liquor volatile suspended solids |
| MRM | Multiple reaction monitoring |
| N.D. | Not determinable |
| NA | Not applicable |
| ND | Not detected |
| NGS | Next-generation sequencing |
| NSAID | Non-steroidal anti-inflammatory drug |
| NSW | New South Wales |
| OH | Oaten hay |
| ORP | Oxidation-reduction potential |
| PcoA | Principal coordinate analysis |
| PEA | Phenylethylamine |
| PL | Polysaccharide lyases |
| PN/PS | Protein/polysaccharide |
| PVDF | Polyvinylidene difluoride |
| QIIME | Quantitative insights into microbial ecology |
| qPCR | Quantitative polymerase chain reaction |
| RMT | Random matrix theory |

| | |
|---|---|
| RUSITEC | Rumen simulation technique apparatus |
| sCOD | Soluble chemical oxygen demand |
| SIP | Stable-isotope probing |
| SMP | Soluble microbial product |
| SPE | Solid-phase extraction |
| SRT | Solids retention time |
| TEA | Triethylamine |
| TMP | Transmembrane pressure |
| TOA | Total organic acids |
| TOC | Total organic carbon |
| TS | Total solids |
| TVFA | Total volatile fatty acid |
| UF | Ultrafiltration |
| UPGMA | Unweighted pair group method with arithmetic mean |
| VFA | Volatile fatty acid |
| VS | Volatile solid |
| VSS | Volatile suspended solids |
| WS | Wheat straw |
| WWTP | Wastewater treatment plant |

## ABSTRACT

Waste/wastewater treatment often rely on microbes and biotransformation for removing contaminants and environmental restoration. Insights into the microbial communities associated with these processes can help develop better operational strategies. Three common environmental engineering processes were investigated in this thesis to demonstrate the application of next-generation sequencing and bioinformatics tools to elucidate the link between microbial community and process performance.

The first process was membrane fouling in membrane bioreactors (MBRs). Nutritional deficiency led to endogenous decay and sludge bulking, which in turn triggered membrane fouling under sub-critical flux. The mixed liquor and fouling layer possessed similar microbial composition. The most dominant filamentous order *Thiotrichales* (>60%) positively correlated with fouling severity. Under high-flux conditions, MBR biofilm and mixed liquor possessed different microbial structures. Low-abundance taxa (<1%) such as *Victivallales* and *Blastocatellia* 11-24 drove the divergence between the two communities. These taxa also played key roles in fouling development and positively correlated with fouling indicators. Knowledge of MBR fouling-associated microbial taxa can help improve fouling control strategies, reduce the cost of membrane cleaning and energy consumption, enhance MBR application and increase the treated water quality.

The second process was lignocellulosic biomass (LCBM) valorisation using rumen microbes. Biomethane potential analysis showed that rumen microbes can produce four times more volatile fatty acids (VFA) than anaerobic sludge. However, VFA accumulation led to pH drop which in turn resulted in process inhibition, suggesting the need for continuous extraction of VFA from the system. A novel rumen-MBR was evaluated, showing continuous VFA production at 438 mg VFA/g substrate. Acetic and propionic acids accounted for >80% of the total VFA produced. Most of the produced VFA (73 ± 15%) was continuously extracted by an ultrafiltration membrane. Shifts in dominant rumen microbes during operation did not impact VFA yield. This work provides an important foundation for the development of a sustainable pathway for producing renewable chemicals in a circular economy.

The third process was chiral inversion of 2-arylpropionic acids (2-APAs) in biological waste and wastewater treatment. Despite possessing highly similar chemical structures, eleven 2-APAs exhibited diverse and distinctive chiral inversion behaviours. Both unidirectional and bidirectional chiral inversions of 2-APAs were observed under aerobic and anaerobic conditions. Potential microbes involved in chiral inversion, including *Candidatus_Microthrix*, *Rhodococcus*, *Mycobacterium*, *Gordonia,* and *Sphingobium*, are aerobic or facultative anaerobic bacteria. This

is the first study to report chiral inversion behaviours of a comprehensive suite of 2-APAs during biological treatment.

# Chapter 1. INTRODUCTION

## 1.1. Background

Microbes exist in all environmental compartments, including soil, sediment, surface water, the ocean, and even the human gut. Despite their microscopic size, microbes can play important roles in the health of the ecological niche in which they reside. They participate in biogeochemical cycles of nutrients in plant and soil ecological systems. Microbes are also critically involved in the breakdown of food in human and animal digestion systems. In contrast, some microbes are capable of causing harmful effects and diseases to the host organism. The knowledge of microbial capabilities can be employed to improve human life. To date, the vast majority of microbes and their diverse metabolic potential still remain to be explored.

A microbial community is a collection of microbes occupying a specific habitat. Microbial communities are often highly complex due to the huge amount of interactions within the community and between microbes and the host environment. In such communities, microbes can play different functions or share the same function, compete for nutrients or cooperate in syntrophic relationships. The microbial community also has high phylogenetic diversity with various uncharacterized microorganisms. The diversity and structure of a microbial community change in response to changes in environmental factors and changes in the community also influence the host environment. The study of microbial community and their host environment is referred to as microbial ecology study.

Two major hurdles to microbial ecology study are the complexity of the microbial community and the lack of cost-effective and robust methods for microbial community characterization. In the past, microbial ecology study has relied upon culture-dependent and labour-intensive approaches, such as cloning and Sanger sequencing or denaturing gradient gel electrophoresis. In addition, these approaches usually detect the most predominant members of the community. Recent years have seen the evolution of next-generation sequencing (NGS) technologies and other high-throughput methods that enable comprehensive studies of the microbial community.

## 1.2. Problem statement

Various environmental engineering processes, such as wastewater treatment or bioremediation, rely on microbes to remove contaminants. Insights into the microbial communities associated with these processes can be used for the enhancement of process stability and efficiency. It appears that one single analytical method is not capable of revealing the total complexity of these microbial communities. The integration of different analytical methods, e.g. metagenomics and metatranscriptomics, amplicon sequencing with 16S rRNA marker gene and bioinformatics tools, has been proposed for microbial ecology study. Each technique reveals information about the microbial community in different aspects such as microbial diversity, microbial composition, and

functional profiles. Thus, their integration has the potential for in-depth analysis of the microbial community to reveal a more complete picture of biological systems.

## 1.3. Research objectives

This research aims to contribute to a more comprehensive understanding of the microbial communities associated with different environmental engineering processes. The specific objectives of this research are to:

- Demonstrate the application of integrative microbial community analysis in environmental engineering processes.
- Investigate the link between environmental factors, microbial community and process performance.
- Propose microbial-based strategies to enhance process stability and efficiency.

## 1.4. Thesis outline

This thesis contains nine chapters and covers three major research topics (Figure 1). Chapter 2 offers a critical literature review of current microbial community analysis techniques, with a focus on NGS, and the background of three biological waste and wastewater processes to be investigated. The first research topic aims to elucidate the microbial community associated with membrane fouling in the membrane bioreactor (MBR) process - a major hurdle for MBR application - at different flux conditions. Chapter 3 characterizes fouling-associated microbes at a sub-critical flux (low flux) and highlights the role of filamentous bacteria in fouling. Chapter 4 systematically investigates fouling-associated microbes at high flux and delineates the difference between the mixed liquor and fouling layer communities. The target of the second research topic is to develop the proof-of-concept of the feasibility of a biomimicry process for lignocellulosic biomass (LCBM) valorisation (Chapter 5 – 6). Chapter 5 illuminates rumen fluid as an abundant source of potent lignocellulolytic-degrading bacteria and its superior potential to produce VFAs compared to anaerobic sludge. Based on findings in Chapter 5, chapter 6 proposes a novel rumen-based anaerobic MBR system for the continuous valorisation of LCBM. The shift in the indigenous rumen microbial community during the continuous operation and the subsequent impact on process performance were also highlighted in Chapter 6. Chapter 7 and Chapter 8 focus on the third research topic, namely the fate of enantiomeric 2-arylpropionic acids (2-APAs) during biological waste and wastewater treatment. These 2-APAs include several non-steroidal anti-inflammatory drugs (NSAIDs) that are environmentally significant. Results from these chapters show that chiral 2-APAs exhibited diverse chiral inversion behaviours despite the high similarity in their chemical structures. Potential microbial genera involved in chiral inversion were also identified in Chapter 8. The conclusion and recommendations for future work are presented in

Chapter 9. Details including the materials and methods of each study will be described in the corresponding chapter.

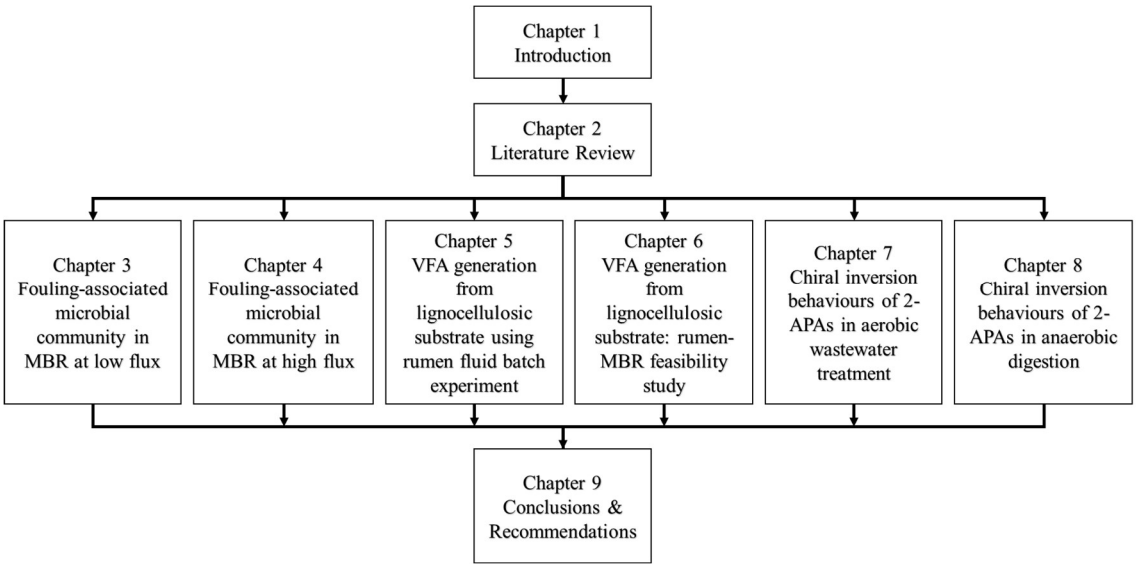


Figure 1. Schematic structure of the thesis.

# Chapter 2. LITERATURE REVIEW

## 2.1. Waste and wastewater treatment & resource recovery

Climate change has occurred at an unprecedented pace, with weather conditions swinging from extreme drought to severe flood over a short time. The prevalence of climate change calls for a more sustainable development strategy – a transition to a circular economy. A circular economy aims to maximise resource utilization and reduce waste by keeping valuable materials in the productive economy for longer. This could be achieved through material reuse, recycling, and recovery. This circular model is an alternative to the linear "take, make, dispose" model, where most manufactured goods are single-use items (not recycled) that usually end up in landfills.

With the current linear economy, about 11.2 billion tonnes of solid waste is generated each year (1). This number will increase due to population growth and unpredictable events, e.g. the COVID-19 global pandemic (2). Waste management plays a key role in mitigating infectious diseases transmission and often involves energy- and emission-intensive processes. Wastewater treatment contributed to >55% of the global methane emissions from the waste sector in 2012 (3). In the paradigm shift towards a circular economy, waste management can also serve as a critical pathway for both pollution prevention and recovery of energy, nutrients, and water. The recognition of economic value in waste and wastewater demands more efficient and economical management of resources, including the development of more effective treatment processes.

Biological treatment is an important waste and wastewater treatment technology and often the key component in any treatment plant. Biological treatment utilizes microorganisms to remove organic contaminants and nutrients (nitrogen and phosphorus) under aerobic/anaerobic conditions. The polluting contaminants could be accumulated in the microbial cell, degraded partially or completely, or transformed into different metabolized. The efficiency of biological treatment processes relies heavily on the microbial communities involved. Thus gaining a comprehensive understanding of such microbial communities is critical for process operation and optimization, as well as the development of novel treatment technologies.

## 2.2. Next-generation sequencing and omics approaches

### 2.2.1. Introduction to microbial ecology study

Microbes are organisms that are invisible by naked eyes. About one trillion species of microbes exist on Earth (4). To date, only a small portion of these microbes has been characterised in detail and they have shown significant impacts on humans and the environment in many aspects. Microbial ecology study aims to develop a comprehensive understanding of the existing microbial biosphere and how their magnificent capacity can be employed to improve human life.

The information gained from microbial ecology study can facilitate environmental engineering applications such as waste treatment or bioremediation. Microbes possess a highly diverse metabolic capability to effectively biodegrade organic matter, including hazardous pollutants such as polycyclic aromatic hydrocarbon, phenolic compounds, and synthetic dyes (5). An example of such application is the use of bioremediation to clean up oil spills in the ocean, during which nutrients were applied at the contaminated site to enhance the rate of oil biodegradation by indigenous hydrocarbon-degrading microorganisms (6). Another example is the implementation of the anaerobic digestion process for solid waste treatment, which involves the use of microbes to biodegrade organic waste to generate valuable products (7).

Microbial ecology study also results in the discovery and application of microbes in food production. A wide range of microbes is capable of converting raw materials into organic acids, alcohols and esters. This process, namely fermentation, has been employed for hundreds of years for food preservation and food production. Products of such applications include yoghurt, cheese, soy sauce, fermented vegetables, and alcoholic beverages. Consumption of fermented food has been proved to have positive impacts on human health (8-10).

Microbial ecology study contributes to the improvement of life quality in other aspects. Microbes are endowed with the power to synthesize valuable materials and chemicals. Their ability to synthesize new substances has been intensively studied and exploited for the production of important chemicals (i.e. amino acids, isoprenoids, organic acids, polymers, and industrial enzymes) (11, 12). Microbes can also be engineered for the production of pharmaceuticals (i.e. vaccines, insulin, and drugs) (13). Microbial production is often more economical and environmental-friendly than other methods, and sometimes it is the only method.

### 2.2.2. Available methods for microbial ecology study

Table 1. Comparing between different methods for microbial ecology study (ASVs - operational taxonomic units, qPCR - quantitative polymerase chain reaction, FISH - fluorescence in situ hybridization, SIP - stable-isotope probing).

| Method | Principle | Information obtained | Ref. |
|---|---|---|---|
| 16S rRNA sequencing | Genomic DNA is extracted from samples. The 16S rRNA gene is amplified and sequenced. Obtained sequences will be compared with reference sequences available in databases, and clustered into ASVs based on their similarity. | Phylogenetic classification, microbial diversity, structure and composition (measured based on ASVs). | (14-17) |
| Microarrays | Genomic DNA is extracted from samples and amplified with primers targeting specific markers. When amplicons are exposed to the microarray containing complementary oligonucleotide probes of the target DNA sequences, hybridization occurs, indicated by fluorescence signal. | Presence and abundance of thousands of genes/species, microbial structure and activities (calculated based on the signal intensity). | (18-21) |
| Fingerprinting | Genomic DNA is extracted from samples and amplified with primers targeting specific markers. DNA fragments are separated by electrophoresis based on the differences in mobility caused by sequence variations. | Changes in microbial composition, identification of dominant members. | (22-26) |
| qPCR | Genomic DNA is extracted from samples and amplified with primers targeting a specific marker. The amplified DNA amount is measured in a real-time manner using intercalating fluorescent dyes or fluorescent probes. | Quantification of microbes present in the samples (calculated based on the fluorescent signal intensity). | (27-30) |

| | | | |
|---|---|---|---|
| FISH | Samples are fixed on a microscope slide. Target sequences of nucleic acid in the sample are hybridized to labelled probes. Hybrids are detected based on fluorescence. | *In situ* phylogenetic identification and enumeration of individual cells. | (31-35) |
| SIP | A stable isotope-labelled substrate is used in the environment. Microbes who utilize the labelled substrate during growth will incorporate the isotopes within their biomass. Their DNA/RNA is then separated for phylogenetic identification by various methods. | Identification of the active population in the microbial community. | (35-38) |
| Integrative "omics" analysis | Analysis of the entire DNA, RNA, expressed protein or metabolites content in a sample. | Microbial community structure and function, interspecies interaction and responses to environmental conditions. | (39, 40) |

A broad range of methods can be applied for microbial ecology study (Table 1). 16S rRNA sequencing and integrative "omics" analysis can produce more informative, comprehensive and useful results than other methods. In addition, other methods (e.g. fingerprinting, qPCR, FISH) can only be used in conjunction with each other or couple with 16S rRNA sequencing. Nevertheless, the 16S rRNA sequencing cannot provide information on the microbial functionality as well as the interactions between community members and with the environment. Integrative "omics" analysis appears to be the only method that can completely achieve the aim of a microbial ecology study.

### 2.2.3. Metagenomics

#### *2.2.3.1. Principle of metagenomics*

The term "metagenomics" refers to the analysis of the entire genetic material of a microbial community at the time of sampling (metagenome) (41). The metagenome is recovered directly from environmental samples and examined by either a sequence-based or a function-based approach. In a sequence-based approach, sequencing technology is applied for the identification of candidate genes and microbes. In a function-based approach, clone library and functional screening are employed to identify bioactive compounds (i.e. enzymes, antibiotics) with desirable functions and their encoding genes (42). The birth of metagenomics resulted in an explosion of new understanding and knowledge in various disciplines such as microbial ecology, microbiology, and biomedical research (43, 44).

Metagenomics allows for the discovery of uncharacterized species and metabolisms. The major part of the Earth microbiome currently remains unculturable due to the limitation of culturing techniques. Culture media (i.e. nutrient composition) often possess low similarity to the natural environment where microbes reside. In addition, finding the optimum culturing conditions (i.e, temperature, oxygen concentration, moisture) for each microbial strain is an arduous task. More importantly, the metabolic activities that microbes express in such artificial conditions might not fully resemble their functional capacity. Furthermore, isolation and characterization of microbes using culture-dependent techniques is a time-consuming and labour-intensive process. Metagenomics analysis eliminates the need to isolate single microbial strains, and offers a powerful tool to explore the genetic functional capacity of unculturable or previously unknown microbes.

Metagenomics analysis can also provide measurements of microbial diversity and composition. In a sequence-based approach, the entire genetic material of the community is sequenced using NGS technologies. NGS can obtain high sequence coverage, which allows the detection of microbes present in the community at low abundances. Estimation of the community diversity can be made from the number of different microbial species present in the sample and the

evenness between them. The community composition is determined by their relative abundances. Metagenomics sequencing can also be coupled with 16S rRNA sequencing to provide taxonomical classification.

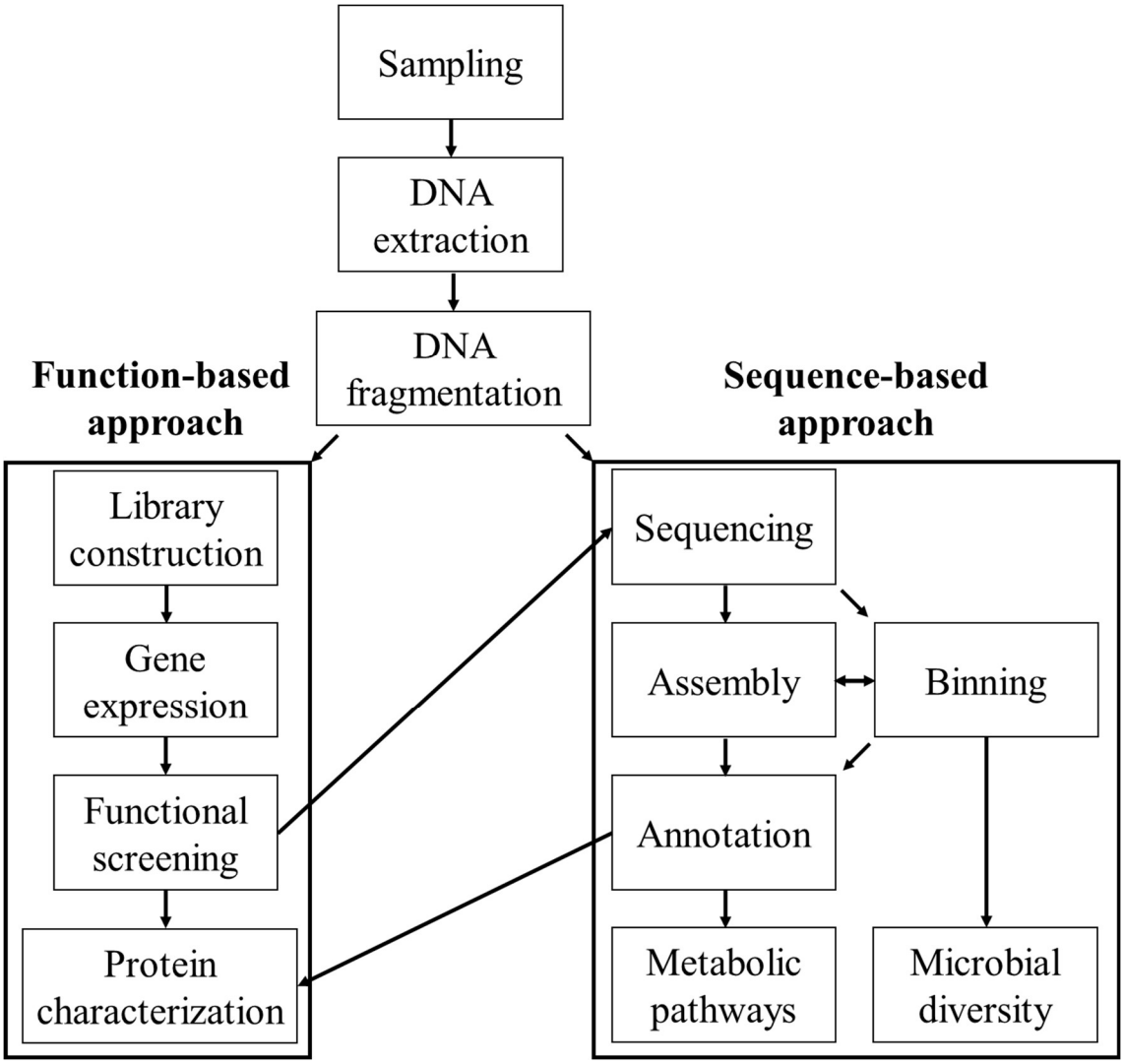


Figure 2. Schematic diagram of metagenomics analysis with the function-based and sequence-based approach.

The first step of a metagenomics analysis is nucleic acid (DNA or RNA) extraction from samples, followed by enrichment and fragmentation. Subsequent steps depend largely on the purpose of the analysis and the corresponding approach (Figure 2). A function-based approach usually serves the purpose of discovering novel bioactive compounds with specific functions. In this approach, a metagenomics library is constructed by ligating DNA fragments with a vector (e.g. plasmid, cosmid, or bacterial artificial chromosome). Next, the ligated vector is transformed into a heterogeneous host for the expression of genomic DNA. This process is referred to as molecular cloning or DNA cloning. Functional screening is carried out and clones that express the function

of interest will be selected for further examination (e.g. characterization of the novel molecule, sequencing the encoding gene).

A sequence-based approach gives an overview of all members in the sample microbial community and their functional capacity. In this approach, DNA fragments are subjected to sequencing, and the original genomes are reconstructed by merging reads via assembly step. Assigning sequences to different taxonomical groups can help improve the accuracy of reads assembly. Microbial diversity is estimated based on taxonomical data. Next, genes prediction and functional annotation are performed based on either the information from the sequence itself or information from available databases. Combining annotated functions with taxonomical information and environmental data, metabolic pathways can be reconstructed to determine the interactions between different microbial guilds in the community, and between the microbial community and the environment.

#### *2.2.3.2. Application of metagenomics*

Metagenomics provides researchers with a tool to unlock the hidden genetic resource of unculturable microbes. The ability to explore the unknown has paved the way for the identification of novel molecules with diverse functions, which can be utilized in various areas. Metagenome-sourced enzymes have been commercialized for use in paper production, fuel and enzyme production, secondary oil and gas recovery, and food industry (45). A number of commercial antibiotics such as tetracycline, rapamycin, erythromycin and biocatalysts for pharmaceuticals are also derived from metagenomics libraries (46).

Knowledge obtained from metagenomics also has significant implications in environmental and ecological studies. Metagenomics broadens the understanding of a microbial community's functional potential in a particular environment or process under study. For example, sequences related to cellulose, hemicellulose and lignin degrading-genes were detected in anaerobic digester treating plant materials (47). Important microbes could be predicted based on their annotated function as well as abundance data. Microbial community function is closely linked to operating parameters (i.e. temperature, and pH) and process performance (48). Such knowledge can contribute to the development of prospective proactive microbiome management strategy to better harness microbial community (i.e. improve process stability and efficiency).

### 2.2.4. Metatranscriptomics

#### *2.2.4.1. Principle of metatranscriptomics*

Although metagenomics can reveal the functional potential of a microbial community, it cannot distinguish whether these functions (genomes) come from cells that are viable, damaged or dead (49). In addition, although many genes are present in the microbial community, not all of them are expressed at the same time. Under different environmental conditions, the microbial

community expresses different sets of genes at different levels. Characterization of the gene expression profile is possible with metatranscriptomics, another “omics” analysis that studies the microbial community metatranscriptome using sequencing technology. Metatranscriptome contains the transcript of all microbes present in the sample at the time of sampling.

Metatranscriptomics analysis can reflect the actual metabolic activity of a microbial community at a given time point. Similar to metagenomics, metatranscriptomics eliminates the need for cultivation and does not require any prior knowledge of the community. When multiple samples are analysed using metatranscriptomics, the whole gene expression profile (which genes were expressed and their expression levels) of a microbial community can be obtained. Thus, metatranscriptomics detects changes in community function and active metabolic pathways under different conditions or over time. In addition, metatranscriptomics distinguishes between constitutively expressed and acutely responsive genes.

While coupling with taxonomical classification, metatranscriptomics can identify microbial groups that are always highly active or only active under certain conditions. Metatranscriptomics combined with taxonomical analysis also reveals the level of correspondence between abundance data and transcriptional activity. The correspondence data will help to confirm whether the most abundant species play the most important functional roles in the community and whether key members of the community possess different gene expression strategies (50). Analysis of the metatranscriptome can also pinpoint the differences in active functions of microbial communities with similar microbial compositions (similar functional and metabolic potential).

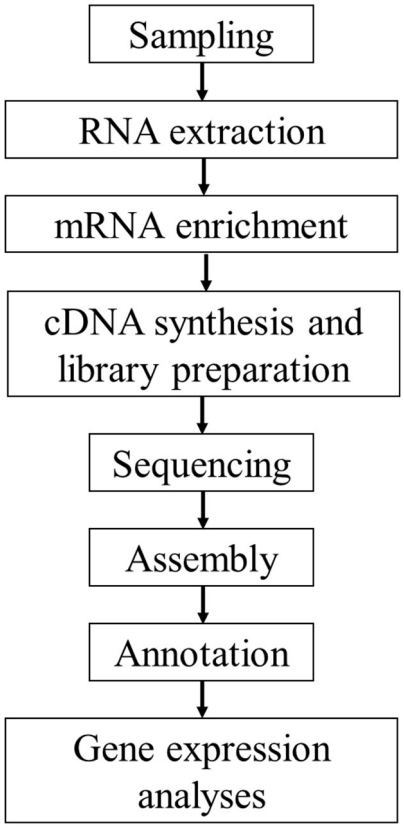


Figure 3. Steps involved in metatranscriptomics analysis.

The standard procedure of a metatranscriptomics analysis shares some common steps with metagenomics analysis using a sequence-based approach (Figure 3). mRNA enrichment needs to be performed after RNA extraction from samples. mRNA is the transcript of coding genes and its abundance is very low compared to other types of RNA. Next, mRNA is subjected to complementary DNA (cDNA) synthesis (to convert to double-stranded DNA) and library preparation, which involves fragmentation of the target sequences and adapters ligation before sequencing. Sequencing reads are subjected to quality control (i.e. filtering non-mRNA reads and trimming low-quality reads) before mapping to the reference genome for annotation. In the case that a reference genome is not available, *de novo* assembly of the reads into contigs is performed after the quality control step. Functional assignment is carried out by aligning the reads to protein databases. Transcript data is normalized and used for the calculations of gene expression levels and patterns.

#### *2.2.4.2. Application of metatranscriptomics*

Metatranscriptomics provides an effective method for the investigation of microbial community immediate regulatory responses to different conditions and the regulating mechanism. This information is valuable, especially in the medical field where human individuals possess distinguished active bacteria groups (51). For example, metatranscriptomics analysis of the

human microbiome can pinpoint the disease-associated bacteria, and reveal the species-specific biases in transcriptional activity and dominant pathways by different microorganisms per host (52). The interaction between human microbiota and immune system or drug metabolism can also be elucidated by metatranscriptomics (51). The gut microbiome may have negative effects on drug efficacy (inactivation of drug) and vice versa (unintended consequences of xenobiotics) (53, 54).

Metatranscriptomics has the capability to discover novel or unrecognized functions, such as stress resistance mechanisms or enzymes involved in metabolism pathways in specific environments. For instance, metatranscriptomics has broadened knowledge about microbial metabolism of organic carbon in Arctic peat soils by unravelling the shift from aerobic to anaerobic metabolism in the deeper peat layers. This shift corresponds to a transition from $CO_2$- to $CH_4$-dominated greenhouse gas emissions, which impacts the global carbon cycle (55). In addition, the integration of functional annotations, taxonomic classification and metagenomics data can help identify the contribution of different taxa (abundant or rare taxa) to the community function. Validation of prevailing models and elucidation of ecological strategies in temperate freshwater microbial communities can be achieved using metatranscriptomics (50).

### 2.2.5. Other omics approaches

Other omics approaches, such as metaproteomics and metabolomics, are increasingly being implemented. Metaproteomics is the analysis of the entire protein complement expressed by the microbial community at the time of sampling (metaproteome), while metabolomics characterizes all the metabolites that were produced (metabolome). These approaches are extremely useful when applied to complex microbial communities where genome/transcriptome assembly and binning of individuals to individual species are arduous tasks. The reason is that metaproteomics and metabolomics do not rely on sequencing technologies. Instead, they employ electrophoresis (metaproteomics) or chromatography techniques (metabolomics) to separate target molecules, followed by spectrometry methods (mass spectrometry, nuclear magnetic resonance, infrared or UV spectroscopy) to acquire data.

While proteins are final products of gene expression, metaproteomics does not necessarily reflect the gene expression profile. There are multiple layers of changes from mRNAs to proteins, including post-transcriptional regulations and post-translational modifications. In addition, proteins are more stable products compared to mRNAs. Thus, although metatranscriptomics focuses on the immediate response of the community to environmental changes, metaproteomics highlights the inherently important metabolic pathways of the community. Metaproteomics can also provide information that is non-attainable using metagenomics or metatranscriptomics, such as protein functions and interactions.

Metabolomics allows for the identification and quantification of metabolites at the same time in a particular environment of interest. Metabolites are direct products of metabolic pathways, and thus can serve as a useful tool for pathway analysis. Metabolites are also closely related to the interaction of the microbial community with the host environment (56). Therefore, investigation of metabolites can unravel the functional dynamics influencing community and host interactions (57). Furthermore, metabolites are means of communication between individuals in the microbial community (signalling process) (56). Metabolomics thereby contributes to the understanding of communication mechanisms that can have significant impacts on gene expression and microbial phenotypes.

Metaproteomics and metabolomics have multiple possible applications ranging from medical to environmental areas. As an example of medical application, metaproteomics has been used to reveal disease-related mechanisms such as the associations between the microbiome and intestinal extracellular vesicle proteins in children with inflammatory bowel disease (58). A more comprehensive understanding of such mechanisms will assist the development of disease control strategies. Meanwhile, drug discovery and pharmacogenomics using metabolomics can pave the way for personalized medicine. In the environmental field, metabolomics can be employed for the study of interactions between the microbial community with biotic and abiotic factors in the environment. Microbial surviving mechanisms and selective forces under stressful conditions can also be examined using metabolomics. This approach has been utilized to elucidate biochemical modes of action of various environmental stressors to both terrestrial and aquatic organisms, as well as predictive biomarkers for these stressors (59).

### 2.2.6. Potential applications of next-generation sequencing

Integrative omics analysis or the multi-omics approach represents the combination of two or more ‘omics’ approaches to examine microbial ecology. Each ‘omics’ approach is a powerful tool that targets a specific class of biological molecules to provide information on a specific aspect of the microbial community. Metagenomics reveals the functional potential; metatranscriptomics indicates the immediate gene expression profile; metaproteomics focuses on the protein expression, functions and interactions; while metabolomics unveils metabolic pathways (Figure 4). Nevertheless, mechanisms underlying biological systems cannot be unravelled by a single ‘omics’ study due to their high complexity (60).

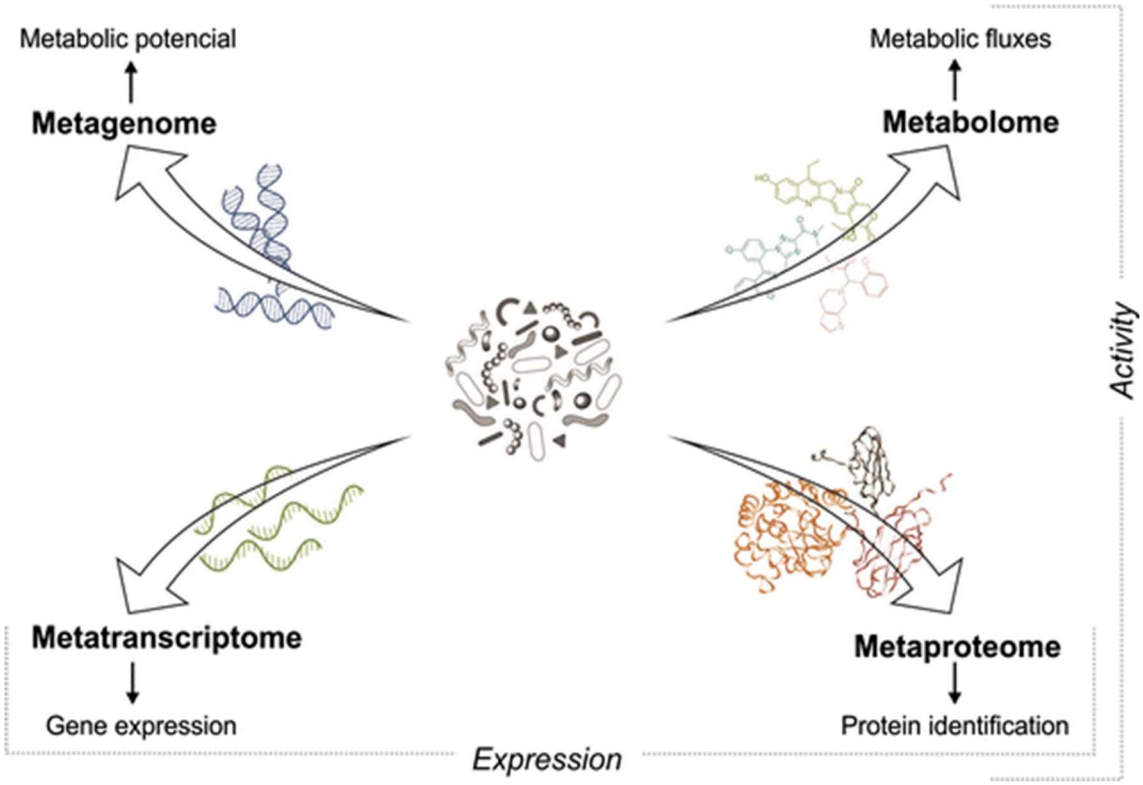


Figure 4. Application of integrative 'omics' analysis of complex microbial communities (from (48)).

As previously mentioned, discrepancies might exist between data obtained from 'omics' approach due to multiple regulations and interactions at each level (genes, transcripts, proteins, metabolites). Thus, when these 'omics' approaches are used in conjunction, they can complement each other to address the detection limit and reduce the detection bias of each approach. In addition, by compiling multiple layers of information obtained, microbial function and metabolism, as well as microbial community responses to environmental factors, can be fully elucidated. The integration of multiple 'omics' will reveal a complete picture of the biological system and subsequently result in novel discoveries that are not accessible through a single 'omics' approach (60). Examples of integrative 'omics' analysis applications are provided in Table 2.

Table 2. Examples of next-generation sequencing and integrative 'omics' analysis application in previous studies.

| **Approaches** | **Study goals** | **Implications** | **Ref.** |
|---|---|---|---|
| Metagenomics and metatranscriptomics | To analyse the metabolic activities of different community members and their possible interactions in a | The knowledge obtained can improve the prediction of cheese flavour, quality, texture and safety, and bioactive metabolites. | (61) |

| | | | |
|---|---|---|---|
| | surface-ripened cheese ecosystem. | | |
| 16S rRNA amplicon sequencing, metagenomics, and metabolomics | To characterize sub- and supragingival biofilms in adults with chronic periodontitis pre- and post-treatment with 0.25% sodium hypochlorite. | The knowledge obtained can enhance the prediction of treatment efficiency. | (62) |
| Metagenomics and metabolomics | To corroborate the host-gut microbiota interactions in patients with cystic fibrosis transmembrane conductance regulator impairment. | The knowledge obtained can be used to develop novel clinical interventions to improve the patient's nutritional status and intestinal function. | (63) |
| Metagenomics, metatranscriptomics, and metabolomics | To study the contributions of individual community members and their interspecies interactions during bisphenol A-degradation. | The knowledge obtained can be applied in future operations such as bioaugmentation of a community or consortium containing the cooperative metabolic groups. | (64) |
| Metagenomics, metatranscriptomics and metaproteomics | To elucidate the influence of the microbiota-host interaction on oak health and disease (acute oak decline). | The knowledge obtained broadens the understanding of the mechanism used by members of the lesion microbiome in plant disease and pathogen defence. | (65) |

Integrative omics approach allows for comprehensive microbial ecology investigation and shows potential applications in multiple processes including those for environmental conservation and protection. Recently, more and more studies were utilized this approach to link operating conditions and microbial community with process performances. The knowledge of the microbial machine behind such processes at the systematic level can contribute to the development of better operational strategies. For example, Nguyen et al. (66) utilized NGS and bioinformatics to investigate effects of operational disturbance and subsequent recovery process on microbial community during a pilot-scale anaerobic co-digestion. Amplicon sequencing of 16S rRNA and *mcrA* marker genes revealed that operational disturbance led to the enrichment of hydrolytic and fermentative bacteria (>57% of the total abundance) and reduction of acetogenic and methanogenic microbes (<9% and <3% of the total abundance, respectively). Acetogens and methanogens population were replenished by inoculum addition, which in turns recovered

digester performance. In another study, Henriet et al. (67) evaluated different sludge bulking mitigation strategies and employed 16S amplicon sequencing and quantitative PCR to monitor the abundance of *Thiothrix* species and glycogen-accumulating bacterium Candidatus *Competibacter* over 1.5 years. Results showed that sludge densification strategy can solve sludge bulking more effectively than polyaluminium chloride addition and volatile fatty acids reduction. Under the scope of this thesis, several environmental engineering applications that can potentially benefit from microbial ecology study using integrative omics analysis have been identified. These applications include membrane-fouling mitigation in membrane bioreactor (MBR), valorisation of lignocellulosic biomass (LCBM), and chiral inversion of 2-arylpropionic acids (2-APAs) in biological waste and wastewater treatment.

## 2.3. Biological treatment processes

### 2.3.1. Membrane bioreactor for wastewater treatment

MBR refers to the integration of membrane filtration with conventional activated sludge (CAS) treatment to produce high-quality treated effluent and achieve complete microbial biomass retention in a much smaller physical footprint. Over the last few decades, MBRs have become an essential process for municipal and industrial wastewater treatment as it offers high effluent quality and low footprint (68, 69). Since 2018, there have been over 700 MBR plants in operation worldwide with a treatment capacity of over 100 MLD/plant (70, 71). Due to increasingly stringent regulations on treated water quality and water reuse initiatives, MBRs are expected to continuously increase in both number and scale (72). However, membrane fouling presents a major challenge to widespread and cost-effective MBR applications (73).

Membrane fouling can be defined as the deposition of foulants on the membrane surface, creating a fouling layer, causing flux decline or increasing transmembrane pressure. Membrane fouling can be classified into biofouling (deposition and growth of microorganisms), organic fouling (deposition of organic substances), and inorganic fouling (deposition of inorganic substances) (74). The presence of the fouling layer reduces membrane permeability, increases transmembrane pressure (TMP) and declines water flux (74, 75). In addition, the growth of microorganisms on the membrane surface can result in membrane deterioration, impaired contaminants rejection and deterioration of permeate quality (76). As a result, membrane fouling can increase MBR operating cost significantly due to the high energy consumption to compensate for the loss of effective pressure, cost for frequent membrane cleaning and replacement. For example, it is estimated that membrane maintenance cost and cleaning chemicals account for 36.9% of MBR operating expenditure in the Netherlands, resulting in a 58% increase compared to CAS process (77-79). Thus, membrane fouling mechanism and mitigation have been subjects of great research interest (80-83).

Membrane fouling occurs in several stages: conditioning, initial attachment, maturation, succession, and dispersion. In the conditioning step, organic (e.g. proteins, polysaccharides, humic acids**)** and inorganic substances in the aqueous solution are deposited onto membrane surface and either block the pores of membranes (if the substance size is less than/comparable to membrane pores), and form a conditioning film (if the size of the substance is larger than membrane pores) and Brownian motion. In the second stage, microbial cells are transported to the conditioning film by fluid dynamic forces (permeation drag, back-diffusion transport and cross-flow velocity). Some pioneer species can easily adhere to the membrane surface via adhesive proteins and electrostatic interactions (initial attachment) (84), e.g. bacteria with small rods and long motile flagella. Such species can rapidly reproduce thanks to the concentrated nutrient (concentration polarisation) near the membrane surface. The conditioning film becomes thicker and is now referred to as biofilm. A large amount of extracellular polymeric substances (EPSs) and soluble microbial products (SMPs) is generated during biofilm growth, forming a layer of glutinous substances, and creating a bridging effect to attract more and more species to the membrane surface**.** Gradually, the biofilm matures and its interior becomes anoxic due to lower oxygen levels, rendering its suitability for the initially attached pioneer species. Climax species that can adapt to the new environmental conditions will be enriched preferentially in the biofilm (succession). Parts of the biofilm are dispersed into the bulk sludge and subpopulations of these detached mature cells can reinitiate biofouling formation on a new site of the membrane (85). It is clear that biofouling plays a key role in membrane fouling development. Biofouling can be considered the most complicated and challenging issue currently hindering MBR applications due to various factors involved (membrane properties, feed-biomass characteristics, and operating conditions).

Techniques to control membrane fouling can be categorized into two groups, namely prevention and mitigation (membrane cleaning). Pre-treatment of the feed water to remove potential foulants is a common strategy for fouling prevention. Fouling mitigation includes backwashing (physical cleaning), chemical, and biological cleaning. Physical cleaning methods such as backwashing or the addition of supporting media (e.g. activated carbon and plastic beads) can remove loosely attached foulants (reversible fouling) (86, 87), while chemical cleaning targets harder-to-remove materials (irreversible fouling). A combination of physical and chemical cleaning is generally applied to maintain sustainable operation of MBRs (88). Despite their effectiveness in foulants removal, membrane damage and production of toxic by-products (which can inhibit microbial in the bulk sludge) are limitations of these methods (89). Thus, more environmental-friendly and membrane-friendly biological cleaning methods have also been developed based on understanding of the nature of biofouling (90-93).

Biological cleaning involves the use of bioactive agents (enzymes and signal molecules) to break down the biofilm. In the biofilm, EPS provides the matrix and nutrients for microbial growth, while signal molecules (auto-inducers) are used for microbial communication (quorum sensing). These molecules play critical role in regulating biofilm formation, and they can be targeted to control biofouling without damaging membrane surface. For example, microbial communication can be interrupted (quorum quenching) by inhibiting the production of auto-inducers, their detection by receptors, or their degradation (94, 95). Although biological methods have been demonstrated to be effective in controlling fouling, the mechanical and biological stability against long-term MBR operation are the main concerns for the practical applications with these methods (75, 81).

Due to the important contribution of biofouling to overall membrane fouling, significant efforts in characterizing membrane fouling microbial communities have been made using different types of MBR including aerobic (96-106), anoxic/aerobic (83, 107-113) and anaerobic MBRs (114, 115). Early investigations mostly applied fingerprinting techniques such as denaturing gradient gel electrophoresis or terminal restriction fragment-length polymorphism for microbial community analysis (96, 97, 107-109, 114, 115), while recent works preferably employed NGS as the technology became more affordable in the last 10 years (83, 98-102, 104-106, 112, 116). Besides characterizing the microbial structure and composition in the biofilm and mixed liquor (bulk sludge), previous works also tried to identify the link between microbial community, fouling propensity, and other operating conditions using statistical and bioinformatics tools such as correlation analysis (100, 117), constrained/gradient analysis (103, 110, 112), and network analysis (100, 113, 116, 118).

Recent research works have resulted in a better understanding of key aspects of the fouling microbial community. Operating parameters such as solids retention time (SRT), dissolved oxygen (DO) level, and temperature can strongly impact microbial community and fouling propensity in MBR (96, 105, 108, 109, 111). However, the impact of these operating parameters on the microbial structure is weaker than the spatial separation between the biofilm and the mixed liquor (96, 109, 116), as well as the micro-environment developed inside the biofilm (115). Most studies also found diverse and distinct communities on the membrane surface compared with the one in the bulk sludge (96-98, 100, 103, 104, 114), indicating that specific groups of microorganisms were selectively growing in the biofilm. Microbial species that develop in the biofilm of an MBR are subjected to its specific operating conditions (83, 98, 100). In addition, the interactions between biofilm microorganisms and their excreted metabolites including EPSs and SMPs were crucial factors that accelerate membrane fouling (96, 102, 107, 109, 110, 114). For example, biofouling succession can change the composition/accumulation of metabolic products in the biofilm, and the accumulation of metabolic products can alter the biofilm micro-

environment and induce biofouling succession (110). The role of low-abundance microbial species in membrane fouling was also recognised in recent works (100, 110, 113).

Despite recent research efforts, a comprehensive understanding of the microbial community during fouling has not been achieved. There are some discrepancies in the literature on the fouling-associated microbial community. For example, Chen et al. (110) and Huang et al. (96) observed that biofilm composition was similar to the mixed liquor composition at low flux, while distinct biofilm communities developed on membrane surfaces at high fluxes despite the high drag force. In contrast, Xu et al. (116) reported fouling at the low-flux condition is a deterministic process and depends on environmental conditions (e.g., substrate types and concentrations) rather than a stochastic dispersal from the bulk sludge, while under the high-flux condition the high drag force unselectively drives species from the mixed liquor to the membrane surface for biofilm formation. These results suggest that more insights into microbial composition and interactions during membrane fouling are needed in order to assist the development of fouling mitigation strategies.

### 2.3.2. Lignocellulosic biomass valorisation using rumen fluid

LCBM refers to plant biomass in the form of agricultural, agro-industrial and forestry wastes, such as rice straw, corn stover, leaves, and any other non-edible parts of the plants (e.g. stalks, cobs, husks, and stems). Due to increasing food demand and rigorous farming conditions, LCBM is the most abundant source of biomass on Earth. Global production of rice straw alone is 731 million tons per year (119). Annual agricultural crop residue in Canada reached 69 million dry tonnes (120), while the number is estimated to be 1.4 billion dry tonnes in the US (121). LCBM comprises of three main components: cellulose (35–50 wt%), hemicellulose (20–35 wt%), and lignin (15–20 wt%) (Table 3). Cellulose is a homogenous biopolymer consisting of linear chains of glucose units linked by β-1,4-glycosidic bonds. These chains aggregated together through hydrogen bonds and van der Waals forces to form a crystalline structure called cellulose microfibrils (122). Hemicellulose possesses a heteropolymeric structure, consisting of various sugar monomers including pentose (xylose, arabinose), hexose (glucose, galactose, mannose), 4-O-methyl glucuronic acid, and galacturonic acid residues (123). Lignin is a highly heterogeneous polymer contructed from cross-linked phenylpropanoid monomers of three types: guaiacyl, syringyl, and hydroxyphenyl (124). Lignin cross-links with hemicellulose and fills the spaces in the plant cell wall between cellulose and hemicellulose. The crystallinity of cellulose, hydrophobicity of lignin, and encapsulation of cellulose by the lignin-hemicellulose matrix together form a rigid structure that is recalcitrant to degradation (125).

Table 3. Chemical composition of various lignocellulosic biomass.

| Lignocellulosic biomass | Composition (% dry weight) | | | References |
|---|---|---|---|---|
| | Cellulose | Hemicellulose | Lignin | |
| **Agriculture waste** | | | | |
| Corn straw | 49.3 | 28.8 | 7.5 | (126) |
| Rice straw | 31.1 | 22.3 | 13.3 | (127) |
| Wheat straw | 35.9 – 48.6 | 23.9 – 27.7 | 8.2 – 19.3 | (128, 129) |
| Sugarcane bagasse | 43.1 | 31.1 | 11.4 | (130) |
| **Forestry waste** | | | | |
| Hardwood | 38 – 51 | 17 – 38 | 21 – 31 | (131) |
| Softwood | 33 – 42 | 22 – 40 | 27 – 32 | (131) |
| Switch grass | 39.5 | 25 | 17.8 | (132) |
| Forage sorghum | 35.6 | 20.2 | 18.2 | (133) |

Previously, LCBM was often considered unavoidable waste, and the majority of LCBM is discarded or burned. Agriculture crop burning is a common practice in Australia, Canada, US, India, and many agriculture production regions around the globe. In India alone, 92 million tons of crop residues are burned each year (134). Farmers consider open burning is considered as the easiest and most economical option to remove crop residue and prepare for the new season (135). This practice contributes to greenhouse gas emissions, air pollution, public health concerns, as well as declining soil organic matter and soil productivity (136). Carbon dioxide emissions from the burning of crop residues are estimated to be in the range of 1.1 and 1.7 Gt per year (137). In recent years, the shift toward sustainable development and circular economy has renewed interest in LCBM as a valuable commodity for the production of biofuels and chemicals. LCBM is an abundant and inexpensive source of carbon in the form of polysaccharides. Cellulose and hemicellulose in LCBM can be broken down into sugar monomers, which in turn can be converted into biogas, biofuels (ethanol, butanol, and diesel) over 200 biochemical compounds (138). This provides a renewable and more sustainable alternative to traditional fossil-fuel-based chemical production. LCBM can be produced quickly and does not interfere with food supply (125). In the US, about 111 million dry tons of primary crop residues are available to collect at farmgate feedstock prices of $60 as of 2011 (139). Nevertheless, LCBM valorisation is hindered by the presence of recalcitrant lignin and the resistance of cellulose and hemicellulose to degradation. Thus, pre-treatment is necessary to increase the digestibility of LCBM.

Various approaches have been developed for pre-treatment of LCBM, with the aim to liberate cellulose from the lignin-hemicellulose matrix, increase cellulose and hemicellulose solubility, increase their accessibility to enzymes and chemicals, and minimize sugar loss (125). Currently available pre-treatment regime falls under the categories: chemical, physical, physio-chemical

and biological approaches. These approaches possess different modes of action, resulting in different yields, advantages and disadvantages (Table 4). Chemical pre-treatment offers high efficiency (4 to 10-fold increase in sugar yield) but associates with expensive reactors and toxic chemicals. The use of physicochemical methods can also increase sugar yield (up to 131%) while involving high energy input. The formation of inhibitory by-products during chemical and physical pre-treatment also affects the yield of the downstream hydrolysis/fermentation process (140). Biological pre-treatment is environmental-friendly, low cost, and efficient (3-4 folds increase in sugar yield) but time-consuming (6 – 28 days) (125, 141).

Table 4. Advantages and disadvantages of current lignocellulosic biomass pre-treatment methods.

| Pre-treatment | Mechanism | Advantages | Limitations | Ref. |
|---|---|---|---|---|
| ***Chemical pre-treatment*** | | | | |
| Alkali | Solubilise lignin and part of hemicellulose | High effectiveness<br>Low sugar loss<br>Mild operating conditions | Time-consuming<br>Conversion of alkali into irrecoverable salts | (142-144) |
| Acids | Solubilize hemicellulose and part of lignin through the cleavage of glucosidic bonds | High product yield within a short time frame | High reactors cost<br>Corrosive and toxic chemicals<br>Formation of inhibitory by-products | (144, 145) |
| Ozone oxidation | Oxidize lignin | Low sugar loss<br>No toxin residues<br>Mild operating conditions | High energy consumption<br>High dose required | (146-148) |
| Ionic liquids & Deep eutectic solvents | Cellulose crystallinity reduction<br>Partial hemicellulose and lignin removal | Non-toxic, non-corrosive<br>High efficiency | High cost<br>Large volume of liquids | (149, 150) |
| ***Physical/physicochemical pre-treatment*** | | | | |
| Mechanical (e.g. milling, grinding) | Reducing particle size and increasing the surface area | Control of final particle size | High energy consumption<br>Cannot degrade lignin, low efficiency | (151) |
| Irradiation (e.g. microwave and ultrasound) | Disrupt lignin and hydrogen bonds | Short treatment time | Extreme operating conditions<br>Formation of inhibitors | (151, 152) |
| Hydrothermal (e.g. hot liquid, steam explosion) | Removal of soluble lignin and hemicellulose | No need for chemical addition | High energy and water consumption | (151, 153) |

| | | | | |
|---|---|---|---|---|
| | | Short treatment time | | |
| ***Biological pre-treatment*** | | | | |
| Microorganisms (Fungi and bacteria) | Microorganisms excrete enzymes to degrade lignin and cellulose | Environmentally friendly<br>No chemical addition<br>Low energy demand | Time-consuming<br>Sugar loss<br>Lower efficiency | (140) |
| Ligninolytic enzymes (e.g. laccase) | Direct application of lignin-degrading enzymes on biomass | Reduced treatment time<br>Selective lignin degradation | High enzyme extraction and purification cost | (154, 155) |

Among all currently available approaches, biological pre-treatment is the most sustainable for LCBM valorisation, as this approach employs naturally occurring microorganisms/enzymes under mild operating conditions. This approach also entails low downstream processing cost and reduce the formation of inhibitors. Various high value-added chemicals generated from the breakdown of lignin during biological pre-treatment can be used as precursors for the production of phenolic acid, vanillin, vanillic acid, cinnamic acid, benzoic acid, and syringaldehyde (140). Biological pre-treatment can be categorized into microbial pre-treatment (fungal, bacterial, microbial consortia and ensiling) and enzymatic pre-treatment. Microbial pre-treatment involves direct use of lignin-degrading (ligninolytic) fungi and/or cellulose-degrading (cellulolytic) bacteria, with white-rot fungi proven to be the most efficient lignin-degrading species (156-158). The major drawbacks of using single strain fungal/bacterial are long pre-treatment time and strict microbial growth conditions (140). These disadvantages could be overcome by the design and exploitation of co-culture systems consisting of fungal-fungal (159), bacterial-bacterial (160), or bacterial-fungal species (161). These microorganisms can carry out synergistic activities to degrade LCBM: fungi break down lignin and cellulose into monomer sugars, which are then metabolized by bacteria into valuable products (161, 162). Microbial consortia also have higher adaptability to operational disturbance and increased substrate utilization compared to single strain pre-treatment, which in turn leads to higher treatment efficiency and productivity (140).

Currently, the design of lignocellulose-degrading microbial consortia involves the combination of single strain fungal/bacterial isolates. However, it is challenging to find strains with positive synergistic interactions (161), and maintain the stability and efficiency of such artificial systems (163, 164). Thus, the use of naturally occurring lignocellulose-degrading microbial consortia is gaining attention in recent years (165, 166). An elegant example of such consortia is the symbionts in the digestive tract of ruminant animals. Microorganisms in the rumen microbial community have evolved for millions of years to digest LCBM; thus, they possess superior cellulolytic activity with the ability to produce at least 21 extracellular hydrolytic enzymes (167). Pre-treatment of LCBM with rumen-enriched cultures showed promising results with cellulose hydrolysis efficiency up to 81% and reduced treatment time (168-172). Rumen microbes degrade LCBM into valuable products: VFAs and biogas, indicating the potential of this process to be incorporated into anaerobic digesters for biogas production.

In recent years, the application of metagenomics and metatranscriptomics for novel lignocellulosic-degrading enzymes screening from natural sources has become increasingly common (173-177). Effective application of omics tools allows for the retrieval of novel enzymes from microbial populations that cannot be maintained in axenic cultures e.g. bovine ruminal protozoan (178). Using omics tools, enzymes with superior characteristics (e.g. thermostable, alkaline-tolerant, and halotolerant) were identified from saline-alkaline lake soil and rumen of

black-goat, cow and sheep (173-177). Such enzymes can catalyze LCBM hydrolysis under harsh conditions and show high potential for various industrial applications including renewable biomass and biofuels production. A newly developed metagenomics-guided strategy (without the construction of metagenomics libraries) also allows for high-throughput screening of new cellulases from environmental metagenomes (179).

Recent advances in omics tools also provide more insights into LCBM degradation by environmental microbes, such as the relative abundance of rRNA genes, functional genes, and transcripts encoding glycoside hydrolases (GH), and render their applications for LCBM valorisation (180-185). Whole-genome sequence analysis of anaerobic fungi *Orpinomyces* strain C1A (isolated from the feces of an Angus steer) revealed the presence of an extremely rich repertoire of lignocellulolytic machinery with considerable functional overlap, consisting of 357 GH genes, 92 carbohydrate esterases, and 24 polysaccharide lyases (PLs) (181). This result was in agreement with the analysis of transcriptomic profiles of the strain C1A when grown on four different types of LCBM (alfalfa, energy cane, corn stover, and sorghum) (180). Comtet-Marre et al. (182) applied metatranscriptomics analysis of rumen of dairy cows fed on a mixed diet and identified GHs families involved in the deconstruction of different plant cell wall components: GH9, GH48, GH5, and GH94 (cellulose), GH10, GH11, and GH43 (hemicellulose), PL11 and GH28 (pectin), and GH13 (starch deconstruction).

Omics tools, with metagenomics being the most common one, can elucidate the shift in microbial community structure and composition during LCBM pretreatment and/or treatment. For example, Baba et al. (186) detected that the predominant phylum shifted from *Bacteroidetes*, composed of amylolytic *Prevotella* spp., to *Firmicutes*, composed of cellulolytic and xylanolytic *Ruminococcus* spp., in only 6 h of pretreatment of rapeseed using cattle rumen fluid, and the relative abundance of two *Ruminococcus* species increased with increasing cellulose and hemicellulose degradation rates. Lee et al. (185) identified an increase in the relative abundance of *Ruminococcus* and *Clostridium* and a decrease in the relative abundance of *Prevotella* and *Fibrobacter* (dominant bacteria in rumen fluid) during pretreatment of waste paper pieces (0.1% w/v). This phenomenon was also observed in the continuous treatment of rice straw using a co-inoculation of ruminal microbiota with methanogenic sludge, with an increase in *Clostridium* and *Ruminococcus* abundances, whereas *Bacteroides*, *Fibrobacter* and *Acetivibrio* disappeared (187). The decrease/disappearance of indigenous bacteria could be attributed to their inability to acclimatize to *in vitro* conditions (e.g., different pH, VFAs) (187). In addition, omics analysis contributes to a better understanding of the relationship between operating conditions, community structure and functional profile, and performance and efficiency during LCBM pretreatment and valorisation. Deng et al. (187) investigated the co-inoculation of ruminal microbiota with methanogenic sludge and found that co-inoculation increased methanogens abundance, allowing

for mutual cooperation between *Methanobrevibacter* and *Ruminococcus*, an increased proportion of bacteria containing GH5 genes, which in turns resulted in increased biogas production. Similarly, enhanced methane production following steam-explosion pretreatment and bioaugmentation with cellulolytic bacteria was well correlated with the increase in abundance of hydrolytic bacterium *Caldicoprobacter*, syntrophic acetate oxidizing bacteria, and the hydrogenotrophic *Methanothermobacter* (188). Previous studies have employed a combination of metagenomics with enzyme activity analysis to link microbial and functional profiles. Baba et al. (189) elucidated that the relative abundance of known lignocellulose-degrading bacteria (*Prevotella*, *Ruminococcus*, *Ruminofilibacter*, *Cellulosilyticum* and *Bacteroides*) corresponded to lignocellulose-degrading enzymatic activities in rapeseed pretreatment. Similarly, Takizawa et al. (190) revealed that the relative abundances of *Selenomonas*, *Porphyromonas*, *Clostridiales* family XI, and *Lachnospiraceae* positively correlated with 40, 50, 52, 53, and 101 kDa endoglucanases during carboxymethyl cellulose degradation.

These previous studies have demonstrated the various applications of omics tools in developing and optimizing LCBM valorisation process. Most studies were performed at batch-scale (191-193), indicating the need for more studies at lab- and pilot-scale before industrial application. Key indigenous bacteria of rumen participating in LCBM degradation (*Prevotella*, *Ruminococcus*, *Fibrobacter*, and *Ruminofilibacter*) have been identified in multiple studies. However, these indigenous bacteria can reduce in populations if they cannot acclimatize to the *in vitro* conditions. Species originating from natural inoculum or bioaugmentation can also suffer from microbial washout, especially in continuous stirred tank reactors. Thus, further studies employing omics tools are needed to provide a more comprehensive understanding of the ruminal microbial community involved in the lignocellulosic degradation process under *in vitro* conditions and contribute to the development of an engineered system to generate valuable products from LCBM.

### 2.3.3. Chiral inversion of non-steroidal anti-inflammatory drugs in biological treatment

Non-steroidal anti-inflammatory drugs (NSAIDs) are a group of emerging contaminants due to their increasing accumulation in the natural environment. NSAIDs are detected in wastewater treatment plants (WWTPs) influents and effluents in Asia, North America and Europe with median concentration ranging from below the method quantification limit to 147,700 ng/L (194). The main reason for such accumulation is their high accessibility as over-the-counter drugs and their wide usage for pain relief. Commonly used NSAIDs include acetaminophen, diclofenac, fenoprofen, ibuprofen, ketoprofen, naproxen and salicylic acid. Another reason is the limited capacity of the waste and wastewater treatment facilities to remove these compounds. In addition, NSAIDs can undergo sorption into sludge and can enter the environment via improper sludge application (195, 196). Environmental accumulation of NSAIDs presents a significant concern due to possible negative impacts. The presence of NSAIDs in the water environment, even at trace

levels, has been known to potentially affect aquatic organisms and disrupt aquatic ecosystems (197). Schmidt et al. (198) reported GST inhibition, lipid peroxidation and DNA damage when fish are exposed to NSAIDs at environmentally relevant concentrations. Moreover, NSAIDs may exhibit toxicity on humans if they enter the food chain via medicated food products and/or products from aquacultural/agricultural systems that are contaminated with NSAIDs.

Most municipal WWTPs are primarily designed to remove organic nutrients, and are not necessarily designed to eliminate NSAIDs and other emerging contaminants. One removal mechanism is the sorption of hydrophobic NSAID into sludge. In addition, NSAIDs could be degraded to biodegradation (199-204), either incomplete (parent drugs are transformed into intermediate products) or complete mineralization (203). Previous studies have reported NSAIDs degradation by ammonia-oxidizing bacteria (205) and by white-rot fungi such as *Phanerochaete chrysoporium* and *Trametes versicolor* (206-209). Removal of NSAIDs also depends on the treatment technology and individual drugs properties (210). In general, NSAIDs that belong to the class 2-APA e.g. ibuprofen, naproxen, and ketoprofen, showed higher removal during WWTP than other NSAIDs and within the range of 45 – 100% (207, 209, 211-213).

Several NSAIDs are chiral compounds, existing in two enantiomers that possess identical chemical structures but different spatial arrangements of atoms around a stereogenic centre. Chiral NSAIDs including ibuprofen, naproxen, ketoprofen, indoprofen, flurbiprofen, carprofen and fenoprofen (214). Chiral enantiomers can exhibit vastly different biological properties (215), and chirality can induce enantioselectivity in a compound's environmental occurrence, fate and toxicity (216-219). For example, (*S*)-ibuprofen was suggested to be preferentially removed during activated sludge, trickling filter and MBR treatment, constructed wetlands, and sand filters (199, 219-221). Meanwhile, Camacho-Muñoz et al. (222) observed enrichment of (S)-ketoprofen during trickling filter treatment. Nevertheless, NSAID drug stereochemistry is often overlooked in environmental studies, and the potential of NSAIDs undergoing chiral inversion in the environment, whereby an enantiomer converts to its antipode, has received limited attention (219, 221).

Microbial analysis has been commonly conducted in studies on NSAIDs degradation studies. Putative ibuprofen- and ketoprofen- degrading microorganisms were isolated from WWTP activated sludge and 16S rRNA sequencing was employed to identify their taxonomic classification (223-225). Promising results from these studies indicate that the isolated bacteria may be useful for bioaugmentation to enhance NSAID removal in WWTPs. The impacts of NSAIDs at environmental concentrations on microbial community assembly and activity were also investigated through microbial analysis. Jiang et al. (226) found that the addition of diclofenac, ibuprofen and naproxen damaged cell walls of microorganisms, and resulted in

increased microbial diversity in sequencing batch reactors. NGS results showed enrichment in *Actinobacteria* and *Bacteroidetes* populations - suggesting their involvement in NSAIDs degradation - while *Micropruina* and *Nakamurella* decreased with the addition of NSAIDs. Grenni et al. (227) employed FISH to evaluate the effect of chronic exposure to naproxen on the natural microbial community of the Tiber River. Analysis of bacterial abundance and composition revealed a decrease in β-*Proteobacteria* and the *Archaea*, and an increase in α- and γ-*Proteobacteria* (227). Similarly, Navrozidou et al. (228) observed a massive increase in the relative abundance of *Alphaproteobacteria* and *Gammaproteobacteria* (from 29.1 to 80.8%) when applying high ibuprofen concentration as the sole carbonaceous feeding substrate in an immobilized cell bioreactor. The shift in feeding conditions, from commercial ibuprofen tablets (containing traces amount of other compounds) + yeast extract to high purity ibuprofen, also resulted in the predominance of *Novosphingobium* and *Rhodanobacter* ($25.5 \pm 10.8\%$ and $25.2 \pm 3.0\%$, respectively), indicating the presence of a specialized ibuprofen-degrading bacterial community in activated sludge (228). More recent studies started applying NGS to investigate the efficiency of novel treatment technologies and their impact on the microbial community (229, 230). At the optimum current intensity of 0.35A, *Thiothrix*, *Flavobacteriaceae*, *Halothiobacillaceae*, *Hydrogenophaga*, and *Comamonadaceae* were key bacteria removing diclofenac and clofibric acid ($79.40 \pm 6.74\%$ and $69.50 \pm 6.26\%$, respectively) in a three-dimensional electrode biological aerated filter (229).

## 2.4. Summary

Information corroborated in this chapter highlights the need to understand and characterise microbial communities associated with MBR fouling, LCBM valorisation, and chiral inversion since microorganisms are key players in all of these processes. Insights into microbial communities will certainly provide valuable and fundamental information for process improvement. NGS sequencing using the 16S rRNA marker gene appears to be the most cost-effective among different techniques available for microbial community characterization. Thus, in this study, 16S rRNA sequencing is selected to characterize the microbial community. In addition, novel bioinformatics tools such as functional prediction analysis (PICRUST), random matrix theory (RMT) network analysis, and differential abundance analysis (ANCOM) were employed to elucidate the roles and relationships between different microbial groups during each process, and the subsequent effect on process performance.

# Chapter 3. FOULING-ASSOCIATED MICROBIAL COMMUNITY IN MEMBRANE BIOREACTOR AT LOW-FLUX CONDITION

This chapter has been published as the following journal article.

Nguyen AQ, Nguyen LN, Johir MAH, Ngo HH, Nghiem LD. Linking endogenous decay and sludge bulking in the microbial community to membrane fouling at sub-critical flux. Journal of Membrane Science Letters. 2022;2(1):100023.

**Summary:** This study examined membrane fouling and associated microbial taxa in a membrane bioreactor operating at a sub-critical flux condition using next-generation amplicon sequencing. The membrane was operated at a sub-critical flux, thus, fouling was not observed until endogenous decay. The observed fouling could be attributed to endogenous decay which was driven by nutrient deficiency at high sludge age and low food-to-microorganisms ratio (decreasing from 0.15 to 0.09 gBOD/gMLVSS.d). Endogenous decay resulted in a sharp decrease of the number of species and evenness between different species (49.7 and 58.9% compared to the inoculum, respectively). The release of dissolved organic matters and cell debris from endogenous decay as well as the excessive growth of filamentous bacteria, e.g. *Thiotrichales* were the main contributors to membrane fouling. The relative abundance of *Thiotrichales* significantly correlated with transmembrane pressure (Pearson R = 0.996, p-value <0.001), indicating this order's contribution to membrane fouling. Other dominant orders in the mixed liquor after endogenous decay such as *Rhizobiales*, *Burkholderiales*, *Rhodospirillales* and *Myxococcales*, *Flavobacteriales* can produce extracellular polymeric substances and aggravating membrane fouling. Fouling layers possess highly similar microbial composition with the mixed liquor, with some filamentous microbial orders, e.g. *Corynebacteriales* and *Oligoflexales* showing increased relative abundance by 6.83 and 5.64 folds, respectively.

## 3.1. Introduction

Membrane bioreactor (MBR) offers numerous advantages over the conventional activated sludge process, including better effluent quality and smaller footprint. A recent life cycle assessment conducted by Banti et al. (231) also showed that MBR has significantly lower environmental impacts e.g. eutrophication potential and global warming potential compared with conventional activated sludge (CAS) treatment plant. Since 2008, more than 2500 MBR plants have been constructed worldwide (232). The estimated global MBR treatment capacity was 20 GLD (gigalitres per day) in 2019 (233). Nevertheless, membrane fouling remains the most challenging issue in MBR operation and limits MBR widespread application. High energy consumption and operational costs associated with membrane cleaning and replacement made retrofitting from CAS to MBR a controversial topic when considering both economical and management aspects

(78, 234). Thus, characterization of membrane fouling, optimization of operating conditions, and development of novel methods for fouling mitigation have attracted great interest (89).

Operating conditions such as permeate flux, solids retention time (SRT), (which affects food-to-microorganism (F/M) ratio), as well as sludge characteristics can have considerable impacts on fouling rate (235-237). Researchers have reach a consensus that operation below the critical flux can minimize membrane fouling (89, 238, 239), due to the restrain of foulants deposition on the membrane surface (240, 241). Nguyen et al. Nguyen et al. (242) reported that applying a low flux of 2 LMH (liters per square meter per hour) can delayed fouling onset for more than 30 days when treating hospital wastewater treatment. Thanh et al. (243) also observed lower fouling rate at low operating fluxes (1.2 and 2.4 LMH) in MBR treatment of high strength leachate from a solid waste transfer station. In addition, operating at sub-critical flux (20 LMH) can result in lower formation of polysaccharides, protein, and high molecular weight organics (~ 48 kDa) than operating above critical flux condition (40 LMH) (244). SRT is another major influencer on membrane fouling, however, the impact of SRT reported in the literature was controversial (245-248). Lower membrane fouling rate was achieved at elevated SRT of 40+ days or even complete sludge retention (235, 245). In contrast, Han et al. (246) found that membrane fouling increased with SRT since sludge particles were more severely deposited on the membrane surface at longer SRT (100 days vs. 30-70 days).

The substrate deficient state (low F/M ratio) created by long SRT can also reduce specific bioactivity and trigger endogenous respiration in microbial cells (245, 246). These conditions are prone to excessive growth of filamentous bacteria (sludge bulking) in the reactor. Filamentous bacteria have greater capacity of energy storage and easier access to nutrients compared to other bacteria (237), making them more resilient under limited substrate conditions. Most previous studies found that membrane fouling behaviour induced by bulking sludge was significantly more severe in comparison with normal sludge (249-251). However, these studies mainly focused on examining sludge characteristics using visual/physiochemical analyses such as floc morphology, relative hydrophobicity, three-dimensional excitation-emission matrix fluorescence spectroscopy (237, 251-254). Investigation of the microbial community presented in bulking sludge will provide more insights into sludge bulking impact on membrane fouling.

This study aims to investigate the fouling mechanism and effect of filamentous bacteria on fouling under long-term operation at sub-critical flux and infinite SRT (complete sludge retention). Next-generation sequencing (NGS) on Illumina Miseq platform was performed to characterize the microbial community profile in the mixed liquor and fouling layer over time. Results from this study can provide the fundamental understanding for fouling mitigation under sub-critical flux condition through optimizing operating conditions.

## 3.2. Materials and Methods

### 3.2.1. Laboratory-scale membrane bioreactor system setup

A laboratory-scale aerobic MBR system was used in this study (Figure 5). The MBR was equipped with a 5 L reactor, two identical hollow fibre membrane modules (Evoqua, Australia), two peristaltic pumps, a digital pressure gauge, and an air pump connected to a diffuser for aeration. The two peristaltic pumps (Masterflex L/S, USA) were used for feeding and permeate extraction. Each of the two membrane modules consisted of 20 polyvinylidene difluoride (PVDF) fibers with a nominal pore size of 0.04 µm and a length of 30 cm (effective surface area of 0.02 $m^2$). One membrane module was submerged in the reactor but was not connected with the pump to examine the biofouling layer under static condition (denoted ST-BF or biofouling layer on static membrane), the other module was connected with the permeate pump to examine the biofouling layer with permeation (denoted as PM-BF or biofouling layer on membrane with permeation). The digital pressure gauge was a high-resolution pressure sensor (±0.1 kPa, John Morris Group, Australia), which was installed between the membrane module and the permeate pump for continuous monitoring of the transmembrane pressure (TMP). The reactor's working volume was maintained at 3 L. The air pump (AquaOne, Australia) aerated the reactor at an air flowrate of 0.4 L/min via a diffuser at the bottom of the reactor.

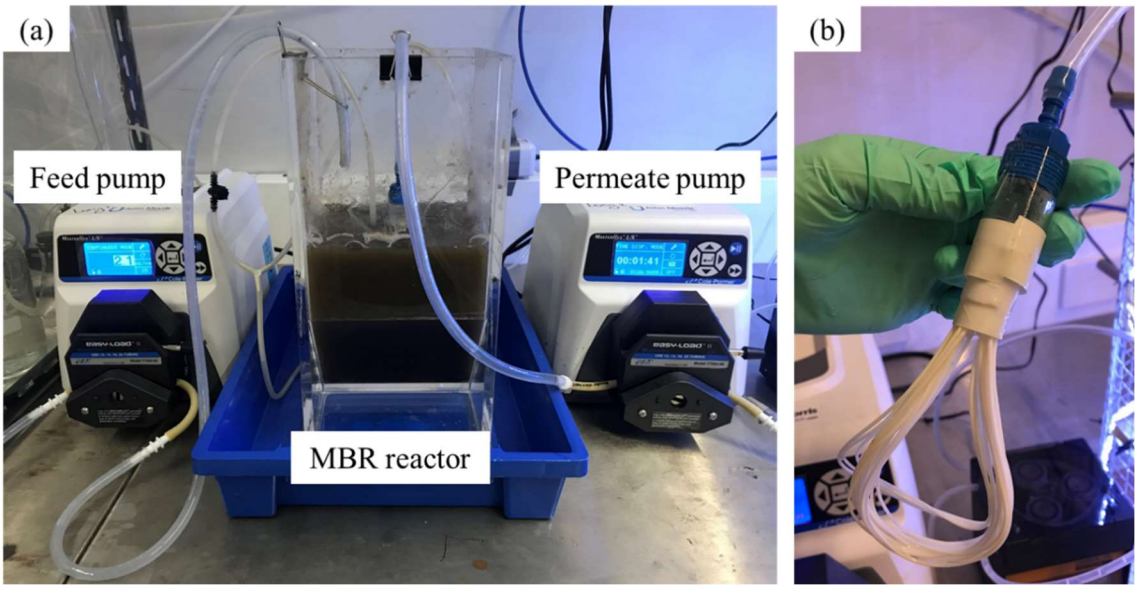


Figure 5. Laboratory-scale membrane bioreactor setup (A) and hollow-fiber membrane module (B).

### 3.2.2. Operating protocol

Activated sludge was collected from a wastewater treatment plant (New South Wales, Australia) and used as the inoculum. The MBR was fed with synthetic wastewater to ensure a consistent composition of carbon, nitrogen, and phosphorus for microbial growth. The synthetic feed has

chemical oxygen demand (COD): total nitrogen: total phosphorus of 150: 6.5: 1, which is similar to the municipal sewage. In detail, the synthetic feed solution (influent) contains the following ingredients in mg/L: glucose (600), peptone (100), urea (35), $KH_2PO_4$ (17.5), $MgSO_4$ (17.5), $FeSO_4$ (10), and sodium acetate (225) as described in previous studies (255, 256). The average total organic carbon (TOC) of the synthetic feed was 238.8 ± 17.0 mg/L. The MBR was operated at a flux of 6.25 LMH corresponding to a hydraulic retention time of 24 h. Prior to the main experimental period and biomass collection for analysis, the MBR was acclimatised under the same operating condition for one month.

The performance of the MBR was evaluated by monitoring effluent, influent, and mixed liquor twice per week. Samples were analysed for pH, DO concentration, TOC, nitrate concentration, mixed liquor suspended solids (MLSS), and mixed liquor volatile suspended solids (MLVSS). MLSS and MLVSS were measured according to the standard method 2540D. TOC was analysed using a TOC-$V_{CSH}$ analyser (Shimadzu, Japan). Nitrate concentration was measured using ion chromatography (Thermo Scientific, Australia). DO concentration of the MBR was maintained at 6.5 ± 1.3 mg/L. No sludge removal was conducted during the experimental period except for MBR performance monitoring purpose, resulting in a SRT of 265 days.

### 3.2.3. DNA extraction and quality monitoring

Duplicate samples of the inoculum were collected at the beginning of the experiment. Duplicate samples of the mixed liquor were collected at the end of the acclimatisation period (day 39), and at severe fouling stage (day 102 and day 142). Biofouling layers on the surface of static membrane (denoted as ST-BF) and membrane with permeation (denoted as PM-BF) were collected at severe fouling stage (day 142) by sonication (72 W, 43 ± 2 kHz) for 2 minutes in Milli Q water, following by centrifuge (3500 rpm, 10 minutes).

Each sample was mixed with 100% v/v ethanol (1:1 v/v) and stored at -20 ºC prior to DNA extraction. Genomic DNA extraction was carried out using DNAeasy PowerSoil Pro Kit (50) (QIAGEN) following the manual's instructions. The integrity, purity and concentration of the extracted DNA were evaluated by NanoDrop® spectrophotometer. DNA concentration of all samples was normalized to 10 ng/µl using DNase/Pyrogen-Free Water before sending to the sequencing facility.

### 3.2.4. Amplicon sequencing and bioinformatics analysis

The universal primer set Pro341F (5'-CCTACGGGNBGCASCAG-3') and Pro805R (5'-GACTACNVGGGTATCTAATCC-3') was used to amplify 16S rRNA V3 – V4 regions of the microbial community. Paired-end amplicon sequencing (2 × 300 bp) was carried out on the Illumina MiSeq platform (Australian Genome Research Facility, Melbourne, Australia).

Raw reads were imported into Quantitative Insights into Microbial Ecology (QIIME) 2 (version 2019.10) for computational analysis (257). Quality filtering, denoising (primer and read trimming), paired-end reads merging, dereplication, chimera filtering and feature clustering (≥ 97% similarity) were performed using the q2-dada2 denoise-paired plugin (258). Forward reads were truncated at position 280 and reverse reads were truncated at position 250 in the 3' end due to decrease in quality. The parameter min-fold-parent-over-abundance was set to 8 in the denoising step. Reads were mapped back to amplicon sequence variant (ASV) with a minimum identity of 97% to obtain the number of reads in each feature.

Taxonomy was assigned to features using the q2-feature-classifier (259) classify-sklearn Naïve Bayes taxonomy classifier against the SILVA database (release 132) (260-262) with a confidence of 0.7. All features were aligned with mafft [8] and used to construct phylogenetics tree with FastTree2 (263) via the q2-phylogeny align-to-tree-mafft-fasttree pipeline. Diversity metrics were estimated using q2-diversity core-metrics-phylogenetic pipeline after samples were rarefied (subsampled without replacement) to 66,500 sequences per sample.

## 3.3. Results and Discussions

### 3.3.1. Membrane bioreactor performance and fouling development under stress condition

Figure 6 shows the basic performance of MBR in three phases: acclimatisation period (day 1 – 39), stable operation (day 40 – 86), endogenous decay and severe fouling (day 87 onwards). During the acclimatisation period, as expected, the biomass growth as well as TOC and nitrate concentration in the mixed liquor and permeate showed considerable fluctuation. Nevertheless, the TOC removal efficiency was high, in the range of 97.4 – 98.7%. After the acclimatisation period, the MBR system showed stable biological treatment performance until day 86. TOC removal efficiency increased to 99.1 – 100%, biomass concentration increased steadily from around 4.3 g/L on day 39 to 7.5 g/L on day 86. MLVSS/MLSS ratio increased from 0.90 ± 0.05 to 0.94 ± 0.03, in other words, active sludge accounts for most of the solids content in the reactor.

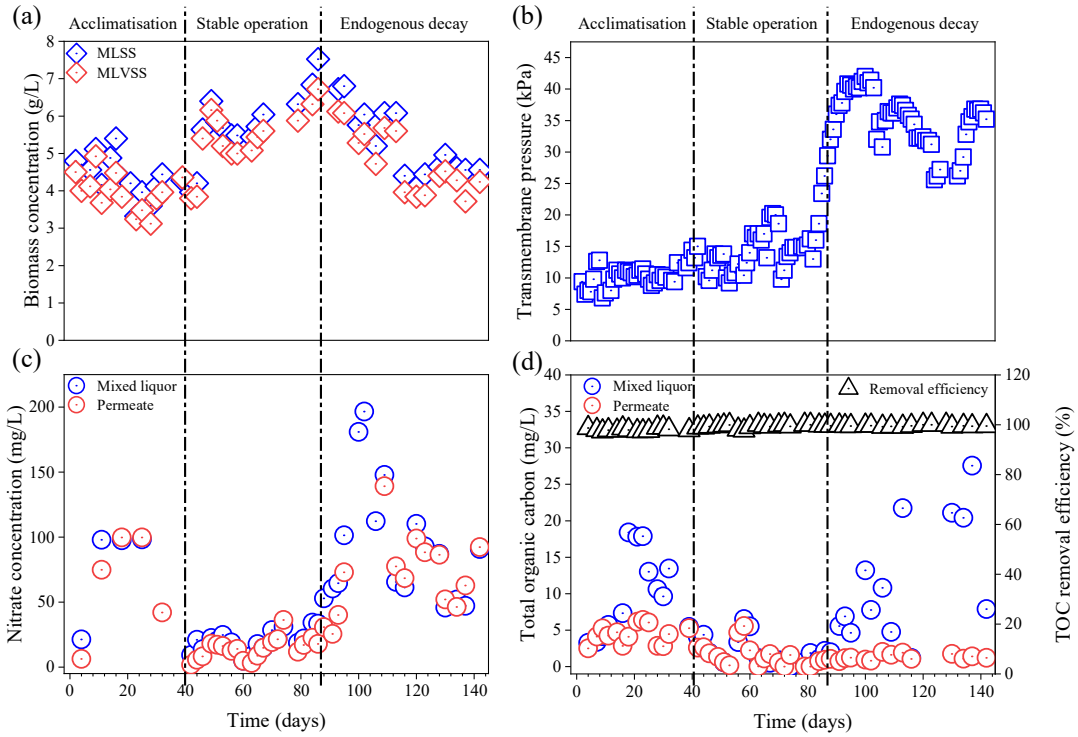


Figure 6. Biomass growth, total organic carbon concentration and removal, nitrate concentration and transmembrane pressure in the MBR during the experimental period.

In the last phase from day 87, endogenous decay resulted in loss in cell mass due to oxidation of internal storage products (Figure 6). Along with the decreased sludge concentration, this process released a large amount of dissolved organic matter (indicated by rapid rise in TOC concentration in the mixed liquor – Figure 6D), soluble nitrogen (Figure 6C) probably in the form of ammonia as presented in Equation 1.

$$C_5H_7O_2N + 5O_2 \rightarrow 5CO_2 + NH_3 + 2H_2O \qquad \text{(Eq. 1)}$$

Stress conditions including nutritional stress, extreme temperatures and oxidative stress are common factors to trigger microbial endogenous decay (264, 265). Since sludge withdrawal was not conducted except for performance monitoring, the MBR operated in a high SRT of 265 days (high sludge age) and with a continuously decreasing F/M ratio (from 0.15 on day 4 to 0.09 gBOD/gMLVSS.d on day 86), which can result in decreased sludge production as identified in a previous study (266). Thus, nutritional stress is likely to be the cause of endogenous decay in this MBR. At the same time with endogenous decay, TMP increased exponentially from 18.6 to 40.8 kPa in 10 days and reached 42 kPa on day 100 (Figure 6B), suggesting that membrane fouling was related to endogenous decay and its successive events e.g. rise in TOC and changes in microbial community (Section 3.3.2).

### 3.3.2. Microbial succession in the mixed liquor after endogenous decay

Table 5. Changes in number of observed species and evenness (Shannon index). ST-BF: biofouling layer on static membrane, PM-BF: biofouling layer on membrane with permeation.

| Sample | Number of observed species | Evenness (Shannon index) |
|---|---|---|
| Inoculum | 1588.5 ± 67.5 | 8.25 ± 0.04 |
| Day 39 (after acclimatisation) | 1191 | 7.65 |
| Day 102 (after endogenous decay) | 798.5 ± 20.5 | 3.39 ± 0.07 |
| Day 142 | 802.5 ± 26.5 | 4.15 ± 0.13 |
| ST-BF | 778 | 3.64 |
| PM-BF | 654 | 3.21 |

Bioinformatics analysis of MBR mixed liquor revealed significant shift in both microbial diversity and composition, especially after endogenous decay. The decrease in diversity of the mixed liquor compared to the inoculum (25% of number of species observed and 7.2% of evenness) during the acclimatisation phase (day 0 to 39) could be attributed to the adaptation of microbes to the new environmental conditions (Table 5). Endogenous decay resulted in another sharp decrease of diversity (day 102), with species richness and evenness 33 and 55.7% lower than day 39. The change in species evenness (Shannon index) caused by endogenous decay was statistically significant (Student t-test, p-value 0.01), indicating the predominance of a few microbial species in the mixed liquor. Both biofouling layers on the surface of static and permeate membrane showed reduced number of species and evenness compared to mixed liquor (Table 5). The number of observed species and evenness in the permeate module fouling layer were slightly lower than those of the static module fouling layer, indicating the impact of permeation drag.

The most dominant order in the mixed liquor after endogenous decay was *Thiotrichales* (Figure 7), accounting for 66.1 ± 3.6 % of the mixed liquor community. *Thiotrichales* are filamentous bacteria involved in activated sludge bulking (267). Besides *Thiotrichales*, other filamentous bacteria including *Saccharibacteria* and *Caldilineales* were also detected in the community (268). It has been reported that long SRT and low F/M induce the growth of filamentous microorganisms (269, 270). Sludge that has been retained too long can become septic, lose its activity, and consequently can deplete the necessary DO in the reactor, which favours the growth of filamentous bacteria (271). In addition, the nutrient compounds in the simulated feed are readily biodegradable and accessible to filamentous bacteria, due to their morphology.

Filamentous bacteria are the backbones within sludge flocs and play pivotal roles in floc formation and floc stability by assisting the aggregation of sludge and colloids (272, 273).

Previous works have reported that the presence of a small quantity of filamentous microorganisms can increase porosity of the sludge and lower sludge adhesion on the membrane surface (274, 275). For example, *Thiotrichales* was presented in the mixed liquor after acclimatisation (day 39) at 13.1%, but did not lead to any membrane fouling effect. Nevertheless, the predominance of *Thiotrichales* after endogenous decay (relative abundance > 60%) indicates excessive growth of filamentous bacteria, which can have detrimental effects on membrane permeation. Bulking sludge showed two to three times higher cake layer resistance than normal sludge (252). In addition, the bulking flocs with irregular shape can easily accumulate on the membrane surface and intertwisted on the membrane fibers due to their irregular morphology (252, 253). The fixing action of filamentous bacteria results in more foulants adhering to membrane and enhance their clinging intensity, which worsen the membrane permeability seriously (252). Sludge bulking also contribute to higher extracellular polymeric substance (EPS) and soluble microbial product (SMP) concentration (237, 253), and variation in the EPS (higher PN/PS ratio), leading to an increase in sludge hydrophobicity and surface negative charge (276) and aggravating membrane fouling.

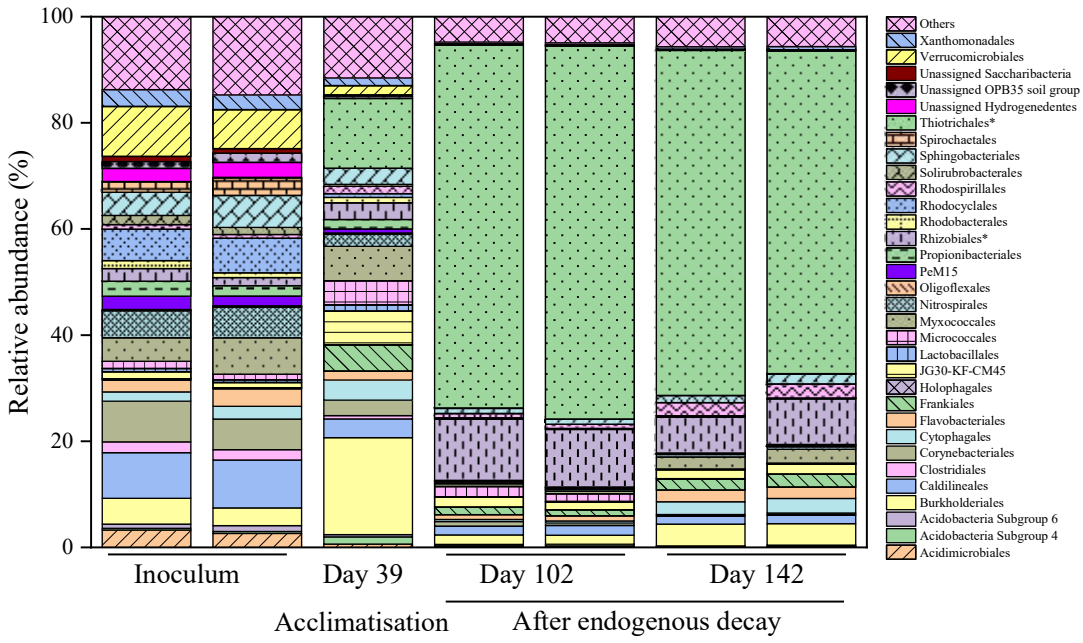


Figure 7. Changes in microbial composition during different phases of MBR operation.

The relative abundance of *Thiotrichales* in the mixed liquor significantly correlated with TMP (Pearson R = 0.996, p-value <0.001), indicating their possible contribution to membrane fouling. Results from this study are consistent with previous reports that exponential increase in TMP due to uncontrolled growth of filamentous bacteria in MBR (273, 277), and Meng et al. (252, 253) observation that membrane fouling was most serious under the sludge bulking condition.

*Rhizobiales* was the second most dominant order in the community (relative abundance of 9.4 ± 1.9%). The high abundance of *Rhizobiales* could be attributed to its involvement in nitrification process (278, 279) of the ammonia release from endogenous decay. Members of *Rhizobiales* have also been reported to produce polar adhesive holdfasts and fimbrae (280-282). Other dominant orders (relative abundance > 1%) such as *Burkholderiales*, *Rhodospirillales* and *Myxococcales*, *Flavobacteriales* can produce EPS, colloids, and biosurfactants which increase their ability to attach to the membrane surfaces (100, 112, 283-285).

### 3.3.3. Effects of endogenous decay and sludge bulking on biofouling layer

As noted in section 3.3.2, diversity indices of the permeation module fouling layer (PM-BF) were slightly lower than those of the static module fouling layer (ST-BF). Dominant microbial orders of the biofouling layers were similar with the mixed liquor, with the static module fouling layer (ST-BF) possessing higher similarity to mixed liquor than the permeation module fouling layer (PM-BF) (Figure 8). In the absence of permeation drag (ST-BF), the biofouling layer is formed mostly by adhesion and gravity deposition. Thus, it is expected that composition of the static module biofouling layer shows more similarly to the mixed liquor than the permeation module fouling layer. The most dominant order was *Thiotrichales*, accounted for 69.8 and 75.3% in the static and permeate module fouling layer, respectively. Several microbial taxa show increased relative abundance in the PM-BF compared to the mixed liquor, including *Corynebacteriales* (6.83 folds), *Oligoflexales* (5.64 folds) and *Holophagales* (27.3 folds). Both *Corynebacteriales* and *Oligoflexales* order consist of filamentous bacteria, e.g. *Mycobacterium* and *Gordonia*, explaining for their higher abundance. Meanwhile, *Holophagales* is an anaerobic taxon that may develop in the inner side of the thick biofouling layer where oxygen is depleted. It has been established that the overgrowth of filamentous bacteria in sludge suspension could result in the formation of a thick (~200 μm) and loose cake layer, compared to a compact and thin (~20 μm) fouling layer at a small quantity of filamentous bacteria (252, 286).

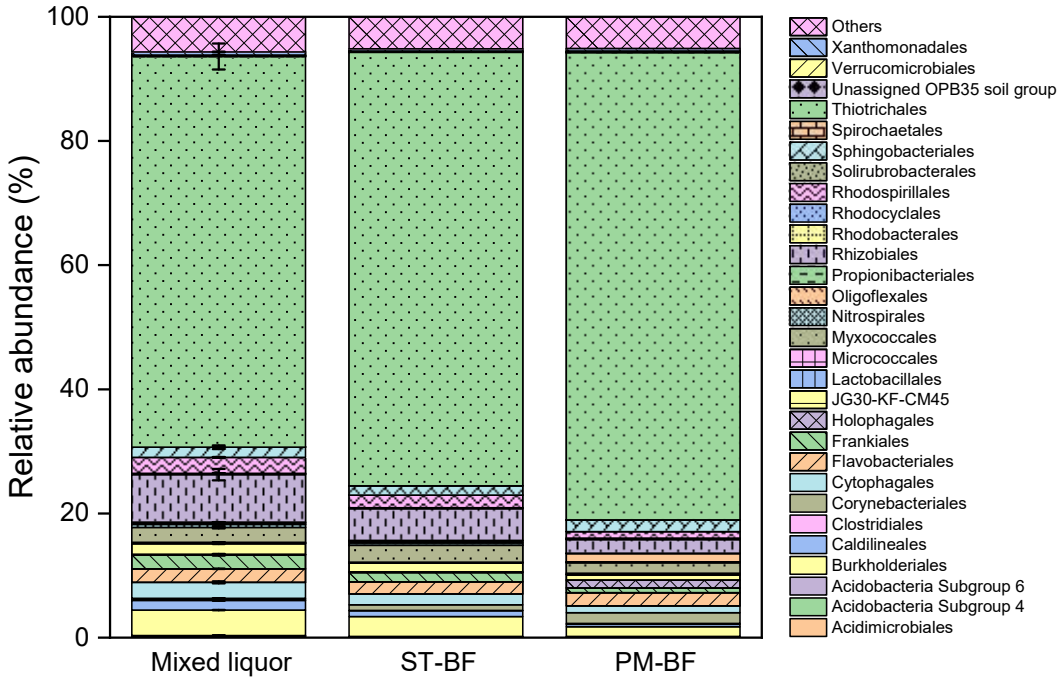


Figure 8. Microbial composition of mixed liquor, biofouling layer on static membrane (ST-BF) and biofouling layer on membrane with permeation (PM-BF).

The spike in amount of foulants released by endogenous decay together with the overgrowth of filamentous bacteria inevitably led to severe membrane fouling, despite the sub-critical flux condition. The low drag force provided by sub-critical flux could not avoid the attachment of filamentous bacteria on the membrane surface. Thus, it is necessary to prevent endogenous decay and excessive growth of filamentous bacteria in order to mitigate MBR fouling while operating at a sub-critical flux condition, through adjustments of operating parameters such as SRT, F/M and DO concentration. SRT could be adjusted by manually change the sludge wasting rate based on the F/M ratio or MLSS concentration. In this study, endogenous decay occurred at low F/M ratio (below 0.1 gBOD/gMLVSS.d). These results suggest the need for regular removal of activated sludge to maintain F/M higher than this threshold of 0.1 gBOD/gMLVSS.d. The results also highlight the role of filamentous bacteria overgrowth as the underlying cause of membrane fouling under sub-critical flux condition. Several strategies to control the proliferation of filamentous bacteria have also been suggested. Banti et al. (273) successfully controlled filamentous bacteria at a medium level using a step-aerating MBR, leading to low TMP values ≤ 2 kPa for more than 90 days of operation. Implementing successive anaerobic and aerobic reactors can also limit/suppress *Thiothrix*-caused bulking in dairy wastewater treatment plants (287). In addition to optimizing the operating parameters, filamentous bacteria can be controlled by chlorination or biocide addition (288). Henriet et al. (67) investigated several strategies to control filamentous bulking caused by *Thiothrix* species in full-scale wastewater treatment plants over

1.5 years. They suggested that polyaluminium chloride addition and VFAs reduction could not permanently solve the fouling problem, while periodic starvation to avoid endogenous decay could be used to reduce fouling at high sludge age.

## 3.4. Conclusion

Under the sub-critical flux condition, nutrient deficiency due to high sludge age and low F/M (decreased from 0.15 to 0.09 gBOD/gMLVSS.d) led to the occurrence of endogenous decay. Once endogenous decay occured, severe membrane fouling can occur even at a sub-critical flux. Membrane fouling during endogenous decay was triggered by the release of dissolved organic matter and cell debris as well as the excessive growth of filamentous bacteria, e.g. *Thiotrichales*. The relative abundance of *Thiotrichales* was positively correlated with TMP increase (Pearson R = 0.996, p-value <0.001). Other dominant orders in the mixed liquor after endogenous decay such as *Rhizobiales*, *Burkholderiales*, *Rhodospirillales* and *Myxococcales*, *Flavobacteriales* can produce EPS and aggravate membrane fouling. Fouling layers possess a highly similar microbial composition with the mixed liquor, with static module showing higher similarity with mixed liquor than permeate module. A few filamentous microbial orders, e.g. *Corynebacteriales* and *Oligoflexales* showing increased relative abundance by 6.83 and 5.64 folds in the permeate module compared to the mixed liquor, respectively.

# Chapter 4. DIFFERENCE IN MICROBIAL COMPOSITION AND INTERSPECIES INTERACTIONS BETWEEN FOULING LAYER AND MIXED LIQUOR AT HIGH-FLUX CONDITION

This chapter has been published as the following journal article.

Nguyen AQ, Nguyen LN, Xu Z, Luo W, Nghiem LD. New insights to the difference in microbial composition and interspecies interactions between fouling layer and mixed liquor in a membrane bioreactor. Journal of Membrane Science. 2022;643:120034.

**Summary:** This work examined the fouling-associated microbial community in a carefully controlled laboratory-scale MBR at different fouling stages. In agreement with the literature, fouling severity was positively correlated with bound polysaccharides and protein content (indicators) in the mixed liquor. Unweighted pair group method with arithmetic mean (UPGMA) clustering analysis with different indices indicated that the biofouling layer (biofilm) and mixed liquor possessed highly similar microbial identity, important differences between the two communities' structures were observed. This is the first comprehensive study to apply differential abundance analysis (ANCOM) to identify microbial taxa driven the divergence in microbial structure, including *Victivallales*, *Coxiellales*, unassigned *Microgenomatia* and *Blastocatellia* 11-24 (all presented at <1% abundance). Network analysis also identified *Victivallales* and *Blastocatellia* 11-24 among the few key players in the mixed liquor and biofilm community, respectively. Despite their low abundances, key players in both communities positively correlated (Pearson's correlation coefficient >0.6) with fouling indicators, confirming their important contributions to fouling propensity. The biofilm community exhibited a more complex structure with higher level of inter-species interaction and prevalence of positive connections (74.6%) compared to the mixed liquor community (42.2%), reflecting higher stability and synergy between microbial taxa in the biofilm. Results from this comprehensive investigation can support the development of new fouling control strategies.

## 4.1. Introduction

Membrane bioreactor (MBR) has many advantages over the conventional activated sludge (CAS) process. These include a smaller physical footprint and better effluent quality suitable for water reuse applications (289). Globally, there are 73 large MBR plants for municipal wastewater with a designed capacity of over 100 ML/d currently in operation or the construction phase (themrbsite.com). There is a much larger number of small and medium MBR plants for municipal and industrial wastewater treatment around the world. Recent scientific progress in membrane fabrication and module design, system integration, and process automation has significantly reduced the cost of wastewater treatment by MBR technology. Thus, there has been a greater

focus on membrane fouling which is inherent in any MBR plant and has become a major hurdle for further improvement in energy efficiency and cost-saving (232).

Numerous techniques have been developed and applied to control fouling during MBR operation (232, 290). They include regular backwashing, membrane cleaning by biocide and oxidising reagents, such as hypochlorite, and modification of membranes and their modules. These techniques are based on chemical and physical processes to remote and disrupt the formation of biofilm on the membrane surface. While they are effective, they cannot completely prevent biofouling regrowth given the direct contact of membrane with microbe-abundant activated sludge (i.e. mixed liquor in MBR). They must be applied frequently, resulting in additional cost and gradual deterioration of membrane performance.

MBR is a biological membrane separation process. As such, biological techniques to control MBR fouling have shown very promising results. Nevertheless, these biological techniques have not yet been applied widely in full-scale operation (74). In 2009, Lee and co-workers (291) demonstrated for the first time a relationship between microbial quorum sensing activities (i.e. the presence of the N-acyl homoserine lactone quorum signalling molecule) and biofilm formation on the membrane surface. Their work has triggered many subsequent investigations to develop biological techniques to control membrane fouling during MBR operation (292, 293). Bacteriophage to inhibit specific bacteria in the biofilm is another promising approach to control biofouling (294). It is essential for these biological techniques to selectively target the biofilm on the membrane surface while maintaining the microbial community in the mixed liquor so that biological performance of the MBR is unaffected. Thus, the key is to understand the difference in microbial composition and inter-species interactions between the biofilm (fouling layer) and mixed liquor.

Recent progress in culture-independent molecular techniques has paved the way for in-depth investigation of the microbial community associated with fouling on the membrane surface in comparison to the mixed liquor (295). Early works on this topic have focused on characterizing the microbial diversity and composition in the fouling layer and mixed liquor (108, 296-298); however, inter-species interactions in each community were rarely examined (100, 116, 118). There is a consensus that the biofilm community differs from the mixed liquor community (100, 298, 299), although the extent of this difference has not been systematically and quantitatively examined. In addition, findings in the literature have been rather inconsistent. For example, Gao et al., (300) reported higher microbial richness and abundance in the bio-cake than that of the bulk sludge. On the other hand, Jo et al. (100) measured biofilm diversity and observed no significant difference from those of activated sludge. Luo et al. (298) reported that the biofilm microbial composition in laboratory-scale MBRs was indistinguishable from that of the mixed liquor during

the initial stage of operation but significantly diverged from the sludge over time and ultimately showed a unique biofilm profile. By contrast, Xu et al. (116) observed a greater similarity between the bio-cake and the bulk sludge as the fouling developed.

On a particular note, previous works often assumed that fouling-associated species were highly abundant microbial taxa or taxa that showed higher relative abundance in the biofilm than the mixed liquor (298, 301). This assumption is problematic because dominant taxa in the biofilm are also abundant in the mixed liquor since the mixed liquor is a major source of inoculum for the biofilm (299). Thus, their high abundances do not necessarily affirm them as key players in the biofilm community. Through network and biomarker analyses, more recent studies have suggested that low-abundance taxa, rather than high-abundance ones, play critical roles in fouling development and biofilm formation (113, 116, 302, 303). Furthermore, the difference between the biofilm and mixed liquor community based on relative abundance may not reflect the actual difference due to the caveat of relative data. Relative abundances are absolute abundances of different species normalized to the total number of sequences detected in the sample. Thus, the change in the absolute abundance of one microbial species can alter the relative abundance of all other species.

Several bioinformatics tools/analyses have been employed for microbial community characterization in MBRs. Alpha diversity indices describe the number of species in a community (i.e. Chao1 index) and the evenness between their proportions in the community (i.e. Shannon index) (116), while coordination analyses such as principal coordinate analysis (PcoA) and non-metric multidimensional scaling based on beta diversity indices (i.e. unweighted UniFrac and Bray-Curtis) show the similarity/dissimilarity between different communities (112, 299). Although less popular than coordination analyses, clustering analyses, including UPGMA, can also depict the similarity/dissimilarity between communities and clearly show the pairwise similarities between samples (100, 109, 304). It is worth noting that the selection of beta diversity index for analysis can influence the extent of dissimilarity between microbial communities since different indices were calculated differently. To address these shortcomings, in recent years, researchers have begun to use network-based techniques for deciphering complex microbial interaction patterns under dynamic conditions such as the composting of organic waste (305) or to compare the fouling evolution between aerobic and anaerobic MBR (303). These techniques may also be useful for delineating the difference in microbial composition and inter-species interactions between the fouling layer and mixed liquor in the MBR.

This study addresses key research gaps identified above, such as the lack of attention on the roles of inter-species interactions in fouling, and the impact of the bioinformatics tools and index used for comparison of different microbial communities. This study aims to delineate the distinction

between biofouling community (biofilm) and suspended community (mixed liquor) and identify the role of individual microbial taxa in fouling development. Comparison in terms of microbial identity profiles was performed using UPGMA clustering analysis was conducted based on unweighted UniFrac distance metric. Differential abundance analysis (ANCOM) was used to specifically identify species with true different abundance over-represented in each community. Phylogenetic molecular ecological network was constructed for both communities to deduce species-species ecological interactions and the role of high- and low-abundance microbial taxa. Results from this study contribute to a more comprehensive understanding the biofouling microbial community structure to address the problem of membrane fouling in MBR operation.

## 4.2. Materials and Methods

### 4.2.1. Laboratory-scale membrane bioreactor system setup

A laboratory-scale aerobic MBR system was used in this study. The MBR was equipped with 6 L glass reactor, a hollow fibre polyvinylidene difluoride (PVDF) membrane module (Mitsubishi Rayon, Japan), a water bath, two peristaltic pumps, a chiller, a pressure sensor and an air pump. The membrane module had a nominal pore size of 0.04 μm and an effective surface area of 0.073 $m^2$. The pressure sensor was a high-resolution pressure sensor (±0.1 kPa, John Morris Group, Australia), which was installed between the membrane module and the permeate pump for continuous monitoring of the transmembrane pressure (TMP). The chiller (Thermoline Australia) was equipped with a stainless-steel heat-exchanging coil. Two peristaltic pumps (Masterflex L/S, USA) were used for feeding and permeate extraction. The reactor's working volume was maintained at 6.0 L. The air pump (AquaOne, Australia) aerated the reactor at an air flowrate of 400 mL/min via a diffuser at the bottom of the reactor.

### 4.2.2. Operating protocol

Activated sludge was transferred from another MBR system (with two identical membrane modules as used in this study). This MBR system was under stable operation for over 2 months and fed with synthetic influent similar to that in this study. Synthetic feed was used to provide carbon, nitrogen, and phosphorus for microbial growth in the MBR. The synthetic feed has chemical oxygen demand (COD): total nitrogen: total phosphorus = 150: 6.5: 1, which is similar to municipal sewage. In details, the synthetic feed solution (influent) contains mg per litre: glucose (600), peptone (100), urea (35), $KH_2PO_4$ (17.5), $MgSO_4$ (17.5), $FeSO_4$ (10), and sodium acetate (225) as described in previous studies (256, 306).

During the acclimatisation period, the MBR was operated at different water fluxes in the range from 11 to 15 LMH to determine a suitable value for a reproducible and representative fouling profile. The membrane module was operated with 9 min "suction" and 1 min "relaxation". TMP profiles of these preliminary fouling runs are shown in Figure 9. The critical flux was 11 LMH.

At flux higher than 11 LMH, the fouling onset was observed within 1-2 days. Based on these preliminary fouling runs, water flux value of 10 LMH was used in this study to achieve reproducible and representative fouling under sub-critical flux condition. The thresholds for three fouling stages were defined as: no-fouling (TMP ≤ 10 kPa) – TMP increases slightly and at slow rate, mild fouling (10 < TMP ≤ 30 kPa) – TMP increases exponentially, and severe fouling (TMP > 30 kPa) – TMP increases gradually and tends to reach a plateau.

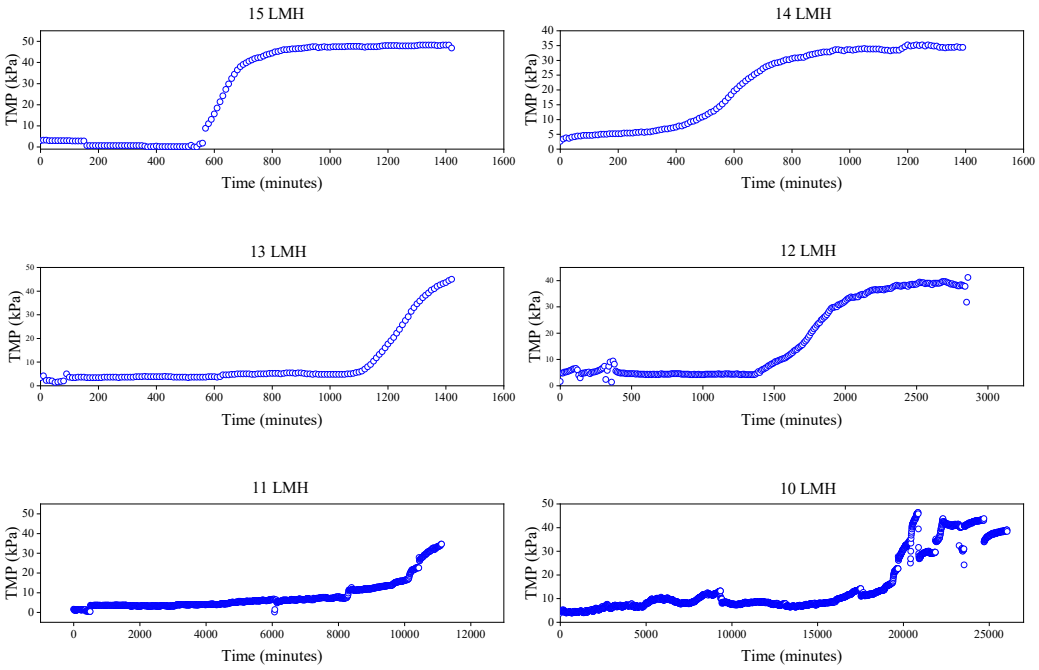


Figure 9. Transmembrane pressure profile of the MBR during preliminary fouling runs in comparison with first biomass collection phases.

In the biomass collection period, three repetitive phases were conducted to capture sufficient DNA samples of mixed liquor and biofilm at different fouling stages. The biomass concentration at the beginning of each fouling cycle was set at 12.4 ± 0.1 g/L. When the TMP reached a threshold, the MBR operation was paused and the membrane module was removed from the reactor for DNA sample collection. At the end of each phase, the membrane module was removed for chemical cleaning. The chemical cleaning protocol was able to fully restore to the membrane permeability to as new condition. Sludge withdrawal was conducted to reset the mixed liquor suspended solids (MLSS) concentration to around 12. 4 ± 0.1 g/L prior to the next phase.

The performance of the MBR was regularly monitored by sampling effluent, influent, and mixed liquor twice per week. Monitored parameters included pH, dissolved oxygen (DO) concentration in the mixed liquor, effluent turbidity, total organic carbon (TOC), MLSS, mixed liquor volatile suspended solids (MLVSS), extracellular polymeric substance (EPS), soluble microbial product

(SMP). MLSS and MLVSS were measured gravimetrically following the method 2540D (307). TOC was analysed using a TOC-$V_{CSH}$ analyser (Shimadzu, Japan). Nitrate concentration was measured using ion chromatography (Thermo Scientific, Australia). The temperature and DO concentration of the MBR was maintained at 20.0 ± 0.1°C and above 3 mg/L, respectively.

### 4.2.3. Extraction of extracellular polymeric substances and soluble microbial products

EPS and SMP concentrations in mixed liquor samples were measured according to the thermal extraction method (308). In brief, 25 mL of mixed liquor sample was centrifuged in a 50 mL tube at 1500×g and 4 ºC for 20 min to collect SMP fraction. The residual sludge was resuspended with 50 mL of 0.9% NaCl solution at room temperature by a vortex mixer for 3 min. The mixture was transferred to an enclosed flask and heated at 80 ºC for 1 h to release bound polysaccharide and bound protein (EPS). Then, the mixture was cooled to room temperature before centrifugation at 1500×g and 4 ºC for 20 min. The supernatant was collected for further analysis and denoted as the EPS fraction. The heating method showed high extraction efficiency compared to other physical extraction methods (62 mg EPS/g VSS, yield 4%) (309).

The phenol–sulfuric acid method (310) was applied for determination of polysaccharides with a series of glucose solutions (0.5 – 50 mg/L, calibration curve $R^2 = 0.97$) as the standard. Protein contents in EPS and SMP fractions were determined by an UV/VIS spectrophotometer (DR5000, HACH) following the modified Lowry method using Total Protein Kit, Micro Lowry, Peterson′s Modification kit (Sigma-Aldrich) with a series of bovine serum albumin solution as the standard (0.5 – 15 mg/L, calibration curve $R^2 = 0.99$).

### 4.2.4. DNA extraction and quality monitoring

As mentioned previously, duplicate samples of the mixed liquor were collected at the beginning of each phase and at three fouling stages (based on TMP). This resulted in 14 DNA samples. The samples from mixed liquor were labelled as MLx.x.x with ML is mixed liquor; first digit is fouling phase number; second digit is fouling stage; third digit is replication number. For example, ML1.3.1 is the mixed liquor sample at fouling phase 1, fouling stage 3 and replication 1.

Duplicate samples of the membrane biofilm were collected at mild- and severe-fouling stages with minor modifications in each phase. In phase 1, no sample collection was conducted under mild fouling condition in phase 1 to maintain the natural progress of biofilm development. In phase 2, only part of the biofilm was collected from the membrane surface under mild fouling condition to minimalize the impact of sampling on biofilm development. Samples were taken from multiple positions on the membrane surface. In phase 3, the entire biofilm was collected under mild fouling condition thus the phase was terminated and no sample collection was conducted under severe fouling condition. This results in slightly different operational periods of each phase: phase 1 (day 14 – 33), phase 2 (day 34 – 49), and phase 3 (day 50 – 56). The biofilm

(a mixture of cake layer and gel layer deposited on the membrane surface) was scrapped off the membrane surface using cotton swabs prior to membrane chemical cleaning. This resulted in 7 DNA samples. The samples from membrane biofilm were labelled as BFx.x.x with BF: biofilm; first digit is fouling phase number; second digit is fouling stage; third digit is replication number. For example, BF1.3.1 is the biofilm sample at fouling phase 1, fouling stage 3 and replication 1. Details of samples collection regime in this study is shown in Figure 11.

Samples were mixed with ethanol (1:1 v/v) and stored at -20 $^{o}$C prior to DNA extraction. Genomic DNA extraction was carried out using QIAamp DNA Stool Mini Kit (QIAGEN) following the manual's instructions. An additional bead-beating step was performed at the beginning of the extraction to enhance DNA yield. The integrity, purity and concentration of the extracted DNA were evaluated by NanoDrop® spectrophotometer. DNA concentration of all samples was normalized to 20 ng/µl using DNase/Pyrogen-Free Water before sending to the sequencing facility.

#### 4.2.5. Amplicon sequencing and bioinformatics analysis

The universal primer set Pro341F (5'-CCTAYGGGRBGCASCAG-3') and Pro806R (5'-GGACTACNNGGGTATCTAAT-3') was used to amplify 16S rRNA V3 – V4 regions of the microbial community. Paired-end amplicon sequencing (2 × 300 bp) was carried out on the Illumina MiSeq platform (UTS Next Generation Sequencing Facility, Sydney, Australia). Raw sequence data were generated with the Illumina *bcl2fastq* pipeline (version 2.20.0.422). All sequencing data in this study are available at the Sequence Read Archive (accession number: PRJNA752525) in the National Center for Biotechnology Information.

Raw reads were imported into Quantitative Insights into Microbial Ecology (QIIME) 2 (version 2020.11.1) for computational analysis (257). Quality filtering, denoising (primer and read trimming), paired-end reads merging, dereplication, chimera filtering and feature clustering (≥ 97% similarity) were performed using the q2-dada2 denoise-paired plugin (258). Forward reads were truncated at position 280 and reverse reads were truncated at position 250 in the 3' end due to decrease in quality. The parameter *min-fold-parent-over-abundance* was set to 4 in the denoising step. Reads were mapped back to amplicon sequence variant (ASV) with a minimum identity of 97% to obtain the number of reads in each feature.

Taxonomy was assigned to features using the q2-feature-classifier (259) classify-sklearn Naïve Bayes taxonomy classifier against the SILVA database (release 132) (260-262) with a confidence of 0.7. All features were aligned with mafft [8] and used to construct phylogenetics tree with FastTree2 (263) via the q2-phylogeny align-to-tree-mafft-fasttree pipeline. Phylogenetic tree was visualized using FigTree (version 1.4.4). Beta diversity metrics (Bray-Curtis dissimilarity) were estimated using q2-diversity core-metrics-phylogenetic pipeline after

samples were rarefied (subsampled without replacement) to 25,000 sequences per sample. 2D PcoA was plotted using Bray-Curtis distance matrix. Statistical analyses were conducted using QIIME2 to test the difference between the mixed liquor and biofilm communities structure (PERMANOVA test), and identify microbial taxa with differential abundance (analysis of composition of microbiomes - ANCOM) (311). Results from ANCOM analysis were visualized using RStudio (version 3.6.1).

#### 4.2.6. Network construction and analysis

The Random Matrix Theory (RMT) based molecular ecological network analysis (MENA) was employed to construct modular networks of microbial taxa in mixed liquor and biofilm at order level (312). Network analysis can provide insights into microbial co-occurrence patterns in the community, keystone species and interactions between community members, rather than the simple species richness and abundance. Only taxa detected in at least 4 samples were included in the analysis. Network construction procedures followed the developer's recommendations on the online pipeline, with a correlation cut-off of 0.8 for both mixed liquor and biofilm networks. Networks were constructed based on Pearson's correlation between microbial orders, and the cut-off for network construction was selected based on Chi-square test on Poisson distribution. Networks were modularized using the greedy modularity optimization method. Pearson's correlations between microbial taxa and environmental traits (EPS and SMP concentration) were also determined using MENA pipeline. Network visualization was carried out using Cytoscape (version 3.8.2) (313). Among-module and within-module connectivity plot was constructed in RStudio (version 3.6.1).

### 4.3. Results and Discussions

#### 4.3.1. Membrane bioreactor performance and fouling development

The MBR system showed stable biological treatment performance and long-term flux profile (Figure 10). High TOC removal (96.3 – 99.1%) was achieved during the experimental period. The average effluent TOC concentration was 3.8 ± 1.6 mg/L. Stable biomass growth was also observed, with biomass concentration (MLSS) increased steadily from around 12 g/L to 18 g/L in 15 days. MLVSS/MLSS ratio was above 0.8 throughout the experimental period, indicating high biomass quality.

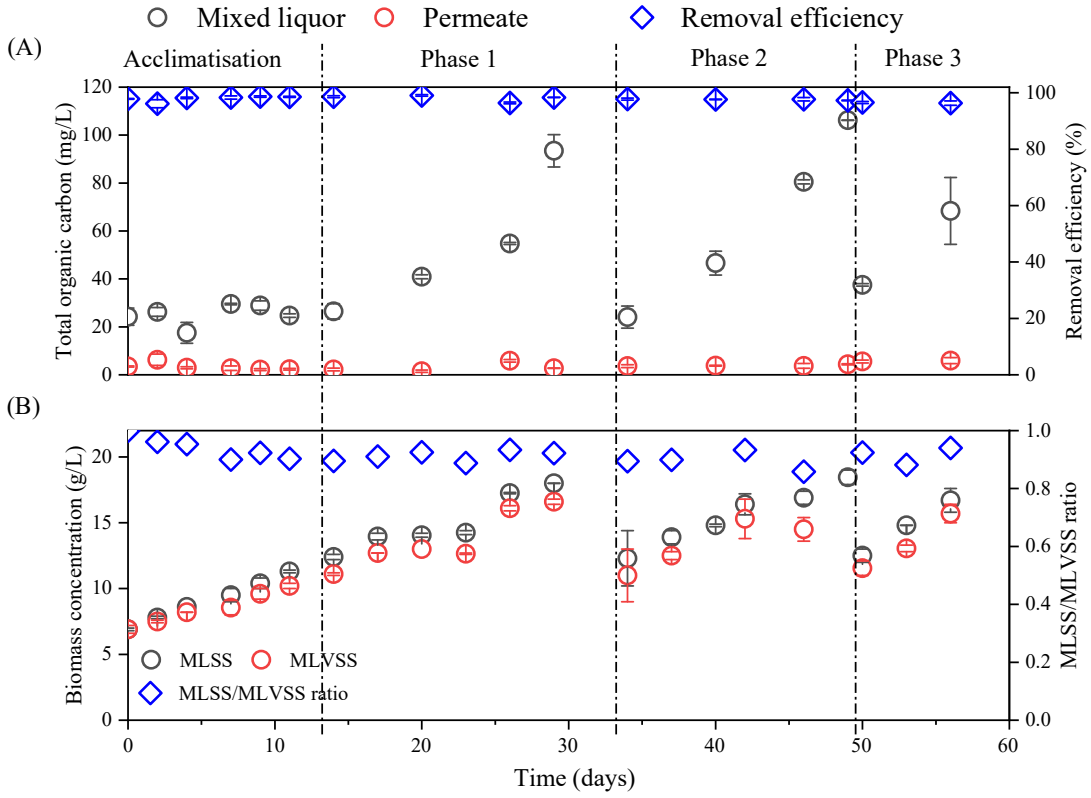


Figure 10. Total organic carbon concentration and removal efficiency (A) and biomass concentration (B) during the experiment. The error bar represents the standard deviation from duplicate samples.

The TMP profiles of individual fouling phases progressed with the operation times (Figure 11). At the beginning of each fouling phase, TMP gradually increased from 5 to 10 kPa. Once the TMP reached 10 kPa, it increased rapidly to over 30 kPa within 4 days (TMP jump). At TMP higher than 30 kPa, the rate of TMP increase was even higher. Thus, for further analysis, membrane fouling was categorised to three stages: (i) no fouling (TMP <10 kPa), (ii) mild fouling (TMP of 10 to 30 kPa), and severe fouling (TMP >30 kPa). Severe fouling condition was associated with high MLSS content in the reactor (Pearson's correlation R = 0.79, p-value < 0.05). The MLSS content was 18 g/L when severe fouling (TMP > 30 kPa) was observed. However, while the increase in MLSS content over time was gradual, the increase in TMP was exponential (Figure 11).

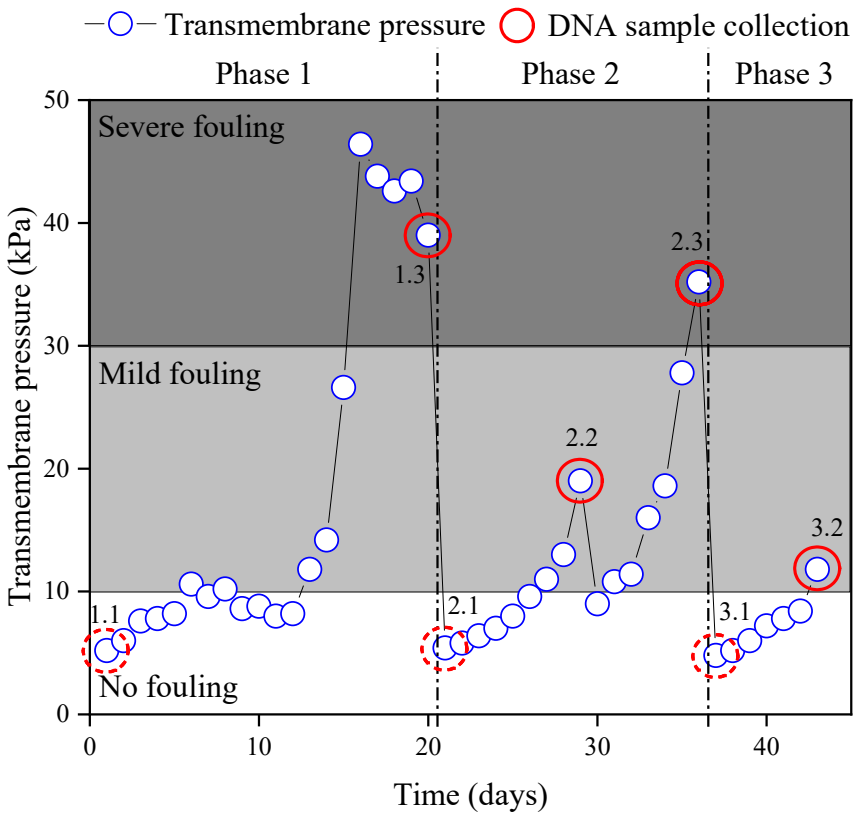


Figure 11. Fouling profile in the membrane bioreactor during the experiment. Each DNA sampling point is marked by a circle and a number. Dashed circles represent the collection of mixed liquor samples only, rounded circles represent the collection of both mixed liquor and biofilm samples. The first digit is the fouling phase number and the second digit is the fouling stage.

There is a correlation between fouling severity and EPS concentration in mixed liquor samples at each fouling phase (Figure 12A&B). EPS and SMP are biopolymers produced by microbial metabolism. Thus, higher microbial activity results in higher release of EPS and SMP. Both EPS and SMP primarily consist of polysaccharides and proteins (314). The concentration of bound polysaccharides increased proportionally from no fouling to mild fouling and was highest at the severe fouling stage. Similarly, bound protein concentration increased with the three corresponding fouling stages (Figure 12B). This phenomenon can also be observed while normalized bound polysaccharides and proteins to the biomass concentration. No clear relationship was observed between fouling and SMP content (i.e. soluble polysaccharides and protein concentration) during the experimental period (Figure 12C&D).

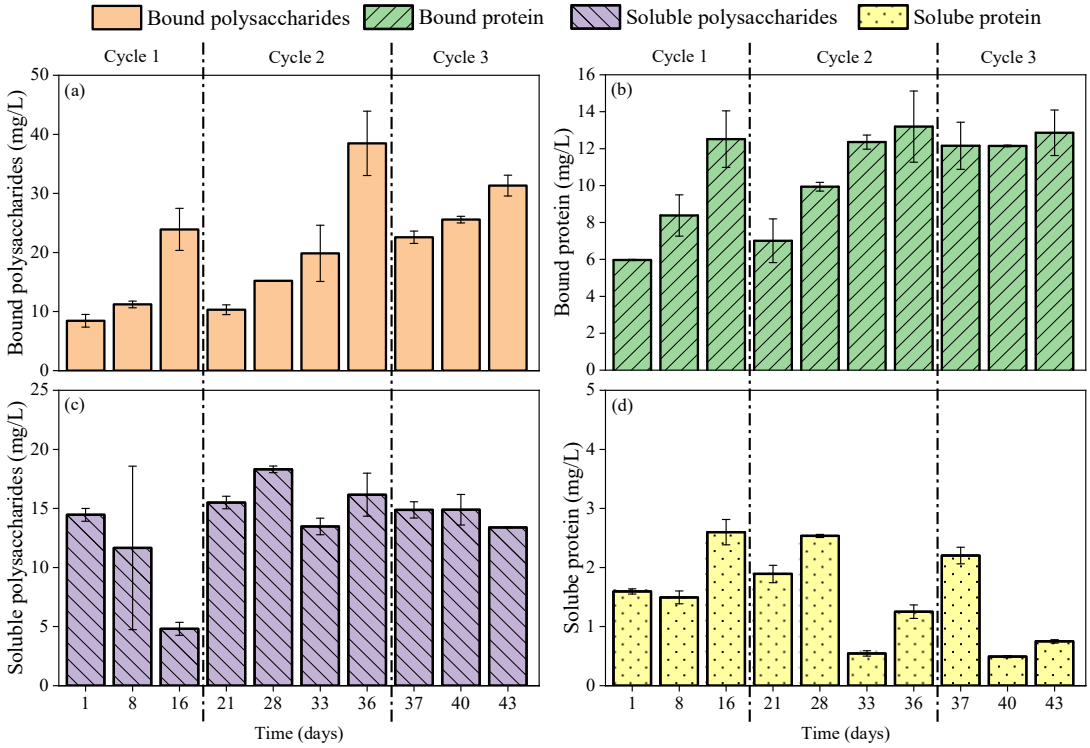


Figure 12. Extracellular polymeric substances (EPS) and soluble microbial products (SMP) concentration in the mixed liquor during the experiment. The error bar represents the standard deviation from duplicate samples.

Results in Figure 12 indicate that EPS governed the fouling process. This is consistent with previous work that reported EPS as a major cause of membrane fouling (109, 315) and correlated strongly with fouling potential and filtration resistance (108, 316). EPS has been shown to play key role in initial adhesion of microbial biofilm to surfaces (317-319). In addition, EPS can facilitate cell adhesion (320), cell cohesion and cell communication in biofilm, through dispersion forces, electrostatic interactions, and hydrogen bonds between polymeric substances (317, 321). This provides the mechanical stability allowing different microorganisms to be retained in long-term close proximity and to establish stable and synergistic community (321). In addition, both low and excessive production of EPS can weaken the aggregation of microbial sludge flocs in the mixed liquor, and the expanded sludge/small sludge flocs can easily adhered to the surface of the membrane, thereby causing biofouling (315). The adsorption of EPS on the membrane surface also contributes to organic fouling and can lead to irreversible fouling (322, 323).

A higher concentration of polysaccharide than protein in both EPS and SMP fractions was observed (Figure 12). The protein/polysaccharide (PN/PS) ratio determines specific interactions (e.g. hydrophobic, van der Waals, electrostatic interaction and cation bridging) between sludge flocs and membrane surface and thus affects membrane fouling (324). In this study, the PN/PS

ratio in EPS and SMP exerted a negative impact on membrane fouling, as fouling propensity increased when PN/PS ratio decreased. The impact of EPS/SMP composition on membrane fouling was also observed in previous studies (324-326). When protein concentration was constant, flux decline became faster and fouling rate increased as PN/PS ratio decreased for PVDF membrane (326).

### 4.3.2. Differences in microbial identity between mixed liquor and biofilm

UPGMA clustering analysis was conducted based on unweighted UniFrac distance metric to reconstruct a dendrogram of DNA samples from the MBR (Figure 13). A small but observable dissimilarity in microbial identity profiles can be seen between the mixed liquor and membrane biofilm (Figure 13). Unweighted UniFrac distance metric calculates the distance between pairs of microbial communities based on the presence/absence of observed microorganisms and phylogenetic distances between these microorganisms (327). The distance between two samples (two tips of the tree) is the sum of all branch lengths connecting between them. Duplicate samples showed small distances to each other (e.g. BF2.3.1 vs BF2.3.2, ML2.1.1 vs. ML2.1.2), confirming the reliability of our sampling procedure and analysis.

The discernible difference between biofilm and mixed liquor samples in terms of microbial identity could be attributed to the presence of unique taxa-specific microbial groups presented in the biofilm that was or was not present (at low abundances) in the mixed liquor and vice versa. This is in agreement with a previous study investigating membrane fouling in five full-scale MBR plants (299). In this study, the biofilm harvested at the severe fouling stage of phase 1 showed higher similarity to the mixed liquor compared to other biofilms. This is possibly due to the deposition of microbes from the mixed liquor onto the biofilm's outer layer due to accumulation of EPS and strong drag force. This observation is also consistent with a previous study by Xu et al., (116) who reported greater similarity between the microbial structure of the biofilm and the mixed liquor as fouling develops at a water flux below the critical flux value.

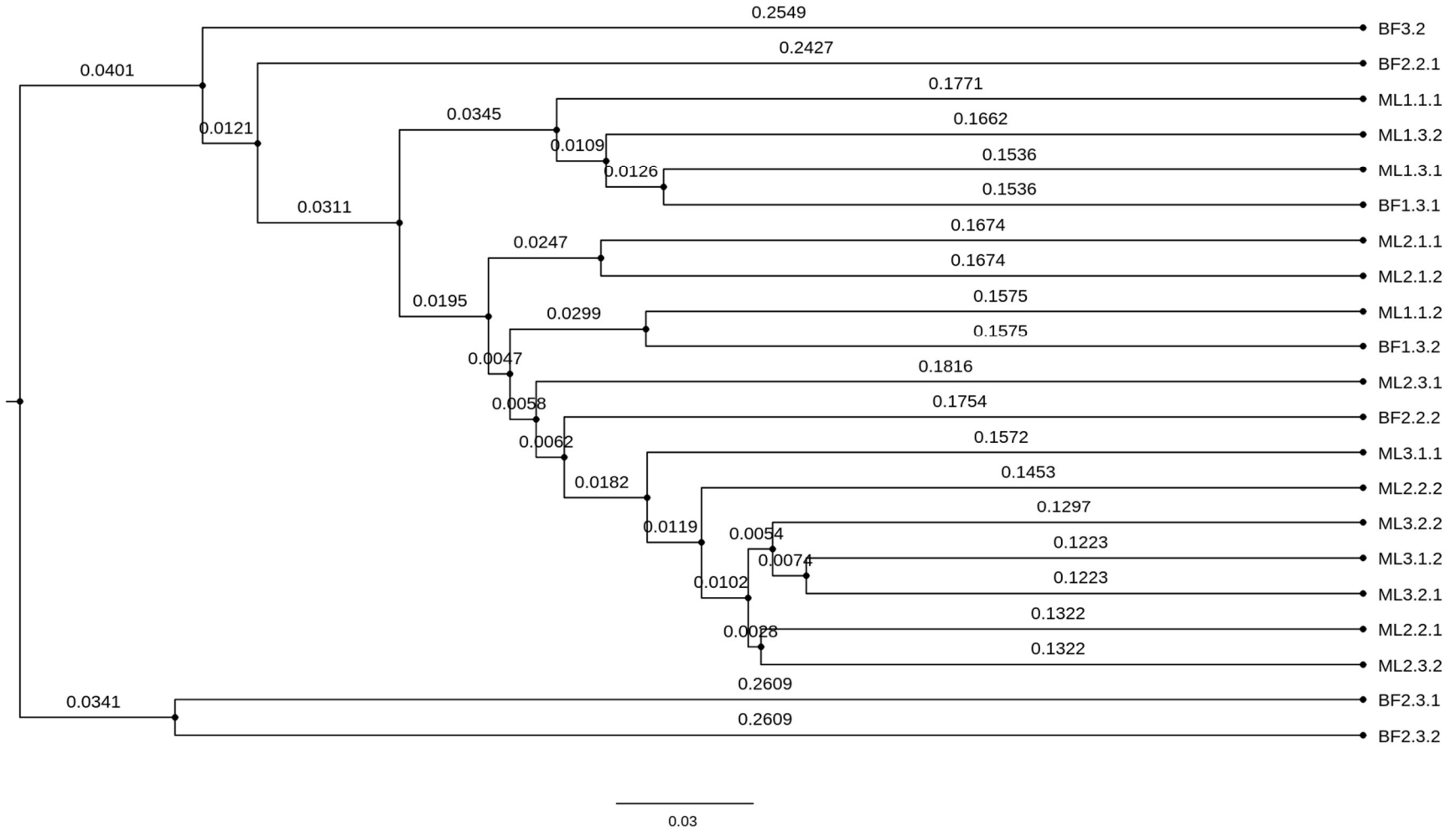


Figure 13. UPGMA clustering dendrogram based on unweighted UniFrac distance metric showing similarity between mixed liquor (ML) and biofilm (BF) microbial identity. BF2.2.2: membrane sample in run 2 fouling stage 2 duplicate 2.

### 4.3.3. Differences in microbial structure between mixed liquor and biofilm

To highlight the difference in microbial structure between the mixed liquor and biofilm, a dendrogram was constructed by UPGMA clustering analysis using the Bray-Curtis dissimilarity (Figure 14). There is a fundamental difference between the unweighted UniFrac distance metric and Bray-Curtis dissimilarity. While unweighted UniFrac distance metric is a binary (presence/absence) system, Bray-Curtis dissimilarity considers both microbial identity and their abundances. A Bray-Curtis dissimilarity of zero (0) between a pair of samples means these two samples share the same taxon with the same abundance (same structure). As a result, it is expected that the dendrogram based on Bray-Curtis dissimilarity quantifies the difference between the mixed liquor and biofilm in terms of microbial structure. The mixed liquor and biofilm microbial communities become more distinguishable under the microbial structure angle compared to microbial identity angle (Figure 14), indicating that microbial abundance was the key driver of the difference between the two communities. Results from PcoA based on Bray-Curtis dissimilarity also support this finding (Figure 15), with mixed liquor and biofilm samples form distinct clusters. The difference between the mixed liquor and biofilm communities was statistically significant (PERMANOVA test, $n = 21$, permutation = 999, pseudo-$F = 3.53$, p-value $< 0.05$) (Figure 16). These results also highlight how diversity index selection strongly impacts the extent of difference between the mixed liquor and biofilm communities.

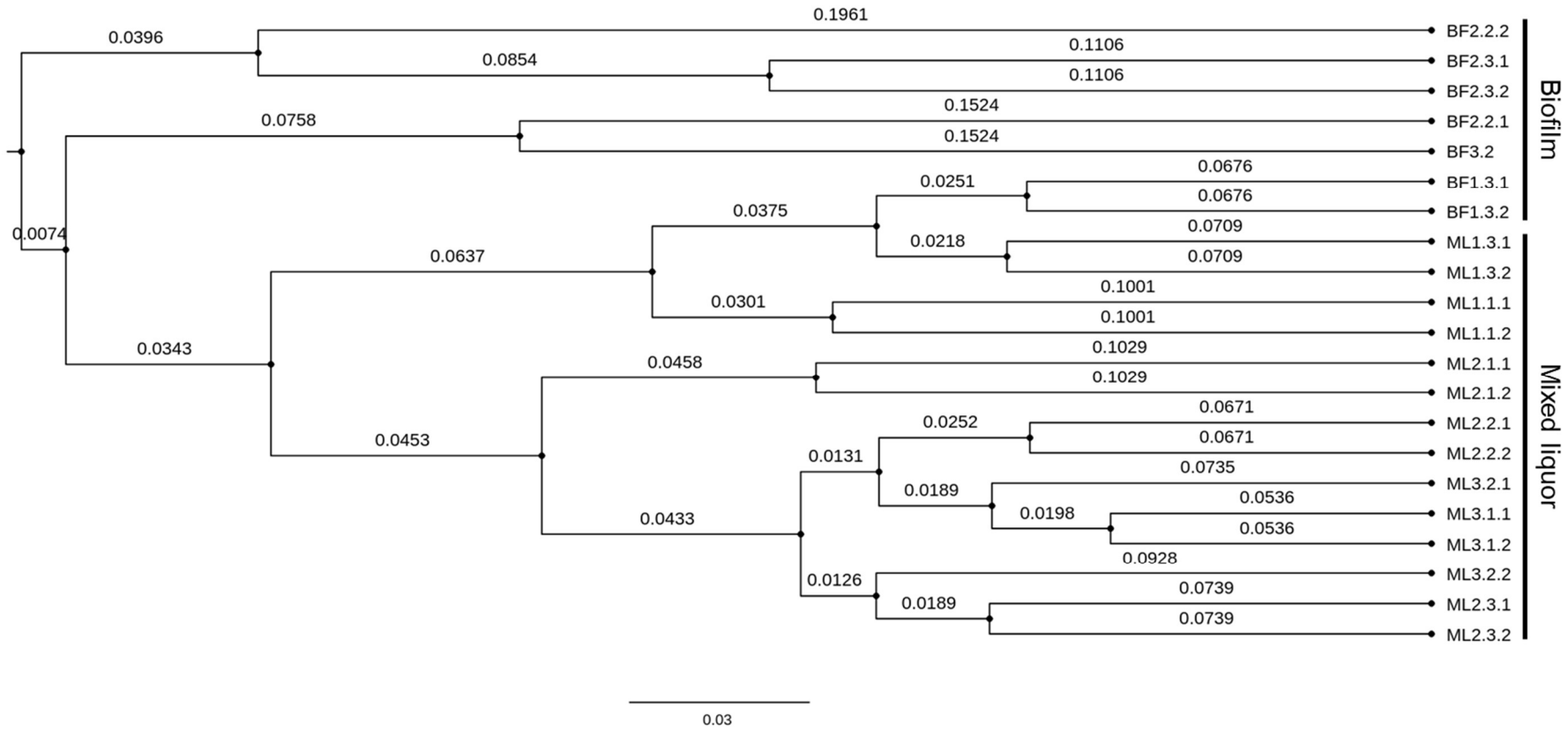


Figure 14. UPGMA clustering based on unweighted Bray-Curtis dissimilarity showing difference between mixed liquor (ML) and biofilm (BF) microbial structure. BF2.2.2: membrane sample in run 2 fouling stage 2 duplicate 2.

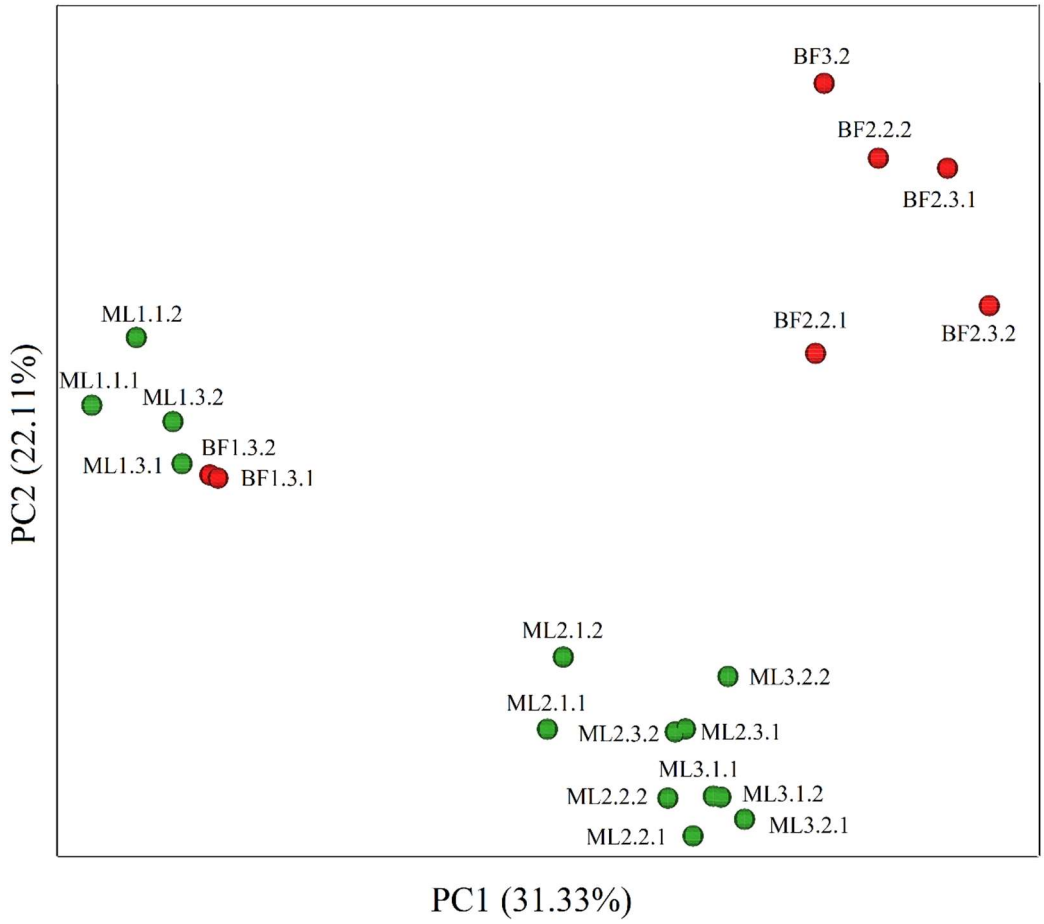


Figure 15. Principal coordinates analysis showing similarity/dissimilarity between mixed liquor (ML) and biofilm (BF) samples microbial community composition.

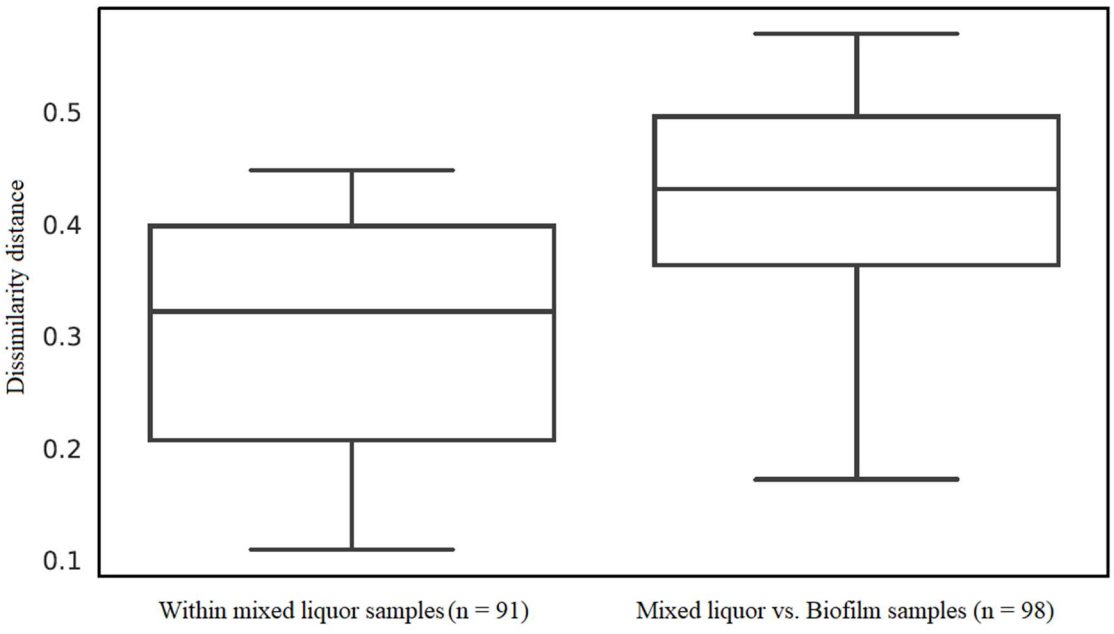

Figure 16. Bray-Curtis dissimilarity distance within mixed liquor samples and between mixed liquor and biofilm samples. The whiskers of the box represent the minimum and maximum values. The bottom and top of the box are the first and third quartiles, respectively, and the line inside the box denotes the median.

Distinct patterns in microbial structure of biofilm (both early and mature) and mixed liquor have been reported previously in lab (112, 113, 304), pilot (98, 297) and full-scale MBR systems (100, 299). This difference in microbial structure could be attributed to different assembly mechanisms and environmental conditions (116, 299). Selective deposition of microorganisms from the mixed liquor to the membrane surface occurs due to multiple factors, such as species mobility and adhesive ability, membrane flux, and membrane properties (328). In addition, biofilm is a microenvironment with high local cell density, resulting in a substantially different level of oxygen and nutrient compared to the mixed liquor (304), with a nutrient concentration gradient forming along the thickness of the biofilm as it developed (329). As such, microorganisms that can adapt to these conditions emerge in the biofilm community, and further drive the divergence between biofilm and mixed liquor microbial structure.

### 4.3.4. Difference in microbial abundance between mixed liquor and biofilm

Since the difference between the two communities was mainly caused by difference in microbial abundance (Section 4.3.3), microbial abundance was further examined. Differential abundance analysis was performed to identify specific microbial taxa that steer the divergence between mixed liquor and biofilm communities. Differential abundance analysis can be used to identify taxa that present in different absolute abundances across two or more environments (sample groups) (330). In this study, a log-ratio-based normalization method (known as ANCOM) was used for differential abundance analysis. This method successively uses each taxon as the reference taxon and transforms the observed abundances to log ratios of the observed abundance of each taxon relative to the reference taxon (311). It controls the false discovery rate at a low level (5%) while maintaining high statistical power (330).

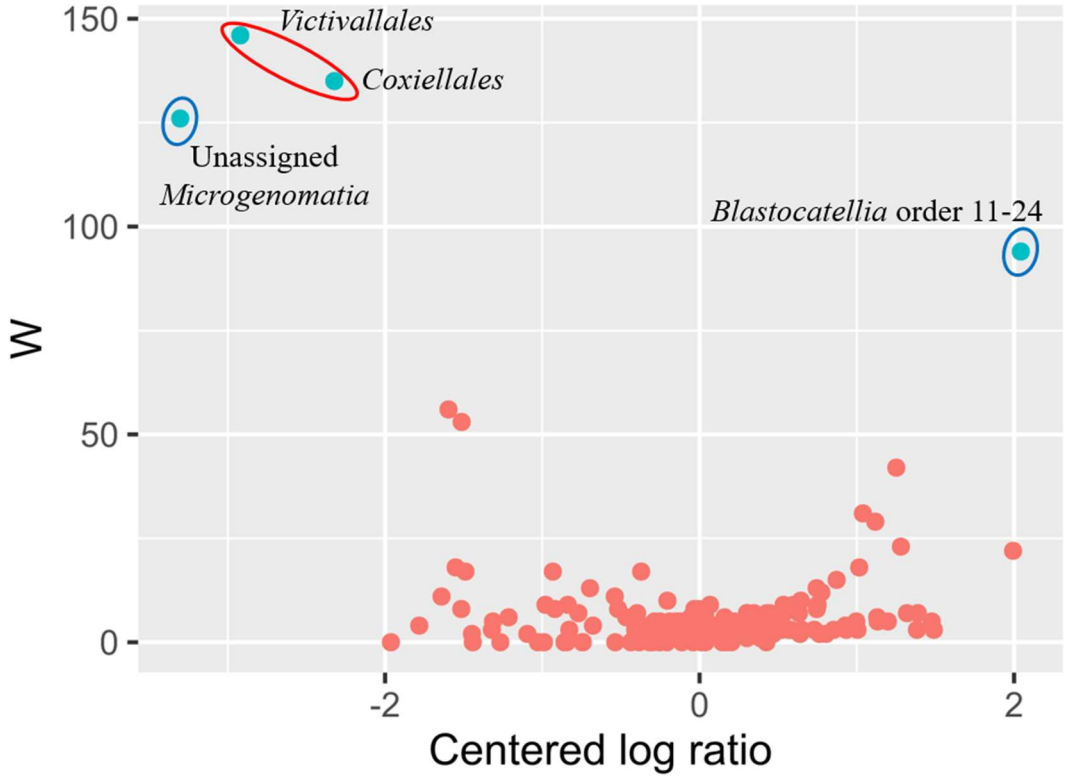


Figure 17. Differential abundance analysis (ANCOM) volcano plot. The W value represents the number of times the null-hypothesis (the average abundance of a given order in the mixed liquor is equal to that in the biofilm) was rejected for a given order. When the W value of an order is high, it is more likely that the order is differentially abundant across sample groups. The 70$^{th}$ percentile of the W distribution is used as the empirical cut-off value. Orders with W values higher than this cut-off are labelled with red circles, and orders with high W values but less than the cut-off are labelled with blue circles. The centered log ratio (clr) is the transformed mean difference in abundance of a given order between the mixed liquor and biofilm groups. A

positive clr means an order is abundant in mixed lqiuor and a negative clr value means a species is abundant in biofilm.

Figure 17 shows only a few orders of differential abundance between mixed liquor and biofilm samples. The W value for an order means that the ratio between that order and W other orders was different across the compared sample groups. Higher W value means higher likelihood that the difference is true (330). Compared to mixed liquor samples, *Victivallales, Coxiellales* and unassigned *Microgenomatia* were enriched in biofilm samples, while *Blastocatellia* order 11-24 was depleted in biofilm samples. Despite their preferential growth in the biofilm, together *Victivallales, Coxiellales* and unassigned *Microgenomatia* only account for a small fraction (<1%) of the biofilm microbial community and can be defined as rare taxa. Rare taxa (<1%) have been identified as biomarkers shaping the difference between MBR bulk sludge and biofilm communities (299), and it was also suggested that these rare taxa play important roles in fouling development (113). Results in Figure 17 corroborate with observations from microbial identity analysis (Section 4.3.2) to confirm the difference in microbial community structure between the mixed liquor and the biofilm on the membrane surface.

### 4.3.5. Key players in mixed liquor compared to biofilm community

Modularized RMT-based ecological networks of mixed liquor and biofilm microbial communities were constructed to reveal the microbial interactions within each community (Figure 18 & Table 6). Cooperative and competing interactions can exist between microbial taxa in a community. Examples of cooperative interactions are cross-feeding, where a taxon feeds on the microbial product of another taxon (331), or mutualistic symbiosis where both taxa benefit from the relationship (332). Microbial taxa can also compete with each other for carbon sources and other nutrients (e.g. oxygen, nitrogen) due to limited space and nutritional resources. The average clustering coefficient, path distance, and modularity of the two empirical networks were significantly higher than that of their corresponding random networks under identical nodes and links, indicating their small-world behaviour and modularity structure (Table 6). The nodes in the network are mainly affiliated with the phylum *Proteobacteria*, *Patescibacteria*, *Acidobacteria*, and *Bacteroidetes* (Figure 18), which have been identified as dominant wastewater phyla.

Table 6. Major topological properties of empirical and random molecular ecological networks (MENs) of bacterial community in mixed liquor and biofilm.

| Sample type | Empirical network | | | | | | 100 random networks | | |
|---|---|---|---|---|---|---|---|---|---|
| | Total nodes | Total edges | Average degree | Average clustering coefficient | Average path distance | Modularity | Average clustering coefficient | Average path distance | Modularity |
| Mixed liquor | 66 | 90 | 2.727 | 0.186 | 4.279 | 0.622 | 0.04 ± 0.02 | 3.65 ± 0.16 | 0.55 ± 0.02 |
| Biofilm | 99 | 354 | 7.152 | 0.363 | 3.423 | 0.499 | 0.12 ± 0.01 | 2.6 ± 0.03 | 0.29 ± 0.01 |

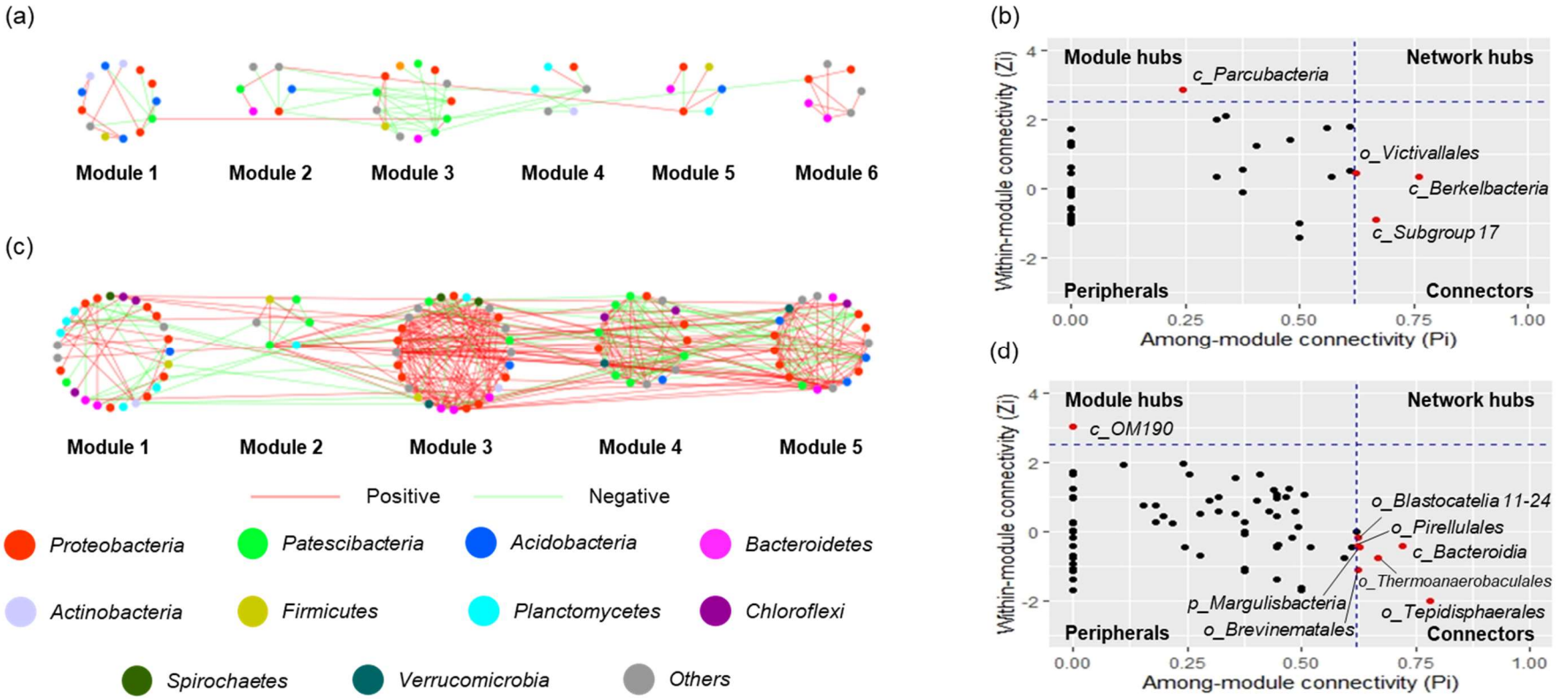


Figure 18. Modularized co-occurrence network analysis revealing the interactions among microbial orders in (a) the mixed liquor and (c) the biofilm community with Z-P plot of species topological roles (b&d). The formed modules with the number nodes more than 5 were selected to construct final modularized co-occurrence network. Each node represents a microbial order. The nodes' colors represent different major phyla (account for >75% of network members). Red and green lines represent positive and negative interactions, respectively.

A higher level of interaction between microbial orders was observed in the biofilm compared to the mixed liquor, indicated by the higher number of nodes, edges, average degree (connectivity) and clustering coefficient (Table 6), suggesting the existence of a more complex microbial structure in the biofilm (116). The higher connectivity also reflects higher stability of the microbial community in the biofilm compared to the mixed liquor, since the removal of a small number of edges will not be able weaken the network. In addition, more positive connections were observed in the biofilm (74.6%) compared to the mixed liquor (42.2%) (Figure 18), suggesting the predominance of syntrophic and mutual relationships in the biofilm. This agrees with assembly mechanisms of mixed liquor and biofilm. Microbial taxa in the mixed liquor are more dispersed (333), while those in the biofilm are placed in close proximity, allowing for intense communication and high synergy, and resulting in their stable co-existence (321).

Microbial orders in each module were densely connected among one another (especially in the biofilm network) and each module could be regarded as a functional ecological unit. The topological role of a taxon could be defined by its position compared with others in its own module and how well it connects to taxa in other modules. As shown in the Z-P plot (Figure 18B&D), the majority of nodes were detected as peripherals with most of their links inside their own modules (93.9 and 91.9% in the mixed liquor and biofilm network, respectively). Only 3 nodes (4.6%) in the mixed liquor network and 6 nodes (7.1%) in the biofilm network were identified as connectors that are highly connected to several modules and are likely to be key players in the community.

A common characteristic between the biofilm and mixed liquor networks is all identified connectors was orders with low relative abundances. For example, the two connectors *Victivallales* and uncultured *Berkelbacteria* only accounted for <0.3% in the mixed liquor community. Similarly, many connectors have negligible to low relative abundance in the biofilm, e.g. *Pirellulales*, *Tepidisphaerales* and unassigned *Bacteroidia* <0.2%. Xu et al. (116) and Zhang et al. (113) also observed that keystone fouling-causing taxa in biofilm networks were present at very low abundances (0.01%–0.93%). By contrast, dominant orders such as *Betaproteobacteriales* and *Chitinophagales* did not appear to play important roles in both communities. These two dominant orders accounted for 55.4 ± 6.1% of the mixed liquor community and 41.8 ± 10.0% of the biofilm community, respectively).

The relationships between microbial taxa with environmental traits were established by the Pearson correlation. The majority of network connectors strongly correlated (correlation coefficient > 0.6) with EPS and SMP, further confirming their contributions to fouling (Table 7 & Table 8). A higher number of correlations was observed between microbial taxa in the biofilm and fouling indicators than that of the mixed liquor. These results suggest that the biofilm microbial community is more fouling-associated. In addition, since keystone fouling-causing taxa only occur in the fouling layer at a very low abundance (<1%), it may be possible to independently regulate them to control fouling without affecting biological performance of the mixed liquor. For example, bacteriophage – a virus that infects and destroys specific host bacterium through cell lysis/disruption actions – can be used to eliminate these fouling-associated taxa in the community (334, 335), with minimal unintentional ecological impacts on other taxa (336). Goldman et al. (337) demonstrated that phages targeting *Pseudomonas aeruginosa*, *Acinetobacter johnsonii* and *Bacillus subtilis* can reduce membrane biofouling by 40% to >60% in ultrafiltration system. Ma et al. (338) also reported effective fouling mitigation with different bacteriophage assisted anti-biofouling strategies in ultrafiltration including phage immobilization on the membrane surface in dead-end filtration system, phage addition into the feed of cross-flow, and phage-assisted cleaning of a biofouled membrane.

Table 7. Pearson correlation between microbial orders in the mixed liquor with fouling indicators. Taxa that were identified as network connectors/module hubs are marked with an asterisk. Taxa that showed strong correlations with fouling indicator (>0.6) are marked with two asterisks.

| **Taxa** | **SMPc** | **SMPp** | **EPSc** | **EPSp** |
|---|---|---|---|---|
| *Absconditabacteriales SR1* | 0.03 | 0.177 | 0.062 | 0 |
| *Acetobacterales* | 0.001 | 0.452 | 0.212 | 0.179 |
| *Anaerolinea 1-20* | 0.025 | 0.36 | 0.113 | 0 |
| *Anaerolineales* | 0.129 | 0.075 | 0.001 | 0.003 |
| *Armatimonadales* | 0.489 | 0.446 | 0.27 | 0.139 |
| *Azospirillales* | 0.585 | 0.214 | 0.011 | 0.103 |
| *Babeliales*** | 0.615 | 0.118 | 0.032 | 0.021 |
| *Bacteroidales* | 0.027 | 0.008 | 0.16 | 0.223 |
| *Bdellovibrionales* | 0.359 | 0.047 | 0.152 | 0.176 |
| *Betaproteobacteriales* | 0.016 | 0 | 0.002 | 0.026 |

| | | | | |
|---|---|---|---|---|
| *Blastocatellales*** | 0.736 | 0.136 | 0.056 | 0.004 |
| *Blastocatellia 11-24* | 0.084 | 0.212 | 0.23 | 0.128 |
| *Caedibacterales*** | 0.906 | 0.588 | 0.072 | 0.284 |
| *Caldilineales* | 0.071 | 0.065 | 0.115 | 0.033 |
| *Candidatus Falkowbacteria*** | 0.135 | 0 | 0.908 | 0.769 |
| *Candidatus Magasanikbacteria* | 0.074 | 0.146 | 0.15 | 0.088 |
| *Candidatus Nomurabacteria* | 0.096 | 0.001 | 0.216 | 0.265 |
| *Candidatus Pacebacteria* | 0.049 | 0.352 | 0.024 | 0.076 |
| *Caulobacterales* | 0.073 | 0.055 | 0.216 | 0.187 |
| *CCM19a* | 0.181 | 0.047 | 0.09 | 0.339 |
| *Chitinophagales* | 0.007 | 0.455 | 0.26 | 0.114 |
| *Chlamydiales* | 0.054 | 0.111 | 0.086 | 0.041 |
| *Chloroflexales* | 0.057 | 0.004 | 0.004 | 0.059 |
| *Chthoniobacterales* | 0 | 0 | 0.139 | 0.115 |
| *Chthonomonadales* | 0.08 | 0.001 | 0.017 | 0.006 |
| *Clostridiales* | 0.283 | 0.007 | 0.028 | 0.025 |
| *Cytophagales* | 0.13 | 0 | 0.082 | 0.051 |
| *Desulfarculales* | 0.47 | 0.291 | 0.034 | 0.166 |
| *Desulfobacterales* | 0.015 | 0.335 | 0.093 | 0.008 |
| *Desulfovibrionales* | 0.31 | 0.037 | 0.183 | 0.193 |
| *Desulfuromonadales* | 0.2 | 0.008 | 0.001 | 0.001 |
| *Diplorickettsiales*** | 0.767 | 0.255 | 0 | 0.033 |
| *Dongiales*** | 0.093 | 0.034 | 0.634 | 0.805 |
| *Erysipelotrichales*** | 0.086 | 0.057 | 0.945 | 0.717 |
| *Fibrobacterales*** | 0.002 | 0.741 | 0.26 | 0.085 |
| *Fimbriimonadales* | 0.201 | 0.073 | 0.005 | 0.026 |
| *Flavobacteriales* | 0.053 | 0.326 | 0.006 | 0 |
| *Frankiales* | 0.065 | 0.004 | 0.15 | 0.139 |

| | | | | |
|---|---|---|---|---|
| *Gammaproteobacteria Incertae Sedis* | 0 | 0.025 | 0.062 | 0.09 |
| *Gemmatales* | 0.033 | 0.038 | 0.377 | 0.281 |
| *Gemmatimonadales* | 0.309 | 0.089 | 0.18 | 0.103 |
| *Holophagales* | 0.096 | 0.075 | 0.039 | 0.034 |
| *Holosporales*** | 0.682 | 0.007 | 0.372 | 0.399 |
| *Hydrogenedentiales* | 0.318 | 0.161 | 0.17 | 0.024 |
| *Isosphaerales* | 0.06 | 0.297 | 0.097 | 0.001 |
| *Lactobacillales* | 0.338 | 0.041 | 0.129 | 0.062 |
| *Legionellales*** | 0.506 | 0.351 | 0.993 | 0.768 |
| *Leptospirales* | 0.054 | 0.002 | 0 | 0.021 |
| *Micrococcales* | 0.149 | 0.196 | 0.006 | 0.009 |
| *Microtrichales* | 0.383 | 0.448 | 0.475 | 0.384 |
| *MVP-88* | 0.148 | 0.269 | 0.018 | 0.044 |
| *Myxococcales* | 0.035 | 0.049 | 0.228 | 0.196 |
| *NB1j* | 0.12 | 0.123 | 0.01 | 0 |
| *Nitrospirales* | 0.002 | 0.117 | 0.056 | 0.128 |
| *Obscuribacterales* | 0.106 | 0.002 | 0.198 | 0.273 |
| *Oligoflexales* | 0.531 | 0.049 | 0.19 | 0.16 |
| *OPB56* | 0.023 | 0.005 | 0.243 | 0.28 |
| *Opitutales* | 0.131 | 0.004 | 0.006 | 0.002 |
| *Paracaedibacterales*** | 0.802 | 0.258 | 0.005 | 0.061 |
| *Pedosphaerales* | 0.085 | 0.107 | 0.151 | 0.161 |
| *Phycisphaeraemle18* | 0.312 | 0.106 | 0 | 0.026 |
| *Phycisphaerales* | 0.037 | 0.034 | 0.029 | 0.061 |
| *Pirellulales* | 0.005 | 0.001 | 0.146 | 0.2 |
| *Planctomycetales* | 0.035 | 0.002 | 0.316 | 0.398 |
| *Propionibacteriales* | 0.023 | 0.006 | 0.294 | 0.252 |
| *Pseudomonadales* | 0.002 | 0.07 | 0.087 | 0.162 |

| | | | | |
|---|---|---|---|---|
| *RBG13549* | 0.111 | 0.003 | 0 | 0.007 |
| *Reyranellales* | 0.294 | 0.178 | 0.095 | 0.079 |
| *Rhizobiales* | 0 | 0.019 | 0.174 | 0.167 |
| *Rhodobacterales* | 0.536 | 0.22 | 0.063 | 0.025 |
| *Rhodospirillales* | 0 | 0.16 | 0.03 | 0.022 |
| *Rickettsiales*** | 0.708 | 0.264 | 0.018 | 0 |
| *Saccharimonadales* | 0.299 | 0.217 | 0.086 | 0.039 |
| *SAR324 clade Marine group B* | 0.027 | 0.057 | 0.079 | 0.157 |
| *SBR1031* | 0.024 | 0.097 | 0.489 | 0.483 |
| *Selenomonadales* | 0.11 | 0.107 | 0.042 | 0.045 |
| *SM1A07* | 0 | 0.236 | 0.019 | 0.078 |
| *Solibacterales* | 0.183 | 0.131 | 0.097 | 0.068 |
| *Sphingobacteriales* | 0.014 | 0.015 | 0.188 | 0.292 |
| *Sphingomonadales* | 0.011 | 0.009 | 0.279 | 0.372 |
| *Spirochaetales* | 0.018 | 0.048 | 0 | 0.046 |
| *Steroidobacterales* | 0.479 | 0.08 | 0.341 | 0.243 |
| *Tepidisphaerales* | 0.389 | 0.002 | 0.014 | 0.004 |
| *Thermales* | 0.377 | 0.322 | 0.022 | 0.004 |
| *Thermoanaerobaculales* | 0.428 | 0.219 | 0.005 | 0.001 |
| *Thermomicrobiales* | 0 | 0.278 | 0.218 | 0.174 |
| *Tistrellales* | 0.161 | 0.278 | 0.205 | 0.119 |
| *Unassigned Acidobacteria* | 0.165 | 0.133 | 0.005 | 0.03 |
| *Unassigned Alphaproteobacteria*** | 0.778 | 0.223 | 0 | 0.028 |
| *Unassigned Bacteroidia* | 0.016 | 0.185 | 0.182 | 0.2 |
| *Unassigned Chloroflexi* | 0 | 0.1 | 0.2 | 0.077 |
| *Unassigned Deltaproteobacteria* | 0.002 | 0.102 | 0.03 | 0.037 |
| *Unassigned Elusimicrobia* | 0.076 | 0.18 | 0.013 | 0.014 |
| *Unassigned LineageIIa* | 0.357 | 0.06 | 0.003 | 0.016 |

| | | | | |
|---|---|---|---|---|
| *Unassigned Microgenomatia* | 0.135 | 0.513 | 0.391 | 0.143 |
| *Unassigned microorganism* | 0.337 | 0.525 | 0.005 | 0.024 |
| *Unassigned OM190* | 0.024 | 0.015 | 0.008 | 0.049 |
| *Unassigned Subgroup 17*** | 0.537 | 0 | 0.592 | 0.653 |
| *Unassigned Subgroup 6* | 0.183 | 0.058 | 0.013 | 0.065 |
| *UnassignedBacteria* | 0.044 | 0.135 | 0.313 | 0.498 |
| *Uncultured Alphaproteobacteria* | 0.219 | 0.091 | 0.055 | 0.071 |
| *Uncultured Berkelbacteria** | 0.378 | 0.617 | 0.483 | 0.466 |
| *Uncultured LCP89*** | 0.008 | 0 | 0.592 | 0.644 |
| *Uncultured OM190* | 0 | 0.09 | 0.04 | 0 |
| *Uncultured Parcubacteria** | 0.13 | 0.322 | 0.202 | 0.09 |
| *Uncultured Pelobacter sp.* | 0.396 | 0.149 | 0.168 | 0.063 |
| *Uncultured Woesearchaeia* | 0.338 | 0.065 | 0.15 | 0.081 |
| *Uncultured WS6 Dojkabacteria* | 0.015 | 0.205 | 0.38 | 0.091 |
| *Verrucomicrobiales* | 0.074 | 0 | 0.215 | 0.229 |
| *Victivallales** | 0.026 | 0.006 | 0.669 | 0.764 |
| *WD260*** | 0.57 | 0.725 | 0.395 | 0.352 |
| *Xanthomonadales* | 0.014 | 0.004 | 0.044 | 0.151 |

Table 8. Pearson correlation between microbial orders in the biofilm with fouling indicators. Taxa that were identified as network connectors/module hubs are marked with an asterisk. Taxa that showed strong correlations with fouling indicator (>0.6) are marked with two asterisks.

| **Taxa** | **SMPc** | **SMPp** | **EPSc** | **EPSp** |
|---|---|---|---|---|
| *Absconditabacteriales SR1*** | 0.279 | 0.701 | 0.465 | 0.074 |
| *Acetobacterales* | 0.163 | 0.25 | 0.516 | 0.116 |
| *Anaerolineales*** | 0.221 | 0.06 | 0.491 | 0.928 |
| *Azospirillales*** | 0.39 | 0.639 | 0.918 | 0.254 |
| *Babeliales* | 0.102 | 0.002 | 0.093 | 0.027 |
| *Bacteroidales* | 0.04 | 0.037 | 0.079 | 0.004 |

| | | | | |
|---|---|---|---|---|
| *Bdellovibrionales* | 0.515 | 0.202 | 0 | 0.006 |
| *Betaproteobacteriales* | 0.165 | 0.074 | 0.024 | 0.015 |
| *Blastocatellales* | 0.529 | 0.269 | 0.026 | 0.001 |
| *Blastocatellia 11-24** | 0.728 | 0.44 | 0.123 | 0.008 |
| *Brevinematales** | 0.075 | 0 | 0.316 | 0.8 |
| *Caedibacterales*** | 0.936 | 0.153 | 0 | 0.042 |
| *Caldilineales* | 0.104 | 0 | 0.095 | 0.023 |
| *Candidate division WOR1 bacterium RIFOXYB2FULL4235*** | 0.499 | 0.969 | 0.535 | 0.4 |
| *Candidatus Collierbacteria* | 0.039 | 0.297 | 0.346 | 0.204 |
| *Candidatus Falkowbacteria* | 0.2 | 0.011 | 0.04 | 0.328 |
| *Candidatus Nomurabacteria* | 0.312 | 0.49 | 0.289 | 0.114 |
| *Candidatus Pacebacteria* | 0 | 0.029 | 0.124 | 0.194 |
| *Candidatus Zambryskibacteria* | 0.082 | 0.07 | 0.095 | 0.004 |
| *Caulobacterales*** | 0.017 | 0.14 | 0.613 | 0.997 |
| *Chitinophagales* | 0.164 | 0.484 | 0.182 | 0.172 |
| *Chlamydiales* | 0.004 | 0.011 | 0 | 0.035 |
| *Chloroflexales* | 0.449 | 0.004 | 0.255 | 0.408 |
| *Chthonomonadales*** | 0.645 | 0.556 | 0.093 | 0.033 |
| *Clostridiales* | 0.016 | 0.114 | 0.369 | 0.085 |
| *Coxiellales* | 0.019 | 0.025 | 0.035 | 0.045 |
| *Cytophagales*** | 0.343 | 0.628 | 0.245 | 0.099 |
| *Desulfarculales*** | 0.579 | 0.199 | 0.78 | 0.54 |
| *Desulfobacterales* | 0 | 0.197 | 0.26 | 0.011 |
| *Desulfovibrionales* | 0.036 | 0.537 | 0.576 | 0.099 |
| *Desulfuromonadales* | 0 | 0.436 | 0.064 | 0.02 |
| *Diplorickettsiales* | 0.134 | 0.201 | 0.136 | 0.009 |
| *Fibrobacterales* | 0.317 | 0.056 | 0.232 | 0.008 |
| *Fimbriimonadales* | 0.451 | 0.412 | 0.016 | 0 |

| | | | | |
|---|---|---|---|---|
| *Flavobacteriales* | 0.14 | 0.195 | 0.088 | 0.093 |
| *Frankiales* | 0.01 | 0.257 | 0.016 | 0.023 |
| *Gammaproteobacteria Incertae Sedis* | 0.104 | 0.035 | 0.065 | 0.121 |
| *Gemmatales* | 0.038 | 0.168 | 0.327 | 0.065 |
| *Gemmatimonadales* | 0.537 | 0.445 | 0.122 | 0.004 |
| *Holophagales* | 0.392 | 0.025 | 0.094 | 0 |
| *Holosporales* | 0.278 | 0.551 | 0.248 | 0.126 |
| *Isosphaerales*** | 0.135 | 0.259 | 0.677 | 0.163 |
| *Lactobacillales* | 0.061 | 0.005 | 0.334 | 0.304 |
| *Leptospirales* | 0.427 | 0.03 | 0.211 | 0.086 |
| *Micrococcales*** | 0.002 | 0.215 | 0.632 | 0.327 |
| *MVP-88* | 0.123 | 0.036 | 0.129 | 0.002 |
| *Myxococcales* | 0.126 | 0.071 | 0.098 | 0.12 |
| *NB1j*** | 0.002 | 0.946 | 0.708 | 0.333 |
| *Nitrospirales*** | 0.706 | 0.097 | 0.056 | 0.023 |
| *Obscuribacterales* | 0.147 | 0.389 | 0.243 | 0.165 |
| *Oligoflexales* | 0.016 | 0 | 0 | 0.035 |
| *OPB56* | 0.024 | 0.005 | 0.108 | 0.004 |
| *Opitutales* | 0.328 | 0.033 | 0.075 | 0.085 |
| *Paracaedibacterales* | 0.768 | 0.272 | 0.013 | 0.016 |
| *Pedosphaerales* | 0.459 | 0.377 | 0.094 | 0.016 |
| *Phycisphaerales* | 0.199 | 0.003 | 0.112 | 0.152 |
| *Pirellulales** | 0.013 | 0.011 | 0.169 | 0.038 |
| *Planctomycetales* | 0.012 | 0.249 | 0.473 | 0.274 |
| *Pseudomonadales* | 0.102 | 0.056 | 0.242 | 0.017 |
| *RBG13549* | 0.383 | 0.119 | 0.006 | 0.166 |
| *Reyranellales* | 0.007 | 0.389 | 0.423 | 0.276 |
| *Rhizobiales* | 0.075 | 0.134 | 0.014 | 0.034 |

| | | | | |
|---|---|---|---|---|
| *Rhodobacterales* | 0.006 | 0.134 | 0.102 | 0.062 |
| *Rhodospirillales* | 0.232 | 0.2 | 0.059 | 0.034 |
| *Rickettsiales*** | 0.704 | 0.2 | 0.002 | 0.013 |
| *Saccharimonadales* | 0.064 | 0.303 | 0 | 0.011 |
| *SAR324 clade Marine group B*** | 0.1 | 0.636 | 0.352 | 0.015 |
| *SBR1031* | 0.109 | 0.004 | 0.321 | 0.526 |
| *Selenomonadales* | 0.134 | 0.378 | 0.158 | 0.001 |
| *Solibacterales*** | 0.798 | 0.378 | 0.041 | 0.012 |
| *Sphingobacteriales* | 0.005 | 0.009 | 0.121 | 0.021 |
| *Sphingomonadales* | 0.195 | 0.158 | 0.305 | 0.035 |
| *Spirochaetales*** | 0.097 | 0.943 | 0.725 | 0.19 |
| *Steroidobacterales* | 0.341 | 0.004 | 0.059 | 0.052 |
| *Synergistales*** | 0.599 | 0.77 | 0.691 | 0.496 |
| *Tepidisphaerales** | 0.82 | 0.083 | 0.997 | 0.956 |
| *Thermales*** | 0.704 | 0.174 | 0.01 | 0.104 |
| *Thermoanaerobaculales** | 0.589 | 0.629 | 0.291 | 0.035 |
| *Tistrellales* | 0.151 | 0.002 | 0.188 | 0.151 |
| *Unassigned Acidobacteria* | 0.325 | 0.01 | 0.204 | 0.155 |
| *Unassigned Alphaproteobacteria*** | 0.889 | 0.206 | 0.01 | 0.019 |
| *Unassigned Bacteria*** | 0.402 | 0.88 | 0.709 | 0.147 |
| *Unassigned Bacteroidia** | 0.173 | 0.325 | 0.495 | 0.509 |
| *Unassigned Chloroflexi* | 0.314 | 0.023 | 0.038 | 0.01 |
| *Unassigned Deltaproteobacteria* | 0.04 | 0.746 | 0.241 | 0.025 |
| *Unassigned LineageIIa* | 0.371 | 0.271 | 0.545 | 0.344 |
| *Unassigned Margulisbacteria** | 0.435 | 0.976 | 0.856 | 0.512 |
| *Unassigned Microgenomatia*** | 0.282 | 0.603 | 0.276 | 0.002 |
| *Unassigned microorganism*** | 0.23 | 0.639 | 0.759 | 0.172 |
| *Unassigned OM190* | 0.228 | 0.119 | 0.155 | 0.112 |

| | | | | |
|---|---|---|---|---|
| *Unassigned Parcubacteria*** | 0.626 | 0.164 | 0.018 | 0.268 |
| *Unassigned Subgroup 6* | 0.332 | 0.426 | 0.27 | 0.072 |
| *Unassigned WS6 Dojkabacteria* | 0.597 | 0.561 | 0.111 | 0.124 |
| *Uncultured Alphaproteobacteria*** | 0.686 | 0 | 0.227 | 0.175 |
| *Uncultured Berkelbacteria* | 0.421 | 0.303 | 0.009 | 0.039 |
| *Uncultured OM190** | 0.083 | 0.222 | 0.633 | 0.311 |
| *Uncultured Parcubacteria* | 0.421 | 0.272 | 0.212 | 0 |
| *Uncultured Woesearchaeia* | 0.017 | 0.29 | 0.13 | 0 |
| *Uncultured WS6 Dojkabacteria* | 0.345 | 0.084 | 0.014 | 0.046 |
| *Verrucomicrobiales* | 0.583 | 0.566 | 0.163 | 0.007 |
| *Victivallales* | 0.235 | 0.048 | 0.05 | 0.007 |
| *Xanthomonadales* | 0.3 | 0.188 | 0.159 | 0.171 |

## 4.4. Conclusion

This study highlights the importance of bioinformatics analysis and index selection for microbial community characterization. Using a combination of complementary bioinformatics analyses i.e. UPGMA clustering analysis, differential abundance analysis and network analysis, this study provides a more complete picture of the difference in microbial community between the fouling layer (biofilm) and mixed liquor and helps to reconcile the discrepancy in the current literature. There is a subtle but critical difference in microbial community structure between the fouling layer and mixed liquor. Although broadly similar in the composition of abundant microbial taxa, the fouling layer (biofilm) shows a higher level of inter-species interaction. Key drivers of the critical difference between the fouling layer and mixed liquor were identified to be low-abundance taxa (<1%) which formed multiple syntrophic interactions with more abundant taxa in the community. These keystone fouling-causing taxa in the fouling layer appear to play critical role in communication and forming syntrophic and mutual interaction with other more abundant taxa within the network. Results from this study are useful for the development of biological techniques that target these specific low-abundance fouling-associated taxa to control fouling in MBR applications.

# Chapter 5. EXAMINING VFA GENERATION FROM LIGNOCELLULOSIC SUBSTRATE BY RUMEN FLUID VS. DIGESTED SLUDGE

This chapter has been published as the following journal article.

Nguyen LN, Nguyen AQ, Johir MAH, Guo W, Ngo HH, Chaves AV, et al. Application of rumen and anaerobic sludge microbes for bio harvesting from lignocellulosic biomass. Chemosphere. 2019;228:702-8.

**Summary:** This work investigated the production of biogas, volatile fatty acids (VFAs), and other soluble organic from lignocellulosic biomass (LCBM) by two microbial communities (i.e. rumen fluid and anaerobic sludge). Biochemical methane potential (BMP) assay was conducted for rumen fluid and anaerobic sludge separately. Four types of abundant LCBM (i.e. wheat straw, oaten hay, lurence hay and corn silage) found in Australia were used. The results show that rumen microbes produced four-time higher VFAs level than that of anaerobic sludge reactors, indicating the possible application of rumen microorganisms for VFAs generation from LCBM. VFA production in the rumen fluid reactors was probably due to the presence of specific hydrolytic and acidogenic bacteria (e.g. *Fibrobacter* and *Prevotella*). VFA production corroborated from the observation of pH drop in the rumen fluid reactors indicated hydrolytic and acidogenic inhibition, suggesting the continuous extraction of VFAs from the reactor. Anaerobic sludge reactors on the other hand, produced more biogas than that of rumen fluid reactors. This observation was consistent with the abundance of methanogens in anaerobic sludge inoculum (3.98% of total microbes) compared to rumen fluid (0.11%). VFA production from LCBM is the building block chemical for bioplastic, biohydrogen and biofuel. The results from this study provide important foundation for the development of engineered systems to generate VFAs from LCBM.

## 5.1. Introduction

LCBM are residues from agricultural and forestry industries with an estimation of 10 billion tons annually. The conventional view of the residues is that they need to be disposed of to prevent the spread of disease in the next cropping season. An alternative view is that the residues, as LCBM, are a great reserve of carbon, the keystone of energy and raw chemical production (339, 340). LCBM has a net calorific value of up to 20 MJ/kg. However, the economic value of alternate uses such as electricity generation through incineration is relatively small due to high moisture content in LCBM. An alternative use of LCBM will probably pave the way for the production of raw chemicals and energy that currently depends on fossil resources. Harvesting processes from LCBM have gained an upward trajectory in the last two decades; however, the recalcitrant structure of LCBM is the main bottleneck that still requires substantial research to overcome (340, 341).

Current methods to extract raw chemicals and energy from LCBM have low productivity (339, 340). This is because the chemical compositions and structure of LCBM (which includes cellulose, hemicellulose and lignin) require high energy or corrosive chemicals to break it down (340, 342). Processes that have been investigated include a physical process (e.g. steam explosion and grinding); chemical process (e.g. sulphuric, nitric acids, sodium hydroxide and urea soaking); and protein engineering to improve the performance of existing lignocellulose-degrading enzymes (340, 343). The physical process methods and chemical process methods are limited in their effectiveness, create environmental hazards, and are energy-intensive. The protein engineering methods have achieved only modest results in improving LCBM hydroxylation (343). This is mostly due to our limited understanding of the mechanisms of biomass hydroxylation and the relatively low activity of currently available hydrolytic enzymes.

Specific microbial communities from a termite gut, from the digestive tract of ruminant animals and from anaerobic digester have shown the capability of degrading LCBM. The rumen microbial community has evolved in the rumen environment for million years to digest LCBM to produce VFAs and biogas. The symbiotic relationship between the rumen and its microbial community has led to the evolution of lignocellulosic-degrading bacteria that have not been found to proliferate elsewhere. Likewise, the microbial community in 1 µL termite gut is also specific for lignocellulosic degradation. Recently, Lazuka et al. (344) has reported that a consortium of lignocellulosic-degrading bacteria can be achieved in an engineered anaerobic reactor under sterile conditions. Anaerobic microbial community from the anaerobic digester has demonstrated the efficiency of converting organic waste to energy (i.e. biogas) (345, 346). Research in the application of these microbial communities for LCBM degradation has gained promising results (165, 166, 168, 340). Takizawa et al. (165) reported that rumen fluid pretreatment of paper sludge increased 3.4 times methane production. Zhang et al. (168) observed an enhancement of cellulose degradation due to rumen microbes addition in anaerobic digestion. Therefore, microbial community sources (e.g. rumen fluid and anaerobic sludge) could be used to produce VFAs and energy from LCBM.

The study aims to investigate the production of VFAs and biogas as well as soluble chemical oxygen demand from LCBM by rumen fluid and anaerobic sludge microbial communities. The production rate was investigated in a biomethane potential assay that provided conditions simulating anaerobic digestion process. 16S rRNA gene-based community was employed to reveal the microbial community composition in rumen fluid and anaerobic sludge. The results of microbial community analysis provided support evidence to the different observations in production rate between two communities. Results from this study provided preliminary background for the development of an engineered system to generate VFAs from LCBM.

## 5.2. Materials and Methods

### 5.2.1. Lignocellulosic biomass and inoculum sources

Four lignocellulosic materials namely wheat straw (WS), lurence hay (LH), oaten hay (OH) and corn silage (CS) were obtained from a local pet store. These are some of the most abundant LCBM in Australia. They were washed with Milli-Q water and dried at 60 °C for 24 h. Then, they were milled and sieved through a 600-µm pore size sieve (Figure 19A). The resultant was characterized for moisture, volatile solid (VS) and ash content and stored in a zip bag at room temperature until use. The VS contents of all four lignocellulosic materials were above 90% (Table 9). These LCBM have substantial levels of COD (500-1000 kg COD/kg biomass). Therefore, these materials have high potential as feedstocks for anaerobic digestion.

Table 9. Characteristics of lignocellulosic biomass (mean ± standard deviation from 3 samples).

| **Materials** | **Moisture (%)** | **VS (%)** | **Ash (%)** | **COD (kg/kg)** |
|---|---|---|---|---|
| Wheat straw (WS) | 2.8 ± 0.5 | 92.5 ± 0.0 | 4.7 ± 0.5 | 846.5 ± 168.9 |
| Lurence hay (LH) | 4.9 ± 0.5 | 91.3 ± 0.2 | 3.8 ± 0.6 | 1014 ± 33.6 |
| Oaten hay (OH) | 4.2 ± 1.1 | 94.6 ± 0.2 | 1.7 ± 0.9 | 531 ± 8.5 |
| Corn silage (CS) | 4.4 ± 0.7 | 95.3 ± 0.5 | 0.3 ± 0.2 | 738.5 ± 112.4 |

Rumen fluid and anaerobic sludge were two inoculum sources (Table 10). The former was collected from a 12-year old fistulated cow after 2 hours feeding. Rumen fluid was strained through two layers of cheesecloth to remove any coarse materials, and then stored in insulated thermos bottles that had been pre-heated with warm water to maintain a temperature of approximately 39ºC during transportation to the laboratory. Anaerobic sludge was obtained from a full-scale anaerobic digester at the wastewater treatment plant in NSW, Australia. Anaerobic sludge was stored in pre-heated insulated thermos bottles during transportation and used within four hours of collection.

Table 10. Key properties of inoculum (mean ± standard deviation of 3 measurements).

| | Rumen fluid | Digested sludge |
|---|---|---|
| TS (%) | 2.2 ± 0.2 | 1.6 ± 0.2 |
| VS (%) | 1.8 ± 0.1 | 1.1 ± 0.2 |
| pH | 7.0 ± 0.0 | 7.3 ± 0.0 |
| Total COD (g/L) | 14.8 ± 1.7 | 1.8 ± 0.5 |

### 5.2.2. Biochemical methane potential assay

Biochemical methane potential (BMP) assay was conducted using a set of test rigs similar to that used by Nghiem et al., (347). The test rigs contained fermentation bottles, a water bath, and a

biogas collection gallery. The fermentation bottles were made of glass with 100 mL active volume. Each bottle was equipped with a rubber stoper and aluminium cap. The water bath was Model TWB-20D Thermoline Scientific Pty Ltd and the biogas collection gallery included a 50-mL syringe connected with the needle via an inter lock. Biogas production was recorded daily following the change of syringe piston position on the graduated syringe.

Inoculum (50 mL) of either rumen fluid or anaerobic sludge, was added with 1.5 g LCBM equivalent to 3% w/v into a 100-mL fermentation glass bottle that was pre-flushed with $N_2$ gas. The bottles were flushed again with $N_2$ gas and immediately sealed with a rubber stopper to maintain anaerobic condition. The fermentation bottles were submerged in a water bath to maintain a constant temperature of 39 ± 1 °C and 35 ± 1 °C for rumen fluid and anaerobic sludge fermentation, respectively (Figure 19B).

The fermentation process was conducted for 7 days with rumen fluid and anaerobic sludge inocula, respectively. For each lignocellulosic material, six fermentation bottles were prepared. Two bottles were taken for soluble COD and total organic acids (TOA) as acetate analysis every two days. Another set of bottles was prepared with only either inoculum or lignocellulosic materials as the controls. Fermentation bottles were mixed manually three times each day.

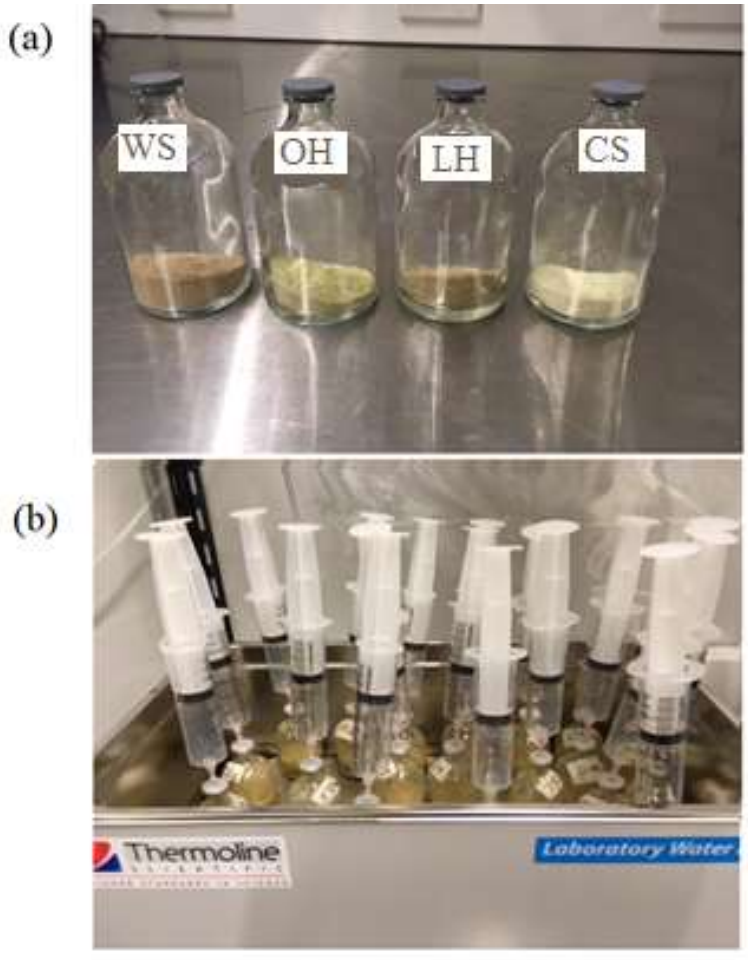

Figure 19. Four selected lignocellulosic biomass: WH = wheat straw; OH = oaten hay; CS = corn silage; LH = lurence hay (a) and a photograph of biomethane potential setup (b).

### 5.2.3. Analytical methods

Moisture, VS and ash content of lignocellulosic biomass were determined according to Standard Methods 1684. Briefly, five grams of lignocellulosic biomass was transferred into a ceramic bowl and dried at 100°C for 24 h. The ceramic bowl was then allowed to cool to room temperature in a desiccating glass chamber. The weight of ceramic bowl and material was recorded. Then the ceramic bowl was heated to 550 °C in a furnace for 15 min. The residual weight was recorded and used to calculate moisture, VS and ash content.

Total chemical oxygen demand (COD) and soluble COD (sCOD) concentration were measured by using digestion vials (Hach, Australia) and Hach DR3900 spectrophotometer program number 435 COD HR, following the US-EPA Standard Method 5220 D.

Total organic acids (TOA) as acetate (mg/L) were measured following US-EPA Standard Method 5560C, including acidification, distillation and titration. Fermented broth (3 mL) from each fermentation bottle was diluted into 200 mL with Milli-Q water. Then 5 mL of 98% $H_2SO_4$ was mixed into samples. The sample was distilled using the Vapodest 300 (Gerhardt Germany) with set up program of heating power 80% and distillate time of 8 min. The final sample was titrated using an Auto Titrator 885 (Metrohm Australia). TOA concentration was calculated using the following equation:

$$\text{Total organic acid } (\frac{\text{mg}}{\text{L}}) = \frac{(\text{mL NaOH sample - mL NaOH blank}) \times \text{N} \times 60000}{\text{mL sample} \times 0.6}$$

Where: N = normality of NaOH and 0.6 is the recovery factor (60%).

### 5.2.4. Microbial community analysis

Rumen microbial community results were obtained from Duarte et al. (348), who sampled rumen fluid from the same fistulated cow. Anaerobic sludge microbial community samples were collected before the inoculation process. Anaerobic sludge was mixed with 100% ethanol (1:1 v/v) to preserve the cells. Detail sample preparation procedure is available elsewhere (66). Briefly, samples were stored in an ice bag during transport and immediately transferred to - 20 °C freezer upon arrival to the laboratory. Genomic DNA was extracted using DNeasy PowerSoil Pro Kit (QIAGEN Pty Ltd, Australia) following the manufacturer's instructions. The integrity, purity and concentration of the extracted DNA were determined by a spectrophotometer (Nanodrop ND2300). The mass of DNA in each sample was always more than 10 µg and the concentration was normalized to 50 ng/µL using DNA/RNA free water. Samples were stored at - 20 °C until DNA sequencing.

The variable regions (V3-V4) on the 16S rRNA gene of extracted DNA were amplified using the universal primers Pro341F (5'-CCTACGGGNBGCASCAG-3') and Pro805R (5'-GACTACNVGGGTATCTAATCC-3') (349). The amplified fragments were sequenced on the Illumina MiSeq sequencing platform at the Australian Genome Research Facility, Australia. Raw paired-end (2×300 bp) 16S rRNA gene sequence data were analyzed according to the Quantitative Insights into Microbial Ecology (QIIME2) pipeline (350). In brief, raw sequences were denoised using DADA2 with the following parameters: trim left-f = 17, trim left-r = 20, trunc-len-f = 280, trucn-len-r = 220, and all other parameters at their default setting. The sequences were clustered into representative OTUs based on a 97% nucleotide identity cut-off. The 16S rRNA gene sequencing generated 120,000 to 450,000 sequences per sample after pre-processing. The taxonomical assignment was performed against MiDAS database version 2.1 (351). The 16S rRNA gene sequences were deposited in GenBank with the accession number PRJNA507317.

## 5.3. Results and Discussions

### 5.3.1. Volatile fatty acids production

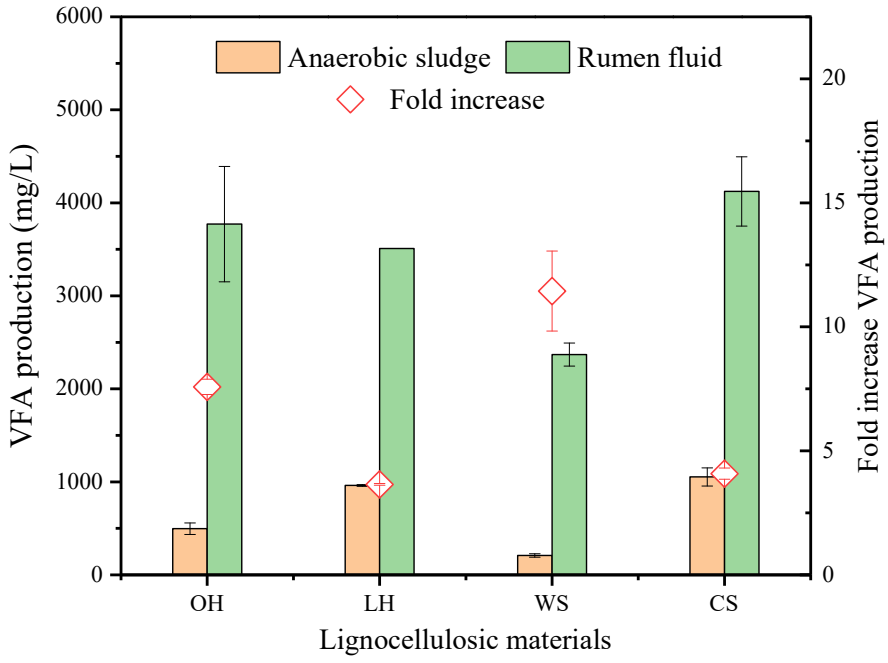


Figure 20. Volatile fatty acid production from anaerobic digestion of lignocellulosic biomass by rumen fluid and digested sludge inocula. Data was recorded after four days incubation. Value and error bars are mean and standard deviation (n = 4).

Rumen fluid is a potential source of microorganisms for bio harvesting of VFAs from LCBM. The rumen fluid reactors generated significantly higher total VFA levels than that of the anaerobic sludge reactor (Figure 20). An average 100 mg VFA per g of LCBM was produced after two days of inoculation with rumen fluid, whereas this value was 23 in the reactors with anaerobic sludge

(an estimated of four times higher). VFAs (i.e. acetic, propionic and butyric acid) are the products of hydrolytic and acidogenic steps during the fermentation process. The level of VFAs indicates the efficiency of hydrolytic and acidogenic processes. Results suggest that rumen fluid microorganisms can hydrolyses LCBM for the production of VFAs. VFAs are building blocks for biodegradable plastics and biofuel. The market for VFAs is growing with an annual demand growth rate of 7.4% (352). The global demand for VFAs (i.e. acetic, butyric, and propionic) is predicted to be about 18 million tons by 2023 (352, 353). The VFAs generation during the incubation of rumen microorganisms with LCBM suggests an alternative source to offset the future VFA demand that currently relies on fossil resources.

Table 11. pH profile in samples during the incubation time (data are mean of two replicates).

| **Time (day)** | **0** | **2** | **4** | **6** |
|---|---|---|---|---|
| Rumen fluid only | 6.95 | 6.98 | 7.01 | 7.04 |
| Rumen fluid + oaten hay | 6.93 | 5.50 | 5.44 | 5.51 |
| Rumen fluid + lurence hay | 7.02 | 5.50 | 5.46 | 5.49 |
| Rumen fluid + wheat straw | 7.01 | 5.68 | 5.59 | 5.59 |
| Rumen fluid + corn silage | 6.98 | 5.25 | 5.23 | 5.29 |
| Digested sludge | 7.54 | 7.6 | 7.58 | 7.46 |
| Digested sludge + oaten hay | 7.20 | 6.53 | 7.02 | 7.12 |
| Digested sludge + lurence hay | 7.23 | 6.11 | 6.47 | 6.5 |
| Digested sludge + wheat straw | 7.31 | 7.03 | 7.1 | 6.9 |
| Digested sludge + corn silage | 7.22 | 6 | 5.8 | 6.1 |

Anaerobic hydrolysis and acidogenesis of LCBM by rumen microbes caused a decline in pH (Table 11). The pH of the reactor dropped from 7.0 to 5.6 after four days incubation. This observation is in consistent with the high level of VFAs production. Extending the incubation period to 6 days resulted in no further pH drop. Therefore, it is inferred that hydrolytic and acidogenic processes were inhibited by high level of VFAs accumulation. Likewise, the VFA concentration profiles along incubation times showed no significantly different after two days incubation with rumen microbes (Figure 21). This study suggests that pH is a detrimental factor to hydrolytic and acidogenic processes. This result is in consistent with the observation that rumen microbes are inhibited at pH below 5.5 (168). On the other hand, hydrolysis and acidogenesis are possible rate-limiting steps in the anaerobic sludge reactor. In consistent with the low level of VFAs production, pH of the reactor was relatively stable (Table 11). In conclusion, VFAs produced from rumen microbe fermentation should be collected from the reactor or on a regular basis.

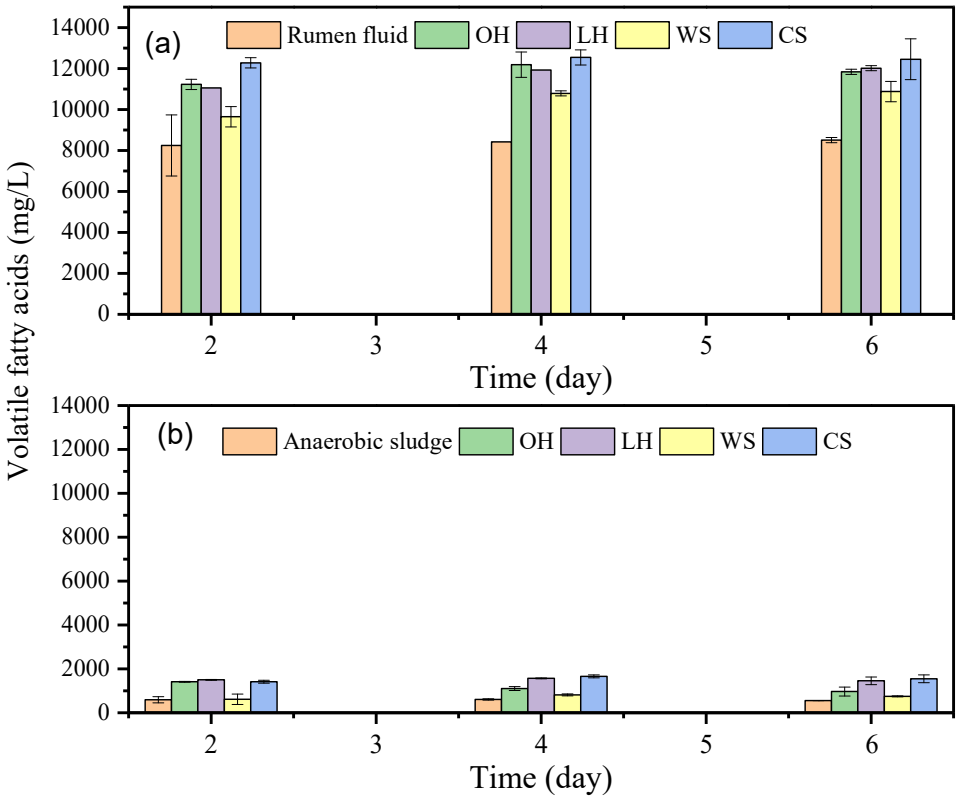


Figure 21. Volatile fatty acid production during the incubation of lignocellulosic biomass with rumen fluid (a) and digested sludge (b). Value and error bars are mean and standard deviation (n = 2).

### 5.3.2. Biogas production

BMP results indicated a higher biogas production from the anaerobic sludge than from rumen fluid reactor (Figure 22). At the end of the incubation period (i.e. 7 days), the BMP bottles with anaerobic sludge produced an average 2.5 times higher biogas than the rumen fluid reactors. Biogas production is a direct indicator of methanogenesis in the anaerobic digestion process. Many studies have demonstrated the positive correlation between biogas production and the abundance of methanogens (66, 354, 355). Results from this study suggest that methanogenesis is a limiting step in the rumen fluid reactor. That is because of the low abundance of methanogens in the rumen fluid (356). Methanogens are often outcompeted by hydrolytic and acidogenic microbes in ruminant microbiota. VFAs compounds, which are substrates for methanogens, are continuously adsorbed in the rumen of host animals (356). Another notable observation is the accumulation of VFAs and drop in pH in rumen fluid reactor (Section 5.3.1). Methanogens are slow-growing microbes and sensitive to pH of the environment. These conditions indicate an onset of the inhibition of the methanogenesis process (357).

Anaerobic sludge reactors produced 120 to 170 mL biogas per g VS added of LCBM (Figure 22). These values are lower than that typically obtained from the anaerobic digestion of municipal solid waste, waste activated sludge and organic wastes (66, 347). This result is likely due to the limitation in hydrolysis and acidogenesis of LCBM by anaerobic sludge microbes. Overall, rumen fluid microbes can be used for the production of VFAs, whereas anaerobic sludge can be used for biogas production. The complementary effect of these two inocula presents a potential solution for bio harvesting from LCBM.

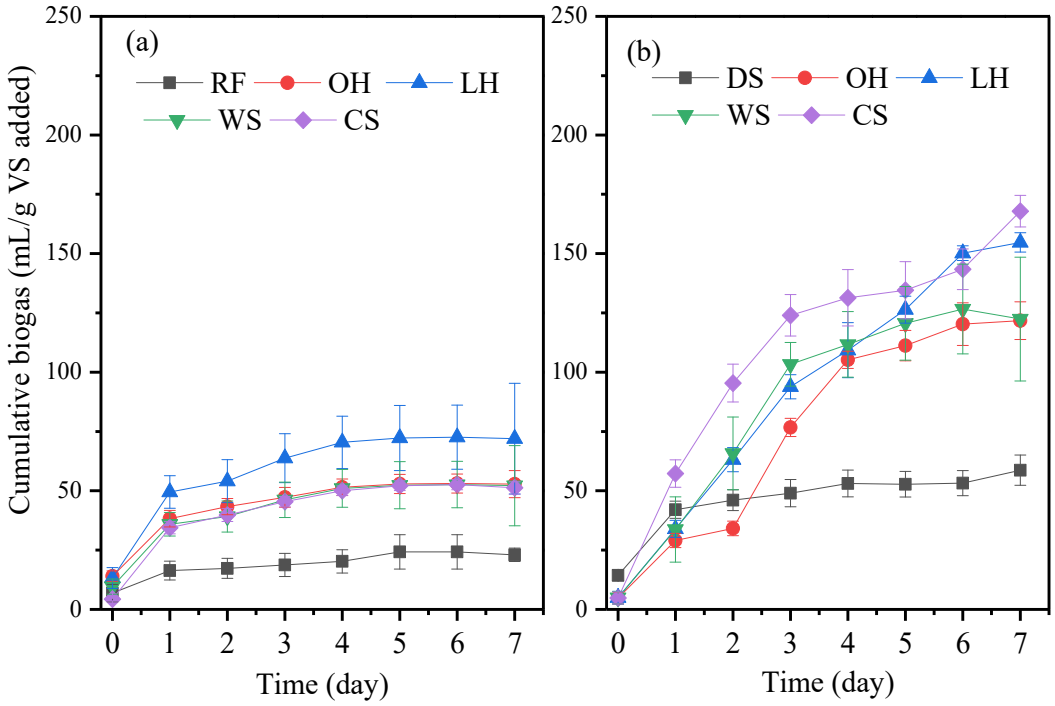


Figure 22. Cumulative biogas production (mL/g VS added) plotted against time from anaerobic digestion of lignocellulosic biomass by rumen fluid (a) and digested sludge (b) inocula. Value and error bars are mean and standard deviation (n = 4).

### 5.3.3. Soluble chemical oxygen demand

Rumen fluid and anaerobic sludge inoculum have an impact on sCOD production from LCBM fermentation (Figure 23). LCBM is insoluble. The control reactor (i.e. contain LCBM only) has negligible amount of sCOD. Therefore, any increase in sCOD is mainly due to the biological conversion of LCBM. The rumen fluid reactors produced 227 (OH), 251 (LH), 187 (WS) and 340 (CS) mg sCOD/g VS added, whereas the anaerobic sludge reactors produced 135 (OH), 32 (LH), 56 (WS) and 256 (CS) mg sCOD/g VS added.

The levels of sCOD depend on the methanogenic microbes. According to the COD balance calculation, Xie et al., (358) estimated about 50% conversion of input COD to biogas. Therefore, the activity of methanogens could negatively correlate with sCOD concentration. In the rumen

fluid reactors, the sCOD concentration was high after two days of inoculation and remained stable towards the end of incubation period (Figure 23). On the other hand, in the anaerobic sludge reactors, the sCOD concentration gradually decreased from day 2 to day 6 (Figure 23). Furthermore, the ratio of sCOD and VFA from rumen fluid reactors (ca. 1.88 [OH], 2.14 [LH], 2.36 [WS], and 2.48 [CS]) was much lower than those of the anaerobic sludge reactors (ca. 7.5 [OH], 10.37 [LH], 8.0 [WS], and 7.11 [CS]). This observation indicated two scenarios (i) sCOD was converted to VFAs in the rumen fluid reactors and (ii) sCOD was converted to VFAs and biogas in the anaerobic sludge.

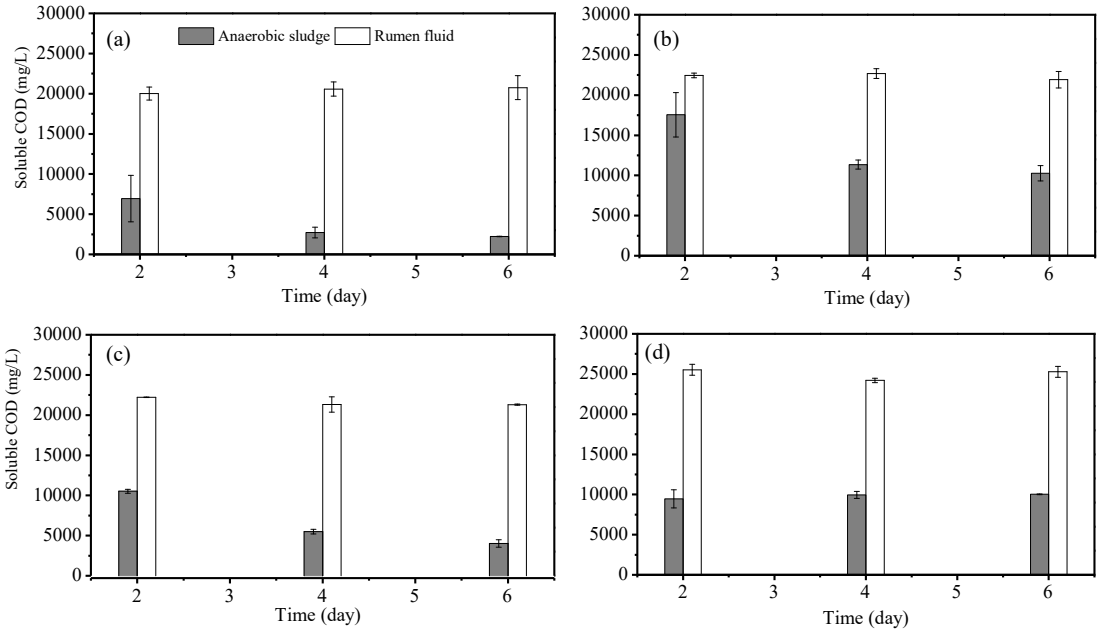


Figure 23. Soluble COD production from anaerobic digestion of lignocellulosic biomass by rumen fluid and digested sludge inocula: (a) control sets with inocula only or lignocellulosic biomass only (a) and tested sets inoculated with WS (b), LH (c), OH (d) and CS (e). Value and error bars are mean and standard deviation (n = 4).

### 5.3.4. Microbial community in rumen fluid and anaerobic sludge inocula

The first difference between rumen fluid and anaerobic sludge microbial communities is the presence of bacteria in the phylum of *Fibrobacteres* (Table 12). The abundance of the phylum *Fibrobacteres* in the rumen fluid (i.e. 8.8%) was significantly higher than that in the anaerobic sludge inoculum (i.e. 0.06%). Bacteria in the phylum of *Fibrobacteres* are the major rumen microbes, allowing for the degradation of plant-based cellulose in ruminant animals. For example, the genus of *Fibrobacter* is specific hydrolytic bacteria that have genes encoding for enzymes cellulases and xylanases. *Fibrobacter succinogenes*, which is one of two cultivated species in the phylum of *Fibrobacter*, effectively degrades crystalline cellulose. Its genome contains high number of genes that were classified into 31 identified cellulases (359). This species also encodes

hemicellulose-degrading enzymes to remove hemicelluloses for other enzymes to attach on cellulose. These enzymes are highly specific for hydrolysis (i.e. cellulolysis) of LCBM (i.e. 30-60% cellulose, 10-25% lignin and 8-40% hemicellulose).

The second difference is the presence of bacteria in the *Prevotellaceae* family in the rumen fluid inoculum (Table 12). In this family, *Prevotella* was dominant in rumen microbiota (348). Baba et al. (186) observed that species in the *Prevotella* family presented at 50.5% of total microbial abundance in the rumen fluid of cattle. Members of the *Prevotella* family such as *P. brevis, P. ruminicola* and *P. bryantii* produce cellulolytic enzymes such as carboxymethyl cellulase and xylanases. The *Prevotella* species function synergistically with other cellulolytic organisms to contribute to the ruminal fibrolytic activity. In contrast, *Prevotellaceae* were present at very low abundance in anaerobic sludge (Table 12). The presence of *Fibrobacter* and *Prevotella* at high abundance and their cellulolytic functions probably explain for the generation of sCOD and VFAs in the reactor inoculated with rumen fluid and LCBM.

Another possible difference between rumen fluid and anaerobic sludge inoculum is the presence of flagellate protozoa and fungi in the rumen fluid. The number of protozoa in the rumen fluid inoculum was $6 \times 10^4$ cells/mL (Figure 24). Endogenous and protozoal enzymes could act independently or synergistically with bacterial enzymes to breakdown LCBM in the rumen. For example, ruminal protozoan *Polyplastron multivesiculatum* comprise a family of 22 carbohydrate-binding module that binds strongly to various crystallinities cellulose (360). Fungi are unique among rumen microorganisms in which they penetrate the cuticle of plant cells. With high levels of cellulases and hemicellulases, rumen fungi hydrolyse or solubilize the entire plant cell wall. However, the potential of rumen protozoa and fungi to degrade more recalcitrant plant walls is not always achieved in the rumen. Future study is recommended to investigate the proliferation of rumen protozoa and fungi in anaerobic digestion of LCBM.

Figure 24. Light microscope photograph (100x magnification) of protozoa in the rumen fluid inoculum.

The compositions and relative abundance of methanogenic communities in the rumen fluid were different from the anaerobic sludge inoculum (Table 12). Three genera including *Methanobacterium, Methanobrevibacter* and *Methanomicrobium* were present at the relative abundance of less than 0.1%. These genera have been described as hydrogenotrophic rumen methanogens. This is consistent with the physiology of the rumen. VFAs, $CO_2$ and $H_2$ are formed during hydrolysis and fermentation of plant polymers in the rumen. While the ruminant consumes VFAs, $CO_2$ and $H_2$ are used by rumen methanogens to produce methane. These methanogens via hydrogenotrophic pathway function as hydrogen sink and thus support the activity of hydrolytic and fermentative bacteria. Consistently, hydrogenotrophic methanogens have been observed in many rumen microbial community studies (356, 361, 362). On the other hand, aceticlastic methanogens dominated the methanogenic community in the anaerobic sludge (Table 12). The genus of *Methanosaeta* is strictly aceticlastic methanogens, presented at 3.16% of total microorganism population. This is consistent with the high abundance of the genera *Methanosaeta* in most of the anaerobic digestion process (357). The genus of *Methanosaeta* is strictly aceticlastic methanogens. Chen et al. (363) reported the robustness of *Methanosaeta* genus at high levels of acetate in anaerobic digestion (44 mM). Overall, the relative abundance of

methanogens in anaerobic sludge was significantly higher than that of rumen fluid, explaining for the high biogas production and no accumulation of VFAs in reactor inoculated with anaerobic sludge.

Results from the analysis of rumen fluid and anaerobic sludge microbial community compositions revealed the possible complementary between two inocula. The co-inoculation of specific lignocellulolytic consortium (i.e. rumen fluid) with the high methanogenic consortium (i.e. anaerobic sludge) can increase the digestion of LCBM for biogas production. Recent studies have achieved some progress in improving anaerobic digestion of cow manure by co-inoculation of cow rumen fluid and anaerobic sludge (364). However, knowledge into the interactions between rumen microbes and anaerobic sludge microbes as well as their associations with the environmental conditions (i.e. may be different from the rumen conditions) is required to fully realise the co-inoculation approach. This study preliminary suggests maintaining the abundance of lignocelulolytic bacteria (e.g. *Fibrobacter* and *Prevotella*) in anaerobic digestion is necessary for the degradation of LCBM.

Table 12. Relative abundance (%) of specific genera in rumen fluid and anaerobic sludge inocula

| **Genera** | **Relative abundance (%)** | | **Ecological function** |
|---|---|---|---|
| | **Rumen fluid (n = 2)*** | **Anaerobic sludge (n = 4)** | |
| **Bacteria** | | | |
| *Fibrobacter* | 8.8 | 0.06 | Hydrolytic |
| *Prevotellaceae* | 35.8 | 0.08 | Hydrolytic |
| *Firmicutes* | 25.9 | 11.4 | Hydrolytic, acidogenic |
| **Methanogens** | | | |
| *Methanobacterium* | 0.01 | 0.003 | Hydrogenotrophic |
| *Methanobrevibacter* | 0.09 | 0.04 | Hydrogenotrophic |
| *Methanomicrobium* | 0.01 | ND | Hydrogenotrophic |
| *Methanolinea* | ND | 0.62 | Aceticlastic |
| *Methanospirillum* | ND | 0.10 | Aceticlastic |
| *Methanosaeta* | ND | 3.16 | Aceticlastic |
| *Methanoculleus* | ND | 0.05 | Aceticlastic |
| *Methanosphaera* | ND | 0.01 | Aceticlastic |
| Total abundance (%) | 0.11 | 3.98 | |

* Data were retrieved from Duarte et al. (348); ND = not detected.

## 5.4. Conclusion

LCBM (i.e. wheat straw, oaten hay, lurence hay and corn silage) can be used for VFAs and biogas production depending on the inoculum sources. Rumen fluid microbes demonstrated the efficiency to digest LCBM into VFAs (at four-time higher than anaerobic sludge). This was likely due to the presence at the high abundance of lignocellulolytic bacteria in the genus of *Fibrobacter* (8.8% of total microbes) and *Prevotella* (35.8%). On the other hand, anaerobic sludge produced higher biogas than rumen fluid reactors. Consistently, the methanogenic abundance in anaerobic sludge was at 3.98% of total microbes, significantly higher than in the rumen fluid inoculum (0.11%). The results of this study suggest the use of rumen fluid microbes together with a continuous extraction of produced VFAs can be an alternative solution to enhance the environmental and economic benefits of LCBM.

# Chapter 6. DERIVATION OF VOLATILE FATTY ACID FROM CROP RESIDUES DIGESTION USING A RUMEN MEMBRANE BIOREACTOR: A FEASIBILITY STUDY

This chapter has been published as the following journal article.

Nguyen AQ, Nguyen LN, Johir MAH, Ngo H-H, Chaves AV, Nghiem LD. Derivation of volatile fatty acid from crop residues digestion using a rumen membrane bioreactor: A feasibility study. Bioresource Technology. 2020;312:123571.

**Summary:** This work evaluates the feasibility of a novel rumen membrane bioreactor (rumen-MBR) to produce volatile fatty acid (VFA) from crop residues (i.e. lignocellulosic biomass - LCBM). Rumen-MBR can provide a sustainable route for VFA production by mimicking the digestive system of ruminant animals. Rumen fluid was inoculated in a reactor coupled with ultrafiltration (UF) membrane and fed with maize silage and concentrate feed at 60:40% (w/w). Continuous VFA production was achieved at an average daily yield of 438 mg VFA/g substrate. The most abundant VFA species were acetic (40-80%) and propionic (10-40%) acids. The majority (73 ± 15%) of produced VFA was transferred through the UF membrane. Shifts in dominant rumen microbes were observed upon the transition from *in vivo* to *in vitro* environment and during reactor operation, however, stable VFA yield was maintained for 35 days, providing the first proof-of-concept of a viable rumen-MBR.

## 6.1. Introduction

Crop residues (i.e. LCBM) present an abundant, inexpensive, renewable and yet untapped carbon-based resource. It is estimated that 146 billion metric tons of LCBM are generated globally each year (365). LCBM can be converted into a variety of valuable products including biofuel, bio-based materials and chemicals; thus can serve as an alternative for fossil fuels in energy and chemical production (340). Utilization of LCBM does not interfere with food production and also incurs lower cost compared to other important biofuel feedstocks (339). The major challenge hindering LCBM application is the recalcitrant structure consisting of cellulose encapsulated in a hemicellulose-pectin-lignin matrix (340).

Ruminant animals such as cows and sheep can readily digest LCBM thanks to their unique rumen microbial community. Rumen fluid harbours bacteria with superior cellulolytic activities (e.g. *Ruminococcus flavefaciens* and *Ruminococcus albus*) and rhythmic coordination between different functional groups (366, 367). Each cellulolytic bacterial strain as well as fungi genus target specific component(s) of LCBM and the combination of different strains ensures complete substrate hydrolysis. The growth of cellulolytic bacteria is promoted as fermenters and acetogens utilize hydrolysis products to generate VFA and hydrogen. The produced VFA (mainly include acetic, propionic and butyric acid) is continuously absorbed by the animal to produce energy (up to 80% of total energy provided to the host animal), while hydrogen is consumed by

hydrogenotrophic methanogens during methanogenesis. Hydrogen removal by methanogens also favours the activity of fermentative and acetogenic bacteria (368).

Exploiting rumen's microbial community is an attractive approach for VFA production from LCBM (369, 370). Previous studies on this topic have demonstrated promising results with VFA yield of up to 377 mg/g substrate (171, 368, 371). High VFA yield can lead to VFA accumulation and trigger pH drop that is detrimental to microorganism growth. Nguyen et al. (368) studied rumen digestion of four different lignocellulosic substrates and observed a rapid increase in VFA concentration to (12,000 mg/L after 2 days of incubation), followed by a pH drop and process inhibition. Thus, continuous removal of the produced VFA from an engineered rumen reactor is required to achieve long-term operation.

Membrane separation is a potential solution for continuous VFA recovery from the reactor. Membrane can provide effective solids/liquids separation, and has shown prominent capacity to separate fermentative products from fermentative broth (372-374). Membrane can also completely prevent the washout of microbes from the reactor based on membrane pore size, which is beneficial for slow-growing rumen microbes. It is envisaged that the combination of rumen microbes with membrane separation in a reactor for continuous generation and removal of VFA can sustain stable operation. The transfer of VFA into a clean matrix (permeate) also facilitates subsequent purification as the final products. Thus, a new rumen-MBR is proposed to alleviate microbe washout and VFA accumulation in the reactor.

This study aims to develop and evaluate the feasibility of a rumen-MBR to derive VFA from LCBM. The VFA yield was determined under similar conditions to the cow's natural rumen and VFA produced was continuously extracted using an UF membrane module. The composition of the VFA produced and their transfer ratios through the UF membrane module were also investigated. Amplicon sequencing of the 16S rRNA marker gene on the Illumina Miseq platform was performed to elucidate how rumen's microbial community changes during the rumen MBR continuous operation and subsequent impacts on VFA yield. Results from this study provide proof of concept of an engineered system to generate VFA from LCBM.

## 6.2. Materials and Methods

### 6.2.1. Preparation of substrate, rumen fluid and artificial saliva

The rumen-MBR was fed with a mixture of maize silage and concentrate feed at 60:40% (w/w) representative of typical cow's diet. These substrates were obtained from The University of Sydney, Corstorphine (Camden Farm Dairy, Cobbitty, NSW 2570, Australia). Substrates were ground into powder using an electrical blender and stored in zip-locked bags at room temperature until use. These substrates were characterized for moisture, volatile solids (VS), ash content and chemical oxygen demand (COD). The VS, COD, moisture, and ash content of maize silage were 87.8%, 1.022 kg/kg, 7.8 and 4.4%, respectively. The high moisture content in maize silage is

similar to other LCBM. The VS, COD, moisture, and ash content of concentrate feed were 81.2%, 1.325 kg/kg, 7.3 and 1.5%, respectively. The VS contents of both substrates were above 80%, indicating substantial levels of organic matters presented. The chemical composition of concentrate feed consists of non-fibre carbohydrates (52. 2%), crude fat (2.7%), crude protein (15.5%) and neutral detergent fibre (20.8%).

Rumen fluid was collected from a 12-year-old fistulated cow 2 h after feeding and used as the rumen microorganism's source. This rumen collection procedure was in accordance with The University of Sydney Animal Ethics Committee (Approved Protocol number 2015/835). The fistulated cow was housed at The University of Sydney, Corstorphine (Camden Farm Dairy, Cobbitty, NSW 2570, Australia). Rumen fluid was strained through two layers of cheesecloth to remove any coarse materials and then stored in insulated thermos bottles that had been pre-heated with warm water to maintain a temperature of approximately 39 ºC during transportation to the laboratory and used immediately. The pH, total solids (TS), VS, and total COD of the rumen fluid were 6.95, 2.79%, 1.85%, and 27.5 g/L, respectively.

A modified version of the McDougall artificial saliva was used to control pH in the rumen-MBR. McDougall saliva solution has been regularly used to control pH in the rumen simulation technique system (375). The modified saliva contains (g/L) of $Na_2HPO_4$ 1.845, $NaHCO_3$ 4.9, NaCl 0.235, KCl 0.285, $MgCl_2.6H_2O$ 0.0305 and $CaCl_2.2H_2O$ 0.0168.

### 6.2.2. Rumen membrane bioreactor

A 3 L Lambda Minifor fermenter (Lambda Pty Ltd, Czech Republic) was used as the rumen-MBR. The reactor was equipped with two peristaltic pumps (i.e. saliva and permeate pump), an overhead mixer, a redox-temperature-pH probe, a temperature control unit and a submerged hollow fibre membrane module (Figure 25). The module was plotted using epoxy resin (Selleys Araldite Ultra Clear, Australia) comprising 20 polyvinylidene difluoride (PVDF) fibres (Dupont, Australia) of 30 cm in length and 0.04 μm in pore size. The effective surface area of the membrane module was approximately 0.02 $m^2$.

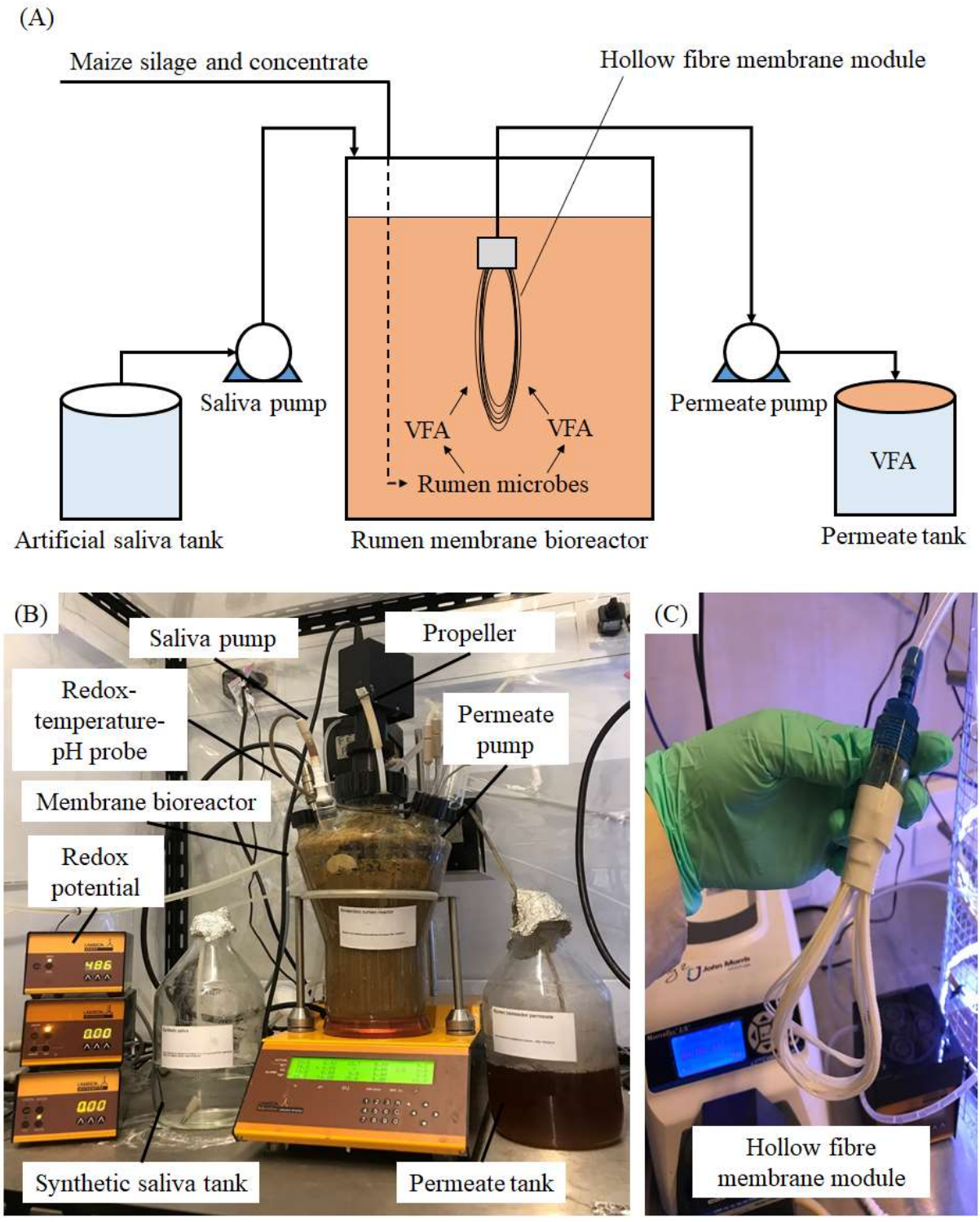


Figure 25. Schematic diagram (A) and real image (B) of the laboratory-scale rumen membrane bioreactor with submerged hollow fibre membrane module (B).

Rumen fluid (1 L) was mixed with saliva (1 L), and 20 g of maize silage: concentrate (60:40 % w/w) to start up the rumen-MBR. Pure $N_2$ gas was purged into the reactor until the oxygen redox potential dropped below -300 mV, indicating the anaerobic condition. The mixture of rumen microorganisms, saliva and substrates was continuously agitated at 150 rpm with one three-bladed

propeller. The temperature control unit was set at 39 °C to simulate the rumen temperature. The feed and permeate pump were continuously operated to achieve a hydraulic retention time (HRT) of 57 h, corresponding to an operating flux of 2.07 L/$m^2$h. The operating flux was kept low to avoid significant membrane fouling in the rumen membrane reactor.

On a daily basis, 100 mL of reactor content was withdrawn from the reactor and 2 g of the substrate mixture in 100 mL of saliva was fed into the reactor to provide a loading rate (LR) of 1 g/L per day (equivalent to 1.14 kg COD/$m^3$ per day). The low LR was applied to avoid insufficient mixing of the substrate and microbial biomass as well as the possible overloading of the system. The SRT in the rumen-MBR was 480 h.

The rumen-MBR was operated for 44 days. The pH and biogas volume were continuously recorded. VFA, TS, VS and soluble COD (sCOD) were measured twice a week.

### 6.2.3. VFA concentration, VFA yield, extent of acidification and transfer ratio

Total VFA (TVFA) concentration in this study was calculated as the sum of individual VFA concentrations. Individual VFA concentration was calculated as below:

$$C_{VFA} = C'_{VFA} \times M \text{ (mg/L)}$$

Where: $C'_{VFA}$ is the VFA concentration expressed as mg/L, $C'_{VFA}$ is the VFA concentration expressed as mmol/L and M is the VFA molar mass.

Daily TVFA yield expressed as mg/g substrate in this study was calculated as below:

$$\text{TVFA yield} = \frac{\text{TVFA}}{\text{LR}} \text{ (mg/g substrate)}$$

Where: TVFA is the total VFA concentration in the reactor and LR is the daily loading rate (g substrate/L).

Daily VFA yields from other studies were calculated from their reported loading rate, VFA concentrations and composition.

Extent of acidification was calculated as:

$$\text{Extent of acidification} = \frac{COD_{VFA}}{\text{sCOD}} \text{ (\%)}$$

Where: $COD_{VFA}$ is the COD equivalent of VFA in the reactor content and was calculated based on the complete oxidation of the individual VFA to $CO_2$ and $H_2O$. The COD conversion factors of acetate, propionate, butyrate (iso-butyrate and n-butyrate), valerate (iso-valerate and n-valerate) and caproate are 1.07, 1.51, 1.82, 2.04, and 2.21, respectively.

To determine the effectiveness of the membrane in terms of transferring VFA to a clean matrix for subsequent extraction, the transfer ratio was calculated as below:

$$\text{Transfer ratio} = 100 \times \frac{C_p}{C_r} \text{ (\%)}$$

Where; $C_p$ is the VFA concentration (mg/L) in the permeate and $C_r$ is the corresponding concentration in the rumen-MBR. The transfer ratio was calculated for TVFA and individual VFA.

### 6.2.4. Analytical procedure

Moisture, TS, VS and ash content were determined according to Standard Methods 1684. Briefly, one gram of substrate was transferred into a ceramic bowl and dried at 100 °C for 24 h. The ceramic bowl was then allowed to cool to room temperature in a desiccating glass chamber. The weight of ceramic bowl and material was recorded and used to calculate TS. Then the ceramic bowl was heated to 550 °C in a furnace for 15 min. The residual weight was recorded and used to calculate moisture, VS and ash content.

Total COD and sCOD concentration were measured by using digestion vials (Hach, Australia) and Hach DR3900 spectrophotometer program number 435 COD HR, following the US-EPA Standard Method 5220 D.

Samples (50 mL) of rumen-MBR content and permeate were taken for quantification of VFA. Samples were centrifuged at 8,300 rpm for 5 minutes and the supernatants were filtered through 1.2 µm filter. The filtrates were mixed with metaphosphoric acid (25% w/v, 5:1 v/v) and centrifuged at 12,000 rpm for 2 minutes on a microcentrifuge (Sigma-Aldrich, Germany). The supernatant (1.2 mL) of was mixed with 0.2 mL crotonic acid solution (0.1 M), vortexed and allowed to stand at room temperature for 30 minutes. The mixture was centrifuged at 12,000 rpm for 10 minutes and the supernatants were transferred to a clean 1.5 mL auto-sampler vial. The VFA determination on Agilent technology 7820A gas-liquid chromatography system, using a DB-FFAP column of dimensions 30 m × 0.32 mm × 1.00 mm, installed with a flame ionization detector set up at 250 ºC, airflow 350 mL/min, $H_2$ fuel flow 30 mL/min, makeup flow ($N_2$) 30 mL/min Split Inlet heated to 225 ºC, 9.526 PSI, Helium total flow 33 mL/min, septum purge flow 3 mL/min, split ratio 5:1, Split Flow 25 mL/min. The oven temperature was set to 150 ºC and held for 1 min, then 5 ºC per minute up to 195 ºC and sustained for 3 min (376).

### 6.2.5. DNA extraction and quality monitoring

Duplicate samples of the inoculum were collected at the beginning of the experiment duplicate samples of rumen-MBR content were collected weekly for microbial community profiling. The inoculum/reactor content was mixed with 100% v/v ethanol (1:1 v/v) and stored at -20 ºC prior to DNA extraction. Genomic DNA extraction was carried out using QIAamp DNA Stool Mini Kit (QIAGEN) following the manual's instructions. The integrity, purity and concentration of the extracted DNA were evaluated by NanoDrop® spectrophotometer. DNA concentration of all samples was normalized to 20 ng/µl using DNase/Pyrogen-Free Water before sending to the sequencing facility.

### 6.2.6. Amplicon sequencing and bioinformatics analysis

The universal primer set Pro341F (5'-CCTACGGGNBGCASCAG-3') and Pro805R (5'-GACTACNVGGGTATCTAATCC-3') was used to amplify 16S rRNA V3 – V4 regions of both bacterial and archaeal communities (377). Paired-end amplicon sequencing (2 × 300 bp) was carried out on the Illumina MiSeq platform (Australian Genome Research Facility, Melbourne, Australia). Raw sequence data were generated with the Illumina *bcl2fastq* pipeline (version 2.20.0.422).

Raw reads were analysed according to Quantitative Insights Into Microbial Ecology (QIIME) 2 (version 2019.10) pipeline (257). In brief, reads were denoised using DADA2 with the following parameters: trunc-len-f = 280, trunc-len-r = 280, trim-left-f = 17, trim left-r = 21, min-fold-parent-over-abundance = 8 and all other parameters as the default setting. Taxonomy assignment was performed against the SILVA database (release 132) (260) with a confidence of 0.7. Rarefaction curves of Observed amplicon sequence variants (ASVs) at a maximum depth of 70,000 showed that all samples approached a saturation plateau at about 68,500 (Figure 26), and this sampling depth was chosen for alpha diversity analysis.

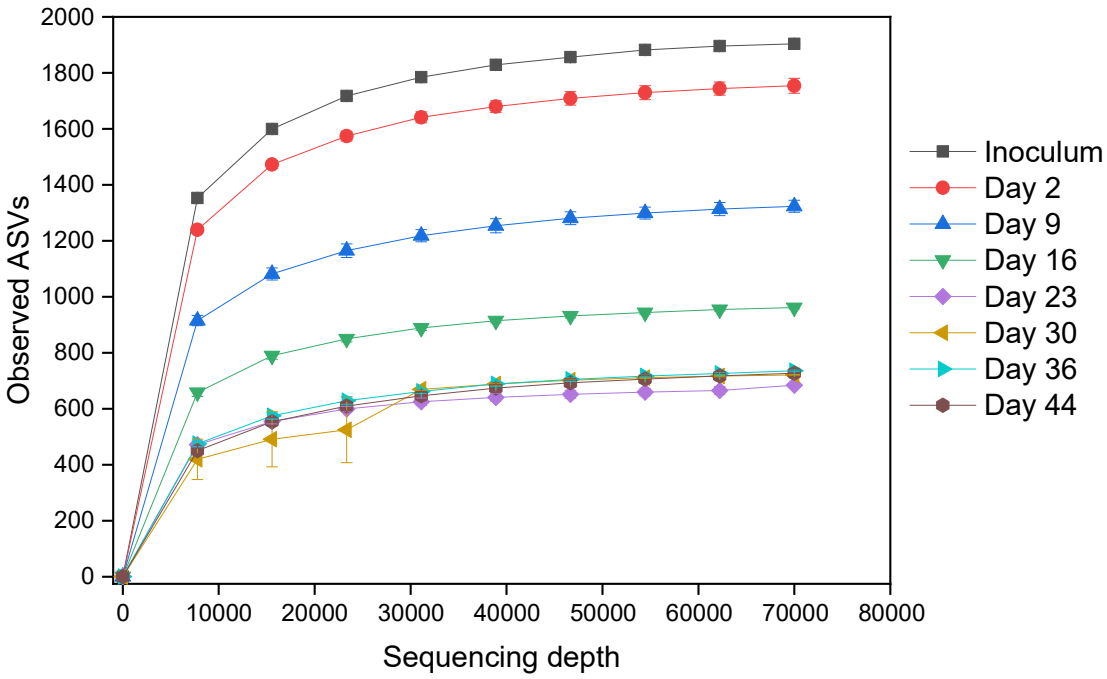


Figure 26. Rarefaction curves of 16S rRNA marker gene amplicon sequences at maximum depth of 70,000.

## 6.3. Results and Discussions

### 6.3.1. Volatile fatty acids yield by the rumen-MBR

### 6.3.2. Total volatile fatty acids yield

The rumen-MBR achieved a stable TVFA yield of 438 ± 87 mg VFA/g substrate from day 9. This stable TVFA yield was recorded for 35 days (Figure 27), which is longer than stable operation periods reported in previous studies using rumen fluid as the inoculum. For example, stable performance was only reported for 8 – 21 days in studies using the rumen simulation technique apparatus (RUSITEC) (375, 378). In another study by Jin et al. (379), stable VFA production was only reported for 18 days at a loading rate of 1% solid content. These authors observed a drastic decrease in VFA production during the first 32 days of the experiment. The decrease in VFA yield was also observed in this study, but mainly during the first 9 days (Figure 27). This decrease was due to the adaptation of rumen microbes after transferring to *in vitro* environment. The adaptation phase is evident by major changes in microbial diversity and composition as revealed by microbial community analysis (Section 6.3.6.2).

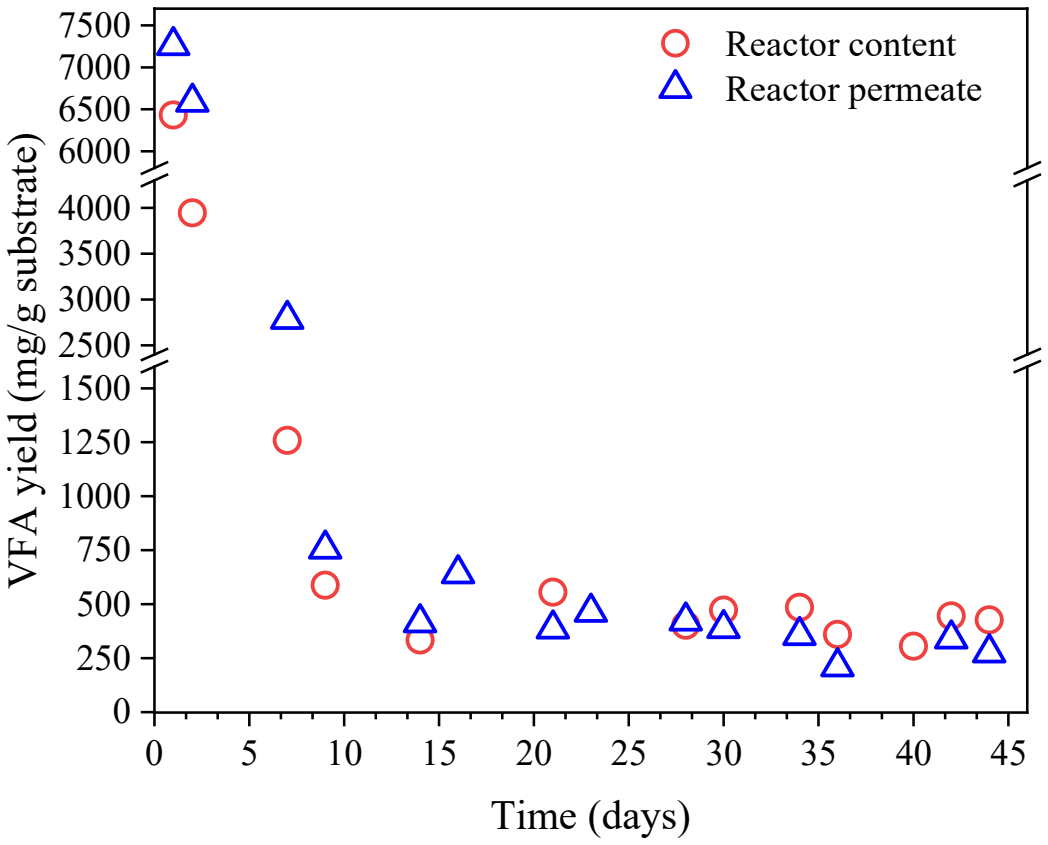


Figure 27. Total volatile fatty acids yield in the rumen membrane bioreactor and permeate during the experimental period.

The rumen-MBR achieved higher VFA yield than most previous studies using rumen fluid as the inoculum (171, 348, 375, 379, 380). VFA yield in these studies ranged from 130.4 to 446.2 mg VFA/g substrate. The higher yield in this study can be attributed to the different reactor configuration (MBR) compared to other studies i.e. RUSITEC fermentation vessels, continuous stirred tank reactor, sequencing batch reactor. The integration of UF membrane allows the achievement of a long solids retention time (SRT) of 480h which provides slow-growing microbes with sufficient time to proliferate in the *in vitro* conditions. Membrane also prevents the washout of slow-growing microbes (as the pore size of the UF membrane used in this study was 0.04 μm) and maintains a high biomass concentration inside the rumen-MBR, which can contribute to high productivity (381). Microbial washout cannot be completely prevented with solids/liquids separation methods used in previous studies such as coarse filtration or sedimentation in sequencing batch reactor. Moreover, membrane enables continuous VFA extraction from the reactor, avoiding VFA loss due to internal conversion reactions as well as process inhibition due to VFA accumulation. Continuous extraction of VFA, while they are being formed, can enhance the rate of VFA production (382). It is noted that the yield from this study (438 mg VFA/g substrate) is slightly lower than the one reported by Barnes et al. (380). These authors observed a VFA yield of 446 mg VFA/g substrate from a sequencing batch reactor inoculated with rumen fluid and fed with fibrous-alpha cellulose (380). The higher yield reported by Barnes et al. (380) can be attributed to the high degradability of their substrate.

### 6.3.3. Volatile fatty acids composition

The VFA composition or the rumen-MBR closely resembles VFA composition in the rumen fluid inoculum (Figure 28). Seven VFA species were detected in both the rumen inoculum and reactor content, with the two most abundant VFA species were acetic acid (59.8 ± 14.5 %) and propionic (24.6 ± 12.2 %). These results were in agreement with VFA composition in previous studies using rumen fluid as the inoculum and similar substrate type and ratio. Ramos et al. (375) found that acetic and propionic acid accounted for 52.2 and 27.1 % of total VFA produced from RUSITEC apparatus fed with hay and concentrate (70: 30%, w/w). In another study by Duarte et al. (378) using hay and concentrate at 66.7: 33.3% (w/w), acetic and propionic accounted for 51.5 and 18.1 % of total VFA. A relatively low but stable presence of branched-chain VFA (iso-butyric and iso-valeric acid) in the rumen-MBR (0.5 – 0.9 mmol/L) was also observed, indicating the digestion of protein content in the substrate. Branched-chain VFA has been shown to play an important role in the growth of ruminal cellulolytic bacteria and their enzyme activities (383).

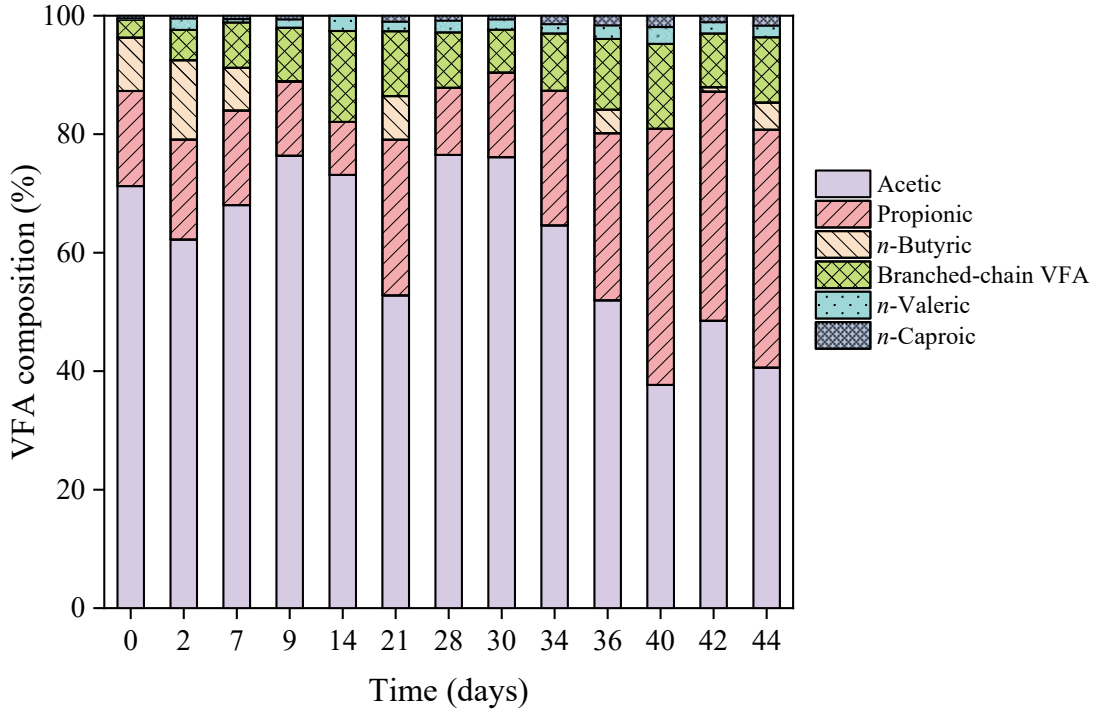


Figure 28. Percentages of individual volatile fatty acids (VFA) of total VFA (based on molar fraction) in the original inoculum (day 0) and rumen membrane bioreactor content (from day 2) during the experimental period. Branched-chain VFA includes iso-butyric and iso-valeric acid.

The predominance of acetic acid in the reactor content shows the potential of the rumen-MBR as a promising option for acetic acid production in the future. Acetic acid is the precursor for synthesising a wide range of important compounds such as vinyl acetate monomer, terephthalic acid, and ethanol. In 2018, the wholesale price of acetic acid was 400–800 €/ton (384). The price of acetic acid is expected to grow at a predicted annual rate of more than 4.3% over the 2019-2024 period due to strong demand (385). Conventional production routes including methanol carbonylation or oxidation of hydrocarbons depend heavily on fossil fuels and emit approximately 3.3 ton $CO2_{eq.}$/ton acetic acid produced (384). Acetic acid production from lignocellulosic biomass using rumen-MBR could be a more sustainable alternative for these production routes.

### 6.3.4. Conversion of the substrate's organic fraction by the rumen-MBR

The digested substrate has a lower VS/TS ratio compared to the original substrate mixture (92.2%), indicating that the organic fraction in the substrate has been utilized by the rumen-MBR (Figure 29). The VS removal efficiency of the reactor was in the range of 28.8 – 49.6 % after day 9, and changes in VS content corresponded with changes in sCOD concentration (Figure 30), indicating that insoluble substrates were converted to soluble products. These changes determine the extent of acidification and dictate the amount of VFA produced during the process (384). Thus, the stable VS removal efficiency and sCOD concentration observed explained for the stable VFA production of the rumen-MBR.

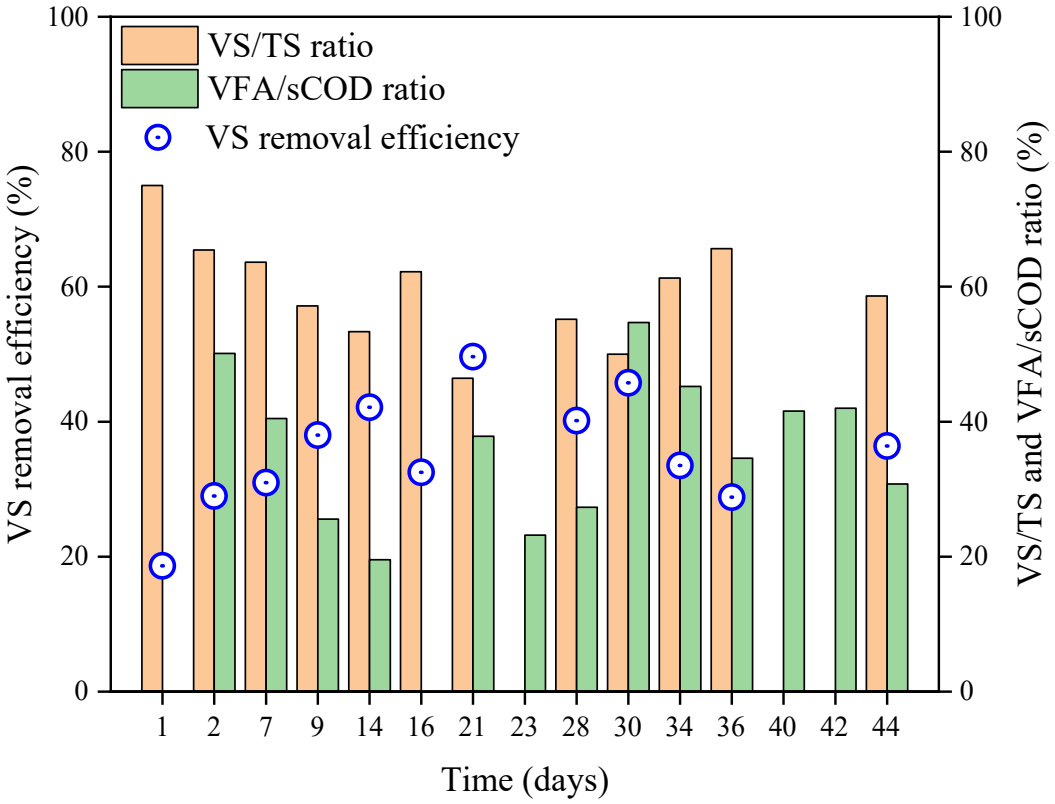


Figure 29. Volatile solids/total solids (VS/TS) ratio, volatile fatty acids/soluble chemical oxygen demand (VFA/sCOD) ratio and VS removal by the rumen membrane bioreactor as a function of time. Samples were collected in a time series and one sample was collected per time.

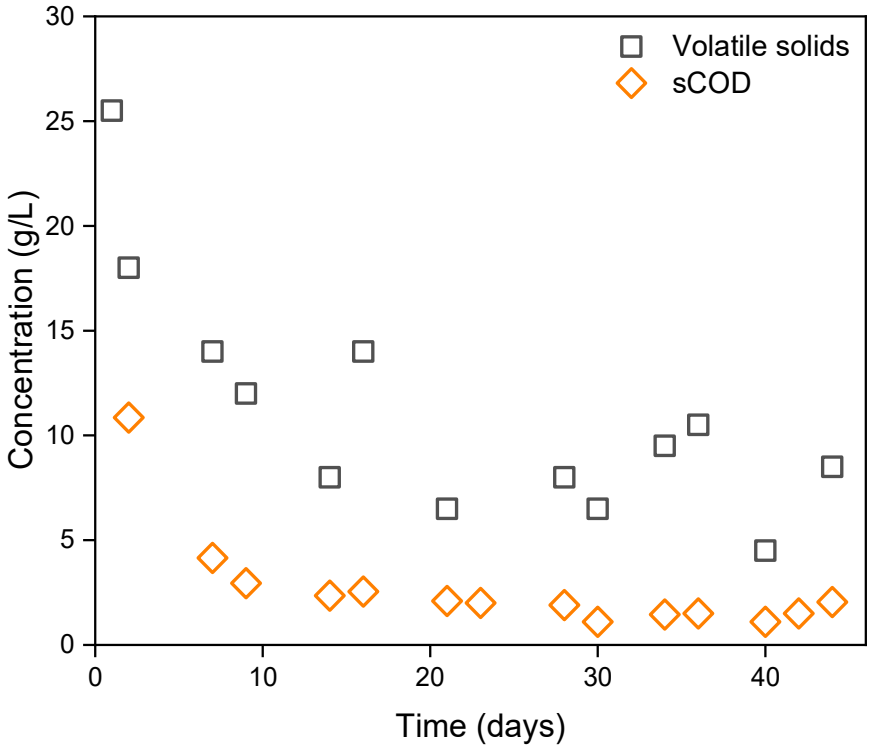


Figure 30. Volatile solids and soluble chemical oxygen demand concentration in the rumen membrane bioreactor over time. Samples were collected in a time series and one sample was collected per time.

The VFA/sCOD ratio shows how much soluble substance is converted into VFA and is commonly used as an indicator of the extent of acidification. The average extent of acidification in the rumen-MBR was 36.4 ± 10.3 % (Figure 29). This value is comparable with the extent of acidification of 40.6% in the rumen fluid inoculum (shown as day 0 in Figure 29), indicating the ability of the rumen-MBR to simulate natural rumen. Due to the recalcitrant structure of lignocellulosic biomass, a higher extent of acidification would be hard to achieve, unless optimal operating conditions or substrate/inoculum pre-treatment are applied. For example, Wang et al. (386) acclimated their inoculum with oilseed rape straw's leachate for 5 months before utilization and observed a 60% extent of acidification during anaerobic digestion of the substrate. A similar extent of acidification was recorded by Kullavanijaya et al. (387) when they performed leachate recirculation to enhance hydrolysis and acidogenesis rates of Napier grass in an anaerobic leach bed reactor.

### 6.3.5. Volatile fatty acids transfer to the permeate

The UF membrane module (0.04 µm nominal pore size) achieved an average transfer ratio of 73 ± 15 % for TVFA (n = 8) (Figure 31). This is the first study to report the continuous transfer of TVFA directly from a rumen reactor using a UF membrane. The transfer ratio observed in this

study was comparable to that of an electrodialysis system (75 %) used by Pan et al. (374) to extract acetic, propionic and butyric acid from fermentation broth. Higher transfer ratios (up to 99%) have been reported in other studies using different extraction methods (e.g. nanofiltration, membrane contractor, solvent extraction) (384). Nevertheless, it is worth mentioning that in these studies the VFA recovery step was separated from VFA production and/or pre-treatment of the broth was performed before recovery (372-374). Overall, the ability of the UF membrane to allow continuous and effective VFA transfer from the rumen-MBR contributes to the system's practical feasibility.

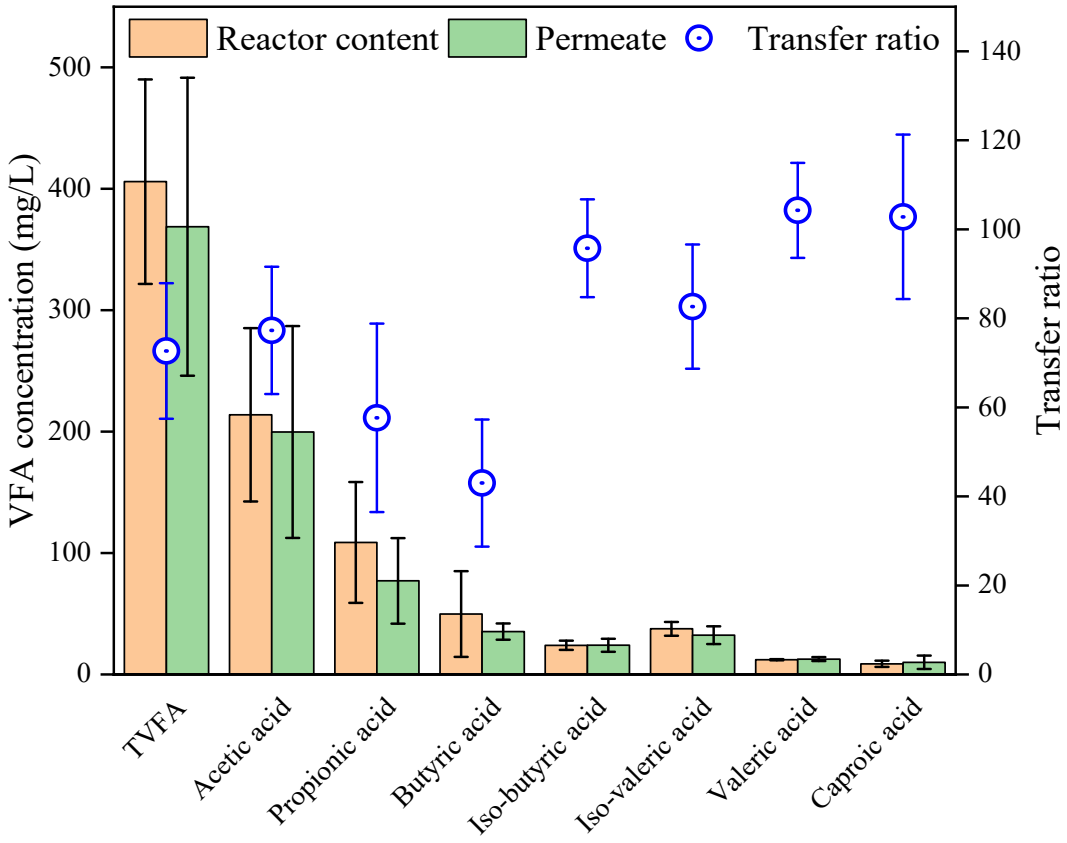


Figure 31. Transfer ratio for total volatile fatty acids and individual volatile fatty acids species. The error bar represents the standard deviation of at least 2 measurements.

The specific transfer ratio for individual VFA was 43 ± 14% for butyric acid, 58 ± 21% for propionic acid, 77 ± 14% for acetic acid, 96 ± 11% for iso-butyric acid, 104 ± 11% for valeric acid, 83 ± 14% for iso-valeric acid and 103 ± 18% for caproic acid (Figure 31). These numbers are comparable with previous studies on membrane filtration for fermentation products recovery. Alexandri et al. (388) reported that 78.5 % lactic acid could be recovered (21.5% loss) by microfiltration module from the fermentation broth of crust bread hydrolysate, while Tessier et al. (389) showed a transfer rate of 81 – 91% of benzylpenicillin from the fermentation broth of

cheese whey liquor using UF membranes. Specific VFA transfer ratio could be enhanced through optimization of filtration conditions (e.g. initial flux/pressure applied, cross-flow velocity, pH).

The UF membrane module was able to operate continuously during the experimental period, which can be explained by the low operating filtration flux applied to the membrane (~2 L/m$^2$h). This flux was relatively low compared to the membrane's typical filtrate flux range (~60 L/m$^2$h) as specified by the manufacturer. However, membrane fouling might become a challenging issue for large-scale operation of rumen-MBR with higher applied pressure/permeate flux and higher loading rates, as fouling can significantly escalate the cost of the process. Tessier et al. (389) observed significant fouling (indicated by up to 74% decrease of permeate flux) after 22 – 34 minutes of UF filtration of cheese whey liquor fermentation broth (initial flux of 65 L/m$^2$h). Therefore, the effect of substrate loading rate and membrane fouling on VFA production from lignocellulosic substrates using the rumen-MBR needs to be investigated in future studies.

### 6.3.6. Rumen microbes and their fates during rumen-MBR operation

#### *6.3.6.1. Rumen microbes' prominent capacity for LCBM degradation*

Rumen fluid inoculum in this study harbours various cellulose-degrader and in total, they accounted for 22.2% of the microbial community (Table 13). Cellulolytic bacteria in this study's inoculum target different components of LCBM. For example, some bacteria digest both cellulose and hemicellulose (xylan), e.g *Ruminococcaceae* (366), some attack hemicellulose and pectin, e.g. *Prevotella* and *Butyrivibrio* (390, 391), while some only degrade cellulose, e.g. *Fibrobacter* (392). This is because each bacterial strain can only produce specific enzyme(s) targeting specific substrate(s). The synergy between multiple cellulolytic bacteria in rumen fluid is the key to efficient degradation of the lignocellulosic substrate.

Table 13. Relative abundances and ecological function of dominant taxa in the rumen fluid inoculum.

| **Functional group** | **Taxon** | **Relative abundance (%)** | **Specific role** | **Reference** |
|---|---|---|---|---|
| Cellulolytic bacteria | *Ruminococcaceae* | 13.3 | degrade cellulose, xylan | Flint et al. (366) |
| | *Prevotella* 1 | 7.5 | degrade xylan, pectin | Krause et al. (390) |
| | *Butyrivibrio* 2 (*Lachnospiraceae*) | 0.5 | degrade xylan, pectin | Palevich et al. (391) |
| | *Fibrobacter* | 0.4 | degrade cellulose | Ransom-Jones et al. (392) |
| | *Pseudobutyrivibrio* (*Lachnospiraceae*) | 0.2 | degrade xylan, pectin | Palevich et al. (391) |
| Non-cellulolytic bacteria | Other *Lachnospiraceae* | 13.2 | acetogenic bacteria | Gagen et al. (393) |
| | *Succiniclasticum* | 10.4 | convert succinate to propionate | Van Gylswyk (394) |
| | Unassigned *Clostridiales* | 7.1 | fermentative bacteria | Nguyen et al. (66) |
| | *Olsenella* | 7.2 | fermentative bacteria | Kraatz et al. (395) |
| | *Corynebacteriaceae* | 3.7 | ferment amino acids | Oliveira et al. (396) |
| | *Veillonellaceae* UCG-001 | 2.0 | fermentative bacteria | Kishimoto et al. (397) |
| | *Acetitomaculum* | 1.3 | acetogenic bacteria | Le Van et al. (398) |
| Methanogens | *Methanobrevibacter* | 14.8 | hydrogenotrophic | Janssen et al. (399) |

| | | | |
|---|---|---|---|
| | *Methanosphaera* | 0.6 | hydrogenotrophic |
| | Unassigned *Methanobacteriaceae* | 0.2 | hydrogenotrophic |

The most dominant cellulolytic taxa in the inoculum were *Ruminococcaceae* (relative abundance of 13.3%) and *Prevotella* (relative abundance of 7.5%), which have been commonly detected in the rumen of various ruminants and other foregut fermenters across the globe (400). Members of *Ruminococcaceae* have been reported to have superior substrate attachment ability compared to other taxa species, comprehensive collections of glucosidase enzymes with high catalytic activity and versatility, as well as novel cell surface-anchored cellulose-binding protein which enhances their degradation capacities (366, 367). Meanwhile, *Prevotella* strains produce a wide range of enzymes (390) that are specialized for hemicellulose and pectin degradation, and this taxon work alongside *Ruminococcaceae* to fully break down lignocellulosic substrates. *Butyrivibrio*, *Fibrobacter*, and *Pseudobutyrivibrio* also contribute to the cellulolytic activity of the rumen inoculum (391, 392), but to a lesser extent than *Ruminococcaceae* and *Prevotella* due to their low relative abundances (< 0.5%).

Other dominant taxa detected in the rumen fluid inoculum are non-cellulolytic microbes that function synergistically with cellulolytic bacteria (Table 13). These microbes including fermenters (*Olsenella*, unassigned *Clostridiales*, *Veillonellaceae* UCG-001, *Corynebacteriaceae*), acetogens (other *Lachnospiraceae*, Succiniclasticum and *Acetitomaculum*) and hydrogenotrophic methanogens (*Methanobrevibacter*, *Methanosphaera* and unassigned *Methanobacteriaceae*) quickly utilize products of cellulolytic bacteria to prevent the feedback inhibition (368). Together, the microbial composition and synergistic interactions between different functional groups in the rumen fluid make it an ideal inoculum source for an engineered system degrading LCBM. This is in agreement with results from a previous study where the superior ability of rumen fluid to degrade lignocellulosic substrates compared to another inoculum (i.e. anaerobic sludge) has been pinpointed to its unique microbial community (368).

### *6.3.6.2. Shifts in microbial composition during rumen-MBR operation*

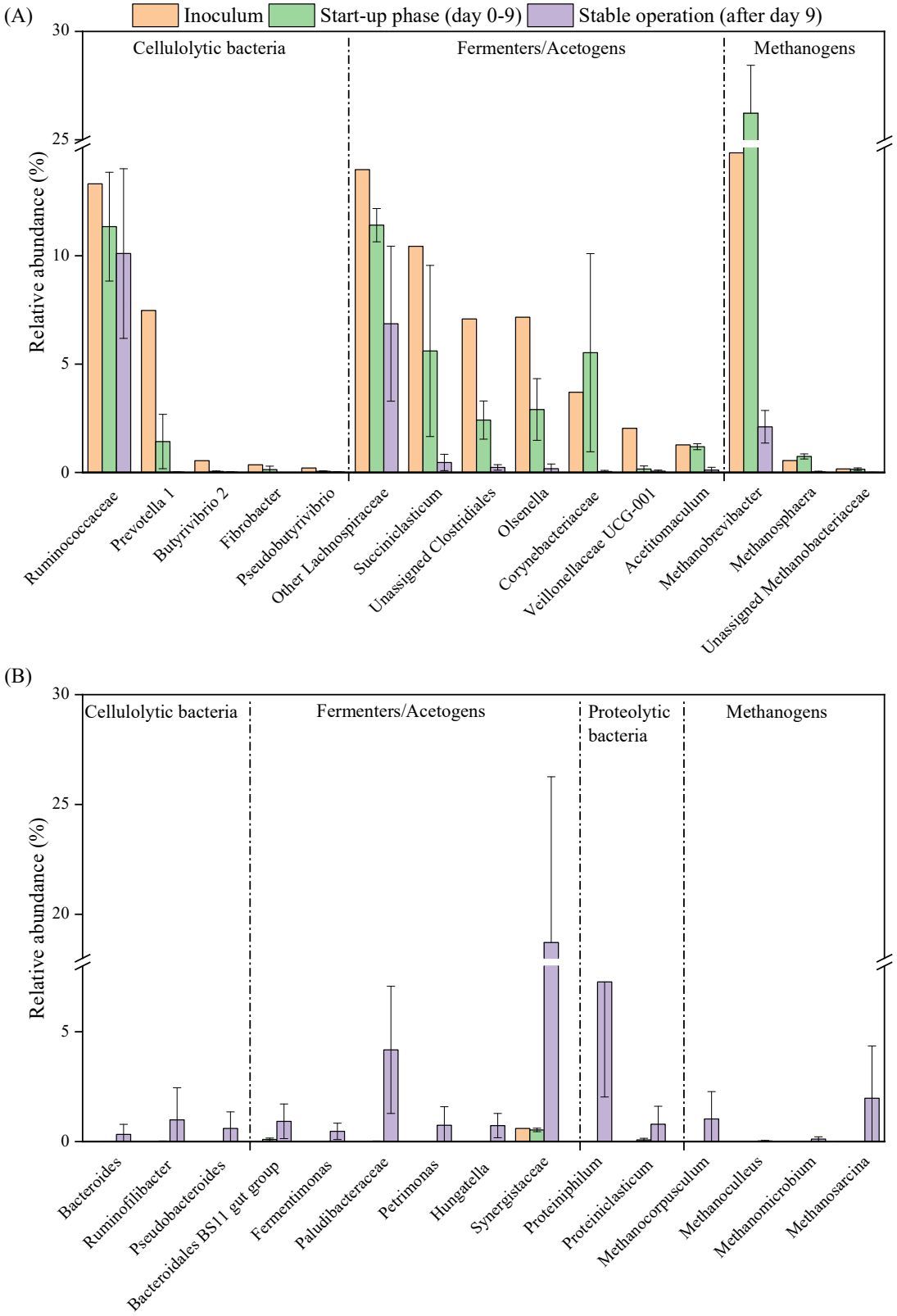


Figure 32. Changes in the relative abundance of dominant taxa from the inoculum during operation of the rumen membrane bioreactor (A) and functional redundancy in the rumen membrane bioreactor are indicated by the emergence of novel functional taxa (B). The error bar

represents the standard deviation of 4 samples for the start-up phase and 10 samples for stable operation phase.

Most dominant taxa in the inoculum showed decreases in their relative abundances during the start-up period of the rumen-MBR (the first 9 days) (Figure 32A). Changes in the microbial community are expected since the *in vitro* environment cannot perfectly simulate the natural environment. This decrease was also accompanied by a reduced diversity level (Table 14), which was also reported in previous studies (401, 402). Specifically, decreases of 19.3% in community richness (Observed ASVs) and 10.5% in evenness (Shannon index) compared to the inoculum were observed in the rumen-MBR during the start-up period. Together these changes explained for the decrease in VFA yield observed during the first 9 days of the experiment.

Table 14. Changes in apha diversity indices of the rumen-MBR microbial community. The percentage decrease (%) calculation was normalized against the values from the inoculum. The error bar represents the standard deviation of 4 samples for the start-up phase and 9 samples for stable operation phase.

| **Index** | **Inoculum** | **Start-up phase (day 0 – 9)** | **% decrease** | **Stable operation (day 10 – 44)** | **% decrease** |
|---|---|---|---|---|---|
| Observed ASVs | 1905 | 1537.3 ± 220.2 | 19.3 | 692.1 ± 107.4 | 63.7 |
| Shannon index | 9.3 | 8.4 ± 0.5 | 10.5 | 5.5 ± 0.4 | 41.0 |

Further decrease in the relative abundance of inoculum's dominant taxa was recorded during the remaining period of the experiment (Figure 32A). These data reflect the experiment selection pressure on the community, where taxa that cannot adapt to the new environment will be eliminated or replaced by other taxa. This was confirmed by sharp decreases in microbial diversity indices (Table 14). The decrease of dominant ruminal taxa can also be attributed to the dilution of the original rumen fluid inoculum. Rumen fluid contains specific nutrients that are essential for the growth of many ruminal microbes, such as hemin for *P. ruminicola*, 3-phenylpropanoic acid for *R. albus*, and mercaptoethanesulfonic acid for *Methanobrevibacter ruminantium* (403). This is the reason why clarified rumen fluid is often supplemented to cultivation media of ruminal bacteria. Meanwhile, in the rumen-MBR the inoculum liquid was continuously diluted by the artificial saliva and thus negatively affected the abundance of inoculum's indigenous taxa.

The rumen-MBR ability to maintain stable performance despite the changes in microbial composition can be attributed to the microbial community functional redundancy. Functional redundancy means multiple taxa can perform the same ecological function (66). Indeed, novel

cellulolytic bacteria such as *Bacteroides* and *Ruminofilibacter* emerged in the rumen-MBR (Figure 32B) to compensate for the reduction of *Ruminococcaceae* and *Prevotella*. Multiple bacteria belong to the order *Bacteroidales* and *Synergistaceae* were also enriched to take over the role in fermentation and acetogenesis steps. Microbial adaptation to the experimental conditions was also indicated by the significant growth of proteolytic bacteria (*Proteiniphilum* and *Proteiniclasticum*) that can utilize the protein content of the concentrate feed. In contrast, there was only a low presence of methanogens in the rumen-MBR after the start-up period (Figure 32B). Methanogens are more susceptible to environmental changes than bacteria and their slow-growing rates make it harder for them to recover after disturbance (66). The decrease in methanogens abundance explains the negligible methane production observed during the experiment.

Other taxa with promoted growth during the operation of the rumen-MBR are also commonly found in the rumen of cow and yak, however, they have unclear functions. These taxa includes *Christensenellaceae* R-7 group (4.4 ± 1.1%), *Rikenellaceae* RC9 gut group (3.0 ± 1.7%), uncultured *Bacteroidales* bacterium Bact_22 (1.7 ± 2.0%), uncultured *Pedosphaeraceae* (0.9 ± 0.8%) and uncultured *Tannerellaceae* (0.7 ± 1.5%) (404, 405). Their high relative abundances and the consistency in their presence in the rumen as previously reported suggest that they play key roles in the rumen digestion of process.

## 6.4. Conclusion

This study demonstrates the proof-of-concept of a rumen-MBR for continuous VFA production from LCBM with an average daily yield of 438 mg/g substrate. The produced VFA contains mostly acetic and propionic acids (over 80% in combined molar fraction). These low molecular weight organic acids can replace petroleum-based raw chemicals in the future. Membrane separation offers a promising solution for VFA removal from the reactor with an average transfer ratio of 73±15%. Shifts in the microbial composition of the rumen-MBR during the stable operation were observed, indicating the role of functional redundancy to support VFA yield.

# Chapter 7. CHIRAL INVERSION OF 2-ARYLPROPIONOIC ACID (2-APA) ENANTIOMERS DURING SIMULATED BIOLOGICAL WASTEWATER TREATMENT

This chapter has been published as the following journal article.

Nguyen AQ, Nguyen LN, McDonald JA, Nghiem LD, Leusch FDL, Neale PA, et al. Chiral inversion of 2-arylpropionic acid (2-APA) enantiomers during simulated biological wastewater treatment. Water Research. 2021:117871.

**Summary:** This study examined the removal and enantio-specific fate of a suite of eleven chiral 2-arylpropionoic acids (2-APAs) during biological wastewater treatment simulated in a laboratory-scale membrane bioreactor (MBR). Using pure (*R*)- and (*S*)- enantiomers in the MBR influent, chiral inversion was determined through the increase in the concentration of the non-dominant enantiomer and changes in the enantiomeric fraction (EF) between the two enantiomers during the treatment process. Effective (> 90%) and similar removal rates between (*R*)- and (*S*)-enantiomers were confirmed for eight 2-APAs. In this study, 2-APAs exhibited diverse and distinctive chiral inversion behaviours: two 2-APAs showed (R→S) unidirectional inversion, three 2-APAs showed (S→R) unidirectional inversion, and six 2-APAs showed bidirectional inversion. This is the first study to report chiral inversion behaviours of a comprehensive suite of 2-APAs with a variety of functional groups substituted onto the aryl ring. A decrease in effluent EF over time was observed for two 2-APAs. This study shows that chiral inversion of 2-APAs varies significantly from compound to compound, despite the high similarity in their chemical structures.

## 7.1. Introduction

Approximately 50% of marketed pharmaceuticals are chiral chemicals (406, 407). There is a growing body of evidence to suggest the ecological implications of some pairs of chiral pharmaceuticals may be variable (214). For example, enantiomers of some widely prescribed pharmaceuticals can have significantly different toxic impacts to model aquatic organisms used in ecotoxicity studies (408-410). However, the vast majority of reported occurrences of pharmaceuticals in the environment do not differentiate between enantiomeric pairs and the role of chirality in their behaviour is generally not studied (411, 412).

2-APAs are a group of chemicals, which include some important non-steroidal anti-inflammatory drugs (NSAIDs), *e.g.*, ibuprofen, ketoprofen, naproxen, and flurbiprofen. These commonly used drugs possess anti-inflammatory and analgesic activities due to their ability to inhibit cyclooxygenase enzymes that promote inflammation (413). Their therapeutic effects have been reported to reside almost exclusively in their (*S)*-enantiomers (eutomers) rather than their (*R)*-enantiomers (distomers) (414). For example, (*S*)-ibuprofen has been reported to be 160 times

more active than (*R*)-ibuprofen (415). Due to the least-cost synthetic route of production, ibuprofen and ketoprofen are most commonly produced and consumed as racemic mixtures of their two enantiomers (407). However, enantiomerically pure (*S*)-ibuprofen (known as 'dexibuprofen') and (*S*)-ketoprofen (known as 'dexketoprofen') are also available (407). Naproxen is only ever manufactured and dispensed as (*S*)-naproxen due to concerns regarding toxicity of (*R*)-naproxen. Neale et al. (215) reported that (*R*)-naproxen is also more toxic to bacteria than (*S*)-naproxen, while (*S*)-flurbiprofen has higher bacterial toxicity and lower algal toxicity than (*R*)-flurbiprofen.

Previous investigations of the changes in EF of emerging contaminants during wastewater treatment have generally assumed that such changes have been solely the consequence of more rapid degradation of one enantiomer relative to the other, termed "enantioselective degradation" (416-419). This assumption may be correct for some chemicals, but an alternative explanation for at least some of the changes in EF may be chiral inversion of one enantiomer to the other. Such processes are well known for some pharmaceuticals during mammalian metabolism (414, 420).

Distinguishing between enantioselective degradation and chiral inversion (in addition to biodegradation) is difficult when racemic mixtures of enantiomeric pairs are examined in biological systems, since either process could lead to reduced concentrations of both enantiomers (214, 421). However, controlled experiments with an enantiomerically pure 2-APA pharmaceutical (naproxen) have revealed that enantiomeric inversion can be observed during simulated biological wastewater treatment processes (422).

Subsequently, enantio-specific analyses of effluents from municipal WWTPs and untreated sewage have provided similar insights. For example, in one study, (*R*)-naproxen was below the method limit of quantification (LOQ) (<1 $ng.L^{-1}$) in untreated sewage but measurable at higher concentrations in WWTP effluents, suggesting that it was produced during wastewater treatment (219). Similarly, a study comparing enantiomeric compositions of naproxen found exclusively (*S*)-naproxen in surface waters from Pakistan where no sewage treatment processes operate, but traces of (*R*)-naproxen in the effluents of a WWTP in Germany (423). That study also reported an identical trend for the naproxen metabolite *o*-desmethyl-naproxen. Despite these observations indicating the occurrence of chiral inversion of naproxen during biological wastewater treatment processes, it is unclear whether equivalent inversion occurs for other 2-APA chemicals.

The aim of this study was to determine whether chiral inversion could be observed for a broader range of 2-APAs during simulated biological wastewater treatment. Furthermore, the study was designed to reveal the direction of chiral inversion, including the possibility that it may occur bidirectionally. Finally, the range of 2-APAs selected for inclusion in this study was intended to

provide insights into the influence of various molecular structures on the observed chiral inversion or biodegradation of 2-APAs.

## 7.2. Materials and Methods

### 7.2.1. Chemicals and consumables

Enantiomerically pure (>95%) 2-APAs analytical standards were used in all experiments. A total of 22 analytes were used, comprising (*R*)- and (*S*)- enantiomers of each of eleven 2-APAs were used, as listed in Table 15.

Table 15. Physicochemical properties of chiral compounds used in this study (data were obtained from the SciFinder database).

| Compound | Molecular structure | Molecular weight (g/mol) | Log *D* at pH 6 25°C | $pK_a$ |
|---|---|---|---|---|
| (*R*)-2-Phenylpropionic acid<br>(*S*)-2-Phenylpropionic acid | 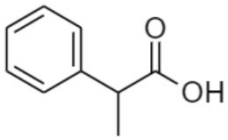 | 150 | 0.04 | 4.3 |
| (*R*)-2-(4-Fluorophenyl)propionic acid<br>(*S*)-2-(4-Fluorophenyl)propionic acid | 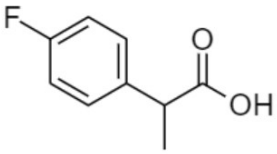 | 168 | 0.29 | 4.3 |
| (*R*)-2-(4-Methoxyphenyl)propionic acid<br>(*S*)-2-(4-Methoxyphenyl)propionic acid | 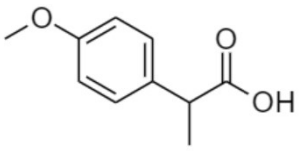 | 180 | 0.32 | 4.5 |
| (*R*)-2-(3-Chlorophenyl)propionic acid<br>(*S*)-2-(3-Chlorophenyl)propionic acid | 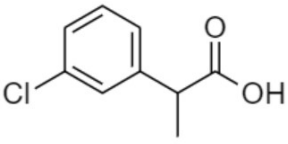 | 185 | 0.58 | 4.2 |
| (*R*)-2-(3-Methylphenyl)propionic acid | 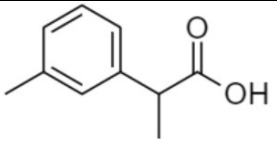 | 164 | 0.66 | 4.4 |

| Compound | Molecular structure | Molecular weight (g/mol) | Log *D* at pH 6 25°C | $pK_a$ |
|---|---|---|---|---|
| (*S*)-2-(3-Methylphenyl)propionic acid | | | | |
| (*R*)-2-(4-Chlorophenyl)propionic acid<br>(*S*)-2-(4-Chlorophenyl)propionic acid | 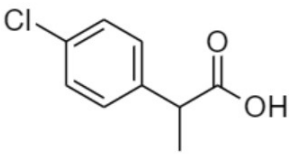 | 185 | 0.68 | 4.2 |
| (*R*)-Ketoprofen<br>(*S*)-Ketoprofen | 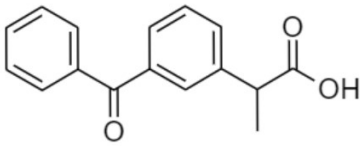 | 254 | 1.14 | 4.2 |
| (*R*)-Naproxen<br>(*S*)-Naproxen | 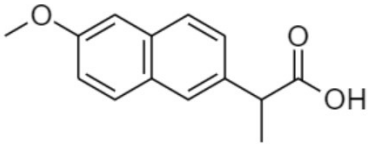 | 230 | 1.69 | 4.8 |
| (*R*)-Flurbiprofen<br>(*S*)-Flurbiprofen | 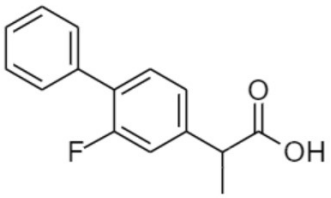 | 224 | 1.80 | 4.1 |
| (*R*)-2-(4-*n*-Butylphenyl)propionic acid<br>(*S*)-2-(4-*n*-Butylphenyl)propionic acid | 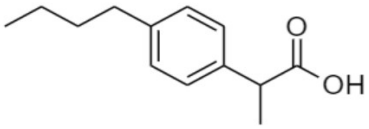 | 206 | 2.08 | 4.4 |
| (*R*)-2-(4-*tert*-Butylphenyl)propionic acid<br>(*S*)-2-(4-*tert*-Butylphenyl)propionic acid | 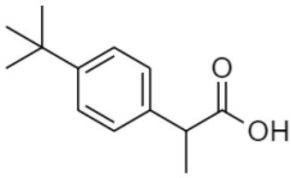 | 206 | 2.23 | 4.5 |

(*R*)-2-(3-Chlorophenyl)propionic acid, (*S*)-2-(3-chlorophenyl)propionic acid, (*R*)-2-(4-chlorophenyl)propionic acid, (*S*)-2-(4-chlorophenyl)propionic acid, (*R*)-2-(4-*tert*-

butylphenyl)propionic acid, and (*S*)-2-(4-*tert*-butylphenyl)propionic acid were purchased from Chem-Space (Monmouth Junction, NJ, USA). (*R*)-2-(4-Fluorophenyl)propionic acid, (*S*)-2-(4-fluorophenyl)propionic acid, (*R*)-2-(3-methylphenyl)propionic acid, (*S*)-2-(3-methylphenyl)propionic acid, (*R*)-2-(4-methoxyphenyl)propionic acid, (*S*)-2-(4-methoxyphenyl)propionic acid, (*R*)-2-(4-*n*-butylphenyl)propionic acid and (*S*)-2-(4-*n*-butylphenyl)propionic acid were purchased from eMolecules (San Diego, CA, USA). (*R*)-Naproxen, (*R*)-ketoprofen, and (*S*)-flurbiprofen were purchased from Sapphire Bioscience. (*R*)-2-Phenylpropionic acid, (S)-2-phenylpropionic acid, (*S*)-naproxen, (*S*)-ketoprofen, and (*R*)-flurbiprofen were purchased from Sigma-Aldrich (St. Louis, MO, USA). Racemic D3-naproxen, D3-ketoprofen, and D3-flurbiprofen were purchased from CDN Isotopes (Pointe-Claire, Quebec, Canada).

Solvents and reagents used in sample preparation were either analytical grade or of a purity > 98%. Acetonitrile (ACN), dichloromethane (DCM), methanol, triethylamine (TEA), ethylchloroformate, (*R*)-1-phenylethylamine (PEA), sulphuric acid, and sodium hydroxide were purchased from Sigma-Aldrich (Castle Hill, NSW, Australia). Water used in analysis was obtained from a Waters Milli-Q Water Purification unit (Millford, CT, USA).

Stock solutions of individual 2-APA enantiomers (approximately 1 g/L) and derivatisation reagents were prepared in anhydrous ACN and stored at 4°C in the dark. From these individual solutions, two working stocks of mixed 2-APAs for calibration standards and experiments were prepared in anhydrous ACN and stored at 4°C in the dark. One stock solution contained pure (*R*)-enantiomers. The other stock solution contained pure (*S*)-enantiomers. As directly analogous internal standards (ISTDs) were not available for some target analytes racemic, a solution of racemic D3-naproxen was prepared in anhydrous ACN at a concentration of 1 mg/L for use as the ISTD.

### 7.2.2. Laboratory-scale membrane bioreactor system

Two identical aerobic MBR systems were operated in parallel. Each system consisted of a 4 L glass reactor and a submerged hollow fibre polyvinylidene difluoride (PVDF) membrane module (Mitsubishi Rayon, Japan) (Figure 33). The membrane module had a nominal pore size and effective surface area of 0.04 μm and 0.073 $m^2$, respectively. A high-resolution pressure sensor (±0.1 kPa, John Morris Group, Australia) was fixed between the membrane module and the suction pump for continuous monitoring of transmembrane pressure (TMP). The two glass reactors were placed in a temperature-controlled water bath to maintain a constant temperature using a temperature control unit (Thermoline, Australia) equipped with a stainless-steel heat exchanging coil. Peristaltic pumps (Masterflex L/S, USA) were used for feeding and permeate extraction, and the reactors' working volumes were maintained at 3 L. Compressed air was used

to aerate the MBR system via diffusers located at the bottom of the reactor at a flow rate of 400 mL/min using an air pump (AquaOne, Australia).

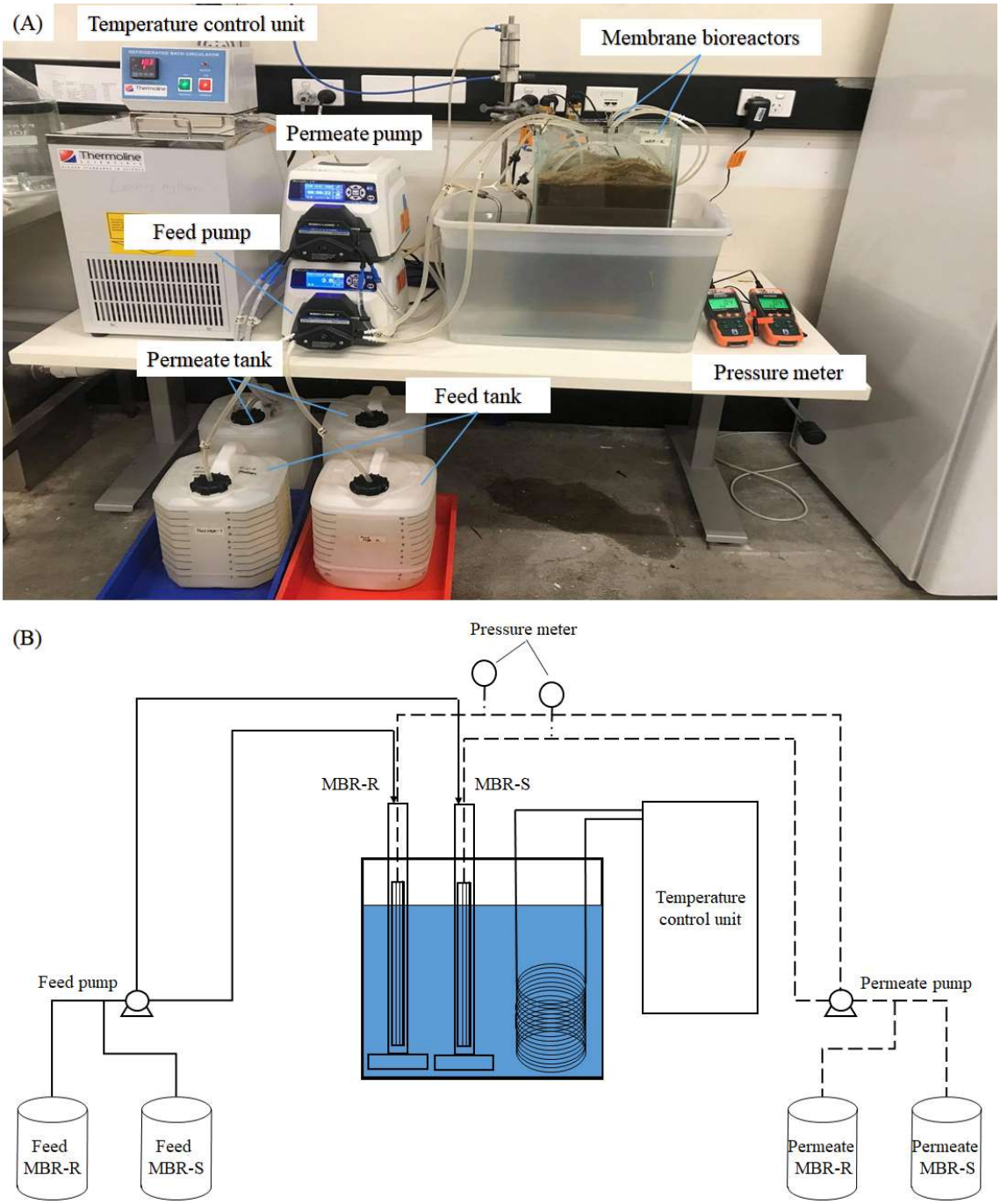


Figure 33. (A) Photo and (B) schematic diagram of laboratory-scale membrane bioreactor systems.

### 7.2.3. MBR experimental protocol

Activated sludge from a full-scale wastewater treatment plant at Sydney Olympic Park (NSW, Australia) was used to inoculate the two MBRs. Synthetic wastewater was used to simulate medium-strength municipal sewage with chemical oxygen demand (COD): total nitrogen: total

phosphorus = 150: 6.5: 1. The concentrated synthetic wastewater was prepared weekly and stored in a refrigerator at 4°C. It was then diluted with tap water on a daily basis to make up a feed solution (influent) containing per litre: glucose (600 mg), peptone (100 mg), urea (35 mg), $KH_2PO_4$ (17.5 mg), $MgSO_4$ (17.5 mg), $FeSO_4$ (10 mg), and sodium acetate (225 mg). The membrane module was operated with 9 min "suction" and 1 min "relaxation" at an average flux of 3.4 LMH.

Chiral 2-APAs were continuously introduced to the MBR influent at a concentration in the range of 1-10 µg/L of each compound. One MBR was dosed with only (*R*)-enantiomers (denoted as MBR-R) and the other MBR was dosed with only (*S*)-enantiomers (denoted as MBR-S).

Samples were collected twice a week to monitor the performance of the two MBRs in terms of standard water quality and operating parameters including pH, dissolved oxygen (DO) concentration, total organic carbon (TOC), mixed liquor suspended solids (MLSS), mixed liquor volatile suspended solids (MLVSS). MLSS and MLVSS were measured according to the Standard Methods for Examination of Water and Wastewater. TOC was analysed using a TOC-$V_{CSH}$ analyser (Shimadzu, Japan). pH and DO of the mixed liquor were monitored using a portable pH/conductivity meter (Hach, Australia). The temperature and DO concentration of both MBRs were maintained at 20.0 ± 0.1°C and above 3 mg/L, respectively. The hydraulic retention time (HRT) was kept at 12 h. Sludge withdrawal was not conducted except for sample collection for analysis purposes, resulting in a sludge retention time of 133 days. Prior to the addition of 2-APAs to the influent, the two MBR systems were operated for approximately two months for acclimatisation to achieve stable and identical performance.

### 7.2.4. Chiral compounds extraction and diastereomer preparation

Duplicate samples of the influent and effluent (500 mL each) were collected on days 1, 4, 7, 10, 14, and 18 after dosing with enantiomerically pure solutions of chiral 2-APAs. Duplicate mixed liquor samples (400 mL) were also collected at the end of the experiment for analysis of chiral 2-APAs in the mixed liquor and sludge phase.

Chiral 2-APAs were extracted from aqueous samples and converted into their respective *R,R* and *R,S*-phenylethylamide diastereomers following a previously described derivatisation method (221) with slight modifications in elution solvent selection. Briefly, samples (500 mL) were acidified to approximately pH 3-4 using sulphuric acid 4M and 50 µL of the ISTD was added. Solid-phase extraction (SPE) was performed using Oasis 500 mg and 60mg hydrophilic/lipophilic balance (HLB) cartridges purchased from Waters (Millford, CT, USA) within 24 h of sample collection. HLB SPE cartridges were pre-conditioned with 5 mL methanol and 5mL Milli-Q water. All samples were then loaded onto the cartridges under vacuum pressure at a flow rate less than 15 mL/min, rinsed with 20 mL Milli-Q water, dried with air at room temperature for 20 min,

and stored at 4°C prior to elution and chiral analysis. Analytes were eluted off the cartridges using a 1:3 ACN/DCM mixture (2 × 3 mL) and combined eluants concentrated to approximately 100 µL under nitrogen. The residue was reconstituted in 300 µL ACN, treated with 30 µL of TEA 50 mM, 40 µL ethyl chloroformate 60 mM, and sonicated for 2 min. Subsequently, 40 µL of (*R*)-PEA 0.5 M was added and the mixture was sonicated for 2 min before the addition of 3 mL sulphuric acid 3 mM. The derivatised analytes were extracted from the mixture in a second SPE step using Oasis HLB cartridges (1 mL, 60 mg) preconditioned with methanol (1 mL) and water (1 mL) adjusted to pH 9.5 using sodium hydroxide. The loaded SPE cartridges were dried under nitrogen and the analytes were eluted using DCM (1 mL) directly into 2 mL autosampler vials prior to analysis.

### 7.2.5. Enantio-specific analysis of chiral compounds

Enantio-specific analysis of the 2-APA *R,R*- and *R,S*-(PEA) diastereomers was conducted following a method previously described by Hashim et al. (221) with some modification. Briefly, target analytes were separated using an Agilent 7890A gas chromatograph equipped with a 30 m HP5-MS (30 m × 250 µm × 0.25 µm) column under a helium flow of 1.2 mL/min. Injection inlet, interface and source temperatures were 270, 260 and 280°C, respectively. An injection volume of 1 µL was used with the inlet in split-less configuration. The oven temperature gradient program was as follows: initial: 120°C, held for 1 min, increased to 240°C at 40°C/min, then to 300°C at 5°C/min and held for 5 min having a run time of 18 min. Target analytes and isotope labelled ISTDs were identified using an Agilent 7000C triple quadrupole mass spectrometer with electron impact ionization source at voltage of 70 eV and a source temperature of 280°C. Multiple reaction monitoring (MRM) mode was employed to monitor analytes. MS1 scans of individual target analytes were performed to obtain suitable precursor ions followed by product ion scans to determine *m/z* transitions and optimise collision energies (CEs). Two MRM transitions were monitored for each target analyte and isotope labelled ISTDs. All monitored transitions and optimized CE are presented in Table 16. The first MRM transition shown was used for quantification, the second used for as a qualifier. Calibration curves showed good linearity with regression coefficients > 0.99 for all analytes. LOQ were defined as the concentration of an extracted analyte giving a signal to noise (s/n) ratio greater than 10. A LOQ of 3 ng/L was determined for all target analytes.

Table 16. Analytical method chromatographic retention times and mass spectral detection conditions.

| **Analyte** | **Retention Time (*R*),(*S*)** | **Precursor ion** | **Product ion** | **Dwell time** | **CollisionEnergy** |
|---|---|---|---|---|---|
| | (min) | (m/z) | (m/z) | (ms) | (v) |
| 2-Phenylpropionic acid PEA | 7.06, 7.25 | 252.9 | 149 | 5 | 5 |
| | | 252.9 | 105.1 | 5 | 20 |
| 2-(4-Fluorophenyl)propionic acid PEA | 6.96, 7.18 | 270.9 | 123 | 5 | 20 |
| | | 270.9 | 105 | 5 | 10 |
| 2-(3-Methylphenyl)propionic acid PEA | 7.61, 7.88 | 266.9 | 163 | 5 | 20 |
| | | 266.9 | 105 | 5 | 10 |
| 2-(3-Chlorophenyl)propionic acid PEA | 8.74, 9.1 | 286.9 | 138 | 5 | 50 |
| | | 286.9 | 105.1 | 5 | 10 |
| 2-(4-Chlorophenyl)propionic acid PEA | 8.89, 9.34 | 286.9 | 138 | 5 | 50 |
| | | 286.9 | 105.1 | 5 | 10 |
| 2-(4-Methoxyphenyl)propionic acid PEA | 9.52, 10.04 | 282.9 | 135.1 | 5 | 10 |
| | | 282.9 | 105 | 5 | 50 |
| 2-(4-*t*-Butylphenyl)propionic acid PEA | 10.2, 10.69 | 308.8 | 147.1 | 5 | 20 |
| | | 308.8 | 161.1 | 5 | 10 |

| | | | | | |
|---|---|---|---|---|---|
| 2-(4-Butylphenyl)propionic acid PEA | 11.25, 11.5 | 308.8 | 119 | 5 | 30 |
| | | 308.8 | 105.1 | 5 | 30 |
| Fluribiprofen PEA | 13.45, 13.67 | 346.9 | 185.2 | 5 | 30 |
| | | 346.9 | 105 | 5 | 30 |
| Naproxen PEA | 13.99, 14.24 | 333.2 | 171.1 | 5 | 35 |
| | | 333.2 | 185.1 | 5 | 10 |
| $D_3$-Naproxen PEA | 14.01, 14.25 | 336 | 171.1 | 5 | 30 |
| | | 336 | 188.1 | 5 | 15 |
| Ketoprofen PEA | 14.89, 15.15 | 357.3 | 105 | 5 | 25 |
| | | 357.3 | 120.1 | 5 | 10 |

Satisfactory method performance was confirmed by processing blank and fortified Milli-Q grade water samples along with experimental batches. No target analyte or ISTD was detected above LOQs in blank samples and extraction recoveries for all target analytes were within 20% of expected values in fortified samples. A fortified extracted sample triplicate gave results with a %RSD of < 5% for all target analytes verifying method precision. Target analyte concentrations were calculated using isotope dilution method with a 6-point calibration curve at 1, 5, 10, 50, 100, 500 ng/mL.

Concentrations of chiral compounds in the solid phase (sludge) were determined according to a method previously described by Wijekoon et al. (424). The solid pellets obtained from the mixed liquor after centrifugation were freeze-dried for 14 h using an Alpha 1–2 LDplus Freeze Dryer (Christ GmbH, Germany). The dried sludge was ground and 0.7 g of sludge powder was transferred to a glass test tube for extraction. The sludge powder was thoroughly mixed with methanol (7.5 mL) using a vortex mixer (VM1, Ratek, Australia) for 3 min, and ultrasonicated for 10 min at 40°C. The sample was centrifuged at 3270×g for 10 min (Alleegra X-12R, Beckman Coulter, USA) and the supernatant was collected in a glass beaker for further analysis. A DCM and methanol mixture (1:1 v/v) (7.5 mL) were added to the remaining sludge, and the process of mixing, ultrasonic extraction, and centrifugation was repeated. The supernatants from both steps were combined, and residual methanol and DCM were purged using nitrogen gas. Finally, Milli-Q water was added to obtain a 500 mL aqueous sample. This sample was then analysed using the analytical method used for aqueous samples described above.

### 7.2.6. Calculation of removal efficiency and enantiomeric fraction

The EF was calculated as follows:

$$EF = \frac{C_M}{C_M + C_O} \qquad \text{Equation 1}$$

Where: $C_M$ is the concentration of the main enantiomer dosed into the reactor i.e. (*R*)-2-APAs for MBR-R and (*S*)-2-APAs for MBR-S, CO is the concentration of the other enantiomer. The EF of all influent samples ranged from 0.97 – 1.00, confirming the purity of enantiomers used in this study.

The removal efficiency of an enantiomer was defined as:

$$\text{Overall removal} = 100 \times \frac{C_F - C_P}{C_F} \qquad \text{Equation 2}$$

Where: $C_F$ and $C_P$ are concentrations of the enantiomer in the MBR feed (influent) and permeate (effluent), respectively. When an enantiomer was not detected, the analytical technique LOQ of 3 ng/L was assigned to concentration value for removal efficiency calculation. Chiral inversion

results in a higher concentration of a specific enantiomer in the effluent than influent, and thus, negative removal of the enantiomer.

The overall removal of an enantiomer can be accounted for by chiral inversion and biotransformation/biodegradation. The percentage accounted by each process was calculated as follows:

$$\text{Chiral inversion (\%)} = 100 \times \frac{C_{OP} - C_{OF}}{C_{MF}} \quad \text{Equation 3}$$

$$\text{Biotransformation (\%)} = \text{Overall removal} - \text{chiral inversion} \quad \text{Equation 4}$$

Where: $C_{MF}$ is the concentration of the main enantiomer in the feed (influent), $C_{OF}$ and $C_{OP}$ are the concentration of the other enantiomer in the feed and permeate, respectively.

Sorption rate of chiral 2-APAs to sludge during MBR treatment was calculated by considering the ratio between the amount of 2-APA detected in sludge and the total amount dosed into the reactor:

$$\text{Sorption rate} = 100 \times \frac{C_{SL} \times V_{SL} \times M_{SL}}{C_F \times V_F \times T} \quad \text{Equation 5}$$

Where: $C_{SL}$ and $C_F$ are the average concentrations of 2-APA in the sludge and the feed. $M_{SL}$ is the sludge concentration in the reactor (g dried sludge/L). $V_{SL}$ is the volume of the reactor mixed liquor (3 L), and $V_F$ is the daily volume of feed (6 L). T was the number of days chiral 2-APAs were dosed into the reactor before sludge sample was collected for analysis (37 days).

#### 7.2.7. Assessment of abiotic changes in enantiomeric fraction

Prior to undertaking the experiments described in this manuscript, control experiments were undertaken to assess the possibility of abiotic changes in EF under laboratory conditions. These experiments involved incubation of chiral 2-APAs (ibuprofen, ketoprofen and naproxen) in laboratory-grade water for up to 21 days, followed by the same SPE and analytical determination applied in this study. These experiments confirmed no observable change in EF under normal laboratory conditions.

### 7.3. Results and Discussions

#### 7.3.1. Membrane bioreactor performance

The two MBRs showed similar performance during the start-up period (Figure 34), allowing for a systematic comparison between (*R*)- and (*S*) enantiomeric inversion during MBR treatment. The MLSS concentration increased steadily from 5.5 ± 0.1 to 9.7 ± 0.2 (n = 2) and from 5.7 ± 0.1 to 8.8 ± 0.2 g/L (n = 2) in the MBR-R and the MBR-S, respectively. Both MBRs showed high MLVSS/MLSS ratios in the range of 0.76 – 0.92, indicating a high number of active

microorganisms. High and stable TOC removal efficiency (> 94%) was achieved in both MBRs. pH of the mixed liquor were stable at 6.55 ± 0.16 (n = 42) and 6.57 ± 0.17 (n = 40) in the MBR-R and the MBR-S, respectively. DO concentration was maintained above 3 mg/L to ensure an aerobic condition in both MBRs.

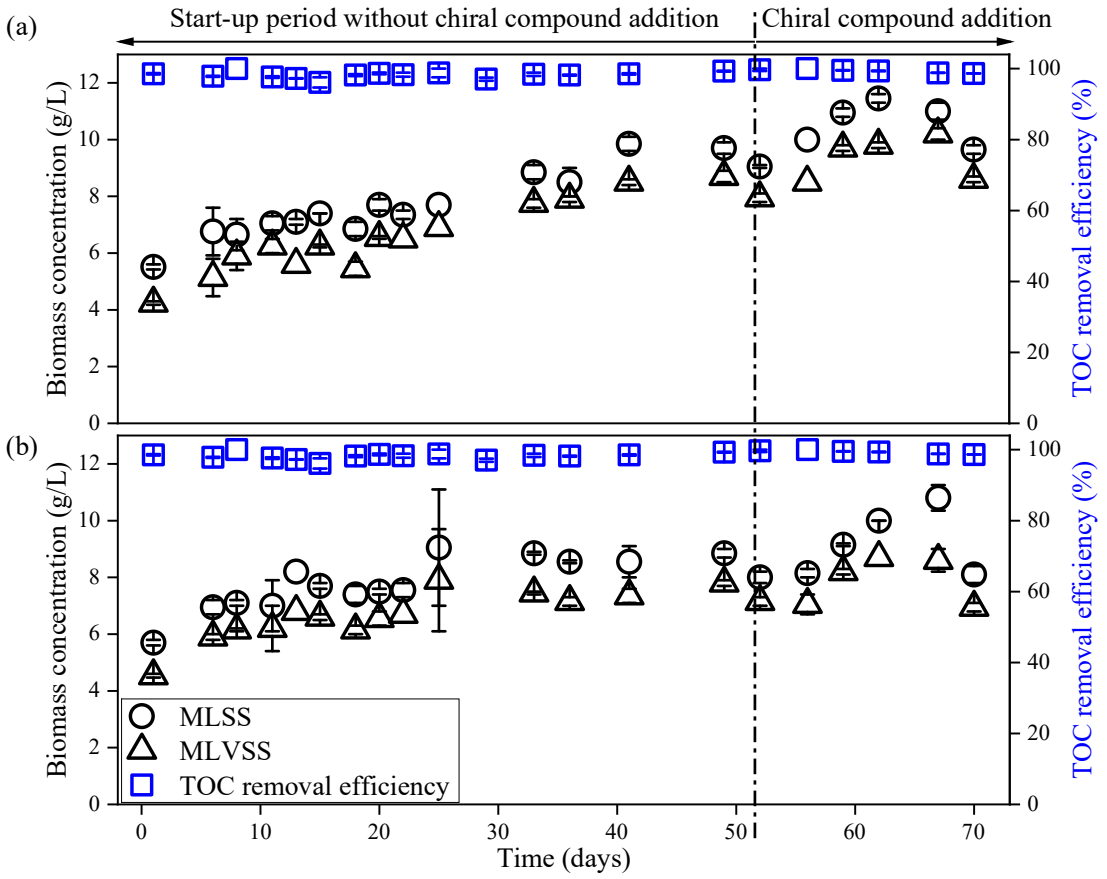


Figure 34. Biomass quality in terms of mixed liquor suspended solids (MLSS) and mixed liquor volatile suspended solids (MLVSS) and total organic carbon (TOC) removal efficiency in: (a) MBR-R receiving (*R*)-2-APAs only and (b) MBR-S receiving (*S*)-2-APAs only. The error bar represents the standard deviation from duplicate samples.

Chiral compound addition and the type of enantiomer dosed did not affect the performance of the two MBRs (Figure 34). Biomass content continued to increase to 11.5 ± 0.2 and 10.8 ± 0.5 g/L (n = 2) in the MBR-R and the MBR-S, respectively, with high MLVSS/MLSS ratio (> 0.85). TOC removal efficiency also increased to 100% during continuous dosing of chiral compounds. Stable operation of both MBRs during the chiral compound addition period allowed for clear determination of chiral inversion occurrence. There was a gradual increase in TMP in both MBRs over time from 0.8 – 1 to 5.2 – 7.6 kPa due to the increasing biomass concentrations (Figure 35). Membrane fouling was not observed during the experimental period due to the low operating flux in this study (3.4 LMH).

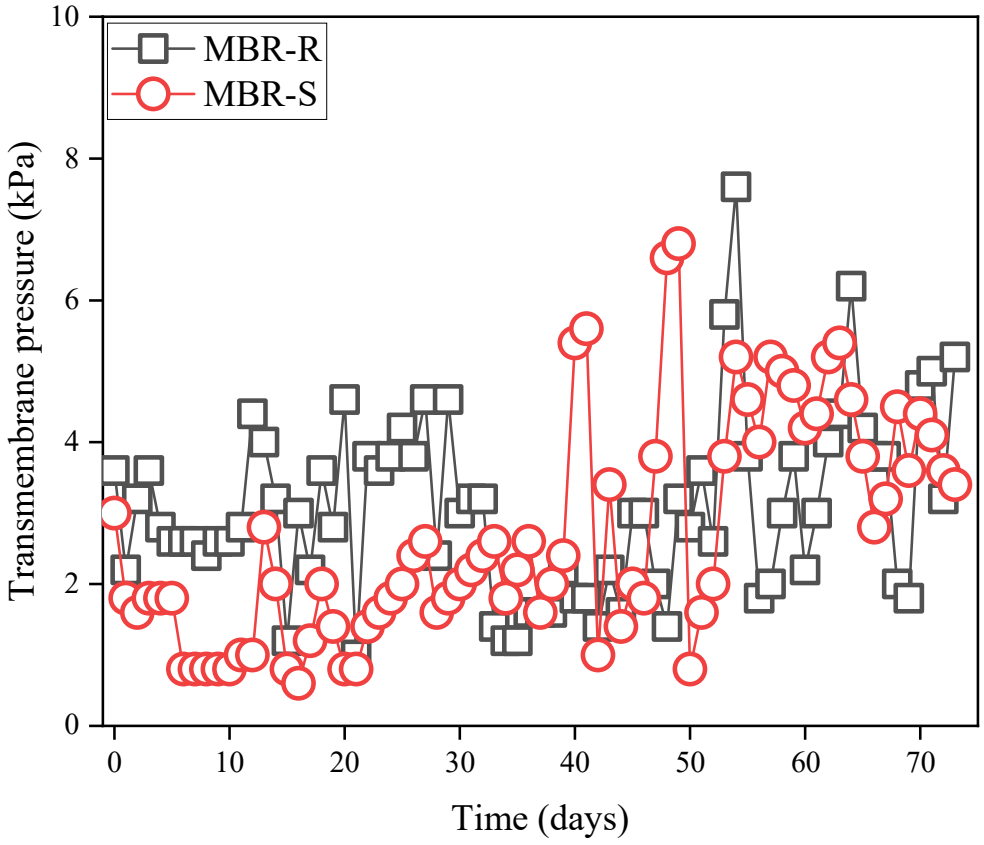


Figure 35. Transmembrane pressure in the two MBR systems during the experimental period.

### 7.3.2. Chiral compound removal efficiency

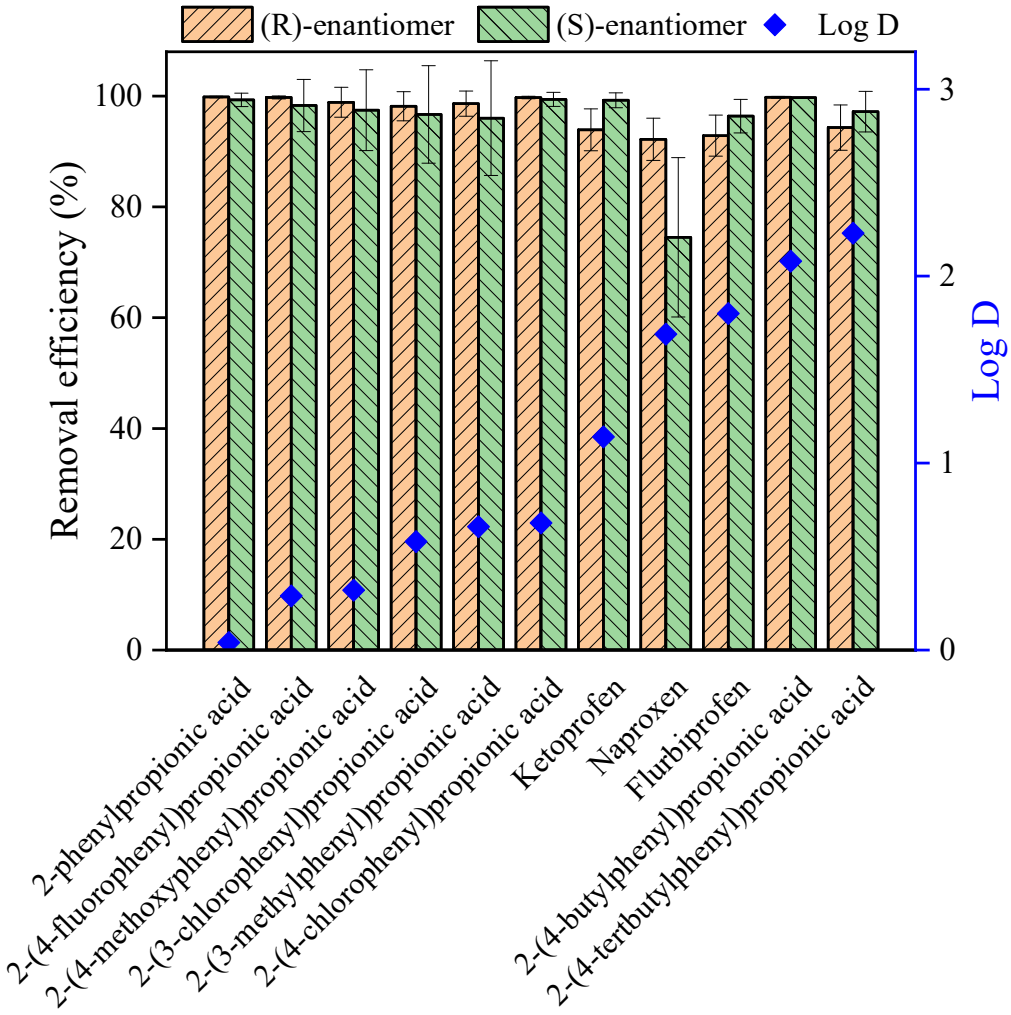


Figure 36. Removal efficiency of (*R*)-2-APAs in the MBR-R (receiving (*R*)-2-APAs only) and (*S*)-2-APAs in the MBR-S (receiving (*S*)-2-APAs only). The error bar represents the standard deviation of eleven measurements (duplicate samples taken twice a week for three weeks). Log D denotes the values at pH 6. Compounds with statistically different removal efficiency of (R)-enantiomer in MBR-R and (S)-enantiomer in MBR-S are marked with asterisks (*: p-value < 0.05, **: p-value < 0.01, ***: p-value < 0.001).

Eleven (*R*)-2-APAs (> 90%) and ten (*S*)-2-APAs (> 96%) were effectively removed in this study (Figure 36). (*S*)-Naproxen was the only exception, with the lowest removal efficiency of 74.5 ± 14.4 % (Figure 36). All compounds investigated here have the same 2-APA skeleton structure. They differ from one another by the substituent groups on the aromatic ring (Table 15). These substituent groups can affect the ability of a compound to participate in biological reactions through steric hindrance and electrostatic shielding, especially for hydrophilic and moderately hydrophobic compounds (log D < 3.2) (425, 426). Steric hindrance at a given atom in a molecule is the congestion caused by the physical presence of the surrounding groups. Steric hindrance can

affect the initial point of enzymatic attack (426) or lead to different metabolism pathways for different enantiomers, which was the case for 3-phenylbutyric acid degradation by *Rhodococcus rhodochrous* PB1 (427). Among the eleven 2-APAs, in terms of molecular structure, naproxen possesses the bulkiest substituent group, resulting in a higher steric hindrance and thus a lower removal efficiency. Naproxen also possesses a polynuclear structure (two fused aromatic rings) that may increase its persistence. This is consistent with previous findings that naproxen can have lower removal efficiency than mononuclear 2-APAs (benzene-based compounds) such as ketoprofen and ibuprofen during wastewater treatment processes (199, 428, 429).

Several mechanisms may contribute to the removal of chiral compounds in MBRs, including biodegradation, biotransformation (including chiral inversion), sorption to sludge and retention by membrane. Hydrophobic organic compounds (log D > 3.2) can be removed via sorption to the sludge phase (425). None of the chiral 2-APAs used in this study is hydrophobic (see their Log D values in Table 15). Under the conditions applied in this study, all APAs are largely ionised and thus negatively charged ($pK_a$ < pH 6). Insignificant sorption to sludge (< 0.25%) was confirmed by the negligible concentrations of (*R*)-2-APAs in the MBR-R sludge phase and (*S*)-2-APAs in the MBR-S sludge phase (Table 17 and Table 18). Membrane retention was also insignificant in this study as confirmed by the similar 2-APA concentration in the MBR mixed liquor and the effluent (Table 17 and Table 18). All 2-APAs investigated here are significantly smaller than the pore size (0.04 μm) of the membrane, thus, their rejection by the membrane was not expected. Thus, both sorption to sludge and membrane retention were insignificant, and biodegradation and biotransformation are the two main removal mechanisms.

Table 17. Sorption of (*R*)-2-APA to MBR-R sludge. Sludge was collected after the chiral addition period (day 37). Daily influent/effluent volume was 6 L. Sludge concentration in MBR-R was 12.76 g dried sludge/L. Concentrations below the limit of quantitation of 3 ng/L were assumed to be 3 ng/L for calculation purposes.

| **Compound** | **Influent conc. (ng/L) (n = 11)** | **Sludge conc. (ng/g dried sludge) (n = 2)** | **Sorption rate (% of total amount)** |
|---|---|---|---|
| (*R*)-2-phenylpropionic acid | 3491 ± 550 | <1 | 0 |
| (*S*)-2-phenylpropionic acid | <3 | <1 | - |
| (*R*)-2-(4-fluorophenyl)propionic acid | 2556 ± 961 | <1 | 0 |
| (*S*)-2-(4-fluorophenyl)propionic acid | <3 | <1 | - |
| (*R*)-2-(4-methoxyphenyl)propionic acid | 6915 ± 2653 | 1.5 ± 1.5 | 0.0004 |
| (*S*)-2-(4-methoxyphenyl)propionic acid | 129 ± 37 | <1 | - |
| (*R*)-2-(3-chlorophenyl)propionic acid | 2060 ± 1142 | <1 | 0 |
| (*S*)-2-(3-chlorophenyl)propionic acid | <3 | 1.0 ± 1.0 | - |
| (*R*)-2-(3-methylphenyl)propionic acid | 5055 ± 959 | <1 | 0 |

| | | | |
|---|---|---|---|
| (*S*)-2-(3-methylphenyl)propionic acid | <3 | <1 | - |
| (*R*)-2-(4-chlorophenyl)propionic acid | 2313 ± 1162 | <1 | 0 |
| (*S*)-2-(4-chlorophenyl)propionic acid | <3 | <1 | - |
| (*R*)-Ketoprofen | 4697 ± 317 | <1 | 0 |
| (*S*)-Ketoprofen | <3 | 5.6 ± 0.1 | - |
| (*R*)-Naproxen | 5222 ± 260 | 6.8 ± 1.3 | 0.02 |
| (*S*)-Naproxen | 123 ± 16 | 41.2 ± 0.3 | - |
| (*R*)-Flurbiprofen | 10030 ± 658 | 145.8 ± 6.0 | 0.25 |
| (*S*)-Flurbiprofen | 185 ± 20 | 41.6 ± 1.4 | - |
| (*R*)-2-(4-n-butylphenyl)propionic acid | 3487 ± 2462 | <1 | 0 |
| (*S*)-2-(4-n-butylphenyl)propionic acid | <3 | 1.7 ± 1.7 | - |
| (*R*)-2-(4-*tert*-butylphenyl)propionic acid | 6040 ± 4464 | 9.0 ± 0.0 | 0.03 |
| (*S*)-2-(4-*tert*-butylphenyl)propionic acid | 81 ± 59 | 1.0 ± 1.0 | - |

Table 18. Sorption of (*S*)-2-APA to MBR-S sludge calculated from mass balance. Sludge was collected after the chiral addition period (day 37). Daily influent/effluent volume was 6 L. Sludge concentration in MBR-R was 8.00 g dried sludge/L at the time of sample collection. Concentrations below the limit of quantitation of 3 ng/L were assumed to be 3 ng/L for calculation purposes.

| **Compound** | **Influent conc. (ng/L) (n = 11)** | **Sludge conc. (ng/g dried sludge) (n = 2)** | **Sorption rate (% of total amount)** |
|---|---|---|---|
| (*R*)-2-phenylpropionic acid | <3 | <1 | - |
| (*S*)-2-phenylpropionic acid | 1030. ± 248 | <1 | 0 |
| (*R*)-2-(4-fluorophenyl)propionic acid | <3 | <1 | - |
| (*S*)-2-(4-fluorophenyl)propionic acid | 1462 ± 326 | <1 | 0 |
| (*R*)-2-(4-methoxyphenyl)propionic acid | <3 | <1 | - |
| (*S*)-2-(4-methoxyphenyl)propionic acid | 1354 ± 355 | <1 | 0 |
| (*R*)-2-(3-chlorophenyl)propionic acid | <3 | <1 | - |
| (*S*)-2-(3-chlorophenyl)propionic acid | 2616 ± 284 | <1 | 0 |
| (*R*)-2-(3-methylphenyl)propionic acid | <3 | <1 | - |
| (*S*)-2-(3-methylphenyl)propionic acid | 1031 ± 154 | <1 | 0 |
| (*R*)-2-(4-chlorophenyl)propionic acid | 27 ± 7 | <1 | - |
| (*S*)-2-(4-chlorophenyl)propionic acid | 1449 ± 144 | <1 | 0 |
| (*R*)-Ketoprofen | <3 | <1 | - |
| (*S*)-Ketoprofen | 20916 ± 7460 | 5.5 ± 0.0 | 0.003 |
| (*R*)-Naproxen | 8 ± 17 | <1 | - |
| (*S*)-Naproxen | 4522 ± 650 | 18.2 ± 0.3 | 0.043 |
| (*R*)-Flurbiprofen | <3 | 54.3 ± 0.4 | - |

| | | | |
|---|---|---|---|
| (*S*)-Flurbiprofen | 5298 ± 1041 | 19.6 ± 0.1 | 0.04 |
| (*R*)-2-(4-n-butylphenyl)propionic acid | <3 | 3.7 ± 2.6 | - |
| (*S*)-2-(4-n-butylphenyl)propionic acid | 1117 ± 300 | <1 | 0 |
| (*R*)-2-(4-*tert*-butylphenyl)propionic acid | <3 | <1 | - |
| (*S*)-2-(4-*tert*-butylphenyl)propionic acid | 1090 ± 159 | <1 | 0 |

Naproxen and ketoprofen removal in MBR treatment has been extensively investigated. By contrast, the removal of the remaining nine 2-APAs appears to have not been previously studied in the literature. (*R*)- and (*S*)- Naproxen and ketoprofen removal efficiencies observed here were higher than those in previous studies (Table 19) using racemic 2-APAs instead of pure enantiomers (422, 425, 430, 431). In agreement with this study, Nguyen et al. (432) reported that the removal of either pure ibuprofen enantiomers by an enzymatic MBR was 20% higher than of racemic ibuprofen. Previous works have confirmed enzymatic degradation as a major biodegradation pathway of naproxen, ketoprofen, and other 2-APAs (433, 434). Further research to simultaneously examine degradation pathway and the fate of pure enantiomers may unravel the underlying reason for the higher removal of pure enantiomers compared to a racemic mixture observed in this study and the literature.

Table 19. Membrane bioreactor removal efficiencies of naproxen and ketoprofen in this study compared to previous studies.

| Compound | Scale | Influent | Influent concentration (µg/L) | SRT (days) | HRT (h) | Removal efficiency (%) | References |
|---|---|---|---|---|---|---|---|
| (*R*)-Ketoprofen | Lab | Synthetic wastewater | 4.70 ± 0.28 | 133 | 12 | 93.9 ± 3.8 | This study |
| (*S*)-Ketoprofen | Lab | Synthetic wastewater | 20.92 ± 0.09 | | | 99.2 ± 1.4 | |
| (*R*)-Naproxen | Lab | Synthetic wastewater | 5.2 ± 0.41 | | | 92.2 ± 3.8 | |
| (*S*)-Naproxen | Lab | Synthetic wastewater | 4.52 ± 1.20 | | | 74.5 ± 14.4 | |
| Ketoprofen | Lab | Synthetic wastewater | 2 | 70 | 24 | 70.5 ± 0.8 | Tadkaew et al. (425) |
| Naproxen | | | | | | 40.1 ± 2.8 | |
| Ketoprofen | Lab | Synthetic wastewater | 2 | 70 | 24 | 67 – 70 | Hashim et al. (422) |
| Naproxen | | | | | | 38 – 47 | |
| Ketoprofen | Lab | Synthetic wastewater | 2 | 70 | 24 | 71 | Alturki et al. (431) |
| Naproxen | | | | | | 40 | |
| Naproxen | Lab | Synthetic wastewater | 50 | 20 | 4 | 84 | Wang et al. (430) |
| Ketoprofen | Pilot | Real wastewater | 50 | 15 | 9 | 98 | Tambosi et al. (428) |
| Naproxen | | | | | | 86 | |
| Ketoprofen | | | | 30 | 13 | 100 | |
| Naproxen | | | | | | 89 | |
| Ketoprofen | Full | Real wastewater | 0.15 – 0.67 | 37 | 35.6 | 80.0 – 95.5 | González-Pérez et al. (435) |
| Naproxen | | | 2.88 – 8.73 | | | 96.5 – 99.8 | |

The two MBRs with feed solution containing (*R*)-enantiomers and (*S*)-enantiomers separately showed similar removal efficiencies of eight chiral 2-APAs (Figure 36). Of the remaining three chiral 2-APAs (*i.e.*, naproxen, ketoprofen and flurbiprofen), one enantiomer was removed at higher rate compared to the other (Student t-test, p-value < 0.05). (*S*)-Enantiomers of ketoprofen and flurbiprofen were better removed than the corresponding (*R*)-enantiomers, while (*R*)-naproxen was better removed than (*S*)-naproxen. In previous studies using racemic compounds, enantioselective degradation (preferential degradation of one enantiomer over the other) was inferred only from the difference in EF between the influent and effluent (199, 436, 437). However, the EF difference could be the result of enantioselective degradation, chiral inversion or a combination of both. The use of pure enantiomers instead of racemic mixtures in this study helps distinguish the two processes and allows for the comparison of each enantiomer's removal efficiency.

### 7.3.3. Chiral inversion behaviour of 2-APAs

The disappearance of an enantiomer is due to the combination of chiral inversion (to the opposite enantiomer) and biotransformation. Thus, the contributions of chiral inversion and biotransformation were calculated for each enantiomer in each sample. From the result in Table 20, the eleven chiral 2-APAs could be divided into 3 groups in terms of chiral inversion behaviour: (1) unidirectional chiral inversion (R→S): two 2-APAs; (2) unidirectional chiral inversion (S→R): three 2-APAs, and (3) bidirectional chiral inversion (R→S and S→R): five 2-APAs. Details on the behaviour of each compound will be discussed further (Section 7.3.3.1 to 7.3.3.3).

Table 20. Breakdown of chiral inversion and biotransformation contribution to overall removal. N.D stands for not determinable.

| Enantiomer | Chiral inversion (%) | Biotransformation (%) | Overall removal (%) |
|---|---|---|---|
| (*R*)-2-Phenylpropionic acid | 0.01 ± 0.04 | 99.8 ± 0.2 | 99.8 ± 0.1 |
| (*S*)-2-Phenylpropionic acid | N.D | 99.3 ± 1.2 | 99.3 ± 1.2 |
| (*R*)-2-(4-Fluorophenyl)propionic acid | 0.33 ± 0.97 | 99.4 ± 1.2 | 99.8 ± 0.3 |
| (*S*)-2-(4-Fluorophenyl)propionic acid | 0.06 ± 0.18 | 98.2 ± 4.9 | 98.3 ± 4.7 |
| (*R*)-2-(4-Methoxyphenyl)propionic acid | N.D | 98.9 ± 2.7 | 98.9 ± 2.7 |

| | | | |
|---|---|---|---|
| (*S*)-2-(4-Methoxyphenyl)propionic acid | 0.15 ± 0.47 | 97.3 ± 7.8 | 97.5 ± 7.3 |
| (*R*)-2-(3-Chlorophenyl)propionic acid | 3.12 ± 4.60 | 95.0 ± 7.2 | 98.2 ± 2.6 |
| (*S*)-2-(3-Chlorophenyl)propionic acid | 0.22 ± 0.69 | 96.5 ± 9.5 | 96.7 ± 8.8 |
| (*R*)-2-(3-Methylphenyl)propionic acid | 0.83 ± 1.00 | 97.8 ± 3.3 | 98.6 ± 2.3 |
| (*S*)-2-(3-Methylphenyl)propionic acid | 0.19 ± 0.59 | 95.8 ± 10.9 | 96.0 ± 10.4 |
| (*R*)-2-(4-Chlorophenyl)propionic acid | 0.37 ± 1.19 | 99.4 ± 1.3 | 99.7 ± 0.2 |
| (*S*)-2-(4-Chlorophenyl)propionic acid | N.D | 99.4 ± 1.3 | 99.4 ± 1.3 |
| (*R*)-Ketoprofen | 3.01 ± 1.71 | 90.9 ± 5.4 | 93.9 ± 3.8 |
| (*S*)-Ketoprofen | 0.05 ± 0.15 | 99.2 ± 1.5 | 99.2 ± 1.4 |
| (*R*)-Naproxen | 20.19 ± 8.80 | 72.0 ± 11.5 | 92.2 ± 3.8 |
| (*S*)-Naproxen | 2.18 ± 0.81 | 72.3 ± 14.8 | 74.5 ± 14.4 |
| (*R*)-Flurbiprofen | N.D | 92.9 ± 3.7 | 92.9 ± 3.7 |
| (*S*)-Flurbiprofen | 9.04 ± 4.79 | 87.3 ± 7.5 | 96.4 ± 3.0 |
| (*R*)-2-(4-n-Butylphenyl)propionic acid | N.D | 99.8 ± 0.2 | 99.8 ± 0.2 |
| (*S*)-2-(4-n-Butylphenyl)propionic acid | N.D | 99.7 ± 0.1 | 99.7 ± 0.1 |
| (*R*)-2-(4-tert-Butylphenyl)propionic acid | N.D | 94.3 ± 4.1 | 94.3 ± 4.1 |
| (*S*)-2-(4-tert-Butylphenyl)propionic acid | 3.99 ± 3.61 | 93.2 ± 7.1 | 97.2 ± 3.7 |

### *7.3.3.1. (R→S) unidirectional chiral inversion*

Unidirectional chiral inversion (R→S) was observed for 2-(4-chlorophenyl)propionic acid and 2-phenylpropionic acid (Figure 37). As described in section 2, the MBR-R was fed with (*R*)-2-APAs, thus (*S*)-enantiomers of these compounds were below the LOQ in the influent. However, they were detected in the effluent, yielding a negative removal efficiency (Figure 37A). Negative removal was not observed for the (*R*)-enantiomers of these compounds in the MBR-S (fed with (*S*)-enantiomers) (Table 21). These results confirm that their chiral inversion was unidirectional in the R→S direction. While the evidence of unidirectional chiral inversion in the R→S direction was conclusive for these two 2-APAs, a very low concentration of the (*S*)-enantiomer in the effluent was noted, resulting in large error bars when reporting the negative removal values of these compounds (Figure 37).

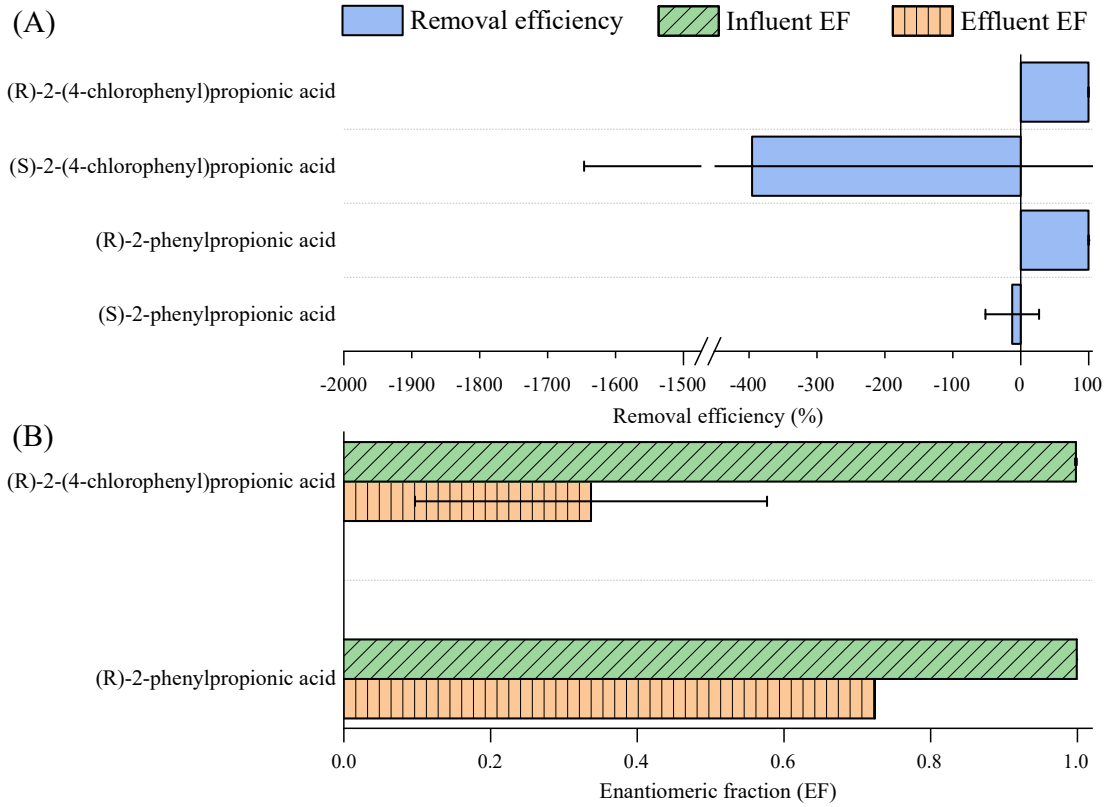


Figure 37. (R→S) chiral inversion depicted through (A) negative removal efficiencies of (*S*)-enantiomers and (B) decrease in enantiomeric fraction (EF) of (*R*)-enantiomers of 2-(4-chlorophenyl)propionic acid and 2-phenylpropionic acid in the MBR-R. Data represent the mean of all samples collected during chiral 2-APA addition period. The error bar represents the standard deviation from eleven measurements (duplicate samples taken twice a week for three weeks).

Corresponding to the increase of (*S*)-enantiomers concentrations, the EF of these compounds significantly decreased from 1.00 in the influent to 0.47 ± 0.12 – 0.58 ± 0.11 (n = 11) in the

effluent (Figure 37B) (Student t-test, $p < 0.05$). This study appears to provide the first evidence of significant chiral inversion of 2-(4-chlorophenyl)propionic acid and 2-phenylpropionic acid during biological wastewater treatment. Previous works have established that microorganisms can perform chiral inversion of 2-phenylpropionic acid, though the direction is substrate- and species-specific (438-440). For example, Hung et al. (441) found that (*R*)-2-phenylpropionic acid was inverted to the (*S*)-enantiomer by the fungi *Cordycep militalis*. Incubations of pure enantiomers with another fungus species (*Verticillium lecanii*) in Sorensen's phosphate buffer confirmed the occurrence of bidirectional inversion (442). Kato et al. (443) reported that the bacteria *Nocardia diaphanozonaia* invert 2-phenylpropionic acid in the (S→R) direction, which was the opposite direction to what was observed in this study.

Table 21. Removal efficiency of 2-APA enantiomers in the two MBR systems.

| **Compound** | **Removal efficiency in MBR-R (fed with (*R*)-2-APAs) (%)** | **Removal efficiency in MBR-S (fed with (*S*)-2-APAs) (%)** |
|---|---|---|
| (*R*)-2-phenylpropionic acid | 99.8 ± 0.1 | - |
| (*S*)-2-phenylpropionic acid | -12.5 ± 39.5 | 99.3 ± 1.2 |
| (*R*)-2-(4-fluorophenyl)propionic acid | 99.8 ± 0.3 | -15.6 ± 49.2 |
| (*S*)-2-(4-fluorophenyl)propionic acid | -312.5 ± 934.8 | 98.3 ± 4.7 |
| (*R*)-2-(4-methoxyphenyl)propionic acid | 98.9 ± 2.7 | -41.6 ± 131.7 |
| (*S*)-2-(4-methoxyphenyl)propionic acid | 78.5 ± 49.1 | 97.5 ± 7.3 |
| (*R*)-2-(3-chlorophenyl)propionic acid | 98.2 ± 2.6 | -132.5 ± 417.5 |
| (*S*)-2-(3-chlorophenyl)propionic acid | -1239.3 ± 1534.0 | 96.7 ± 8.8 |
| (*R*)-2-(3-methylphenyl)propionic acid | 98.6 ± 2.3 | -47.7 ± 150.9 |
| (*S*)-2-(3-methylphenyl)propionic acid | -1322.8 ± 1435.9 | 96.0 ± 10.4 |
| (*R*)-2-(4-chlorophenyl)propionic acid | 99.7 ± 0.2 | 87.9 ± 5.1 |
| (*S*)-2-(4-chlorophenyl)propionic acid | -395.6 ± 1250.9 | 99.4 ± 1.3 |
| (*R*)-Ketoprofen | 93.9 ± 3.8 | -149.8 ± 324.1 |
| (*S*)-Ketoprofen | -4706.0 ± 2632.6 | 99.2 ± 1.4 |
| (*R*)-Naproxen | 92.2 ± 3.7 | -3136.9 ± 1396.4 |
| (*S*)-Naproxen | -867.2 ± 361.2 | 74.5 ± 14.4 |
| (*R*)-Flurbiprofen | 92.9 ± 3.7 | -16573.9 ± 9298.1 |
| (*S*)-Flurbiprofen | 61.2 ± 23.1 | 96.4 ± 3.0 |
| (*R*)-2-(4-n-butylphenyl)propionic acid | 99.8 ± 0.2 | - |
| (*S*)-2-(4-n-butylphenyl)propionic acid | - | 99.7 ± 0.1 |
| (*R*)-2-(4-*tert*-butylphenyl)propionic acid | 94.3 ± 4.1 | -1618.7 ± 1777.9 |
| (*S*)-2-(4-*tert*-butylphenyl)propionic acid | 85.6 ± 10.6 | 97.2 ± 3.7 |

### *7.3.3.2. (S→R) unidirectional chiral inversion*

Unidirectional chiral inversion in the (S→R) direction was observed for flurbiprofen, 2-(4-*tert*-butylphenyl)propionic acid and 2-(4-methoxyphenyl)propionic acid (Figure 38). The concentrations of their (*R*)-enantiomers in the effluent of the MBR-S (receiving (*S*)-2-APAs only) were higher than that of the influent, resulting in negative removal efficiencies. By contrast, negative removal was not observed for the (*S*)-enantiomers of these compounds in the MBR-R (fed with (*R*)-enantiomers) (Table 21).

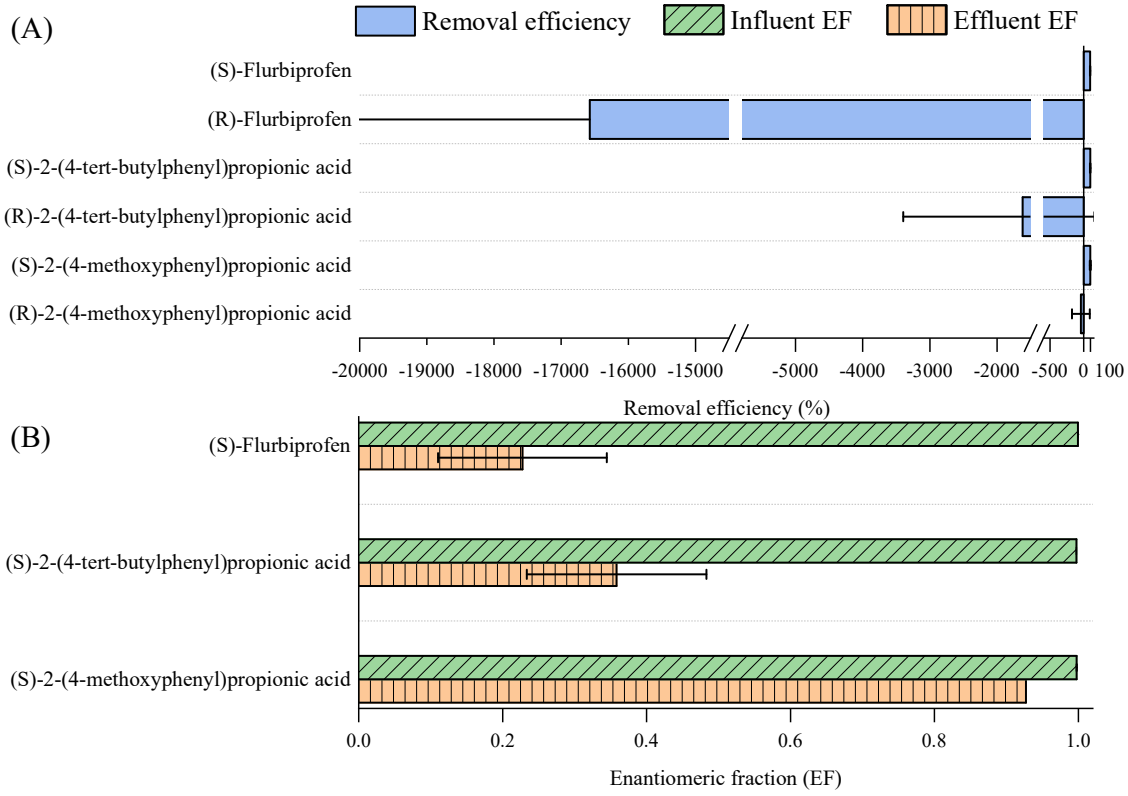


Figure 38. (S→R) chiral inversion depicted through (A) negative removal efficiencies of (*R*)-enantiomers and (B) decrease in enantiomeric fraction (EF) of (*S*)-enantiomers of Flurbiprofen, 2-(4—*tert*-butylphenyl)propionic acid and 2-(4-methoxyphenyl)propionic acid in the MBR-S. Data represent the mean of all samples collected during chiral 2-APA addition period. The error bar represents the standard deviation from eleven measurements (duplicate samples taken twice a week for three weeks).

The EF of (*S*)-flurbiprofen, (*S*)-2-(4-*tert*-butylphenyl)propionic acid and (*S*)-2-(4-methoxyphenyl)propionic acid were significantly different between influent (1.00) and effluent ($0.23 \pm 0.12 - 0.54 \pm 0.12$, $n = 11$) of the MBR-S (Student t-test, $p < 0.05$). It is noted that the effluent EF decreased over time for (*S*)-flurbiprofen (Table 22). Figure 38 appears to be the first set of data on chiral inversion of these 2-APAs during biological wastewater treatment. The direction of flurbiprofen chiral inversion in previous studies examining single bacterial species

was species-specific (443, 444). The fungus *V. lecanii* carried out bidirectional inversion of flurbiprofen, with (R→S) enantiomer as the more significant direction (the opposite of what was observed in this study) (444). The fungus *C. militalis* can invert flurbiprofen from (*R*) to (*S*)-antipode, while the bacteria *N. diaphanozonaria* did not show any chiral inversion activity on this compound (443).

Table 22. Average influent enantiomeric fraction (EF) and effluent EF of (*S*)-2-APA enantiomer in MBR-S during chiral compound dosing period. The column names under effluent EF represent the number of days after chiral dosing commenced and the duplicate number. Compounds that show decreasing effluent EF over time are marked with an asterisk. N.D stands for not determinable. In case where the concentration of one enantiomer was assumed to be LOD (3 ng/L) for EF calculation, a greater than (≥) sign is placed in front of the EF.

| **Compound** | **Influent EF (n = 11)** | **Effluent EF** | | | | | | | | | | |
|---|---|---|---|---|---|---|---|---|---|---|---|---|
| | | **D1** | **D4.1** | **D4.2** | **D7.1** | **D7.2** | **D10.1** | **D10.2** | **D14.1** | **D14.2** | **D18.1** | **D18.2** |
| (*S*)-2-phenylpropionic acid | 1.00 ± 0.00 | ≥ 0.91 | N.D | N.D | N.D | N.D | N.D | N.D | N.D | N.D | N.D | N.D |
| (*S*)-2-(4-fluorophenyl)propionic acid | 1.00 ± 0.00 | 0.94 | N.D | N.D | N.D | N.D | N.D | N.D | N.D | N.D | N.D | N.D |
| (*S*)-2-(4-methoxyphenyl)propionic acid | 1.00 ± 0.00 | 0.93 | N.D | N.D | N.D | N.D | N.D | N.D | N.D | N.D | N.D | N.D |
| (*S*)-2-(3-chlorophenyl)propionic acid | 1.00 ± 0.00 | 0.92 | 0.91 | ≥ 0.91 | ≥ 0.86 | ≥ 0.77 | ≥ 0.80 | ≥ 0.81 | ≥ 0.72 | ≥ 0.70 | ≥ 0.71 | ≥ 0.60 |
| (*S*)-2-(3-methylphenyl)propionic acid | 1.00 ± 0.00 | 0.94 | ≥ 0.86 | ≥ 0.84 | ≥ 0.71 | ≥ 0.60 | ≥ 0.66 | ≥ 0.71 | N.D | N.D | ≥ 0.53 | N.D |
| (*S*)-2-(4-chlorophenyl)propionic acid | 0.98 ± 0.00 | ≥ 0.94 | N.D | N.D | N.D | N.D | N.D | N.D | N.D | N.D | N.D | N.D |
| (*S*)-Ketoprofen | 1.00 ± 0.00 | 0.90 | ≥ 0.97 | ≥ 0.98 | 0.86 | ≥ 0.96 | ≥ 0.95 | ≥ 0.96 | ≥ 0.91 | ≥ 0.93 | ≥ 0.91 | ≥ 0.87 |
| *(*S*)-Naproxen | 1.00 ± 0.00 | 0.95 | 0.94 | 0.94 | 0.94 | 0.94 | 0.90 | 0.89 | 0.85 | 0.85 | 0.74 | 0.74 |
| *(*S*)-Flurbiprofen | 1.00 ± 0.00 | 0.45 | 0.37 | 0.37 | 0.25 | 0.25 | 0.18 | 0.19 | 0.14 | 0.14 | 0.09 | 0.08 |
| (*S*)-2-(4-n-butylphenyl)propionic acid | 1.00 ± 0.00 | N.D | N.D | N.D | ≥ 0.50 | N.D | N.D | N.D | N.D | N.D | N.D | N.D |

Chiral inversion could lead to the increase in the concentration of the more biologically active or more toxic enantiomers. For example, (*R*)-flurbiprofen was found to have a greater effect on photosystem II inhibition in green algae than (*S*)-flurbiprofen, while only (*R*)-flurbiprofen induced ethoxyresorufin-O-deethylase (EROD) activity in fish cells (215). (*R*)-2-(4-tert-Butylphenyl)propionic acid) was around 1.6 times more potent than the (*S*)-enantiomer in the EROD assay ($EC_{IR1.5}$ of 7.9 mg/L for (*S*)- compared to 4.9 mg/L for (*R*)-), while only (*R*)-2-(4-methoxyphenyl)propionic acid-induced EROD activity ($EC_{IR1.5}$ of 4.5 mg/L) (unpublished results).

The EROD assay, which is described in detail in Neale et al. (215), was conducted with an exposure period of 6 h, rather than 24 h. The shorter exposure period was selected since a previous study found this was the optimal exposure period for pharmaceuticals including 2-APAs ibuprofen and ketoprofen (445). Linear concentration-effect curves for EROD activity for the two enantiomers of 2-(4-tert-Butylphenyl)propionic acid and the two enantiomers of 2-(4-Methoxyphenyl)propionic acid are provided in the  (Figure 39 and Figure 40).

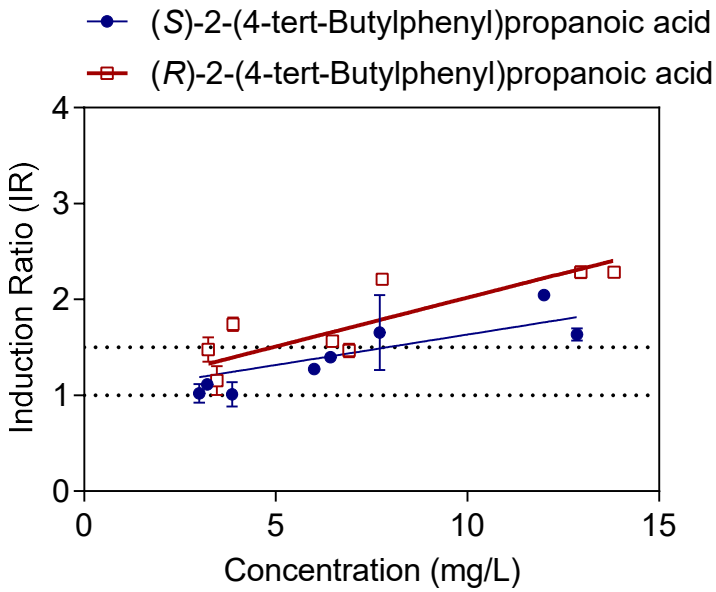


Figure 39. Linear concentration-effect curves for EROD activity for (R)- and (S)-2-(4-tert-Butylphenyl)propionic acid enantiomers.

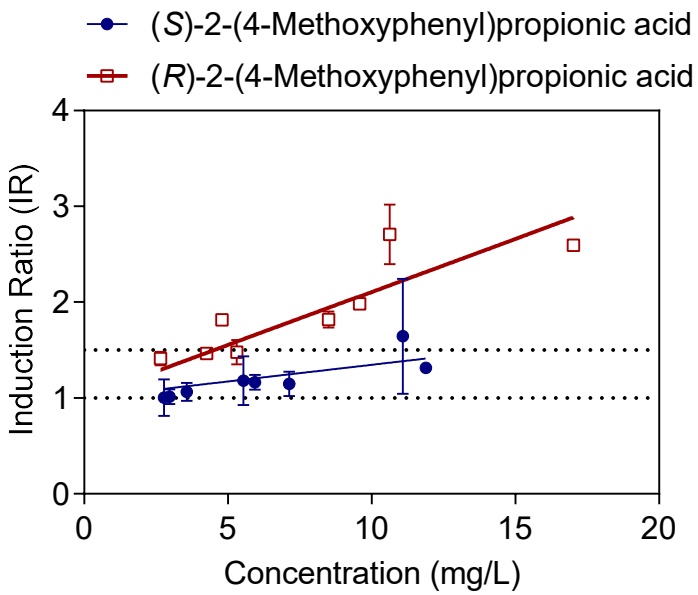


Figure 40. Linear concentration-effect curves for EROD activity for (R)- and (S)-2-(4-Methoxyphenyl)propionic acid enantiomers.

#### *7.3.3.3. Bidirectional chiral inversion*

Six 2-APAs including naproxen, ketoprofen, 2-(3-methylphenyl)propionic acid, 2-(3-chlorophenyl)propionic acid, 2-(4-fluorophenyl)propionic acid, and 2-(4-butylphenyl)propionic acid exhibited bidirectional chiral inversion. This may be observed in Figure 41 and Figure 42 which show negative removal of both (*S*)- and (*R*)-enantiomers, respectively, of these 2-APAs. The concentration of the (*S*)-enantiomer of naproxen, ketoprofen, 2-(3-methylphenyl)propionic acid, 2-(3-chlorophenyl)propionic acid, 2-(4-fluorophenyl)propionic acid in the effluent of the MBR-R was higher than that of the influent, resulting in negative removal efficiencies (Figure 41A). Correspondingly, their EF dropped significantly from 0.98 – 1.00 in the influent to the range between 0.25 ± 0.08 and 0.64 ± 0.07 in the effluent (n = 11) (Figure 41B). In the MBR-S, the concentration of (*R*)-enantiomer in the effluent was also higher than the effluent, resulting in negative removal efficiencies (Figure 42A). The chiral inversion extent for these compounds appears to be greater in the (R→S) direction than (S→R).

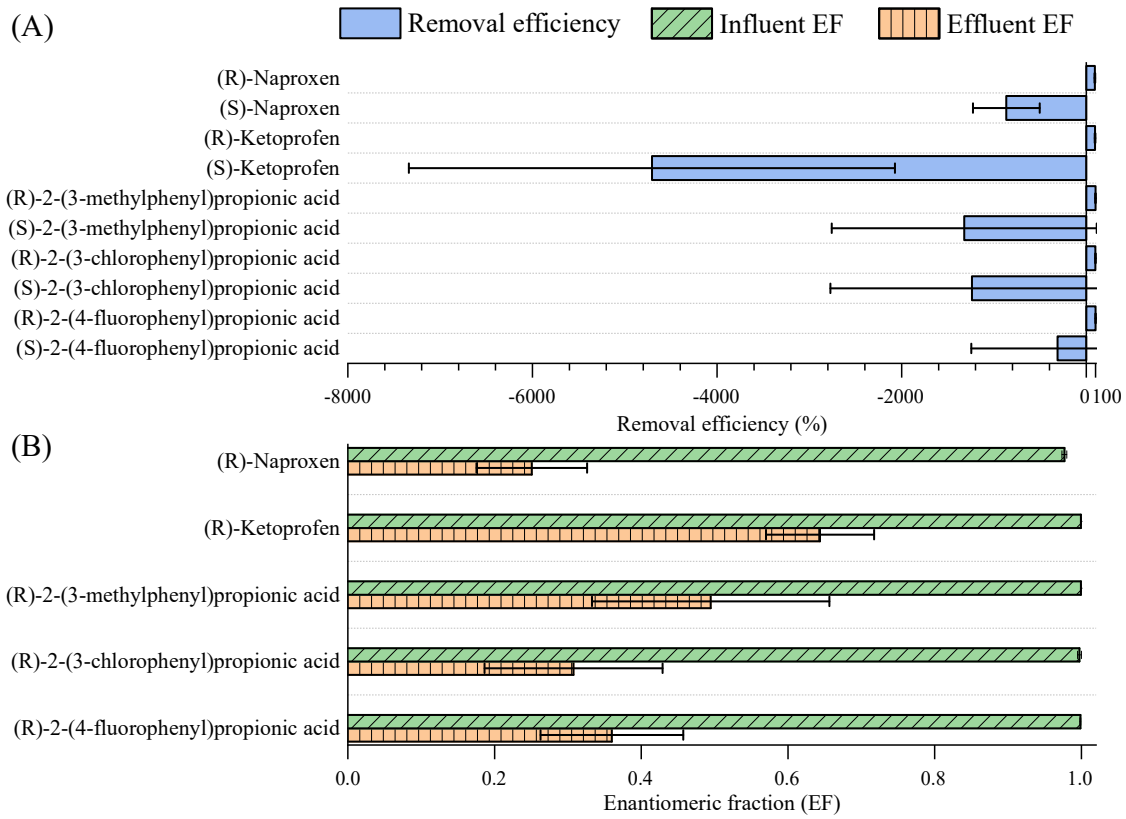


Figure 41. (R→S) chiral inversion depicted through (A) negative removal efficiencies of (*S*)-enantiomers and (B) decrease in enantiomeric fraction (EF) of (*R*)-enantiomers of naproxen, ketoprofen, 2-(3-methylphenyl)propionic acid, 2-(3-chlorophenyl)propionic acid and 2-(4-fluorophenyl)propionic acid in the MBR-R. The error bar represents the standard deviation from eleven measurements (duplicate samples taken twice a week for three weeks).

It is noted that for 2-(4-butylphenyl)propionic acid, there was no evidence from influent and effluent data to support the occurrence of chiral inversion. Nevertheless, (*S*)-2-(4-butylphenyl)propionic acid was not detected in the influent of MBR-R but was detected at 1.7 ± 1.7 ng/g in the sludge phase and 9.0 ± 0.0 ng/L in the mixed liquor supernatant (Table 17). Similarly, (*R*)-2-(4-butylphenyl)propionic acid was not detected in the influent of MBR-S but was detected at 3.7 ± 2.6 ng/g in the sludge phase, suggesting that bidirectional inversion also occurred for this 2-APA (Table 18).

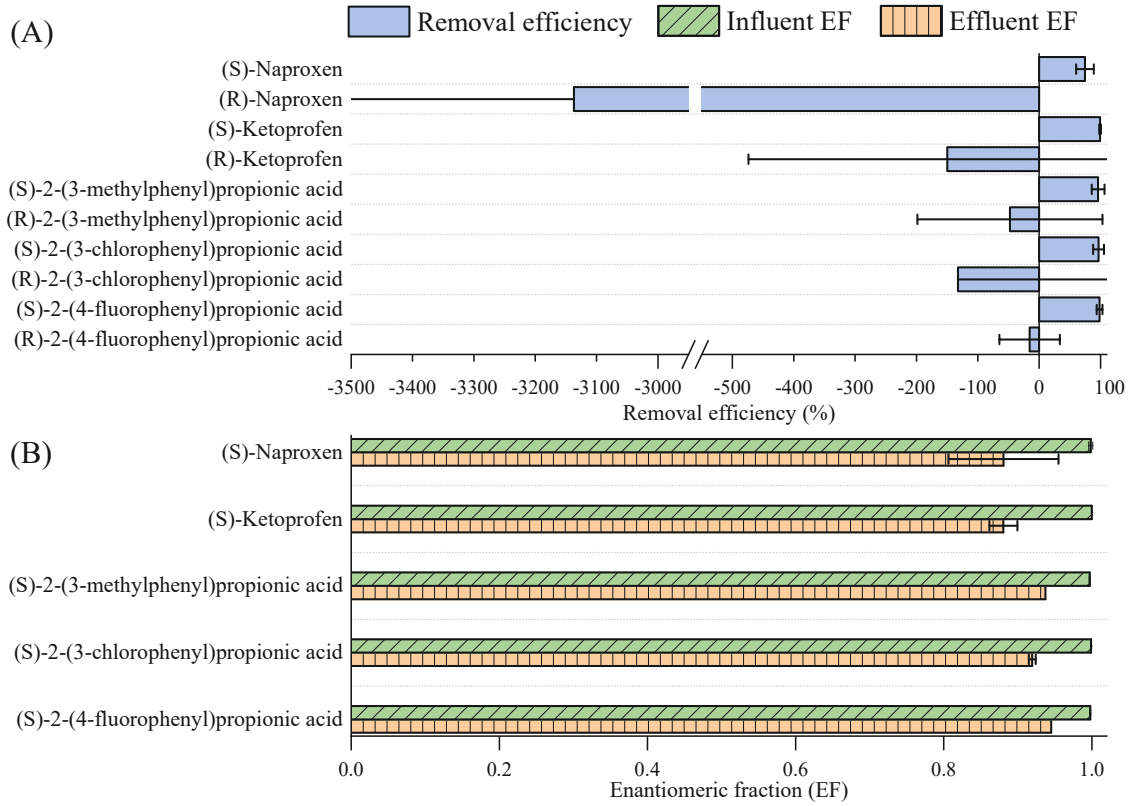


Figure 42. (S→R) chiral inversion depicted through (A) negative removal efficiencies of (*R*)-enantiomers and (B) decrease in enantiomeric fraction (EF) of (*S*)-enantiomers of naproxen, ketoprofen, 2-(3-methylphenyl)propionic acid, 2-(3-chlorophenyl)propionic acid and 2-(4-fluorophenyl)propionic acid in the MBR-S. Data represent the mean of all samples collected during chiral 2-APA addition period. The error bar represents the standard deviation from eleven measurements (duplicate samples taken twice a week for three weeks).

Bidirectional inversion of naproxen and ketoprofen in biological systems has been previously reported (432, 444, 446). Bidirectional inversion of naproxen was observed in an enzymatic MBR dosed with laccase from the fungus *Pleurotus ostreatus*, and in complex microbial communities such as soil microcosms (432, 446). Nguyen et al. (432) also observed that (R→S) was the dominant inversion direction, with 14 ± 4% of (*R*)-naproxen in the influent undergoing inversion to (*S*)-naproxen, and only 4% of (*S*)-naproxen in the influent undergoing inversion to (*R*)-naproxen. Nevertheless, since naproxen chiral inversion is bidirectional, it is difficult to confirm whether this results from the enantioselectivity of chiral inversion enzymes (different rates of inversion for different enantiomers) or other interactions between two enantiomers. This is the first time the (R→S) chiral inversion of naproxen has been demonstrated in a wastewater treatment process. Since (*R*)-naproxen is metabolised into (*S*)-naproxen in the human body, this is the dominant enantiomer detected in raw wastewater and (S→R) inversion has been frequently observed (222, 447). However, it is known that naproxen exhibits different chiral inversion

behaviour in different environments. For example, experiments with the fungus *Verticillium lecanii* resulted in (R→S) chiral inversion (444), while observations from a microcosm experiment with activated sludge from wastewater treatment plant were of (S→R) inversion (448). Ketoprofen has been found to undergo bidirectional inversion by different fungi and fungal enzymes (432, 444, 449). However, it was reported that the (S→R) inversion was more significant than the (R→S) inversion (444), which is different from this study.

Similar to (*S*)-flurbiprofen, the effluent EF of naproxen (both enantiomers) decreased over time (Table 22 & Table 23). The decrease in effluent EF could be due to varying rates of metabolism and chiral inversion as a consequence of microbial adaptation. Analysis of the MBR microbial community associated with chiral inversion may bring more insights into this phenomenon. The results in this study highlight the significance of using pure enantiomer over racemic mixture in confirming the occurrence of chiral inversion. When racemic solutions of 2-(3-chlorophenyl)propionic acid and 2-(4-methoxyphenyl)propionic acid were dosed into culture media of *N. diaphanozonaia*, no inversion activity was observed (443). Ketoprofen frequently showed minor EF change from influent to effluent (increased from 0.54 – 0.58 to 0.61 – 0.68) during wastewater treatment and microcosm studies, but this observation was attributed to enantioselective degradation of the two enantiomers rather than chiral inversion (220, 222, 450).

Table 23. Average influent enantiomeric fraction (EF) and effluent EF of (*R*)-2-APA enantiomer in MBR-R during chiral compound dosing period. The column names under effluent EF represent the number of days after chiral dosing commenced and the duplicate number. Compounds that show decreasing effluent EF over time are marked with an asterisk. N.D stands for not determinable. In case where the concentration of one enantiomer was assumed to be LOD (3 ng/L) for EF calculation, a greater than (≥) sign is placed in front of the EF.

| **Compound** | **Influent EF (n = 11)** | **Effluent EF** | | | | | | | | | | |
|---|---|---|---|---|---|---|---|---|---|---|---|---|
| | | **D1** | **D4.1** | **D4.2** | **D7.1** | **D7.2** | **D10.1** | **D10.2** | **D14.1** | **D14.2** | **D18.1** | **D18.2** |
| (*R*)-2-phenylpropionic acid | 1.00 ± 0.00 | 0.72 | N.D | N.D | N.D | ≥ 0.71 | N.D | N.D | N.D | N.D | ≥ 0.72 | ≥ 0.72 |
| (*R*)-2-(4-fluorophenyl)propionic acid | 1.00 ± 0.00 | 0.22 | N.D | N.D | N.D | ≥ 0.61 | N.D | N.D | N.D | N.D | 0.44 | 0.41 |
| (*R*)-2-(4-methoxyphenyl)propionic acid | 0.98 ± 0.00 | 0.70 | N.D | N.D | ≥ 0.86 | ≥ 0.84 | N.D | N.D | N.D | N.D | 0.73 | 0.73 |
| (*R*)-2-(3-chlorophenyl)propionic acid | 1.00 ± 0.00 | 0.47 | 0.16 | 0.16 | 0.42 | 0.42 | ≥ 0.22 | 0.17 | N.D | ≥ 0.32 | 0.33 | 0.33 |
| (*R*)-2-(3-methylphenyl)propionic acid | 1.00 ± 0.00 | 0.68 | 0.31 | 0.30 | 0.65 | 0.65 | 0.33 | 0.29 | 0.51 | 0.40 | 0.67 | 0.66 |
| (*R*)-2-(4-chlorophenyl)propionic acid | 1.00 ± 0.00 | 0.10 | N.D | N.D | N.D | ≥ 0.58 | N.D | N.D | N.D | N.D | N.D | N.D |
| (*R*)-Ketoprofen | 1.00 ± 0.00 | 0.69 | 0.59 | 0.58 | 0.64 | 0.66 | 0.59 | 0.55 | 0.62 | 0.59 | 0.78 | 0.77 |
| *(*R*)-Naproxen | 0.98 ± 0.00 | 0.43 | 0.32 | 0.33 | 0.22 | 0.21 | 0.23 | 0.21 | 0.17 | 0.19 | 0.22 | 0.22 |
| (*R*)-Flurbiprofen | 0.98 ± 0.00 | 0.91 | 0.91 | 0.91 | 0.90 | 0.90 | 0.91 | 0.92 | 0.89 | 0.91 | 0.92 | 0.93 |
| (*R*)-2-(4-n-butylphenyl)propionic acid | 1.00 ± 0.00 | N.D | N.D | N.D | ≥ 0.76 | ≥ 0.73 | N.D | N.D | ≥ 0.82 | ≥ 0.60 | ≥ 0.70 | ≥ 0.78 |
| (*R*)-2-(4-*tert*-butylphenyl)propionic acid | 0.99 ± 0.00 | 0.97 | 0.97 | 0.97 | 0.97 | 0.97 | 0.97 | 0.96 | 0.96 | 0.97 | 0.97 | 0.97 |

The 2-APAs investigated here only differed from one another by a substituent group of the benzyl ring but exhibited significantly different chiral inversion behaviours (Table 15). The underlying reason could be the impact of substituent groups on the chiral inversion process, or different microbial species with different chiral inversion mechanisms are responsible for the inversion of different compounds. Steric hindrance caused by substituent groups can affect the initial point of enzymatic attack and the metabolism pathway for different enantiomers (426, 427). Liu et al. (426) observed that the bacteria *Xanthobacter flavus* PA1 initially attacked 2-phenylbutyric acid at the β-C atom of the carboxyl alkyl side chain through hydroxylation, not at the aromatic ring, and suggested that the reason to be steric hindrance of the chiral carboxyl alkyl moiety attached on the benzene ring. Simoni et al. (427) examined the metabolism of chiral 3-Phenylbutyric acid by *R. rhodochrous* PB1 and showed that the (*R*)-enantiomer was initially demethylated at the chiral centre of the carboxyl alkyl side chain to decrease the steric hindrance and further metabolized via meta ring cleavage; whereas the (*S*)-enantiomer is only cometabolically oxidized to (*S*)-3-(2,3-dihydroxyphenyl)butyric acid without ring cleavage. Thus, it is possible that steric hindrance of the substituent group can impact chiral inversion behaviour of 2-APAs. Kato et al. (443) demonstrated that chiral inversion enzymes of *N. diaphanozonaria* accept 2-phenylpropionic acid and 2-fluorophenylacetic acid, but did not show any activity on compounds with higher steric bulkiness (*e.g*. 2-phenylbutanoic acid, 2-methoxyphenylacetic acid, and 3-hydroxy-2-phenylpropanoic acid). Consequently, a mechanistic understanding of chiral biotransformation of 2-APAs remains lacking and a future research need.

## 7.4. Conclusion

This study examined the chiral inversion behaviour of a suite of pharmaceutically active 2-arylpropionic acids (2-APAs) using pure (*R*) and (*S*)-enantiomers during biological wastewater treatment. High and similar removal efficiencies of (*R*) and (*S*)-forms were observed (>90%) for most pure 2-APA enantiomers. The eleven 2-APAs investigated here differ from one another by just one substituent group attached to the 2-APA backbone but show diverse and distinctive chiral inversion behaviours. Two 2-APAs showed chiral inversion in the (R→S) direction, three 2-APAs showed chiral inversion in the (S→R) direction, and six 2-APAs showed bidirectional chiral inversion. Compounds exhibiting bidirectional inversion also show greater inversion from (R→S) than from (S→R). Time-dependent changes in effluent EF were observed for two 2-APAs.

# Chapter 8. CHIRAL INVERSION OF 2-ARYLPROPIONOIC ACID (2-APA) ENANTIOMERS DURING ANAEROBIC DIGESTION

This chapter has been published as the following journal article.

Nguyen QA, Vu HP, McDonald JA, Nguyen LN, Leusch FDL, Neale PA, et al. Chiral Inversion of 2-Arylpropionic Acid Enantiomers under Anaerobic Conditions. Environmental Science & Technology. 2022;56(12):8197-208.

**Summary:** This work examined chiral inversion of 2-arylpropionic acids (2-APAs) under anaerobic conditions and the associated microbial community. The anaerobic condition was simulated by two identical anaerobic digesters (R1 and R2). Each digester was fed with substrate containing eleven either pure (*R*)- or pure (*S*)-2-APA enantiomers, respectively. Chiral inversion was evidenced by concentration increase of the other enantiomer in the digestate and changes in the enantiomeric fraction between the two enantiomers. Both digesters showed similar and poor removal of 2-APAs (≤30%, except for naproxen) and diverse chiral inversion behaviours under anaerobic conditions. Four compounds exhibited (S→R) unidirectional inversion (flurbiprofen, ketoprofen, naproxen, and 2-(4-*tert*-butylphenyl)propionic acid) and the remaining seven compounds showed bidirectional inversion. Several aerobic and facultative anaerobic bacterial genera (*Candidatus_Microthrix, Rhodococcus, Mycobacterium, Gordonia, Sphingobium*) were identified in both digesters and predicted to harbour the 2-arylpropionyl-CoA epimerase (enzyme involved in chiral inversion) encoding gene. These genera presented at low abundances (< 0.5 and < 0.2% in R1 and R2, respectively), explaining the limited extent of chiral inversion observed in this study.

## 8.1. Introduction

The fate of chiral compounds in wastewater treatment is a subject of scientific importance. Many biologically active organic compounds are chiral (451). Chiral compounds exist in two enantiomers (or stereoisomers) of the same chemical formula but cannot geometrically superimpose onto each other by any combination of rotations, translations, and conformational changes. About half of all pharmaceuticals on the market are chiral and their enantiomers may exhibit vastly different responses in ecotoxicity studies (452, 453). For example, (*S*)-ibuprofen is 160 times more therapeutically active than (*R*)-ibuprofen (454). Thus, chiral inversion (i.e. the transformation from one enantiomer to the other) has an important implication for the toxicology of chiral compounds in the environment. However, to date, understanding of the chiral inversion behaviour between enantiomers is still limited. Most reported occurrences of pharmaceuticals in the environment do not differentiate between enantiomeric pairs and the role of chirality in their environmental toxicology has often been omitted.

Recent works on chiral inversion behaviour of pharmaceuticals in wastewater treatment have focused on a unique group of chiral compounds called 2-APAs. They have the same chiral center and only differ from one another by one substituent group. Several 2-APAs (e.g. ibuprofen, ketoprofen, naproxen, and flurbiprofen) are important non-steroidal anti-inflammatory drugs (NSAIDs), widely used for pain relief due to their anti-inflammatory and analgesic properties. These drugs can be obtained over the counter, thus, they are also ubiquitous in wastewater and environmental waters impacted by wastewater (194, 455). The removal of NSAIDs by biological wastewater treatment through degradation and sorption has been a subject of intensive study in recent years (456-458). Just like other chiral pharmaceuticals, most NSAIDs exist in enantiomeric pairs with similar physico-chemical properties but vastly different biological and pharmaceutical properties. The therapeutic effects of NSAIDs reside almost exclusively in their (*S*)-enantiomers (eutomers) rather than their (*R*)-enantiomers (459). (*R*)-Naproxen showed higher bacterial toxicity than (*S*)-naproxen, while (*S*)-flurbiprofen exhibited higher bacterial toxicity and lower algal toxicity than (*R*)-flurbiprofen (215). Nevertheless, most previous work on the fate and removal of NSAIDs during treatment process did not take into account the role of chirality in the behaviour of enantiomeric pairs (460, 461).

Previous works have converged to a consensus that chiral inversion is substrate- and species-specific. (*R*)-Naproxen is inverted into (*S*)-naproxen by human and rat metabolism (462, 463), while ketoprofen does not undergo a substantial metabolic inversion in humans but exhibits unidirectional inversion in dogs, sheep, cattle and horses (449). Based on enantio-specific analyses of effluents from municipal WWTPs and untreated sewage, chiral inversion of NSAIDs can be expected during wastewater treatment (219). Indeed, recent studies of NSAIDs and other 2-APAs derivatives in controlled reactors have confirmed the occurrence of chiral inversion in aerobic wastewater treatment processes (432, 448, 464). In a previous study, using pure enantiomers, Nguyen et al. (464) reported diverse chiral inversion behaviours of eleven 2-APAs during membrane bioreactor (MBR) treatment. They observed unidirectional inversion in the (R→S) and (S→R) direction as well as bidirectional chiral inversion of these 2-APAs under aerobic conditions. These results also highlighted that chiral inversion can impact the compound's actual ecotoxicity after the treatment process, which needs to be taken into consideration for environmental risk assessment.

It is noteworthy that previous works have focussed almost exclusively on aerobic wastewater treatment processes. In practice, wastewater treatment involves both aerobic and anaerobic processes. In most wastewater treatment plants (WWTPs), the solids from wastewater and waste activated sludge are anaerobically treated by anaerobic digestion (AD) to produce biogas and biosolids which can be used as a renewable fuel and biofertilizer, respectively (345, 465). While

energy and resource recovery by AD can provide significant economic benefits, there is also an increasing concern with such applications due to the ubiquitous occurrence of trace organic contaminants especially pharmaceutical residues in biosolids (455, 466). Owing to their possible adverse effects on living organisms (467, 468), the presence of trace organic contaminants including household chemicals, personal care products, and pharmaceuticals in biosolids pose a great risk to public health and the environment (466).

While it is clear that chiral inversion is biologically mediated (446, 450), current knowledge on chiral inversion of 2-APAs by microorganisms is still limited with a few mechanistic studies performed on single bacterial/fungal strains (443, 469). In addition, waste and wastewater treatment processes often involve complex microbial communities rather than a single strain, and the relationship between such communities and chiral inversion has not been comprehensively studied. Next-generation sequencing (NGS) is a useful tool for in-depth investigation of the microbial community in different environmental matrixes, especially in the waste/wastewater treatment context (48, 470). 16S rRNA sequencing can also be combined with complementary tools such as functional prediction tools (e.g. PICRUST2) to provide information about the functional composition of sampled communities (471). This study aims to provide new insights into chiral inversion under well-controlled anaerobic conditions using pure enantiomers of eleven 2-APAs. NGS and functional prediction analysis were employed to elucidate possible microbial species involved in chiral inversion.

## 8.2. Materials and Methods

### 8.2.1. Chemicals and consumables

2-APAs with enantiomeric purity of at least 95% were used in this study. Naproxen, ketoprofen, and flurbiprofen were selected as representatives of NSAIDs, along with eight other 2-APA derivatives that differ from one another only by one substituent group. Key physico-chemical properties of the eleven 2-APAs in this study are summarised in Table 24.

Table 24. Physicochemical properties of chiral compounds used in this study (data were obtained from the SciFinder database).

| Compound | Molecular structure | Molecular weight (g/mol) | Log D at pH 8 25°C | $pK_a$ |
|---|---|---|---|---|
| (*R*)-2-Phenylpropionic acid<br>(*S*)-2-Phenylpropionic acid | 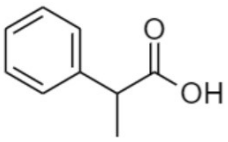 | 150 | -1.7 | 4.3 |
| (*R*)-2-(4-Fluorophenyl)propionic acid<br>(*S*)-2-(4-Fluorophenyl)propionic acid | 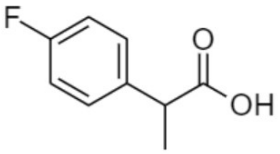 | 168 | -1.44 | 4.3 |
| (*R*)-2-(4-Methoxyphenyl)propionic acid<br>(*S*)-2-(4-Methoxyphenyl)propionic acid | 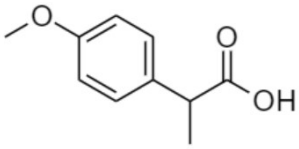 | 180 | -1.47 | 4.5 |
| (*R*)-2-(3-Chlorophenyl)propionic acid<br>(*S*)-2-(3-Chlorophenyl)propionic acid | 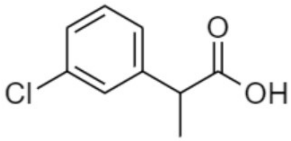 | 185 | -1.08 | 4.2 |
| (*R*)-2-(3-Methylphenyl)propionic acid<br>(*S*)-2-(3-Methylphenyl)propionic acid | 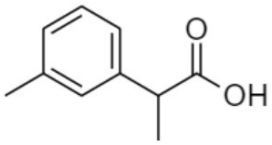 | 164 | -1.08 | 4.4 |
| (*R*)-2-(4-Chlorophenyl)propionic acid<br>(*S*)-2-(4-Chlorophenyl)propionic acid | 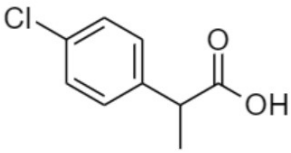 | 185 | -1.0 | 4.2 |
| (*R*)-Ketoprofen<br>(*S*)-Ketoprofen | 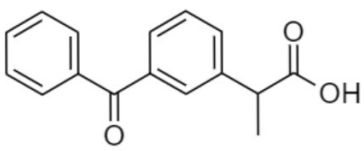 | 254 | -0.55 | 4.2 |

| Compound | Molecular structure | Molecular weight (g/mol) | Log D at pH 8 25°C | $pK_a$ |
|---|---|---|---|---|
| (*R*)-Naproxen<br>(*S*)-Naproxen | 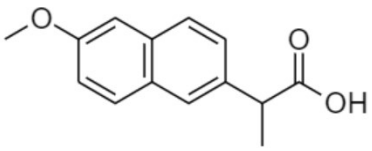 | 230 | -0.18 | 4.8 |
| (*R*)-Flurbiprofen<br>(*S*)-Flurbiprofen | 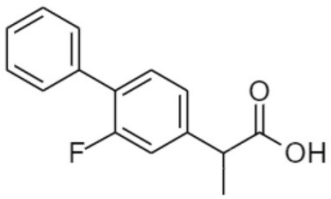 | 224 | 0.16 | 4.1 |
| (*R*)-2-(4-*n*-Butylphenyl)propionic acid<br>(*S*)-2-(4-*n*-Butylphenyl)propionic acid | 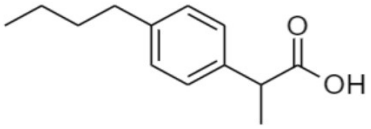 | 206 | 0.31 | 4.4 |
| (*R*)-2-(4-*tert*-Butylphenyl)propionic acid<br>(*S*)-2-(4-*tert*-Butylphenyl)propionic acid | 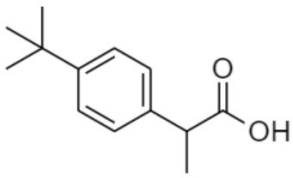 | 206 | 0.45 | 4.5 |

Of these enantiomeric 2-APAs, (*R*)-2-(3-chlorophenyl)propionic acid, (*S*)-2-(3-chlorophenyl)propionic acid, (*R*)-2-(4-chlorophenyl)propionic acid, (*S*)-2-(4-chlorophenyl)propionic acid, (*R*)-2-(4-*tert*-butylphenyl)propionic acid, and (*S*)-2-(4-*tert*-butylphenyl)propionic acid were purchased from Chem-Space (Monmouth Junction, NJ, USA). (*R*)-2-(4-Fluorophenyl)propionic acid, (*S*)-2-(4-fluorophenyl)propionic acid, (*R*)-2-(3-methylphenyl)propionic acid, (*S*)-2-(3-methylphenyl)propionic acid, (*R*)-2-(4-methoxyphenyl)propionic acid, (*S*)-2-(4-methoxyphenyl)propionic acid, (*R*)-2-(4-*n*-butylphenyl)propionic acid and (*S*)-2-(4-*n*-butylphenyl)propionic acid were purchased from eMolecules (San Diego, CA, USA). (*R*)-Naproxen, (*R*)-ketoprofen, and (*S*)-flurbiprofen were purchased from Sapphire Bioscience. (*R*)-2-Phenylpropionic acid, (S)-2-phenylpropionic acid, (*S*)-naproxen, (*S*)-ketoprofen, and (*R*)-flurbiprofen were purchased from Sigma-Aldrich (St. Louis, MO, USA).

All solvents and reagents in the study were of analytical grade. Acetonitrile (ACN), dichloromethane (DCM), methanol, triethylamine (TEA), ethylchloroformate, (*R*)-1-phenylethylamine (PEA), sulphuric acid, and sodium hydroxide were purchased from Sigma-Aldrich (Castle Hill, NSW, Australia). Water used in analysis was obtained from a Waters Milli-Q Water Purification unit (Millford, CT, USA).

Stock solutions of individual 2-APA enantiomers (approximately 1 g/L) and derivatisation reagents were prepared in anhydrous ACN and stored at 4 °C in the dark. From these individual stock solutions, two working stock solutions of 2-APAs were prepared in anhydrous ACN and stored at 4 °C in the dark for calibration standards and experiments. One working stock solution contained pure (*R*)-enantiomers. The other working stock solution contained pure (*S*)-enantiomers. As isotope-labelled standards were not available for all target analytes, a solution of racemic D3-naproxen, D3-ketoprofen, and D3-flurbiprofen was purchased from CDN Isotopes (Pointe-Claire, Quebec, Canada) and used as the surrogate internal standard (ISTD).

### 8.2.2. Laboratory-scale anaerobic digesters system

This study was conducted using a laboratory-scale AD system with two identical anaerobic digesters designated as R1 and R2 (Figure 43). Each digester consisted of a 1 L jacketed glass reactor with mixing paddle, rubber head plate with seven ports (Moubio Fermentor Company, Taiwan), a temperature control unit (Thermoline Scientific, Australia), a peristaltic hose pump (Masterflex L/S, USA), and a biogas counter (Ritter Company™, MilliGascounter). Digestate from a full-scale anaerobic digestion plant in Sydney (NSW, Australia) was used as the inoculum.

The AD system was fed using synthetic feed solution containing per litre: glucose (16 g), peptone (3 g), urea (0.7 g), $KH_2PO_4$ (0.7 g), $MgSO_4$ (1.015 g), $FeSO_4$ (0.7 g), and sodium acetate (9 g). Chemical oxygen demand (COD) and total nitrogen of the feed were 25.34 ± 1.3 and 1.6 g/L ± 0.05, respectively. The working volume of each digester was maintained at 900 mL. Both digesters were fed every day by first withdrawing 90 mL of digestate and then replacing it with 90 mL of feed, resulting in 10 days of hydraulic retention time/solids retention time (HRT/SRT) and an organic LR of 2.5 kg COD/$m^3$.d. The temperature and oxidation-reduction potential (ORP) of all digesters were maintained at 38.0 ± 0.1°C and below -460 mV, respectively. Prior to the addition of 2-APAs to the feed, the AD system was operated for over 30 days (3 SRT) for acclimatisation to achieve stable and identical performance between the two digesters. After acclimatisation, chiral 2-APAs were added to the feed at 1-10 µg/L of each enantiomer for 35 days. One digester (R1) was dosed with only (*R*)-enantiomers and the other digester (R2) was dosed with only (*S*)-enantiomers.

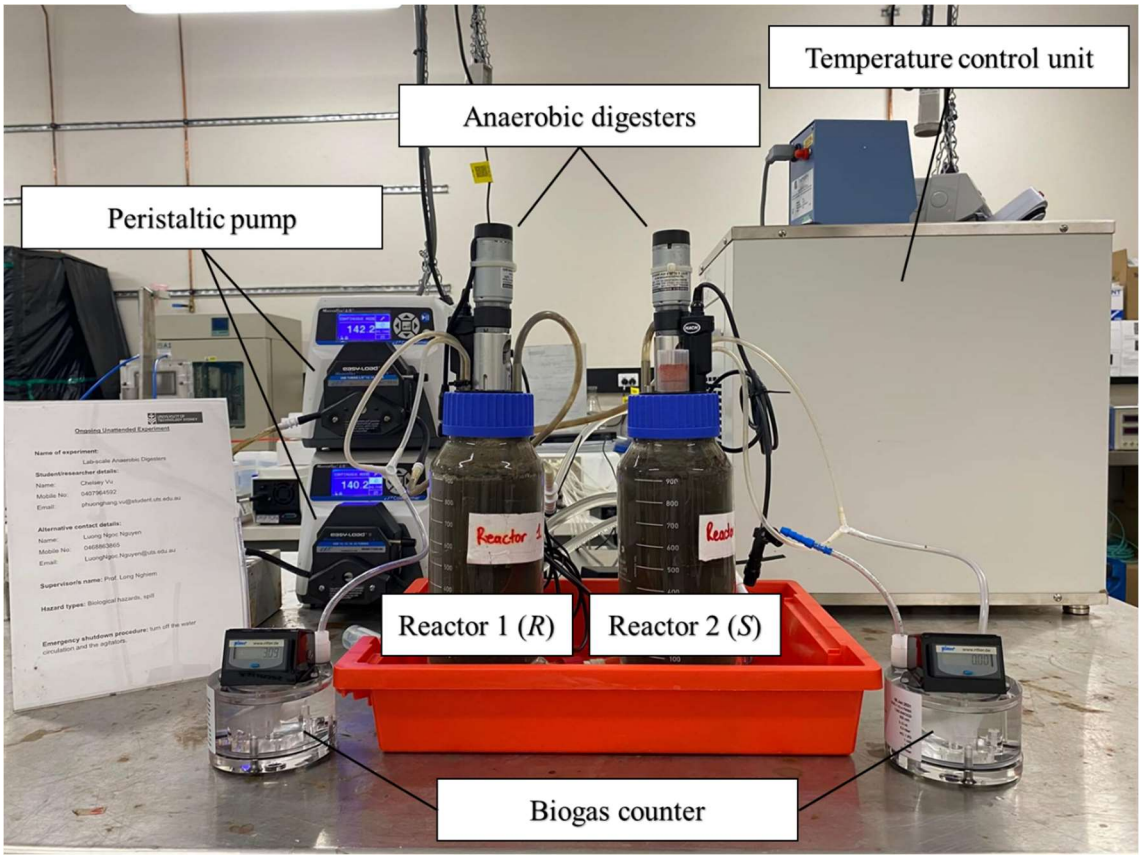


Figure 43. Laboratory-scale anaerobic digestion system.

### 8.2.3. Analytical methods

#### *8.2.3.1. Sample collection regime*

Of the 90 mL of digestate withdrawn from each digester every day, 25 mL was used for determining pH, TS, VS, and COD to monitor the digester performance; 10 mL each was used for DNA extraction and microbial analysis. Digester performance parameters were monitored twice a week. DNA extraction was conducted once a week. The remaining digestate was combined over three consecutive days and stored in a glass bottle at 4 ºC in the dark for settling. Approximately 120 mL of the supernatant was collected from each of these combined samples for enantiomeric analysis. All glass bottles were carefully cleaned with soap and tap water, methanol, and Milli-Q water to remove any trace of chiral compounds.

#### *8.2.3.2. Anaerobic digesters performance*

pH and ORP were monitored using a portable pH/conductivity meter (Hach, Australia). Total solids (TS) and volatile solids (VS) were determined according to Standard Methods 1684. The digestate was diluted 50 times using Milli-Q water and the diluted sludge was used for COD measurement using digestion vials (Hach, Australia) and Hach DR3900 spectrophotometer program number 435 COD HR, following the US-EPA Standard Method 5220D.

#### *8.2.3.3. Chiral compounds analyses*

The supernatant collected in Section 8.2.3.1 was filtered using 1.1 μm glass fiber paper (Filtech, Australia). Duplicate samples of the filtered supernatant (50 mL each) were transferred to separated glass bottles, diluted 10 times with Milli-Q water into 500 mL, and spiked with 50 ng of the ISTD. Duplicate samples of the feed (50 mL each) were prepared in the same protocol, filtered, diluted 10 times with Milli-Q water into 500 mL, and mixed with 50 μL of the ISTD. Solid-phase extraction, diastereomers preparation, and enantio-specific analysis of chiral 2-APAs were performed following a previously described analytical method (464).

#### *8.2.3.4. Removal efficiency and enantiomeric fraction*

The enantiomeric fraction (EF) was calculated as:

$$EF = \frac{C_M}{C_M + C_O} \qquad \text{Equation 1}$$

Where: $C_M$ is the concentration of the main enantiomer dosed into the digester, i.e. (*R*)-2-APAs for R1 and (*S*)-2-APAs for R2, and $C_O$ is the concentration of the other enantiomer.

The removal efficiency of an enantiomer was defined as:

$$\text{Overall removal} = 100 \times \frac{C_F - C_D}{C_F} \qquad \text{Equation 2}$$

Where: $C_F$ and $C_D$ are concentrations of the enantiomer in the AD feed and digestate, respectively.

#### *8.2.3.5. Bioinformatics analyses*

In total, 24 digestate samples were collected from the acclimatisation and chiral compound addition phases for microbial community analysis using a previous described protocol (255). Briefly, each sample was mixed with ethanol (1:1 v/v) and stored at -20 ºC prior to DNA extraction. Genomic DNA extraction was carried out using the DNAeasy PowerSoil Pro Kit (QIAGEN). The integrity, purity and concentration of the extracted DNA were evaluated by NanoDrop® spectrophotometer. DNA concentration of all samples was normalized to around 25 ng/μL using DNase/Pyrogen-Free Water before sending to the sequencing facility.

The universal primer set Pro341F (5'-CCTACGGGNGGCWGCAG-3') and Pro805R (5'-GACTACHVGGGTATCTAATCC-3') was used to amplify 16S rRNA V3 – V4 regions of the microbial community. Paired-end amplicon sequencing (2 × 300 bp) was carried out on the

Illumina MiSeq platform (UTS Next Generation Sequencing Facility, Sydney, Australia). Raw sequence data were generated with the Illumina *bcl2fastq* pipeline (version 2.20.0.422). All sequencing data in this study are available at the Sequence Read Archive (accession number: PRJNA809105) in the National Center for Biotechnology Information.

Raw reads were imported into Quantitative Insights Into Microbial Ecology (QIIME) 2 (version 2021.2.0) for computational analysis (257). Quality filtering, denoising (primer and read trimming), paired-end reads merging, dereplication, chimera filtering and feature clustering (≥ 97% similarity) were performed using the q2-dada2 denoise-paired plugin (258). Forward reads were truncated at position 270 and reverse reads were truncated at position 220 in the 3' end due to decrease in quality. Reads were mapped back to amplicon sequence variants (ASVs) with a minimum identity of 97% to obtain the number of reads in each feature. Taxonomy was assigned to features using the q2-feature-classifier (259) classify-sklearn Naïve Bayes taxonomy classifier against the SILVA database (release 138.99) (260-262) with a confidence of 0.7. Statistical analyses were conducted to identify microbial taxa with differential abundance (ANCOM) (311). Results from ANCOM analysis were visualized using RStudio (version 3.6.1).

Functional prediction was performed using PICRUST2 (471) with the script picrust2_pipeline.py with option --per_sequence_contrib and –stratified to get the contribution of each ASV (taxa) to the enzyme epimerase (EC:5.1.99.4) abundance in each sample. This enzyme was previously determined to associate with chiral inversion (443, 472). Taxa with the highest contribution to enzyme abundance were selected for relative abundance analysis.

## 8.3. Results and Discussions

### 8.3.1. Anaerobic digester performance

Both digesters showed stable and identical performance (Figure 44), allowing for a systematic comparison between (*R*)- and (*S*) enantiomeric inversion during AD. The daily biogas production gradually became stable with an average of 967.2 ± 185.0 and 966.3 ± 169.8 mL/day from R1 and R2, respectively (Figure 44A). The two digesters also showed similar performance in all other basic parameters including COD removal efficiencies, TS contents, VS/TS ratio, and pH (Figure 44B-D).

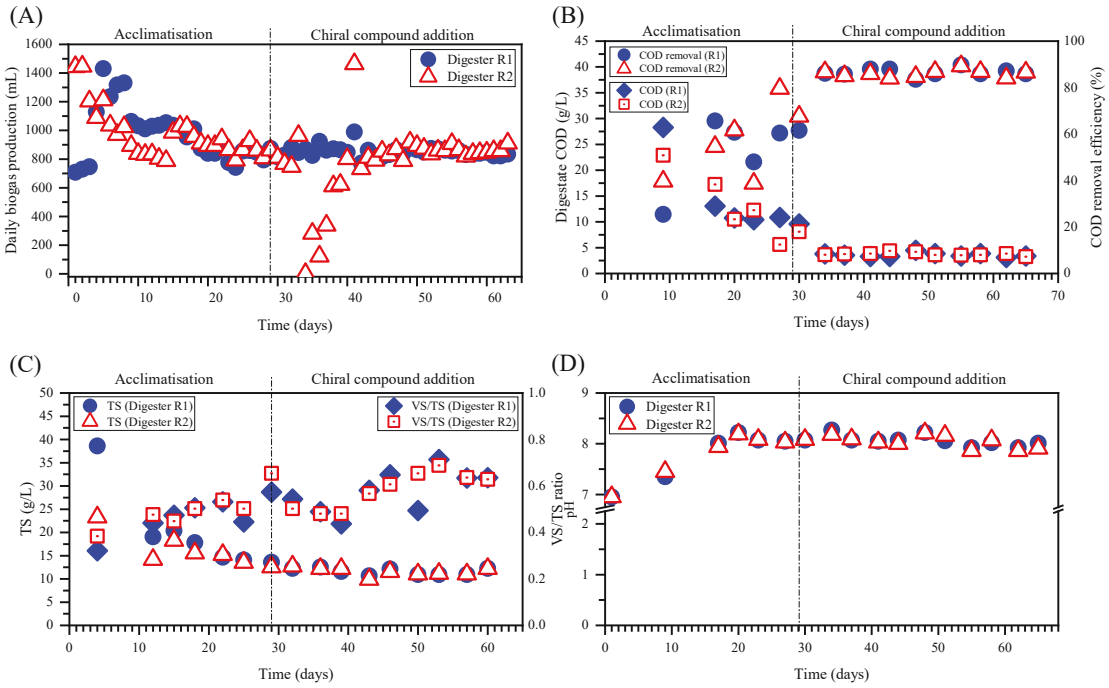


Figure 44. Performance of the two anaerobic digesters during the experimental period in terms of (a) daily biogas production, (b) chemical oxygen demand (COD) concentration and COD removal efficiency, (c) digestate quality including total solids content and volatile solids/total solids (VS/TS) ratio, and (d) pH of the digestate. R1 was dosed with (R)-enantiomers and R2 was dosed with (S)-enantiomers.

Chiral compound addition and the type of enantiomer dosed did not have any observable disturbance on the performance of both digesters (Figure 44). COD removal efficiencies were maintained above 80% in both digesters during the chiral compound addition phase (Figure 44B). Digestate from R1 and R2 showed relatively constant TS contents of 11.6 ± 0.7 and 11.5 ± 0.8, respectively, and the digestates' VS/TS ratios were also identical in this phase (Figure 44C). Biogas productions in two digesters were stable (Figure 44A), notwithstanding a temporary drop in digester R2 biogas production between day 34 to day 37 due to an experimental error (the isolation valve was accidentally left open during feeding allowing acid from the biogas meter to backflow into the digester). Nevertheless, all other performance parameters remained stable (Figure 44) and the biogas production quickly returned to the same level of R1. Overall, the two lab-scale anaerobic digesters had steady and similar performance throughout the experimental period, allowing for clear determination of chiral inversion occurrence.

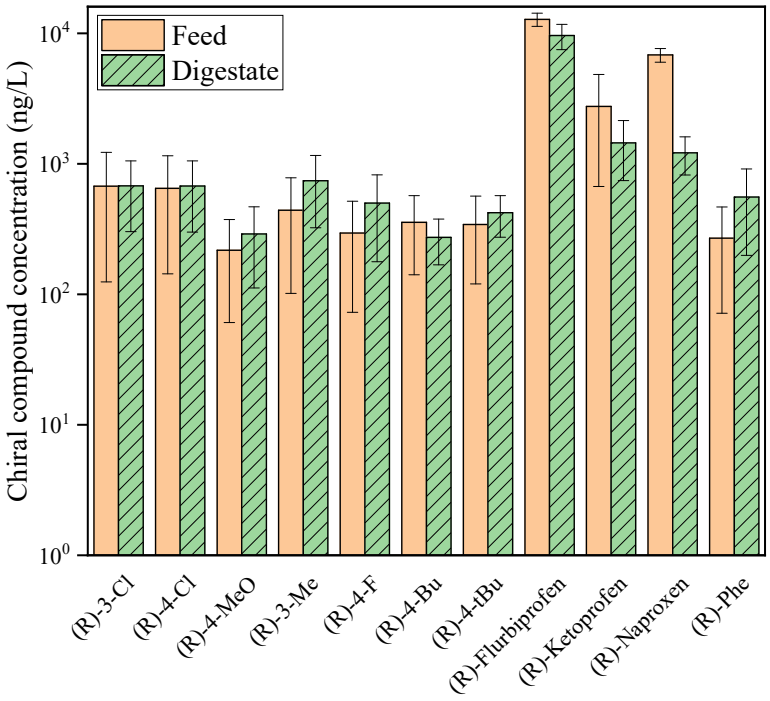


Figure 45. Concentration of (*R*)-enantiomers of 2-APAs in the feed and digestate of digester R1. Data represent the mean of all samples collected during chiral 2-APA addition period. The error bar represents the standard deviation from at least 14 measurements.

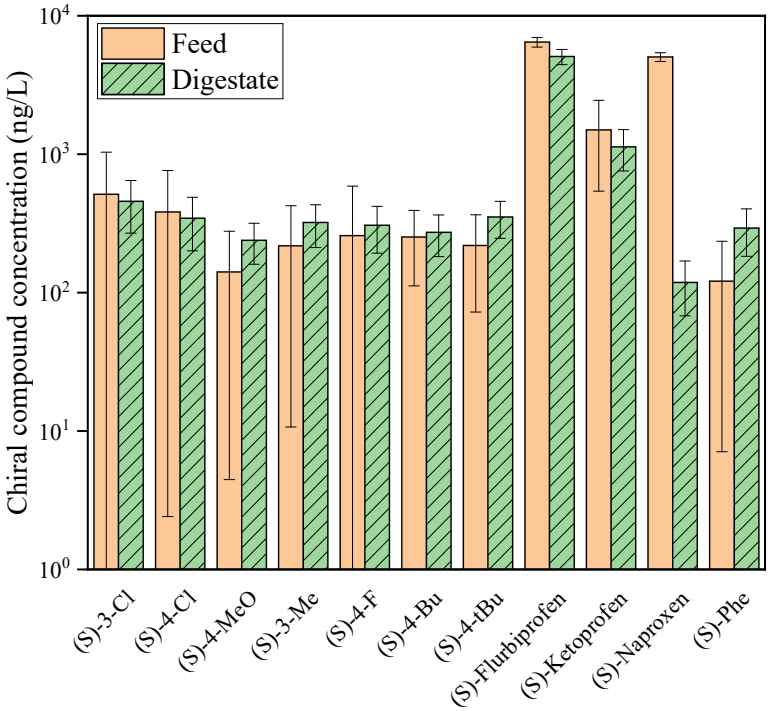


Figure 46. Concentration of (*S*)-enantiomers of 2-APAs in the feed and digestate of digester R2. Data represent the mean of all samples collected during chiral 2-APA addition period. The error bar represents the standard deviation from at least 13 measurements.

As expected, biological degradation of most chiral 2-APAs by anaerobic digestion was small or negligible as reflected by the similarity between the main enantiomer concentrations in the feed and the digestate of both digesters (Figure 45, Figure 46). Naproxen was an exception with a removal efficiency of 83% by digester R1 and 97.5% by digester R2. These results are in good agreement with previous studies investing the removal efficiency of NSAIDs by anaerobic digestion (424, 457). Phan et al. (457) observed that naproxen was well removed (> 83%) in both aqueous and solid phases of a pilot-scale AD system. Wijekoon et al. (424) also reported high removal of naproxen (74.7%), and low removal of all other NSAIDs, e.g. ketoprofen and ibuprofen (25.3 – 27.2%), in an anaerobic MBR. Naproxen possesses electron-donating functional group but no electron-withdrawing functional group, which enhances its susceptibility to biodegradation in an anaerobic system (424).

### 8.3.2. Chiral inversion under anaerobic conditions

A chiral compound can undergo either unidirectional or bidirectional inversion. In the former, the compound can only be converted from one enantiomer to the other but not in the opposite direction. In the latter, chiral inversion in both directions can occur. Chiral inversion under anaerobic conditions was observed for all eleven 2-APAs in this study, evidenced in the appearance of an enantiomer that was not initially present in the feed or at a higher concentration than in the feed. In this study, unidirectional inversion was observed with four 2-APAs and bidirectional inversion was observed with the remaining seven 2-APAs.

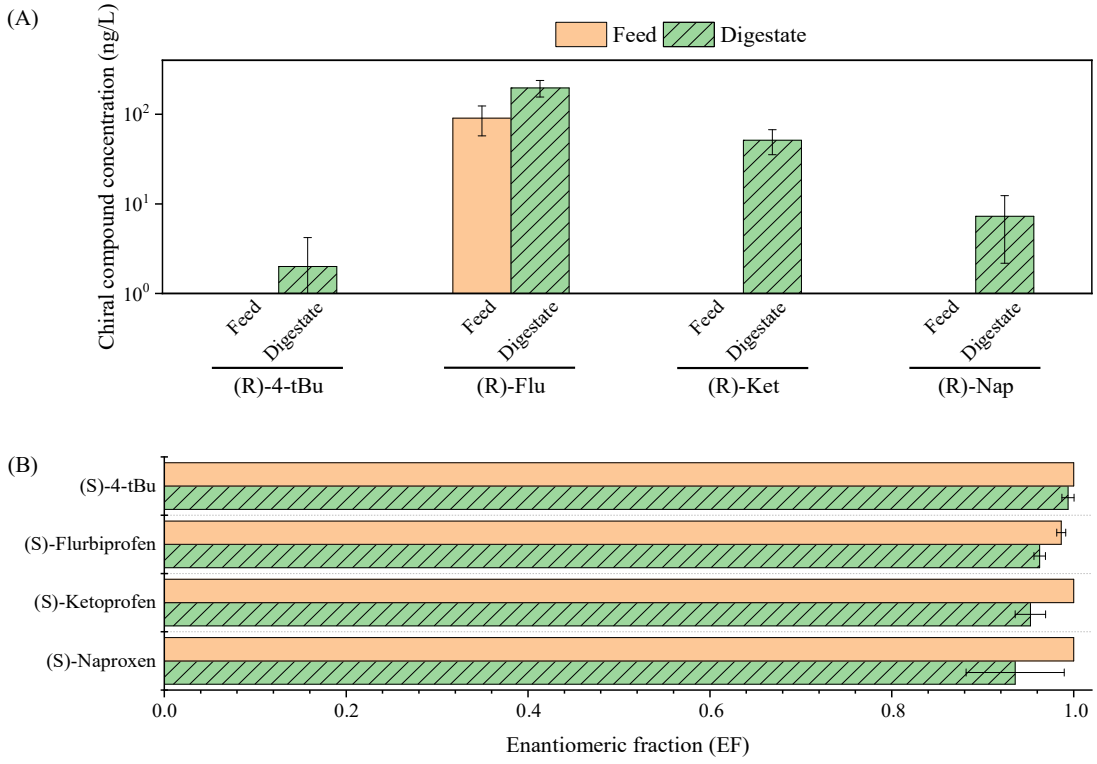

Figure 47. (S→R) chiral inversion of 2-(4-*tert*-butylphenyl)propionic acid (4-tBu), flurbiprofen (Flu), ketoprofen (Ket), and naproxen (Nap) depicted through detection of (*R*)-enantiomers and the decrease in enantiomeric fraction in the digestate of digester R2 (dosed with pure (*S*)-enantiomers). Data represent the mean of all samples collected during chiral 2-APA addition period. The error bar represents the standard deviation from at least 13 measurements.

The four 2-APAs that showed unidirectional chiral inversion are 2-(4-*tert*-butylphenyl)propionic acid, flurbiprofen, ketoprofen, and naproxen. The (*R*)-enantiomers were consistently detected in the digestate of digester R2 (dosed with (*S*)-2-APAs) at statistically higher concentrations than in the feed (Student t-test, $p < 0.05$), indicating the occurrence of chiral inversion (Figure 47A). It is interesting to note that chiral version of these compounds only occurred in the (S→R) direction (Figure 47). The (*S*)-enantiomers were either absent in the digestate, or detected at a lower concentration than in the feed of digester R1 (dosed with (*R*)-2-APAs).

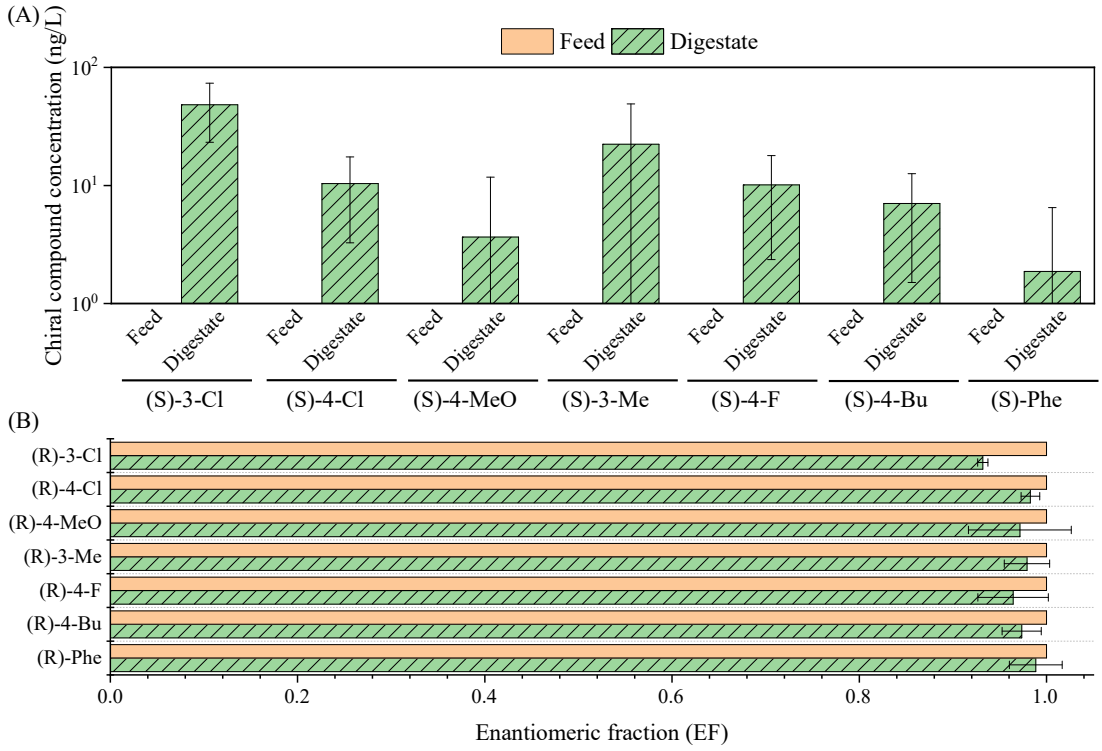


Figure 48. (R→S) chiral inversion of 2-(3-chlorophenyl)propionic acid (3-Cl), 2-(4-chlorophenyl)propionic acid (4-Cl), 2-(4-methoxyphenyl)propionic acid (4-MeO), 2-(3-methylphenyl)propionic acid (3-Me), 2-(4-fluorophenyl)propionic acid (4-F), 2-(4-butylphenyl)propionic acid (4-Bu), and 2-phenylpropionic acid (Phe) depicted through the detection of (*S*)-enantiomers and decrease in the enantiomeric fraction in the digestate of digester R1 (dosed with pure (*R*)-enantiomers). Data represent the mean of all samples collected

during chiral 2-APA addition period. The error bar represents the standard deviation from at least 14 measurements.

Bidirectional inversion was observed for seven 2-APAs, including 2-(3-chlorophenyl)propionic acid, 2-(4-chlorophenyl)propionic acid, 2-(4-methoxyphenyl)propionic acid, 2-(3-methylphenyl)propionic acid, 2-(4-fluorophenyl)propionic acid, 2-(4-butylphenyl)propionic acid, and 2-phenylpropionic acid (Figure 48, Figure 49) (Student t-test, $p < 0.05$). The concentrations of the (*S*)-enantiomer of these compounds in the digestate of R1 (dosed with (*R*)-2-APAs) and (*R*)-enantiomers in the digestate in digester R2 (dosed with (*S*)-2-APAs) were higher than that of the feed (Figure 49A). In both directions, the newly formed enantiomers were detected at low concentrations (sometimes <10 ng/L), and since the removal of most (*R*)- and (*S*)-2-APAs was poor (Section 8.3.1), these data indicate that the inversion rate in anaerobic system was limited.

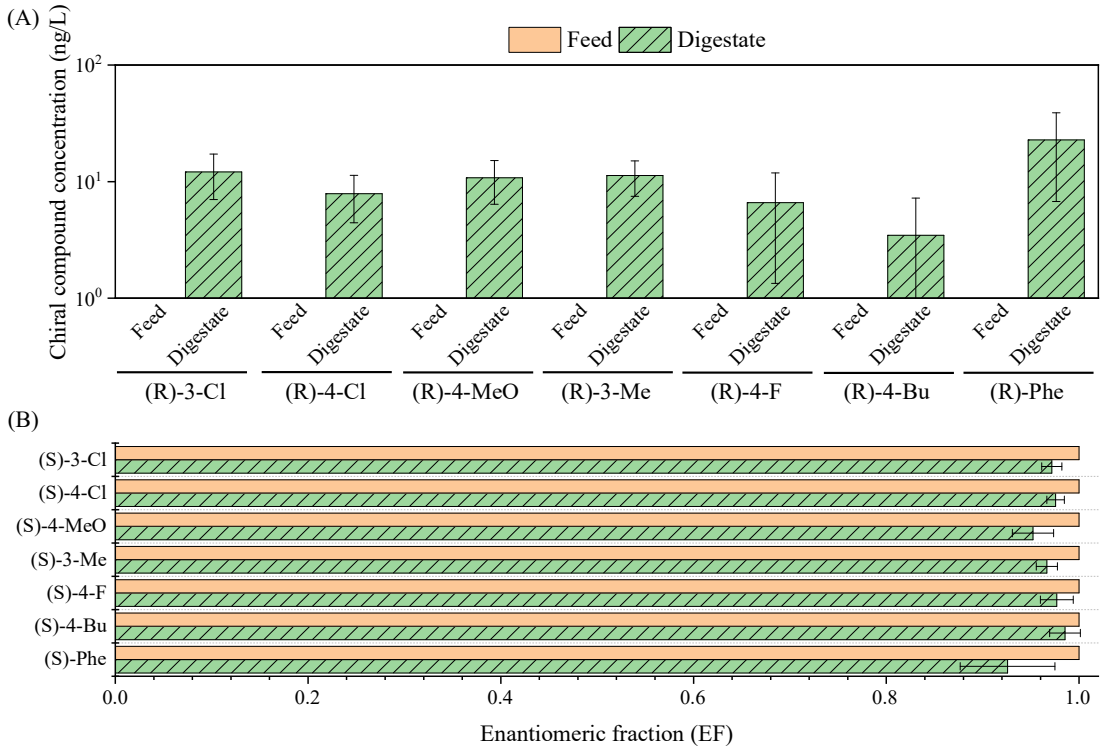


Figure 49. (S→R) chiral inversion of 2-(3-chlorophenyl)propionic acid (3-Cl), 2-(4-chlorophenyl)propionic acid (4-Cl), 2-(4-methoxyphenyl)propionic acid (4-MeO), 2-(3-methylphenyl)propionic acid (3-Me), 2-(4-fluorophenyl)propionic acid (4-F), 2-(4-butylphenyl)propionic acid (4-Bu), and 2-phenylpropionic acid (Phe) depicted through the detection of (*R*)-enantiomers and the decrease in enantiomeric fraction in the digestate of digester R2 (dosed with pure (*S*)-enantiomers). Data represent the mean of all samples collected during chiral 2-APA addition period. The error bar represents the standard deviation from at least 13 measurements.

This study appears to provide the first evidence of chiral inversion of a wide range of 2-APAs during anaerobic biological waste treatment. Although chiral inversion of all eleven 2-APAs in this study under anaerobic conditions can be statistically confirmed, the rate of chiral inversion is low when compared the concentration of the newly formed enantiomer in the digestate to the opposite enantiomer in the feed. Results from this study also demonstrate that the type of biological system can impact chiral inversion behaviour of 2-APAs. Chiral inversion behaviours observed under anaerobic and aerobic conditions were similar for six compounds: 2-(3-chlorophenyl)propionic acid, 2-(3-methylphenyl)propionic acid, 2-(4-fluorophenyl)propionic acid, 2-(4-butylphenyl)propionic acid, 2-(4-*tert*-butylphenyl)propionic acid, and flurbiprofen (Table 25). Meanwhile, discrepancies were observed in the chiral inversion behaviour of the remaining five compounds (432, 464). In addition, chiral inversion under anaerobic conditions happened at a limited extent compared to under aerobic conditions. These differences in chiral inversion behaviour could be due to the difference between aerobic and anaerobic microbial communities. It has previously been established that chiral inversion behaviour is substrate- and species-specific (438-440) (Table 25). Ketoprofen showed bidirectional inversion by a pure culture of the fungus *Verticillium lecanii* (444), but unidirectional (R→S) inversion by another fungus *Cordycep militalis* (440). Microorganisms responsible for chiral inversion under aerobic conditions might be different from that under anaerobic conditions, resulting in different inversion behaviours. It is also possible that the growth of microorganisms that can perform chiral inversion in aerobic systems is restricted under anaerobic conditions. Thus, microbial community analysis and a functional prediction tool were employed to bring more insights into the underlying mechanism (Section 8.3.3).

Table 25. Summary of 2-APAs chiral inversion in microbial systems showing that inversion is substrate- and species-specific. NA: compound not studied, -: no inversion activity, 1: (R→S) unidirectional inversion observed, 2: (S→R) unidirectional inversion observed, 3: bidirectional inversion observed.

| **Compound** | **Anaerobic digester (this study)** | **Aerobic MBR (221, 464)** | **Enzymatic MBR (fungi *Pleurotus ostreatus* laccase) (432)** | **Wastewater treatment plant (219, 448, 473)** | **Bacteria – *Norcardi diaphanozon aria* JCM3208 (443, 474)** | **Bacteria – *Norcardia corallina* B-276 (475)** | **Fungi – *Verticillium lecanii* (439, 444)** | **Fungi – *Cordycep militalis* (440)** |
|---|---|---|---|---|---|---|---|---|
| 2-Phenylpropionic acid | 3 | 1 | NA | NA | 2 | NA | 3 | 1 |
| 2-(4-Fluorophenyl)propionic acid | 3 | 3 | NA | NA | - | NA | NA | NA |
| 2-(4-Methoxyphenyl)propionic acid | 3 | 2 | NA | NA | - | NA | NA | NA |
| 2-(3-Chlorophenyl)propionic acid | 3 | 3 | NA | NA | - | NA | NA | NA |
| 2-(3-Methylphenyl)propionic acid | 3 | 3 | NA | NA | NA | NA | NA | NA |
| 2-(4-Chlorophenyl)propionic acid | 3 | 1 | NA | NA | - | NA | NA | NA |
| Ketoprofen | 2 | 3 | 3 | N/A | NA | NA | 3 | 1 |
| Naproxen | 2 | 3 | 3 | 2 | NA | NA | NA | NA |
| Flurbiprofen | 2 | 2 | NA | NA | - | NA | 1 | 1 |
| 2-(4-*n*-Butylphenyl)propionic acid | 3 | 3 | NA | NA | NA | NA | NA | NA |
| 2-(4-*tert*-Butylphenyl)propionic acid | 2 | 2 | NA | NA | NA | NA | NA | NA |
| Ibuprofen | NA | NA | 3 | NA | - | 2 | 1 | 1 |
| Indoprofen | NA | NA | NA | NA | NA | NA | 1 | 1 |
| Fenoprofen | NA | NA | NA | NA | NA | NA | 1 | 1 |
| Suprofen | NA | NA | NA | NA | NA | NA | 1 | 1 |

### 8.3.3. Role of microbial community during chiral inversion

#### *8.3.3.1. Microbial composition prior to chiral addition*

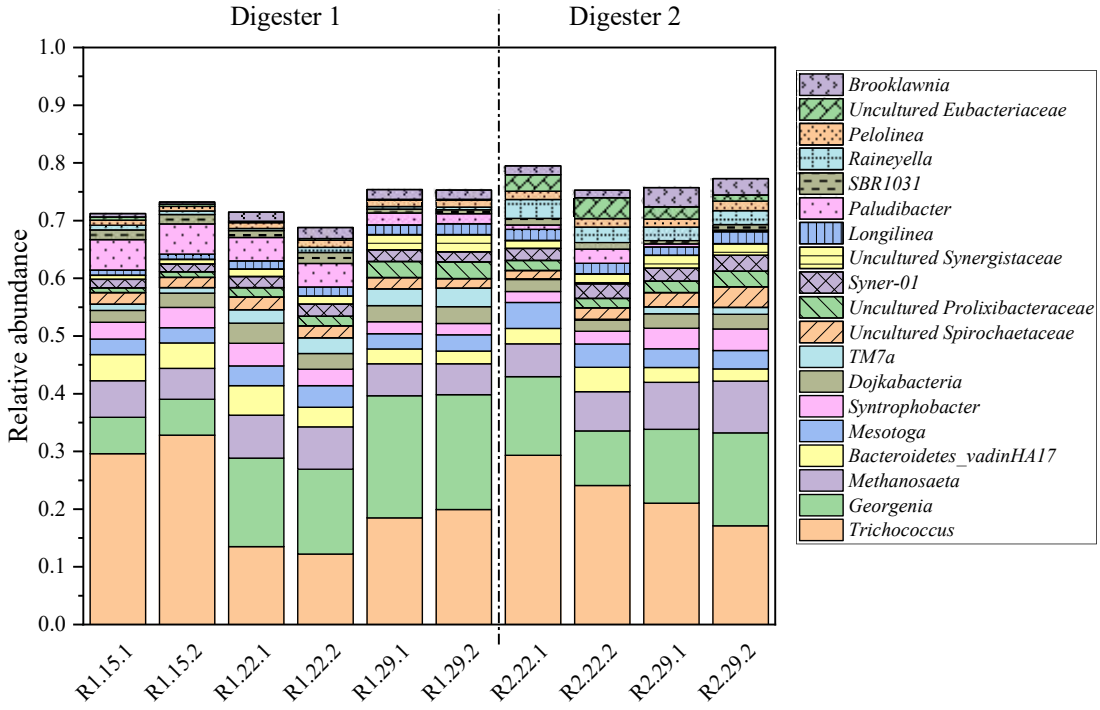


Figure 50. Microbial composition in the two anaerobic digesters during acclimatisation phase. Top 15 dominant genera from each digester were shown. Each sample is labelled using a combination of letter and digit in the format Rx.y.z, with x represents the digester number, y represents the day of operation, and z represents the duplicate number.

Microbial community analysis revealed stable and comparable microbial profiles between the two digesters during the acclimatisation phase (Figure 50). Dominant microbial genera in the two digesters were similar both in terms of identity and relative abundance. These genera are involved in fundamental functional groups of AD process (Table 26). The majority of them are hydrolytic and fermentative bacteria, such as *Trichococcus* (476), *Georgenia* (477), and *Mesotoga* (478). The sum relative abundance of hydrolytic and fermentative bacteria was in the range of 50.9 – 60.8 and 54.2 – 63.0% in digester R1 and R2, respectively. The high abundance of hydrolytic and fermentative bacteria could be attributed to the highly biodegradable feed composition. Nguyen et al. (479) also reported high abundance of hydrolytic and fermentative bacteria (up to 74.8%) while adding carbon-rich substrate into anaerobic digesters treating sewage sludge. Dominant acetogenic bacteria included *Syntrophobacter*, uncultured *Synergistaceae*, and uncultured *Spirochaetaceae* (480-483), accounted for a total of 7.6 – 9.6 and 9.7 – 13.2% in digester R1 and R2, respectively. *Methanosaeta* was the dominant methanogenic archaea, accounting for 6.2 ± 0.9 and 7.4 ± 1.3% of the community in digester R1 and R2, respectively, while

*Methanobacterium* presented at < 1.3% in both digesters. This indicates that acetoclastic methanogenesis was the main methane-producing pathway. Overall, there was a good balance between different functional groups in both digesters, ensuring no product accumulation (e.g. VFAs) and allowing for process stability and efficiency (66). The high similarity between the two digester microbial profiles also explains for the identical performance observed (Section 8.3.1).

Table 26. Dominant genera belong to different functional groups in the two anaerobic digesters and their relative abundances during acclimatisation phase.

| **Functional group** | **Genus** | **Ref.** | **Relative abundance in digester R1 (%)** | **Relative abundance in digester R2 (%)** |
|---|---|---|---|---|
| Hydrolysis and acidogenesis | *Trichococcus* | (476) | 21.1 ± 7.7 | 22.9 ± 4.5 |
| | *Georgenia* | (477) | 13.9 ± 5.9 | 13.0 ± 2.4 |
| | *Mesotoga* | (478) | 3.0 ± 0.4 | 3.7 ± 0.6 |
| | *TM7a* | (484) | 2.2 ± 0.9 | 0.7 ± 0.6 |
| | *Longilinea* | (485) | 1.4 ± 0.4 | 1.8 ± 0.2 |
| | *Paludibacter* | (486) | 3.7 ± 1.4 | 1.0 ± 0.8 |
| | *Raineyella* | (487) | 0.6 ± 0.2 | 2.7 ± 0.4 |
| | *Brooklawnia* | (488) | 1.3 ± 0.6 | 2.3 ± 0.9 |
| Acetogenesis | *Syntrophobacter* | (480), (481) | 2.9 ± 0.7 | 2.9 ± 0.8 |
| | Uncultured *Eubacteriaceae* | (489) | 0.3 ± 0.1 | 2.4 ± 0.9 |
| | Uncultured *Synergistaceae* | (482) | 1.6 ± 0.9 | 1.8 ± 0.3 |
| | Uncultured *Spirochaetaceae* | (483) | 2.0 ± 0.2 | 2.4 ± 0.8 |
| Methanogenesis | *Methanosaeta* | (481) | 6.2 ± 0.9 | 7.4 ± 1.3 |
| | *Methanobacterium* | | 1.1 ± 0.3 | 0.7 ± 0.1 |

#### *8.3.3.2. Impact of chiral addition on microbial composition*

The majority of dominant genera remained the same after 2-APA addition (Figure 51). Some genera showed decreased relative abundance compared to acclimatisation phase, including *Paludibacter* and *Syntrophobacter* in digester R1, *Brooklawnia*, *Longilinea*, *Raineyella* and uncultured *Eubacteriaceae* in digester R2. Members of these genera are hydrolytic-acidolytic and acetogenic bacteria (Table 26). Nevertheless, the decrease in abundance of these genera was

compensated by the emergence of other genera that perform the same function. The abundance of hydrolytic-acidolytic bacteria *Trichococcus* increased from 21.1 ± 7.7 to 30.3 ± 4.0% in digester R1, and from 22.9 ± 4.5 to 26.8 ± 5.4% in digester R2. Newly emerged bacteria belong to this functional group included *Anaerobium* (490), *Blvii28_wastewater_sludge_group* (491), and *Endomicrobium* (492, 493) (Figure 51). The acetogenic bacteria uncultured *Synergistaceae* also showed increased abundance during the chiral addition phase compared to acclimatisation phase, which made up for the decrease abundance of *Syntrophobacter* and uncultured *Eubacteriaceae*. These results show functional redundancy within the microbial community (494), allowing for the maintenance of stable performance in both digesters despite the shift in microbial composition.

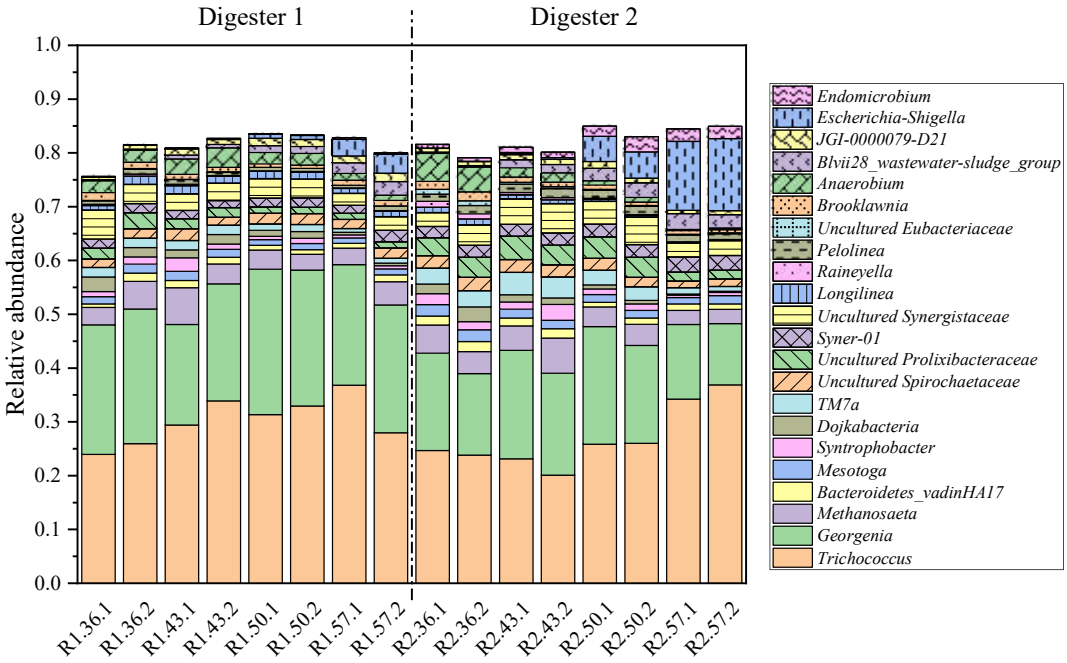


Figure 51. Microbial composition in the two anaerobic digesters during 2-APA addition phase. Top 15 dominant genera from each digester were shown. Each sample is labelled using a combination of letter and digit in the format Rx.y.z, with x represents the digester number, y represents the day of operation, and z represents the duplicate number.

Differential abundance analysis was performed to identify genera with significance changes in absolute abundance after chiral addition (Figure 52). Two genera (*Blvii28_wastewater_sludge_group* and *Dehalobacter*) were detected by differential abundance analysis in both digesters, indicating that these genera emergences were independent of the type of enantiomers dosed. While *Blvii28_wastewater_sludge_group* participates in hydrolysis-acidogenesis (491), the genera *Dehalobacter* is known to be involved in dechlorination process

of polychlorinated biphenyls and trichloromethane (495). This genus has been detected in full-scale WWTP anaerobic digesters at $2.6 \times 10^4$ copies of 16S rRNA genes per gram of digestate (496). It was also suggested that *Dehalobacter* growth is not limited to organohalide respiration, as these genera can also perform dichloromethane fermentation to acetate (497). The enrichment of *Dehalobacter* in both digesters (Figure 52) could be attributed to the addition of 2-APAs containing halogens in the substituent group, e.g. 2-(3-chlorophenyl)propionic acid, 2-(4-chlrophenyl)propionic acid, 2-(4-fluorophenyl)propionic acid, and flurbiprofen.

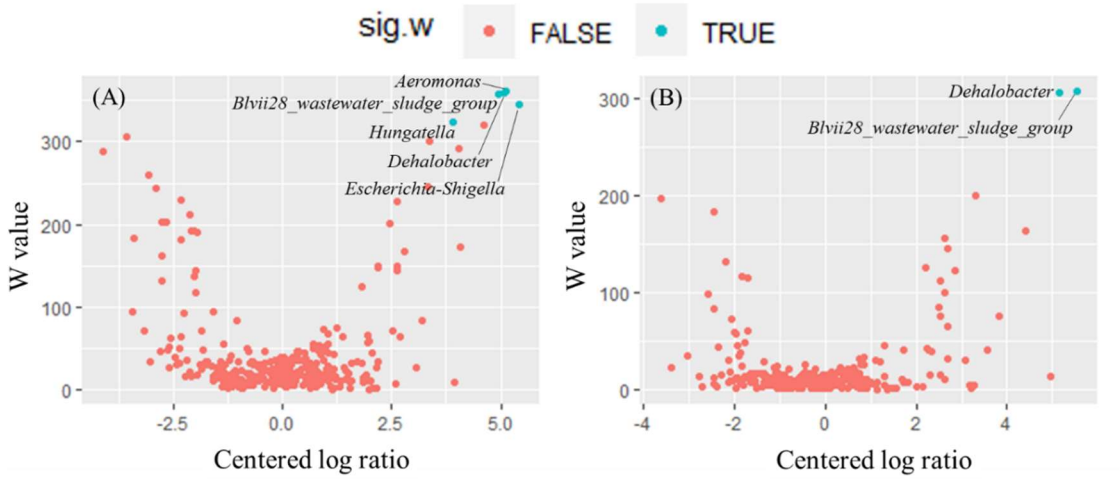


Figure 52. Differential abundance analysis showing microbial genera enriched after chiral addition in (a) digester R1 dosed with (*R*)-2-APAs, and (b) digester R2 dosed with (*S*)-2-APAs. The W value represents the number of times the null-hypothesis (the average abundance of a given genus in the community before chiral addition is equal to that after chiral addition) was rejected for a given genus. When the W value of a genus is high, it is more likely that the genus is differentially abundant across sample groups. The 70$^{th}$ percentile of the W distribution is used as the empirical cut-off value forsignificance. Genera that showed significant changes in abundance between the acclimatisation and chiral addition phases were marked with blue colour. The centered log ratio is the transformed mean difference in abundance of a given genus between the community before (acclimatisation phase) and after chiral addition. A positive centered log ratio means a genus is abundant in the community after chiral addition.

#### *8.3.3.3. Functional prediction reveals microbes involved in chiral inversion*

Chiral inversion by microorganisms is an important subject for further scientific investigation. Based on previous work on the role of bacteria such as *V. lecanii* and *N. diaphanozonaria* (443, 469) in facilitating microbial chiral inversion, the process is proposed to be similar to that in a mammalian system. In other words, chiral inversion involves three steps (Figure 53): formation of an 'activated' coenzyme A derivative with one enantiomer (catalyzed by acyl-CoA-

synthetase), enzymatic epimerisation of the acyl-CoA thioester derivatives (catalyzed by 2-arylpropionyl-CoA epimerase), and hydrolysis to produce the other enantiomer (469). A homologue of mammalian 2-arylpropionyl-CoA epimerase (also known as α-methylacyl-CoA racemase (472)) has been identified in the bacterium *Mycobacterium tuberculosis*. This enzyme showed racemization activity on (*S*)-2-methylmyristoyl-CoA, and (*R,S*)-ibuprofenoyl-CoA (498-500). Detailed study on the structure of this epimerase has shown that its active site geometry agrees with a 1,1-proton transfer mechanism (deprotonation and protonation), and the inversion of the chirality is caused by the interchange of the positions of the $C^{\alpha}$ hydrogen atom and the $C^{\beta}$ atom (499). The enzyme structures also indicate that the acyl chains of the (*S*)- and (*R*)-substrate bind to separate S-pocket and R-pocket, respectively (499).

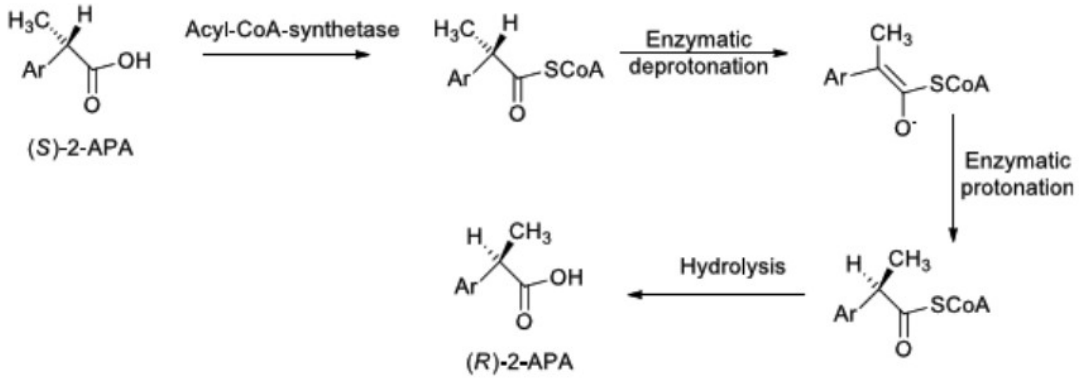


Figure 53. Proposed mechanisms of chiral inversion by microorganisms (from Khan (450)).

Functional prediction analysis identified several taxa harbouring 2-arylpropionyl-CoA epimerase encoding gene in the digester. Taxa with high predicted gene abundances belonged to five genera: *Candidatus_Microthrix, Rhodococcus, Mycobacterium, Gordonia,* and *Sphingobium* (Table 27, Table 28). Of these genera, *Rhodococcus, Mycobacterium,* and *Gordonia* are in the same order (*Corynebacteriales*) with bacteria (*N. diaphanozonaria JCM3208* and *N. corallina* B-276) that have been reported to perform chiral inversion of 2-APAs (i.e. ibuprofen and 2-phenylpropanoic acid) (443, 475). Members of *Rhodococcus* have also been reported to perform chiral inversion of secondary alcohols and aryloxypropionic acid (501, 502). Thus, it is possible that the five genera identified in this study were responsible for 2-APA chiral inversion. These are aerobic or facultative bacteria but can survive in a viable yet nonculturable state (low metabolic activity and do not divide) under anaerobic conditions (503), thus, they have low abundance in the digesters (< 0.5 and < 0.2% in digester R1 and R2, respectively, Table 29). The low abundance of these epimerase-associated genera is consistent with the small rate of chiral inversion observed in this study (Section 8.3.2).

Table 27. Predicted abundance of 2-arylpropionyl-CoA epimerase gene in digester R1 dosed with (*R*)-enantiomers. *f_*: family, *g_*: genus, *s_*: species.

| **Taxa** | **R1.15.1** | **R1.15.2** | **R1.22.1** | **R1.22.2** | **R1.29.1** | **R1.29.2** | **R1.36.1** | **R1.36.2** | **R1.43.1** | **R1.43.2** | **R1.50.1** | **R1.50.2** | **R1.57.1** | **R1.57.2** |
|---|---|---|---|---|---|---|---|---|---|---|---|---|---|---|
| *g__Candidatus_Microthrix* | 82 | 34 | 10 | 24 | 28 | 32 | 18 | 20 | 0 | 10 | 0 | 6 | 0 | 0 |
| *g__Rhodococcus* | 36 | 0 | 72 | 224 | 362 | 250 | 296 | 350 | 228 | 186 | 86 | 82 | 92 | 108 |
| *g__Mycobacterium* | 26 | 0 | 0 | 0 | 18 | 9 | 0 | 0 | 0 | 0 | 0 | 0 | 0 | 0 |
| *g__Gordonia* | 18 | 0 | 30 | 48 | 48 | 42 | 57 | 66 | 0 | 12 | 0 | 0 | 0 | 0 |
| *s__Sphingopyxis_granuli* | 0 | 0 | 0 | 23 | 12 | 10 | 14 | 0 | 6 | 10 | 0 | 3 | 0 | 0 |
| *f__Xanthobacteraceae* | 0 | 0 | 0 | 6 | 9 | 7 | 0 | 15 | 0 | 9 | 0 | 0 | 0 | 0 |
| *s__Pseudomonas_stutzeri* | 0 | 0 | 0 | 0 | 0 | 0 | 0 | 0 | 0 | 0 | 0 | 17 | 7 | 20 |
| *g__Brevundimonas* | 0 | 0 | 0 | 7 | 0 | 3.5 | 2.5 | 2.5 | 0 | 0 | 0 | 0 | 0 | 0 |
| *s__Paracoccus_alkenifer* | 0 | 0 | 0 | 0 | 0 | 10 | 0 | 14 | 10 | 0 | 0 | 0 | 0 | 0 |
| *g__Ottowia* | 0 | 0 | 0 | 0 | 0 | 0 | 1.5 | 0 | 0 | 0 | 0 | 0 | 0 | 0 |
| *f__Sphingomonadaceae* | 0 | 0 | 0 | 0 | 7 | 5 | 0 | 0 | 0 | 0 | 0 | 0 | 0 | 0 |

Table 28. Predicted abundance of 2-arylpropionyl-CoA epimerase gene in digester R2 dosed with (*S*)-enantiomers. *f_*: family, *g_*: genus, *s_*: species.

| **Taxa** | **R2.22.1** | **R2.22.2** | **R2.29.1** | **R2.29.2** | **R2.36.1** | **R2.36.2** | **R2.43.1** | **R2.43.2** | **R2.50.1** | **R2.50.2** | **R2.57.1** | **R2.57.2** |
|---|---|---|---|---|---|---|---|---|---|---|---|---|
| *g__Candidatus_Microthrix* | 114 | 156 | 102 | 86 | 60 | 42 | 18 | 24 | 0 | 4 | 0 | 0 |
| *g__Rhodococcus* | 54 | 30 | 30 | 36 | 36 | 30 | 20 | 0 | 0 | 18 | 20 | 0 |
| *g__Mycobacterium* | 0 | 28 | 0 | 0 | 0 | 0 | 0 | 0 | 0 | 0 | 0 | 0 |
| *g__Sphingobium* | 31 | 52 | 5 | 14 | 0 | 0 | 0 | 0 | 7 | 3 | 15 | 6 |
| *g__Brevundimonas* | 4 | 3.5 | 0 | 0 | 0 | 0 | 0 | 0 | 0 | 0 | 0 | 0 |
| *s__Pseudomonas_guangdongensis* | 0 | 0 | 0 | 0 | 0.6 | 1.6 | 0 | 1.6 | 1 | 2.8 | 1.4 | 0 |
| *g__PeM15* | 0 | 2 | 0 | 0 | 0 | 0 | 0 | 0 | 0 | 0 | 0 | 0 |
| *g__Rhodobacter* | 0 | 0 | 0 | 8 | 4 | 0 | 0 | 0 | 0 | 0 | 0 | 0 |

Table 29. Relative abundance of taxa predicted to harbour 2-arylpropionyl-CoA epimerase gene in the two digesters. *f_*: family, *g_*: genus, *s_*: species. ND: not detected.

| **Taxa** | **Relative abundance in digester R1 (%)** | | **Relative abundance in digester R2 (%)** | |
|---|---|---|---|---|
| | **Acclimatisation** | **Chiral addition** | **Acclimatisation** | **Chiral addition** |
| *g__Candidatus_Microthrix* | 0.046 ± 0.022 | 0.008 ± 0.009 | 0.138 ± 0.037 | 0.021 ± 0.024 |
| *g__Rhodococcus* | 0.214 ± 0.176 | 0.229 ± 0.110 | 0.048 ± 0.025 | 0.018 ± 0.015 |
| *g__Mycobacterium* | 0.012 ± 0.012 | ND | 0.011 ± 0.011 | ND |
| *g__Gordonia* | 0.027 ± 0.016 | 0.013 ± 0.020 | ND | ND |
| *g__Sphingobium* | ND | ND | 0.062 ± 0.041 | 0.011 ± 0.013 |
| *s__Sphingopyxis_granuli* | 0.014 ± 0.016 | 0.009 ± 0.009 | ND | ND |
| *f__Xanthobacteraceae* | 0.009 ± 0.009 | 0.007 ± 0.013 | ND | ND |
| *s__Pseudomonas_stutzeri* | ND | 0.010 ± 0.014 | ND | ND |
| *g__Brevundimonas* | 0.013 ± 0.018 | 0.004 ± 0.005 | 0.010 ± 0.011 | ND |
| *s__Paracoccus_alkenifer* | 0.002 ± 0.003 | 0.003 ± 0.005 | ND | ND |
| *g__Ottowia* | ND | 0.002± 0.004 | ND | ND |
| *f__Sphingomonadaceae* | 0.005 ± 0.007 | ND | ND | ND |
| *s__Pseudomonas_guangdongensis* | ND | ND | ND | 0.010 ± 0.008 |
| *g__PeM15* | ND | ND | 0.001 ± 0.002 | ND |
| *g__Rhodobacter* | ND | ND | 0.006 ±0.007 | 0.001 ± 0.003 |

## 8.4. Conclusion

This study validated the occurrence of chiral inversion of 2-APAs during anaerobic waste treatment. The suite of eleven 2-APAs exhibited diversion chiral inversion behaviour with both unidirectional and bidirectional inversion, although they only differ from one another by one substituent group attached to the backbone. Shifts in microbial composition induced by chiral compound addition did not impact the digesters' performance, which could be attributed to functional redundancy. Most microbial genera predicted to be involved with chiral inversion are aerobic or facultative anaerobic, including *Candidatus_Microthrix*, *Rhodococcus*, *Mycobacterium*, *Gordonia,* and *Sphingobium*, and presented at low abundances in both digesters (< 0.5 and < 0.2% in R1 and R2, respectively), explains for the limited extent of chiral inversion observed.

# Chapter 9. CONCLUSION AND RECOMMENDATIONS

## 9.1. Conclusion

This thesis work has unravelled new insights into biochemical processes for wastewater treatment and bioremediation using state-of-the-art and powerful research tools including metagenomics, bioinformatics, and enantiomeric analysis. Research findings reported here can be used to develop new technologies or optimise the performance of existing processes for biological treatment of wastewater and organic waste.

Membrane fouling-associated microbial community was investigated in membrane bioreactors (MBRs) under low- and high-flux conditions (Chapter 3 & Chapter 4). Endogenous decay and excessive growth of filamentous bacteria (i.e. *Thiotrichales*) could contribute to membrane fouling under the low-flux condition (Chapter 3). Endogenous decay was caused by nutrient deficiency and high sludge age since there was no sludge withdrawal (except for performance monitoring analysis). The biofouling layer (biofilm) possessed highly similar microbial composition to the mixed liquor, with *Thiotrichales* as the predominant microbial taxa. This could be attributed to the tendency of filamentous bacteria to attach on the membrane surface and their fixing action that draws more colloids and other foulants to the membrane. An anaerobic microbial taxon (*Holophagales*) showed 27.3 fold increase in relative abundance in the biofilm compared to the mixed liquor, which could be explained by the lack of oxygen in the thick biofilm formed by filamentous bacteria.

Under the high-flux condition (Chapter 4), the fouling profile was reproducible and the biofilm community showed critical differences from the mixed liquor community. This work highlights the importance of the type of bioinformatics tools and indices used for analysis, since the extent of difference shown between biofilm and mixed liquor can vary based on the analysis. For example, with the unweighted pair group method with arithmetic mean (UPGMA) clustering analysis, the difference between the mixed liquor and biofilm is much clearer when the Bray-Curtis dissimilarity index was used (comparing in terms of microbial composition) compared to when the unweighted UniFrac distance was used (comparing in terms of microbial identity). Results from these two UPGMA analyses highlighted that the difference between mixed liquor and biofilm were driven mainly by the difference in microbial abundance and not microbial identity. Differential abundance analysis (ANCOM) complements UPGMA analyses by identifying which microbial taxa have driven the divergence between mixed liquor and biofilm. ANCOM analysis is conducted based on absolute abundance data rather than relative abundance data like in previous studies, thus it can avoid the caveat of relative data. Results from ANCOM analysis point out that low-abundance (< 1%) microbial taxa e.g. *Victivallales* and *Blastocatellia* 11–24 were those with true differential abundance, and these taxa were also identified as key

players in the two communities through network analysis. Key players in both biofilm and mixed liquor communities strongly correlated with extracellular polymeric substance (EPS) concentration. Network analysis also revealed the distinct pattern in biofilm vs. mixed liquor networks, with higher level of inter-species interaction and prevalence of positive connections (74.6%) in the biofilm compared to the mixed liquor community (42.2%), which could be explained by the assembly mechanism of the biofilm where microorganisms stay in close proximity in EPS matrix.

The evaluation of two inocula (rumen fluid vs. anaerobic sludge) for lignocellulosic biomass digestion was described in Chapter 5. Rumen fluid showed remarkable capability to convert lignocellulosic biomass (LCBM) into volatile fatty acid (VFA) compared to anaerobic sludge (4 times higher VFA yield). The significantly higher VFA yield could be attributed to the presence of specific lignocellulolytic bacteria e.g. *Fibrobacter* and *Prevotella* that can easily break down the recalcitrant structure of the substrate during hydrolysis and acidogenesis steps. However, the rapid acidification and VFA production led to a sharp decline in pH and inhibited the process only after four days of incubation (shown by no further increase in VFA production). VFA accumulation also inhibited methanogens as they are slow-growing microbes and sensitive to sudden changes in environmental pH. These results suggest that continuous separation of VFAs from the reactor can enhance process efficiency. Meanwhile, hydrolysis and acidogenesis were the rate-limiting steps in the anaerobic sludge reactor rather than methanogenesis.

One critical element of this thesis is the development of a novel biomimicry system – the rumen-MBR – which was described in Chapter 6. The integration of an ultrafiltration membrane to a rumen-inoculated system allowed for continuous and effective VFA separation, which in turn avoids process inhibition due to VFA accumulation and promotes continuous and stable VFA generation. The total VFA yield achieved with this system (438 mg VFA/g substrate) was higher than that of the batch study described in Section 4.1 (100 mg VFA/g substrate) and other studies on continuous rumen-based systems. The extent of substrate acidification and VFA composition (type and percentage of each VFA) observed in the rumen-MBR closely resembles VFA composition in the rumen fluid inoculum. These results indicated that the developed system has partly succeeded in simulating the digestion of LCBM and absorption of VFA in cow's rumen. Furthermore, the high transfer rate of total VFA from the rumen-MBR to the permeate (73 ± 15%) facilitates subsequent VFA purification to obtain the final product. The studied operating conditions could not facilitate the complete maintenance of the rumen indigenous microbial community (reduced abundance of lignocellulolytic bacteria e.g. *Ruminococcaceae* and *Prevotella* and methanogens). Nevertheless, after the acclimatisation period, the rumen-MBR showed stable operation, which could be attributed to functional redundancy – the emergence of new microbial taxa that perform same function with the lost taxa e.g. *Bacteroides* and

*Ruminofilibacter*. The success of rumen-MBR system creates an opportunity for VFA production from LCBM instead of fossil fuels in the future.

Chapter 7 examined the removal and enantio-specific fate of chiral 2-arylpropionic acids (2-APAs) during biological wastewater treatment. The dosing of pure (*R*)- and (*S*)- enantiomers into two parallel MBRs (MBR-R and MBR-S) allowed for the clear distinction between enantioselective degradation and chiral inversion (the transformation from one enantiomer to the other enantiomer). All compounds showed effective removal (>90%) except (*S*)-naproxen (74.5 ± 14.4 %), which could be attributed to its higher steric hindrance and polynuclear structure (two fused aromatic rings). Removals of (*R*)-enantiomers in MBR-R and (*S*)-enantiomers in MBR-S were similar for eight compounds. Chiral inversion was observed for all compounds investigated, with two showing unidirectional (R→S) inversion, three showing unidirectional (S→R) inversion, and the rest showing bidirectional inversion. Chiral inversion accounted for 0.01 – 20.19% of the compound removal efficiency. For compounds that exhibited bidirectional inversion, (R→S) appeared to be the more dominant inversion direction. This is the first time chiral inversion behaviours of an extensive suite of 2-APAs in a well-controlled biological wastewater treatment process have been reported.

Built upon the previous work in Chapter 7, chiral inversion of 2-APAs during anaerobic waste treatment was validated in Chapter 8. Both (S→R) unidirectional (flurbiprofen, ketoprofen, naproxen, and 2-(4-*tert*-butylphenyl)propionic acid) and bidirectional inversion (the remaining seven compounds) were observed. There was a high agreement in chiral inversion behaviours under aerobic and anaerobic conditions (6/11 compounds). Differential abundance analysis revealed the enrichment of *Dehalobacter* during chiral compounds addition phase, which could be linked to the 2-APAs containing halogens in the substituent group, e.g. 2-(3-chlorophenyl)propionic acid, 2-(4-chlrophenyl)propionic acid, 2-(4-fluorophenyl)propionic acid, and flurbiprofen. Functional prediction analysis identified several microbial genera potentially involved in chiral inversion, including *Candidatus_Microthrix*, *Rhodococcus*, *Mycobacterium*, *Gordonia,* and *Sphingobium*. These genera are predicted to harbour the gene encoding 2-arylpropionyl-CoA epimerase, the enzyme catalysing the second step of chiral inversion. Since chiral inversion could occur under both aerobic and anaerobic conditions, this process can lead to the increase in the concentration of the more biologically active or more toxic enantiomers in the treated products. Results from these works suggested the need for better monitoring strategies of 2-APAs in waste and wastewater treatment process.

## 9.2. Recommendations

Results from this thesis have demonstrated the application of novel microbial characterization technologies (next-generation sequencing) and bioinformatics tools to provide a more

comprehensive understanding of the microbial community involved in environmental engineering processes, develop novel waste/wastewater treatment technology, and mitigate current process operational challenge for enhanced process stability and efficiency. This research can be extended further. For further application of NGS and bioinformatics tools to improve biological waste and wastewater treatment, the following topics can be considered in future research.

- Despite operating at low (sub-critical) flux, endogenous decay and sludge bulking can result in membrane fouling. Thus, future research should be conducted on optimizing MBR operating conditions (e.g. nutrient and dissolved oxygen) to prevent sludge bulking occurrence.
- The potential of specifically targeting keystone fouling-associated taxa in the MBR mixed liquor should be examined in future studies. Since these taxa were presented in low abundances, it is unlikely for the regulation of their growth to affect biological performance of the MBR.
- The complementary effect between rumen fluid and anaerobic sludge is shown in Chapter 5 suggests a possible combination between the two inocula (rumen fluid for the VFA production and anaerobic sludge for biogas production), which should be investigated in future studies.
- Due to the substrate's recalcitrant structure, pre-treatment of the LCBM before feeding into the rumen-MBR is recommended to enhance acidification rate and VFA yield. In addition, the effect of substrate loading rate and membrane fouling on VFA production should be investigated in future studies to improve the system's scalability. Furthermore, the frequent supplement of clarified rumen fluid during rumen-MBR operation should be considered to provide specific nutrients that are essential for the growth of many ruminal microbes, which would assist the maintenance of indigenous rumen microbial community and enhance VFA yield.
- Removal of pure enantiomers of naproxen and ketoprofen was higher compared to the removal previously reported for racemic solution. Further research to simultaneously examine degradation pathway and the fate of pure enantiomers may unravel the underlying reason for this phenomenon.
- Despite the only difference in substituent group, the eleven 2-APAs studied exhibited significantly different chiral inversion behaviours. Analysis of the MBR microbial community associated with chiral inversion may bring more insights into the chiral inversion mechanism and the effect of substituent group in the process.

## REFERENCES


1. Solid waste management: UN Environmental Programme; [Available from: https://www.unep.org/explore-topics/resource-efficiency/what-we-do/cities/solid-waste-management.
2. Nghiem LD, Iqbal HMN, Zdarta J. The shadow pandemic of single use personal protective equipment plastic waste: A blue print for suppression and eradication. Case Studies in Chemical and Environmental Engineering. 2021;4:100125.
3. Nguyen TKL, Ngo HH, Guo W, Chang SW, Nguyen DD, Nghiem LD, et al. Insight into greenhouse gases emissions from the two popular treatment technologies in municipal wastewater treatment processes. Science of The Total Environment. 2019;671:1302-13.
4. Locey KJ, Lennon JT. Scaling laws predict global microbial diversity. Proceedings of the National Academy of Sciences. 2016:201521291.
5. Mikesková H, Novotný Č, Svobodová K. Interspecific interactions in mixed microbial cultures in a biodegradation perspective. Applied Microbiology & Biotechnology. 2012;95(4):861-70.
6. Atlas RM, Hazen TC. Oil biodegradation and bioremediation: a tale of the two worst spills in U.S. history. Environmental science & technology. 2011;45(16):6709-15.
7. Recovering Value from Waste: Anaerobic Digester System Basics. In: Agency USEP, editor. 2012.
8. Kim B, Hong VM, Yang J, Hyun H, Im JJ, Hwang J, et al. A Review of Fermented Foods with Beneficial Effects on Brain and Cognitive Function. Preventive nutrition and food science. 2016;21(4):297-309.
9. Sonestedt E, Wirfalt E, Wallstrom P, Gullberg B, Orho-Melander M, Hedblad B. Dairy products and its association with incidence of cardiovascular disease: the Malmo diet and cancer cohort. European journal of epidemiology. 2011;26(8):609-18.
10. Chilton SN, Burton JP, Reid G. Inclusion of fermented foods in food guides around the world. Nutrients. 2015;7(1):390-404.
11. Hara KY, Araki M, Okai N, Wakai S, Hasunuma T, Kondo A. Development of bio-based fine chemical production through synthetic bioengineering. Microbial cell factories. 2014;13:173-.
12. Lee JW, Kim HU, Choi S, Yi J, Lee SY. Microbial production of building block chemicals and polymers. Current Opinion in Biotechnology. 2011;22(6):758-67.
13. Sanchez-Garcia L, Martín L, Mangues R, Ferrer-Miralles N, Vázquez E, Villaverde A. Recombinant pharmaceuticals from microbial cells: a 2015 update. Microbial Cell Factories. 2016;15(1):33.
14. Fitamo T, Treu L, Boldrin A, Sartori C, Angelidaki I, Scheutz C. Microbial population dynamics in urban organic waste anaerobic co-digestion with mixed sludge during a change in feedstock composition and different hydraulic retention times. Water Research. 2017;118:261-71.
15. Singh P, Karimi A, Devendra K, Waldroup PW, Cho KK, Kwon YM. Influence of penicillin on microbial diversity of the cecal microbiota in broiler chickens. Poultry science. 2013;92(1):272-6.
16. Bernhard AE, Colbert D, McManus J, Field KG. Microbial community dynamics based on 16S rRNA gene profiles in a Pacific Northwest estuary and its tributaries. FEMS microbiology ecology. 2005;52(1):115-28.
17. Kimura H, Ishibashi J-I, Masuda H, Kato K, Hanada S. Selective Phylogenetic Analysis Targeting 16S rRNA Genes of Hyperthermophilic Archaea in the Deep-Subsurface Hot Biosphere. Applied and Environmental Microbiology. 2007;73(7):2110.

18. Loy A, Kusel K, Lehner A, Drake HL, Wagner M. Microarray and functional gene analyses of sulfate-reducing prokaryotes in low-sulfate, acidic fens reveal cooccurrence of recognized genera and novel lineages. Appl Environ Microbiol. 2004;70(12):6998-7009.
19. Wilson KH, Wilson WJ, Radosevich JL, DeSantis TZ, Viswanathan VS, Kuczmarski TA, et al. High-density microarray of small-subunit ribosomal DNA probes. Applied and environmental microbiology. 2002;68(5):2535-41.
20. Wu L, Thompson DK, Li G, Hurt RA, Tiedje JM, Zhou J. Development and evaluation of functional gene arrays for detection of selected genes in the environment. Applied and environmental microbiology. 2001;67(12):5780-90.
21. Barnett MJ, Toman CJ, Fisher RF, Long SR. A dual-genome Symbiosis Chip for coordinate study of signal exchange and development in a prokaryote-host interaction. Proceedings of the National Academy of Sciences of the United States of America. 2004;101(47):16636-41.
22. Das M, Royer TV, Leff LG. Diversity of Fungi, Bacteria, and Actinomycetes on Leaves Decomposing in a Stream. Applied and Environmental Microbiology. 2007;73(3):756.
23. Pradhan A, Seena S, Pascoal C, Cássio F. Can Metal Nanoparticles Be a Threat to Microbial Decomposers of Plant Litter in Streams? Microbial Ecology. 2011;62(1):58-68.
24. Raviraja NS, Nikolcheva LG, Bärlocher F. Diversity of Conidia of Aquatic Hyphomycetes Assessed by Microscopy and by DGGE. Microbial Ecology. 2005;49(2):301-7.
25. Reeson AF, Jankovic T, Kasper ML, Rogers S, Austin AD. Application of 16S rDNA-DGGE to examine the microbial ecology associated with a social wasp Vespula germanica. Insect Molecular Biology. 2003;12(1):85-91.
26. Díez B, Pedrós-Alió C, Marsh TL, Massana R. Application of Denaturing Gradient Gel Electrophoresis (DGGE) To Study the Diversity of Marine Picoeukaryotic Assemblages and Comparison of DGGE with Other Molecular Techniques. Applied and Environmental Microbiology. 2001;67(7):2942.
27. Ni S-Q, Gao B-Y, Wang C-C, Lin J-G, Sung S. Fast start-up, performance and microbial community in a pilot-scale anammox reactor seeded with exotic mature granules. Bioresource Technology. 2011;102(3):2448-54.
28. Huang Z, Gedalanga PB, Asvapathanagul P, Olson BH. Influence of physicochemical and operational parameters on Nitrobacter and Nitrospira communities in an aerobic activated sludge bioreactor. Water Research. 2010;44(15):4351-8.
29. Lee PK, Macbeth TW, Sorenson KS, Jr., Deeb RA, Alvarez-Cohen L. Quantifying genes and transcripts to assess the in situ physiology of "Dehalococcoides" spp. in a trichloroethene-contaminated groundwater site. Appl Environ Microbiol. 2008;74(9):2728-39.
30. Zhang Z, Qu Y, Li S, Feng K, Wang S, Cai W, et al. Soil bacterial quantification approaches coupling with relative abundances reflecting the changes of taxa. Scientific Reports. 2017;7(1):4837.
31. Schmidt H, Eickhorst T. Detection and quantification of native microbial populations on soil-grown rice roots by catalyzed reporter deposition-fluorescence in situ hybridization. FEMS microbiology ecology. 2014;87(2):390-402.
32. Hoshino T, Schramm A. Detection of denitrification genes by in situ rolling circle amplification-fluorescence in situ hybridization to link metabolic potential with identity inside bacterial cells. Environmental microbiology. 2010;12(9):2508-17.

33. Smolina I, Miller NS, Frank-Kamenetskii M. PNA-based microbial pathogen identification and resistance marker detection: an accurate, isothermal rapid assay based on genome-specific features. Artificial DNA, PNA & XNA. 2010;1(2):1-7.
34. Behrens S, Losekann T, Pett-Ridge J, Weber PK, Ng WO, Stevenson BS, et al. Linking microbial phylogeny to metabolic activity at the single-cell level by using enhanced element labeling-catalyzed reporter deposition fluorescence in situ hybridization (EL-FISH) and NanoSIMS. Appl Environ Microbiol. 2008;74(10):3143-50.
35. Ito T, Yoshiguchi K, Ariesyady HD, Okabe S. Identification and quantification of key microbial trophic groups of methanogenic glucose degradation in an anaerobic digester sludge. Bioresource Technology. 2012;123:599-607.
36. Hungate BA, Mau RL, Schwartz E, Caporaso JG, Dijkstra P, van Gestel N, et al. Quantitative Microbial Ecology through Stable Isotope Probing. Applied and Environmental Microbiology. 2015;81(21):7570.
37. Haichar FeZ, Roncato M-A, Achouak W. Stable isotope probing of bacterial community structure and gene expression in the rhizosphere of Arabidopsis thaliana. FEMS microbiology ecology. 2012;81(2):291-302.
38. Limam RD, Chouari R, Mazeas L, Wu TD, Li T, Grossin-Debattista J, et al. Members of the uncultured bacterial candidate division WWE1 are implicated in anaerobic digestion of cellulose. MicrobiologyOpen. 2014;3(2):157-67.
39. Yang F-C, Chen Y-L, Tang S-L, Yu C-P, Wang P-H, Ismail W, et al. Integrated multi-omics analyses reveal the biochemical mechanisms and phylogenetic relevance of anaerobic androgen biodegradation in the environment. The Isme Journal. 2016;10:1967.
40. Roume H, Heintz-Buschart A, Muller EEL, May P, Satagopam VP, Laczny CC, et al. Comparative integrated omics: identification of key functionalities in microbial community-wide metabolic networks. Npj Biofilms And Microbiomes. 2015;1:15007.
41. Handelsman J, Rondon MR, Brady SF, Clardy J, Goodman RM. Molecular biological access to the chemistry of unknown soil microbes: a new frontier for natural products. Chemistry & Biology. 1998;5(10):R245-R9.
42. Rabausch U, Juergensen J, Ilmberger N, Böhnke S, Fischer S, Schubach B, et al. Functional screening of metagenome and genome libraries for detection of novel flavonoid-modifying enzymes. Applied and environmental microbiology. 2013;79(15):4551-63.
43. Pindjakova J, Sartini C, Lo Re O, Rappa F, Coupe B, Lelouvier B, et al. Gut Dysbiosis and Adaptive Immune Response in Diet-induced Obesity vs. Systemic Inflammation. Frontiers in microbiology. 2017;8:1157.
44. Berini F, Casciello C, Marcone GL, Marinelli F. Metagenomics: novel enzymes from non-culturable microbes. FEMS microbiology letters. 2017;364(21).
45. Berini F, Casciello C, Marcone GL, Marinelli F. Metagenomics: novel enzymes from non-culturable microbes. FEMS Microbiology Letters. 2017;364(21).
46. Cowan D, Meyer Q, Stafford W, Muyanga S, Cameron R, Wittwer P. Metagenomic gene discovery: past, present and future. Trends in Biotechnology. 2005;23(6):321-9.
47. Jaenicke S, Ander C, Bekel T, Bisdorf R, Dröge M, Gartemann K-H, et al. Comparative and Joint Analysis of Two Metagenomic Datasets from a Biogas Fermenter Obtained by 454-Pyrosequencing. PLOS ONE. 2011;6(1):e14519.
48. Cabezas A, de Araujo JC, Callejas C, Galès A, Hamelin J, Marone A, et al. How to use molecular biology tools for the study of the anaerobic digestion process? Reviews in Environmental Science and Bio/Technology. 2015;14(4):555-93.

49. Gosalbes MJ, Durbán A, Pignatelli M, Abellan JJ, Jiménez-Hernández N, Pérez-Cobas AE, et al. Metatranscriptomic approach to analyze the functional human gut microbiota. PloS one. 2011;6(3):e17447-e.
50. Tsementzi D, Poretsky R, Rodriguez-R LM, Luo C, Konstantinidis KT. Evaluation of metatranscriptomic protocols and application to the study of freshwater microbial communities. Environmental Microbiology Reports. 2014;6(6):640-55.
51. Bashiardes S, Zilberman-Schapira G, Elinav E. Use of Metatranscriptomics in Microbiome Research. Bioinformatics and biology insights. 2016;10:19-25.
52. Schirmer M, Franzosa EA, Lloyd-Price J, McIver LJ, Schwager R, Poon TW, et al. Dynamics of metatranscription in the inflammatory bowel disease gut microbiome. Nature Microbiology. 2018;3(3):337-46.
53. Haiser HJ, Turnbaugh PJ. Is It Time for a Metagenomic Basis of Therapeutics? Science. 2012;336(6086):1253.
54. Maurice CF, Haiser HJ, Turnbaugh PJ. Xenobiotics shape the physiology and gene expression of the active human gut microbiome. Cell. 2013;152(1-2):39-50.
55. Tveit AT, Urich T, Svenning MM. Metatranscriptomic Analysis of Arctic Peat Soil Microbiota. Applied and Environmental Microbiology. 2014;80(18):5761.
56. Aguiar-Pulido V, Huang W, Suarez-Ulloa V, Cickovski T, Mathee K, Narasimhan G. Metagenomics, Metatranscriptomics, and Metabolomics Approaches for Microbiome Analysis. Evolutionary bioinformatics online. 2016;12(Suppl 1):5-16.
57. Marcobal A, Kashyap PC, Nelson TA, Aronov PA, Donia MS, Spormann A, et al. A metabolomic view of how the human gut microbiota impacts the host metabolome using humanized and gnotobiotic mice. The ISME journal. 2013;7(10):1933-43.
58. Zhang X, Deeke SA, Ning Z, Starr AE, Butcher J, Li J, et al. Metaproteomics reveals associations between microbiome and intestinal extracellular vesicle proteins in pediatric inflammatory bowel disease. Nature Communications. 2018;9(1):2873.
59. Lankadurai BP, Nagato EG, Simpson MJ. Environmental metabolomics: an emerging approach to study organism responses to environmental stressors. Environmental Reviews. 2013;21(3):180-205.
60. Zhang W, Li F, Nie L. Integrating multiple 'omics' analysis for microbial biology: application and methodologies. Microbiology (Reading, England). 2010;156(Pt 2):287-301.
61. Dugat-Bony E, Straub C, Teissandier A, Onésime D, Loux V, Monnet C, et al. Overview of a Surface-Ripened Cheese Community Functioning by Meta-Omics Analyses. PLOS ONE. 2015;10(4):e0124360.
62. Califf KJ, Schwarzberg-Lipson K, Garg N, Gibbons SM, Caporaso JG, Slots J, et al. Multi-omics Analysis of Periodontal Pocket Microbial Communities Pre- and Posttreatment. mSystems. 2017;2(3):e00016-17.
63. Vernocchi P, Del Chierico F, Russo A, Majo F, Rossitto M, Valerio M, et al. Gut microbiota signatures in cystic fibrosis: Loss of host CFTR function drives the microbiota enterophenotype. PloS one. 2018;13(12):e0208171-e.
64. Yu K, Yi S, Li B, Guo F, Peng X, Wang Z, et al. An integrated meta-omics approach reveals substrates involved in synergistic interactions in a bisphenol A (BPA)-degrading microbial community. Microbiome. 2019;7(1):16-.
65. Broberg M, Doonan J, Mundt F, Denman S, McDonald JE. Integrated multi-omic analysis of host-microbiota interactions in acute oak decline. Microbiome. 2018;6(1):21-.
66. Nguyen AQ, Nguyen LN, Phan HV, Galway B, Bustamante H, Nghiem LD. Effects of operational disturbance and subsequent recovery process on microbial

community during a pilot-scale anaerobic co-digestion. International Biodeterioration & Biodegradation. 2019;138:70-7.
67. Henriet O, Meunier C, Henry P, Mahillon J. Filamentous bulking caused by Thiothrix species is efficiently controlled in full-scale wastewater treatment plants by implementing a sludge densification strategy. Scientific Reports. 2017;7(1):1430.
68. Yang W, Cicek N, Ilg J. State-of-the-art of membrane bioreactors: Worldwide research and commercial applications in North America. Journal of Membrane Science. 2006;270(1):201-11.
69. Huang X, Xiao K, Shen Y. Recent advances in membrane bioreactor technology for wastewater treatment in China. Frontiers of Environmental Science & Engineering in China. 2010;4(3):245-71.
70. Skinner S. Interactive map: History of municipal membrane bioreactor installations (up to 2018): The MBR site; 2018 [Available from: https://www.thembrsite.com/municipal-mbrs/interactive-map-history-municipal-mbr-installations/.
71. Judd S. Largest MBR plants (over 100 MLD) – Worldwide: The MBR site; 2018 [updated 20-08-2021. Available from: https://www.thembrsite.com/largest-mbr-plants/largest-membrane-bioreactor-plants-worldwide/.
72. Santos A, Ma W, Judd SJ. Membrane bioreactors: Two decades of research and implementation. Desalination. 2011;273(1):148-54.
73. Le-Clech P. Membrane bioreactors and their uses in wastewater treatments. Applied Microbiology and Biotechnology. 2010;88(6):1253-60.
74. Wang Z, Ma J, Tang CY, Kimura K, Wang Q, Han X. Membrane cleaning in membrane bioreactors: A review. Journal of Membrane Science. 2014;468:276-307.
75. Bachosz K, Vu MT, Nghiem LD, Zdarta J, Nguyen LN, Jesionowski T. Enzyme-based control of membrane biofouling for water and wastewater purification: A comprehensive review. Environmental Technology & Innovation. 2022;25:102106.
76. Luo W, Xie M, Hai FI, Price WE, Nghiem LD. Biodegradation of cellulose triacetate and polyamide forward osmosis membranes in an activated sludge bioreactor: Observations and implications. Journal of Membrane Science. 2016;510:284-92.
77. van Bentem AGN, Nijman N, Schyns PFT, Petri CP. MBR Varsseveld: 5 years of operational experience. Water Practice and Technology. 2010;5(1):wpt2010013.
78. Hao XD, Li J, van Loosdrecht MCM, Li TY. A sustainability-based evaluation of membrane bioreactors over conventional activated sludge processes. Journal of Environmental Chemical Engineering. 2018;6(2):2597-605.
79. Larrea A, Rambor A, Fabiyi M. Ten years of industrial and municipal membrane bioreactor (MBR) systems – lessons from the field. Water Science and Technology. 2014;70(2):279-88.
80. Bagheri M, Mirbagheri SA. Critical review of fouling mitigation strategies in membrane bioreactors treating water and wastewater. Bioresource Technology. 2018;258:318-34.
81. Aslam M, Ahmad R, Kim J. Recent developments in biofouling control in membrane bioreactors for domestic wastewater treatment. Separation and Purification Technology. 2018;206:297-315.
82. Costa RE, Battistelli AA, Bernardelli JKB, Bassin JP, Belli TJ, Lapolli FR. Assessing the performance and microbial community of hybrid moving bed and conventional membrane bioreactors treating municipal wastewater. Environmental Technology. 2019;40(6):716-29.

83. Abass OK, Fang F, Zhuo M, Zhang K. Integrated interrogation of causes of membrane fouling in a pilot-scale anoxic-oxic membrane bioreactor treating oil refinery wastewater. Sci Total Environ. 2018;642:77-89.
84. Redman JA, Walker SL, Elimelech M. Bacterial Adhesion and Transport in Porous Media: Role of the Secondary Energy Minimum. Environmental Science & Technology. 2004;38(6):1777-85.
85. Karatan E, Watnick P. Signals, Regulatory Networks, and Materials That Build and Break Bacterial Biofilms. Microbiology and Molecular Biology Reviews. 2009;73(2):310-47.
86. Hai FI, Yamamoto K, Nakajima F, Fukushi K. Bioaugmented membrane bioreactor (MBR) with a GAC-packed zone for high rate textile wastewater treatment. Water Research. 2011;45(6):2199-206.
87. Johir MAH, Aryal R, Vigneswaran S, Kandasamy J, Grasmick A. Influence of supporting media in suspension on membrane fouling reduction in submerged membrane bioreactor (SMBR). Journal of Membrane Science. 2011;374(1):121-8.
88. Zsirai T, Buzatu P, Aerts P, Judd S. Efficacy of relaxation, backflushing, chemical cleaning and clogging removal for an immersed hollow fibre membrane bioreactor. Water Research. 2012;46(14):4499-507.
89. Meng F, Zhang S, Oh Y, Zhou Z, Shin H-S, Chae S-R. Fouling in membrane bioreactors: An updated review. Water Research. 2017;114:151-80.
90. Bao Q, Xie L, Ohashi H, Hosomi M, Terada A. Inhibition of Agrobacterium tumefaciens biofilm formation by acylase I-immobilized polymer surface grafting of a zwitterionic group-containing polymer brush. Biochemical Engineering Journal. 2019;152:107372.
91. Lee B, Yeon K-M, Shim J, Kim S-R, Lee C-H, Lee J, et al. Effective Antifouling Using Quorum-Quenching Acylase Stabilized in Magnetically-Separable Mesoporous Silica. Biomacromolecules. 2014;15(4):1153-9.
92. Grover N, Plaks JG, Summers SR, Chado GR, Schurr MJ, Kaar JL. Acylase-containing polyurethane coatings with anti-biofilm activity. Biotechnology and Bioengineering. 2016;113(12):2535-43.
93. Meshram P, Dave R, Joshi H, Dharani G, Kirubagaran R, Venugopalan VP. A fence that eats the weed: Alginate lyase immobilization on ultrafiltration membrane for fouling mitigation and flux recovery. Chemosphere. 2016;165:144-51.
94. Rehman ZU, Leiknes T. Quorum-Quenching Bacteria Isolated From Red Sea Sediments Reduce Biofilm Formation by Pseudomonas aeruginosa. Frontiers in microbiology. 2018;9.
95. Xu H, Liu Y. Control and Cleaning of Membrane Biofouling by Energy Uncoupling and Cellular Communication. Environmental Science & Technology. 2011;45(2):595-601.
96. Huang L-N, De Wever H, Diels L. Diverse and Distinct Bacterial Communities Induced Biofilm Fouling in Membrane Bioreactors Operated under Different Conditions. Environmental Science & Technology. 2008;42(22):8360-6.
97. Zhang K, Choi H, Dionysiou DD, Sorial GA, Oerther DB. Identifying pioneer bacterial species responsible for biofouling membrane bioreactors. Environmental microbiology. 2006;8(3):433-40.
98. Lim S, Kim S, Yeon K-M, Sang B-I, Chun J, Lee C-H. Correlation between microbial community structure and biofouling in a laboratory scale membrane bioreactor with synthetic wastewater. Desalination. 2012;287:209-15.
99. Gonzalez-Martinez A, Leyva-Diaz JC, Rodriguez-Sanchez A, Munoz-Palazon B, Rivadeneyra A, Poyatos JM, et al. Isolation and metagenomic characterization of bacteria

associated with calcium carbonate and struvite precipitation in a pure moving bed biofilm reactor-membrane bioreactor. Biofouling. 2015;31(4):333-48.
100. Jo SJ, Kwon H, Jeong S-Y, Lee C-H, Kim TG. Comparison of microbial communities of activated sludge and membrane biofilm in 10 full-scale membrane bioreactors. Water Research. 2016;101:214-25.
101. El-Fadel M, Sleem F, Hashisho J, Saikaly PE, Alameddine I, Ghanimeh S. Impact of SRT on the performance of MBRs for the treatment of high strength landfill leachate. Waste Management. 2018;73:165-80.
102. Fortunato L, Pathak N, Ur Rehman Z, Shon H, Leiknes T. Real-time monitoring of membrane fouling development during early stages of activated sludge membrane bioreactor operation. Process Safety and Environmental Protection. 2018;120:313-20.
103. Takada K, Hashimoto K, Soda S, Ike M, Makio T, Nakayama Y, et al. Microbial Communities on the Submerged Membranes in Full-Scale Membrane Bioreactors Treating Municipal Wastewater. Journal of Environmental Engineering. 2018;144(1):04017084.
104. Takada K, Shiba T, Yamaguchi T, Akane Y, Nakayama Y, Soda S, et al. Cake layer bacterial communities during different biofouling stages in full-scale membrane bioreactors. Bioresource Technology. 2018;259:259-67.
105. Zhijun R, Pengfei W, Jiayu T, Zhiliu Z. Effects of a low-strength magnetic field on the characteristics of activated sludge for membrane fouling mitigation. RSC Advances. 2019;9(16):9180-6.
106. Liu Y, Liu Q, Li J, Ngo HH, Guo W, Hu J, et al. Effect of magnetic powder on membrane fouling mitigation and microbial community/composition in membrane bioreactors (MBRs) for municipal wastewater treatment. Bioresource Technology. 2018;249:377-85.
107. Gao D, Fu Y, Ren N. Tracing biofouling to the structure of the microbial community and its metabolic products: A study of the three-stage MBR process. Water Research. 2013;47(17):6680-90.
108. Gao D-W, Wen Z-D, Li B, Liang H. Membrane fouling related to microbial community and extracellular polymeric substances at different temperatures. Bioresource Technology. 2013;143:172-7.
109. Gao D-w, Fu Y, Tao Y, Li X-x, Xing M, Gao X-h, et al. Linking microbial community structure to membrane biofouling associated with varying dissolved oxygen concentrations. Bioresource Technology. 2011;102(10):5626-33.
110. Chen CH, Fu Y, Gao DW. Membrane biofouling process correlated to the microbial community succession in an A/O MBR. Bioresour Technol. 2015;197:185-92.
111. Ahmed Z, Cho J, Lim B-R, Song K-G, Ahn K-H. Effects of sludge retention time on membrane fouling and microbial community structure in a membrane bioreactor. Journal of Membrane Science. 2007;287(2):211-8.
112. Takimoto Y, Hatamoto M, Ishida T, Watari T, Yamaguchi T. Fouling Development in A/O-MBR under Low Organic Loading Condition and Identification of Key Bacteria for Biofilm Formations. Scientific Reports. 2018;8(1):11427.
113. Zhang S, Zhou Z, Li Y, Meng F. Deciphering the core fouling-causing microbiota in a membrane bioreactor: Low abundance but important roles. Chemosphere. 2018;195:108-18.
114. Gao D-W, Zhang T, Tang C-YY, Wu W-M, Wong C-Y, Lee YH, et al. Membrane fouling in an anaerobic membrane bioreactor: Differences in relative abundance of bacterial species in the membrane foulant layer and in suspension. Journal of Membrane Science. 2010;364(1-2):331-8.

115. Gao WJ, Lin HJ, Leung KT, Schraft H, Liao BQ. Structure of cake layer in a submerged anaerobic membrane bioreactor. Journal of Membrane Science. 2011;374(1-2):110-20.
116. Xu R, Yu Z, Zhang S, Meng F. Bacterial assembly in the bio-cake of membrane bioreactors: Stochastic vs. deterministic processes. Water Research. 2019;157:535-45.
117. Song D, Zhang W, Liu C, Wang P, Sun Z, Zhao L, et al. Development of a novel anoxic/oxic fed-batch membrane bioreactor (AFMBR) based on gravity-driven and partial aeration modes: A pilot scale study. Bioresour Technol. 2018;270:255-62.
118. Jeong S-Y, Yi T, Lee C-H, Kim TG. Spatiotemporal dynamics and correlation networks of bacterial and fungal communities in a membrane bioreactor. Water Research. 2016;105:218-30.
119. Pinzi S, Dorado MP. 4 - Vegetable-based feedstocks for biofuels production. In: Luque R, Campelo J, Clark J, editors. Handbook of Biofuels Production: Woodhead Publishing; 2011. p. 61-94.
120. Paul S, Dutta A. Challenges and opportunities of lignocellulosic biomass for anaerobic digestion. Resources, Conservation and Recycling. 2018;130:164-74.
121. Kumar R, Singh S, Singh OV. Bioconversion of lignocellulosic biomass: biochemical and molecular perspectives. Journal of Industrial Microbiology and Biotechnology. 2008;35(5):377-91.
122. Harris D, Bulone V, Ding S-Y, DeBolt S. Tools for Cellulose Analysis in Plant Cell Walls. Plant Physiology. 2010;153(2):420-6.
123. Gírio FM, Fonseca C, Carvalheiro F, Duarte LC, Marques S, Bogel-Łukasik R. Hemicelluloses for fuel ethanol: A review. Bioresource Technology. 2010;101(13):4775-800.
124. Lu Y, Lu Y-C, Hu H-Q, Xie F-J, Wei X-Y, Fan X. Structural Characterization of Lignin and Its Degradation Products with Spectroscopic Methods. Journal of Spectroscopy. 2017;2017:8951658.
125. Vu HP, Nguyen LN, Vu MT, Johir MAH, McLaughlan R, Nghiem LD. A comprehensive review on the framework to valorise lignocellulosic biomass as biorefinery feedstocks. Science of The Total Environment. 2020;743:140630.
126. Song Z, GaiheYang, Liu X, Yan Z, Yuan Y, Liao Y. Comparison of Seven Chemical Pretreatments of Corn Straw for Improving Methane Yield by Anaerobic Digestion. PLOS ONE. 2014;9(4):e93801.
127. Chen W-H, Pen B-L, Yu C-T, Hwang W-S. Pretreatment efficiency and structural characterization of rice straw by an integrated process of dilute-acid and steam explosion for bioethanol production. Bioresource Technology. 2011;102(3):2916-24.
128. Saha BC, Iten LB, Cotta MA, Wu YV. Dilute acid pretreatment, enzymatic saccharification and fermentation of wheat straw to ethanol. Process Biochemistry. 2005;40(12):3693-700.
129. Kaparaju P, Serrano M, Thomsen AB, Kongjan P, Angelidaki I. Bioethanol, biohydrogen and biogas production from wheat straw in a biorefinery concept. Bioresource Technology. 2009;100(9):2562-8.
130. Martín C, Klinke HB, Thomsen AB. Wet oxidation as a pretreatment method for enhancing the enzymatic convertibility of sugarcane bagasse. Enzyme and Microbial Technology. 2007;40(3):426-32.
131. Tarasov D, Leitch M, Fatehi P. Lignin–carbohydrate complexes: properties, applications, analyses, and methods of extraction: a review. Biotechnology for Biofuels. 2018;11(1):269.
132. Li C, Knierim B, Manisseri C, Arora R, Scheller HV, Auer M, et al. Comparison of dilute acid and ionic liquid pretreatment of switchgrass: Biomass recalcitrance,

delignification and enzymatic saccharification. Bioresource Technology. 2010;101(13):4900-6.
133. Li B-Z, Balan V, Yuan Y-J, Dale BE. Process optimization to convert forage and sweet sorghum bagasse to ethanol based on ammonia fiber expansion (AFEX) pretreatment. Bioresource Technology. 2010;101(4):1285-92.
134. Bhuvaneshwari S, Hettiarachchi H, Meegoda JN. Crop Residue Burning in India: Policy Challenges and Potential Solutions. International Journal of Environmental Research and Public Health. 2019;16(5).
135. Chawala P, Sandhu HAS. Stubble burn area estimation and its impact on ambient air quality of Patiala & Ludhiana district, Punjab, India. Heliyon. 2020;6(1).
136. Venkatramanan V, Shah S, Rai AK, Prasad R. Nexus Between Crop Residue Burning, Bioeconomy and Sustainable Development Goals Over North-Western India. Frontiers in Energy Research. 2021;8.
137. Smil V. Crop Residues: Agriculture's Largest Harvest: Crop residues incorporate more than half of the world's agricultural phytomass. BioScience. 1999;49(4):299-308.
138. Isikgor FH, Becer CR. Lignocellulosic biomass: a sustainable platform for the production of bio-based chemicals and polymers. Polymer Chemistry. 2015;6(25):4497-559.
139. (Leads) RDPaBJS. U.S. Billion-Ton Update: Biomass Supply for a Bioenergy and Bioproducts Industry. In: Energy USDo, editor. Oak Ridge, TN: Oak Ridge National Laboratory; 2011.
140. Zabed HM, Akter S, Yun J, Zhang G, Awad FN, Qi X, et al. Recent advances in biological pretreatment of microalgae and lignocellulosic biomass for biofuel production. Renewable and Sustainable Energy Reviews. 2019;105:105-28.
141. Mahmoodi P, Karimi K, Taherzadeh MJ. Hydrothermal processing as pretreatment for efficient production of ethanol and biogas from municipal solid waste. Bioresource Technology. 2018;261:166-75.
142. Xu JK, Sun RC. Chapter 19 - Recent Advances in Alkaline Pretreatment of Lignocellulosic Biomass. In: Mussatto SI, editor. Biomass Fractionation Technologies for a Lignocellulosic Feedstock Based Biorefinery. Amsterdam: Elsevier; 2016. p. 431-59.
143. Kim JS, Lee YY, Kim TH. A review on alkaline pretreatment technology for bioconversion of lignocellulosic biomass. Bioresource Technology. 2016;199:42-8.
144. Singh J, Suhag M, Dhaka A. Augmented digestion of lignocellulose by steam explosion, acid and alkaline pretreatment methods: A review. Carbohydrate Polymers. 2015;117:624-31.
145. Jönsson LJ, Martín C. Pretreatment of lignocellulose: Formation of inhibitory by-products and strategies for minimizing their effects. Bioresource Technology. 2016;199:103-12.
146. Wu J, Upreti S, Ein-Mozaffari F. Ozone pretreatment of wheat straw for enhanced biohydrogen production. International Journal of Hydrogen Energy. 2013;38(25):10270-6.
147. Coca M, González-Benito G, García-Cubero MT. Chapter 18 - Chemical Oxidation With Ozone as an Efficient Pretreatment of Lignocellulosic Materials. In: Mussatto SI, editor. Biomass Fractionation Technologies for a Lignocellulosic Feedstock Based Biorefinery. Amsterdam: Elsevier; 2016. p. 409-29.
148. M'Arimi MM, Mecha CA, Kiprop AK, Ramkat R. Recent trends in applications of advanced oxidation processes (AOPs) in bioenergy production: Review. Renewable and Sustainable Energy Reviews. 2020;121:109669.

149. Mancini G, Papirio S, Lens PNL, Esposito G. Solvent Pretreatments of Lignocellulosic Materials to Enhance Biogas Production: A Review. Energy & Fuels. 2016;30(3):1892-903.
150. Yoo CG, Pu Y, Ragauskas AJ. Ionic liquids: Promising green solvents for lignocellulosic biomass utilization. Current Opinion in Green and Sustainable Chemistry. 2017;5:5-11.
151. Kumar B, Bhardwaj N, Agrawal K, Chaturvedi V, Verma P. Current perspective on pretreatment technologies using lignocellulosic biomass: An emerging biorefinery concept. Fuel Processing Technology. 2020;199:106244.
152. Abraham A, Mathew AK, Park H, Choi O, Sindhu R, Parameswaran B, et al. Pretreatment strategies for enhanced biogas production from lignocellulosic biomass. Bioresource Technology. 2020;301:122725.
153. Ahmed B, Aboudi K, Tyagi VK, Álvarez-Gallego CJ, Fernández-Güelfo LA, Romero-García LI, et al. Improvement of Anaerobic Digestion of Lignocellulosic Biomass by Hydrothermal Pretreatment. Applied Sciences. 2019;9(18).
154. Chan JC, Paice M, Zhang X. Enzymatic Oxidation of Lignin: Challenges and Barriers Toward Practical Applications. ChemCatChem. 2020;12(2):401-25.
155. Brémond U, de Buyer R, Steyer J-P, Bernet N, Carrere H. Biological pretreatments of biomass for improving biogas production: an overview from lab scale to full-scale. Renewable and Sustainable Energy Reviews. 2018;90:583-604.
156. Akyol Ç, Ince O, Bozan M, Ozbayram EG, Ince B. Biological pretreatment with Trametes versicolor to enhance methane production from lignocellulosic biomass: A metagenomic approach. Industrial Crops and Products. 2019;140:111659.
157. Mustafa AM, Poulsen TG, Sheng K. Fungal pretreatment of rice straw with Pleurotus ostreatus and Trichoderma reesei to enhance methane production under solid-state anaerobic digestion. Applied Energy. 2016;180:661-71.
158. Vasco-Correa J, Ge X, Li Y. Fungal pretreatment of non-sterile miscanthus for enhanced enzymatic hydrolysis. Bioresource Technology. 2016;203:118-23.
159. Kalyani D, Lee K-M, Kim T-S, Li J, Dhiman SS, Kang YC, et al. Microbial consortia for saccharification of woody biomass and ethanol fermentation. Fuel. 2013;107:815-22.
160. Maki M, Iskhakova S, Zhang T, Qin W. Bacterial consortia constructed for the decomposition of Agave biomass. Bioengineered. 2014;5(3):165-72.
161. Hu J, Xue Y, Guo H, Gao M-t, Li J, Zhang S, et al. Design and composition of synthetic fungal-bacterial microbial consortia that improve lignocellulolytic enzyme activity. Bioresource Technology. 2017;227:247-55.
162. Minty JJ, Singer ME, Scholz SA, Bae C-H, Ahn J-H, Foster CE, et al. Design and characterization of synthetic fungal-bacterial consortia for direct production of isobutanol from cellulosic biomass. Proceedings of the National Academy of Sciences. 2013;110(36):14592.
163. Zuroff TR, Xiques SB, Curtis WR. Consortia-mediated bioprocessing of cellulose to ethanol with a symbiotic Clostridium phytofermentans/yeast co-culture. Biotechnology for Biofuels. 2013;6(1):59.
164. Kato S, Haruta S, Cui Zong J, Ishii M, Igarashi Y. Stable Coexistence of Five Bacterial Strains as a Cellulose-Degrading Community. Applied and Environmental Microbiology. 2005;71(11):7099-106.
165. Takizawa S, Baba Y, Tada C, Fukuda Y, Nakai Y. Pretreatment with rumen fluid improves methane production in the anaerobic digestion of paper sludge. Waste Management. 2018;78:379-84.

166. Wang S, Zhang G, Zhang P, Ma X, Li F, Zhang H, et al. Rumen fluid fermentation for enhancement of hydrolysis and acidification of grass clipping. Journal of Environmental Management. 2018;220:142-8.
167. Wang Y, McAllister TA. Rumen Microbes, Enzymes and Feed Digestion-A Review. Asian-Australas J Anim Sci. 2002;15(11):1659-76.
168. Zhang L, Chung J, Jiang Q, Sun R, Zhang J, Zhong Y, et al. Characteristics of rumen microorganisms involved in anaerobic degradation of cellulose at various pH values. RSC Advances. 2017;7(64):40303-10.
169. Barragán-Trinidad M, Carrillo-Reyes J, Buitrón G. Hydrolysis of microalgal biomass using ruminal microorganisms as a pretreatment to increase methane recovery. Bioresource Technology. 2017;244:100-7.
170. Giménez JB, Aguado D, Bouzas A, Ferrer J, Seco A. Use of rumen microorganisms to boost the anaerobic biodegradability of microalgae. Algal Research. 2017;24:309-16.
171. Hu Z-H, Yu H-Q. Application of rumen microorganisms for enhanced anaerobic fermentation of corn stover. Process Biochemistry. 2005;40(7):2371-7.
172. Yue Z-B, Yu H-Q, Harada H, Li Y-Y. Optimization of anaerobic acidogenesis of an aquatic plant, Canna indica L., by rumen cultures. Water Research. 2007;41(11):2361-70.
173. Zhao J, Guo C, Zhang L, Tian C. Biochemical and functional characterization of a novel thermoacidophilic, heat and halo-ionic liquids tolerant endo-β-1,4-glucanase from saline-alkaline lake soil microbial metagenomic DNA. International Journal of Biological Macromolecules. 2018;118:1035-44.
174. Song Y-H, Lee K-T, Baek J-Y, Kim M-J, Kwon M-R, Kim Y-J, et al. Isolation and characterization of a novel endo-β-1,4-glucanase from a metagenomic library of the black-goat rumen. Brazilian Journal of Microbiology. 2017;48(4):801-8.
175. Garg R, Srivastava R, Brahma V, Verma L, Karthikeyan S, Sahni G. Biochemical and structural characterization of a novel halotolerant cellulase from soil metagenome. Scientific Reports. 2016;6(1):39634.
176. Motamedi E, Sadeghian Motahar SF, Maleki M, Kavousi K, Ariaeenejad S, Moosavi-Movahedi AA, et al. Upgrading the enzymatic hydrolysis of lignocellulosic biomass by immobilization of metagenome-derived novel halotolerant cellulase on the carboxymethyl cellulose-based hydrogel. Cellulose. 2021;28(6):3485-503.
177. Patel M, Patel HM, Dave S. Determination of bioethanol production potential from lignocellulosic biomass using novel Cel-5m isolated from cow rumen metagenome. International Journal of Biological Macromolecules. 2020;153:1099-106.
178. Findley Seth D, Mormile Melanie R, Sommer-Hurley A, Zhang X-C, Tipton P, Arnett K, et al. Activity-Based Metagenomic Screening and Biochemical Characterization of Bovine Ruminal Protozoan Glycoside Hydrolases. Applied and Environmental Microbiology. 2011;77(22):8106-13.
179. Yang C, Xia Y, Qu H, Li A-D, Liu R, Wang Y, et al. Discovery of new cellulases from the metagenome by a metagenomics-guided strategy. Biotechnology for Biofuels. 2016;9(1):138.
180. Couger MB, Youssef NH, Struchtemeyer CG, Liggenstoffer AS, Elshahed MS. Transcriptomic analysis of lignocellulosic biomass degradation by the anaerobic fungal isolate Orpinomyces sp. strain C1A. Biotechnology for Biofuels. 2015;8(1):208.
181. Youssef Noha H, Couger MB, Struchtemeyer Christopher G, Liggenstoffer Audra S, Prade Rolf A, Najar Fares Z, et al. The Genome of the Anaerobic Fungus Orpinomyces sp. Strain C1A Reveals the Unique Evolutionary History of a Remarkable Plant Biomass Degrader. Applied and Environmental Microbiology. 2013;79(15):4620-34.

182. Comtet-Marre S, Parisot N, Lepercq P, Chaucheyras-Durand F, Mosoni P, Peyretaillade E, et al. Metatranscriptomics Reveals the Active Bacterial and Eukaryotic Fibrolytic Communities in the Rumen of Dairy Cow Fed a Mixed Diet. Frontiers in microbiology. 2017;8.
183. Dai X, Tian Y, Li J, Su X, Wang X, Zhao S, et al. Metatranscriptomic Analyses of Plant Cell Wall Polysaccharide Degradation by Microorganisms in the Cow Rumen. Applied and Environmental Microbiology. 2015;81(4):1375-86.
184. Brulc Jennifer M, Antonopoulos Dionysios A, Berg Miller Margret E, Wilson Melissa K, Yannarell Anthony C, Dinsdale Elizabeth A, et al. Gene-centric metagenomics of the fiber-adherent bovine rumen microbiome reveals forage specific glycoside hydrolases. Proceedings of the National Academy of Sciences. 2009;106(6):1948-53.
185. Lee CG, Baba Y, Asano R, Fukuda Y, Tada C, Nakai Y. Identification of bacteria involved in the decomposition of lignocellulosic biomass treated with cow rumen fluid by metagenomic analysis. Journal of Bioscience and Bioengineering. 2020;130(2):137-41.
186. Baba Y, Matsuki Y, Mori Y, Suyama Y, Tada C, Fukuda Y, et al. Pretreatment of lignocellulosic biomass by cattle rumen fluid for methane production: Bacterial flora and enzyme activity analysis. Journal of Bioscience and Bioengineering. 2017;123(4):489-96.
187. Deng Y, Huang Z, Ruan W, Zhao M, Miao H, Ren H. Co-inoculation of cellulolytic rumen bacteria with methanogenic sludge to enhance methanogenesis of rice straw. International Biodeterioration & Biodegradation. 2017;117:224-35.
188. Mulat DG, Huerta SG, Kalyani D, Horn SJ. Enhancing methane production from lignocellulosic biomass by combined steam-explosion pretreatment and bioaugmentation with cellulolytic bacterium Caldicellulosiruptor bescii. Biotechnology for Biofuels. 2018;11(1):19.
189. Baba Y, Matsuki Y, Takizawa S, Suyama Y, Tada C, Fukuda Y, et al. Pretreatment of Lignocellulosic Biomass with Cattle Rumen Fluid for Methane Production: Fate of Added Rumen Microbes and Indigenous Microbes of Methane Seed Sludge. Microbes Environ. 2019;34(4):421-8.
190. Takizawa S, Asano R, Fukuda Y, Feng M, Baba Y, Abe K, et al. Change of Endoglucanase Activity and Rumen Microbial Community During Biodegradation of Cellulose Using Rumen Microbiota. Frontiers in microbiology. 2020;11.
191. Xing B-S, Han Y, Wang XC, Wen J, Cao S, Zhang K, et al. Persistent action of cow rumen microorganisms in enhancing biodegradation of wheat straw by rumen fermentation. Science of The Total Environment. 2020;715:136529.
192. Nagler M, Kozjek K, Etemadi M, Insam H, Podmirseg SM. Simple yet effective: Microbial and biotechnological benefits of rumen liquid addition to lignocellulose-degrading biogas plants. Journal of Biotechnology. 2019;300:1-10.
193. Dollhofer V, Dandikas V, Dorn-In S, Bauer C, Lebuhn M, Bauer J. Accelerated biogas production from lignocellulosic biomass after pre-treatment with Neocallimastix frontalis. Bioresource Technology. 2018;264:219-27.
194. Tran NH, Reinhard M, Gin KY-H. Occurrence and fate of emerging contaminants in municipal wastewater treatment plants from different geographical regions-a review. Water Research. 2018;133:182-207.
195. Cortés JM, Larsson E, Jönsson JÅ. Study of the uptake of non-steroid anti-inflammatory drugs in wheat and soybean after application of sewage sludge as a fertilizer. Science of The Total Environment. 2013;449:385-9.

196. Verlicchi P, Zambello E. Pharmaceuticals and personal care products in untreated and treated sewage sludge: Occurrence and environmental risk in the case of application on soil — A critical review. Science of The Total Environment. 2015;538:750-67.
197. Parolini M. Toxicity of the Non-Steroidal Anti-Inflammatory Drugs (NSAIDs) acetylsalicylic acid, paracetamol, diclofenac, ibuprofen and naproxen towards freshwater invertebrates: A review. Science of The Total Environment. 2020;740:140043.
198. Schmidt W, O'Rourke K, Hernan R, Quinn B. Effects of the pharmaceuticals gemfibrozil and diclofenac on the marine mussel (Mytilus spp.) and their comparison with standardized toxicity tests. Marine Pollution Bulletin. 2011;62(7):1389-95.
199. Matamoros V, Hijosa M, Bayona JM. Assessment of the pharmaceutical active compounds removal in wastewater treatment systems at enantiomeric level. Ibuprofen and naproxen. Chemosphere. 2009;75(2):200-5.
200. Nakada N, Tanishima T, Shinohara H, Kiri K, Takada H. Pharmaceutical chemicals and endocrine disrupters in municipal wastewater in Tokyo and their removal during activated sludge treatment. Water Research. 2006;40(17):3297-303.
201. Onesios KM, Yu JT, Bouwer EJ. Biodegradation and removal of pharmaceuticals and personal care products in treatment systems: a review. Biodegradation. 2009;20(4):441-66.
202. Verlicchi P, Al Aukidy M, Zambello E. Occurrence of pharmaceutical compounds in urban wastewater: Removal, mass load and environmental risk after a secondary treatment—A review. Science of The Total Environment. 2012;429:123-55.
203. Patel M, Kumar R, Kishor K, Mlsna T, Pittman CU, Mohan D. Pharmaceuticals of Emerging Concern in Aquatic Systems: Chemistry, Occurrence, Effects, and Removal Methods. Chemical Reviews. 2019;119(6):3510-673.
204. Petrie B, McAdam EJ, Lester JN, Cartmell E. Obtaining process mass balances of pharmaceuticals and triclosan to determine their fate during wastewater treatment. Science of The Total Environment. 2014;497-498:553-60.
205. Dawas-Massalha A, Gur-Reznik S, Lerman S, Sabbah I, Dosoretz CG. Co-metabolic oxidation of pharmaceutical compounds by a nitrifying bacterial enrichment. Bioresource Technology. 2014;167:336-42.
206. Cruz-Morató C, Ferrando-Climent L, Rodriguez-Mozaz S, Barceló D, Marco-Urrea E, Vicent T, et al. Degradation of pharmaceuticals in non-sterile urban wastewater by Trametes versicolor in a fluidized bed bioreactor. Water Research. 2013;47(14):5200-10.
207. Rodarte-Morales AI, Feijoo G, Moreira MT, Lema JM. Operation of stirred tank reactors (STRs) and fixed-bed reactors (FBRs) with free and immobilized Phanerochaete chrysosporium for the continuous removal of pharmaceutical compounds. Biochemical Engineering Journal. 2012;66:38-45.
208. Marco-Urrea E, Pérez-Trujillo M, Blánquez P, Vicent T, Caminal G. Biodegradation of the analgesic naproxen by Trametes versicolor and identification of intermediates using HPLC-DAD-MS and NMR. Bioresource Technology. 2010;101(7):2159-66.
209. Vasiliadou IA, Sánchez-Vázquez R, Molina R, Martínez F, Melero JA, Bautista LF, et al. Biological removal of pharmaceutical compounds using white-rot fungi with concomitant FAME production of the residual biomass. Journal of Environmental Management. 2016;180:228-37.
210. Kasprzyk-Hordern B, Dinsdale RM, Guwy AJ. The removal of pharmaceuticals, personal care products, endocrine disruptors and illicit drugs during wastewater treatment and its impact on the quality of receiving waters. Water Research. 2009;43(2):363-80.

211. Marco-Urrea E, Aranda E, Caminal G, Guillén F. Induction of hydroxyl radical production in Trametes versicolor to degrade recalcitrant chlorinated hydrocarbons. Bioresource Technology. 2009;100(23):5757-62.
212. Ahmed MB, Zhou JL, Ngo HH, Guo W, Thomaidis NS, Xu J. Progress in the biological and chemical treatment technologies for emerging contaminant removal from wastewater: A critical review. Journal of Hazardous Materials. 2017;323:274-98.
213. Yu T-H, Lin AY-C, Lateef SK, Lin C-F, Yang P-Y. Removal of antibiotics and non-steroidal anti-inflammatory drugs by extended sludge age biological process. Chemosphere. 2009;77(2):175-81.
214. Petrie B, Camacho-Muñoz D. Analysis, fate and toxicity of chiral non-steroidal anti-inflammatory drugs in wastewaters and the environment: a review. Environmental Chemistry Letters. 2021;19(1):43-75.
215. Neale PA, Branch A, Khan SJ, Leusch FDL. Evaluating the enantiospecific differences of non-steroidal anti-inflammatory drugs (NSAIDs) using an ecotoxicity bioassay test battery. Science of The Total Environment. 2019;694:133659.
216. Eaglesham A, Scott A, Petrie B. Multi-residue enantioselective analysis of chiral drugs in freshwater sediments. Environmental Chemistry Letters. 2020;18(6):2119-26.
217. Kasprzyk-Hordern B. Pharmacologically active compounds in the environment and their chirality. Chemical Society Reviews. 2010;39(11):4466-503.
218. Ribeiro AR, Castro PML, Tiritan ME. Chiral pharmaceuticals in the environment. Environmental Chemistry Letters. 2012;10(3):239-53.
219. Khan SJ, Wang L, Hashim NH, Mcdonald JA. Distinct Enantiomeric Signals of Ibuprofen and Naproxen in Treated Wastewater and Sewer Overflow. Chirality. 2014;26(11):739-46.
220. Caballo C, Sicilia MD, Rubio S. Enantioselective determination of representative profens in wastewater by a single-step sample treatment and chiral liquid chromatography–tandem mass spectrometry. Talanta. 2015;134:325-32.
221. Hashim NH, Khan SJ. Enantioselective analysis of ibuprofen, ketoprofen and naproxen in wastewater and environmental water samples. Journal of Chromatography A. 2011;1218(29):4746-54.
222. Camacho-Muñoz D, Petrie B, Lopardo L, Proctor K, Rice J, Youdan J, et al. Stereoisomeric profiling of chiral pharmaceutically active compounds in wastewaters and the receiving environment – A catchment-scale and a laboratory study. Environment International. 2019;127:558-72.
223. Almeida B, Oehmen A, Marques R, Brito D, Carvalho G, Barreto Crespo MT. Modelling the biodegradation of non-steroidal anti-inflammatory drugs (NSAIDs) by activated sludge and a pure culture. Bioresource Technology. 2013;133:31-7.
224. Murdoch RW, Hay AG. The biotransformation of ibuprofen to trihydroxyibuprofen in activated sludge and by Variovorax Ibu-1. Biodegradation. 2015;26(2):105-13.
225. Zhou NA, Lutovsky AC, Andaker GL, Gough HL, Ferguson JF. Cultivation and characterization of bacterial isolates capable of degrading pharmaceutical and personal care products for improved removal in activated sludge wastewater treatment. Biodegradation. 2013;24(6):813-27.
226. Jiang C, Geng J, Hu H, Ma H, Gao X, Ren H. Impact of selected non-steroidal anti-inflammatory pharmaceuticals on microbial community assembly and activity in sequencing batch reactors. PLOS ONE. 2017;12(6):e0179236.
227. Grenni P, Patrolecco L, Ademollo N, Tolomei A, Barra Caracciolo A. Degradation of Gemfibrozil and Naproxen in a river water ecosystem. Microchemical Journal. 2013;107:158-64.

228. Navrozidou E, Melidis P, Ntougias S. Biodegradation aspects of ibuprofen and identification of ibuprofen-degrading microbiota in an immobilized cell bioreactor. Environmental Science and Pollution Research. 2019;26(14):14238-49.
229. Feng Y, Guo M, Jia X, Liu N, Li X, Li X, et al. Combined effects of electrical current and nonsteroidal antiinflammatory drugs (NSAIDs) on microbial community in a three-dimensional electrode biological aerated filter (3DE-BAF). Bioresource Technology. 2020;309:123346.
230. Żur J, Michalska J, Piński A, Mrozik A, Nowak A. Effects of Low Concentration of Selected Analgesics and Successive Bioaugmentation of the Activated Sludge on Its Activity and Metabolic Diversity. Water. 2020;12(4).
231. Banti DC, Tsangas M, Samaras P, Zorpas A. LCA of a Membrane Bioreactor Compared to Activated Sludge System for Municipal Wastewater Treatment. Membranes. 2020;10(12).
232. Krzeminski P, Leverette L, Malamis S, Katsou E. Membrane bioreactors – A review on recent developments in energy reduction, fouling control, novel configurations, LCA and market prospects. Journal of Membrane Science. 2017;527:207-27.
233. Judd S. MBR global capacity, https://www.thembrsite.com/largest-mbr-plants/membrane-bioreactor-global-capacity 2019 [cited 2021. Available from: https://www.thembrsite.com/largest-mbr-plants/membrane-bioreactor-global-capacity.
234. Gao T, Xiao K, Zhang J, Xue W, Wei C, Zhang X, et al. Techno-economic characteristics of wastewater treatment plants retrofitted from the conventional activated sludge process to the membrane bioreactor process. Frontiers of Environmental Science & Engineering. 2021;16(4):1.
235. Van den Broeck R, Van Dierdonck J, Nijskens P, Dotremont C, Krzeminski P, van der Graaf JHJM, et al. The influence of solids retention time on activated sludge bioflocculation and membrane fouling in a membrane bioreactor (MBR). Journal of Membrane Science. 2012;401-402:48-55.
236. Wu B, Kitade T, Chong TH, Lee JY, Uemura T, Fane AG. Flux-Dependent Fouling Phenomena in Membrane Bioreactors under Different Food to Microorganisms (F/M) Ratios. Separation Science and Technology. 2013;48(6):840-8.
237. Pan JR, Su Y-C, Huang C, Lee H-C. Effect of sludge characteristics on membrane fouling in membrane bioreactors. Journal of Membrane Science. 2010;349(1):287-94.
238. Bacchin P, Aimar P, Field RW. Critical and sustainable fluxes: Theory, experiments and applications. Journal of Membrane Science. 2006;281(1):42-69.
239. Field RW, Wu D, Howell JA, Gupta BB. Critical flux concept for microfiltration fouling. Journal of Membrane Science. 1995;100(3):259-72.
240. Li X, Li J, Wang J, Wang H, Cui C, He B, et al. Direct monitoring of sub-critical flux fouling in a horizontal double-end submerged hollow fiber membrane module using ultrasonic time domain reflectometry. Journal of Membrane Science. 2014;451:226-33.
241. Kimura K, Miyoshi T, Naruse T, Yamato N, Ogyu R, Watanabe Y. The difference in characteristics of foulants in submerged MBRs caused by the difference in the membrane flux. Desalination. 2008;231(1):268-75.
242. Nguyen T-T, Bui X-T, Vo T-D-H, Nguyen D-D, Nguyen P-D, Do H-L-C, et al. Performance and membrane fouling of two types of laboratory-scale submerged membrane bioreactors for hospital wastewater treatment at low flux condition. Separation and Purification Technology. 2016;165:123-9.
243. Thanh BX, Dan NP, Visvanathan C. Low flux submerged membrane bioreactor treating high strength leachate from a solid waste transfer station. Bioresource Technology. 2013;141:25-8.

244. Johir MAH, George J, Vigneswaran S, Kandasamy J, Sathasivan A, Grasmick A. Effect of imposed flux on fouling behavior in high rate membrane bioreactor. Bioresource Technology. 2012;122:42-9.
245. Ouyang K, Liu J. Effect of sludge retention time on sludge characteristics and membrane fouling of membrane bioreactor. Journal of Environmental Sciences. 2009;21(10):1329-35.
246. Han S-S, Bae T-H, Jang G-G, Tak T-M. Influence of sludge retention time on membrane fouling and bioactivities in membrane bioreactor system. Process Biochemistry. 2005;40(7):2393-400.
247. Deb A, Gurung K, Rumky J, Sillanpää M, Mänttäri M, Kallioinen M. Dynamics of microbial community and their effects on membrane fouling in an anoxic-oxic gravity-driven membrane bioreactor under varying solid retention time: A pilot-scale study. Science of The Total Environment. 2022;807:150878.
248. Fu C, Yue X, Shi X, Ng KK, Ng HY. Membrane fouling between a membrane bioreactor and a moving bed membrane bioreactor: Effects of solids retention time. Chemical Engineering Journal. 2017;309:397-408.
249. Tian Y, Chen L, Zhang S, Cao C, Zhang S. Correlating membrane fouling with sludge characteristics in membrane bioreactors: An especial interest in EPS and sludge morphology analysis. Bioresource Technology. 2011;102(19):8820-7.
250. Li J, Li Y, Ohandja D-G, Yang F, Wong F-S, Chua H-C. Impact of filamentous bacteria on properties of activated sludge and membrane-fouling rate in a submerged MBR. Separation and Purification Technology. 2008;59(3):238-43.
251. Meng F, Yang F. Fouling mechanisms of deflocculated sludge, normal sludge, and bulking sludge in membrane bioreactor. Journal of Membrane Science. 2007;305(1):48-56.
252. Meng F, Yang F, Xiao J, Zhang H, Gong Z. A new insight into membrane fouling mechanism during membrane filtration of bulking and normal sludge suspension. Journal of Membrane Science. 2006;285(1):159-65.
253. Meng F, Zhang H, Yang F, Li Y, Xiao J, Zhang X. Effect of filamentous bacteria on membrane fouling in submerged membrane bioreactor. Journal of Membrane Science. 2006;272(1):161-8.
254. Wang Z, Wang P, Wang Q, Wu Z, Zhou Q, Yang D. Effective control of membrane fouling by filamentous bacteria in a submerged membrane bioreactor. Chemical Engineering Journal. 2010;158(3):608-15.
255. Nguyen AQ, Nguyen LN, Xu Z, Luo W, Nghiem LD. New insights to the difference in microbial composition and interspecies interactions between fouling layer and mixed liquor in a membrane bioreactor. Journal of Membrane Science. 2022;643:120034.
256. Nguyen LN, Hai FI, Kang J, Price WE, Nghiem LD. Removal of emerging trace organic contaminants by MBR-based hybrid treatment processes. International Biodeterioration & Biodegradation. 2013;85:474-82.
257. Bolyen E, Rideout JR, Dillon MR, Bokulich NA, Abnet CC, Al-Ghalith GA, et al. Reproducible, interactive, scalable and extensible microbiome data science using QIIME 2. Nature Biotechnology. 2019;37(8):852-7.
258. Callahan BJ, McMurdie PJ, Rosen MJ, Han AW, Johnson AJA, Holmes SP. DADA2: High-resolution sample inference from Illumina amplicon data. Nature Methods. 2016;13(7):581-3.
259. Bokulich NA, Kaehler BD, Rideout JR, Dillon M, Bolyen E, Knight R, et al. Optimizing taxonomic classification of marker-gene amplicon sequences with QIIME 2's q2-feature-classifier plugin. Microbiome. 2018;6(1):90.

260. Glöckner FO, Yilmaz P, Quast C, Gerken J, Beccati A, Ciuprina A, et al. 25 years of serving the community with ribosomal RNA gene reference databases and tools. Journal of Biotechnology. 2017;261:169-76.
261. Yilmaz P, Parfrey LW, Yarza P, Gerken J, Pruesse E, Quast C, et al. The SILVA and "All-species Living Tree Project (LTP)" taxonomic frameworks. Nucleic Acids Research. 2013;42(D1):D643-D8.
262. Quast C, Pruesse E, Yilmaz P, Gerken J, Schweer T, Yarza P, et al. The SILVA ribosomal RNA gene database project: improved data processing and web-based tools. Nucleic Acids Research. 2012;41(D1):D590-D6.
263. Price MN, Dehal PS, Arkin AP. FastTree 2 – Approximately Maximum-Likelihood Trees for Large Alignments. PLOS ONE. 2010;5(3):e9490.
264. Rice KC, Bayles KW. Molecular control of bacterial death and lysis. Microbiol Mol Biol Rev. 2008;72(1):85-109.
265. Hazan R, Sat B, Engelberg-Kulka H. Escherichia coli mazEF-mediated cell death is triggered by various stressful conditions. J Bacteriol. 2004;186(11):3663-9.
266. Van Loosdrecht MCM, Henze M. Maintenance, endogeneous respiration, lysis, decay and predation. Water Science and Technology. 1999;39(1):107-17.
267. Guo F, Zhang T. Profiling bulking and foaming bacteria in activated sludge by high throughput sequencing. Water Research. 2012;46(8):2772-82.
268. Kindaichi T, Yamaoka S, Uehara R, Ozaki N, Ohashi A, Albertsen M, et al. Phylogenetic diversity and ecophysiology of Candidate phylum Saccharibacteria in activated sludge. FEMS microbiology ecology. 2016;92(6):fiw078.
269. Dunkel T, de León Gallegos EL, Bock C, Lange A, Hoffmann D, Boenigk J, et al. Illumina sequencing for the identification of filamentous bulking and foaming bacteria in industrial activated sludge plants. International Journal of Environmental Science and Technology. 2018;15(6):1139-58.
270. Kowalska E, Paturej E, Zielińska M. Use of Lecane inermis for control of sludge bulking caused by the Haliscomenobacter genus. Desalination and Water Treatment. 2016;57(23):10916-23.
271. Zaidi NS, Muda K, Sohaili J, Loan LW, Sillanpää M. Enhancement of nitrification efficiency during sludge bulking by magnetic field under long sludge retention time. 3 Biotech. 2020;10(9):408.
272. Li B-B, Peng Z-Y, Zhi L-L, Li H-B, Zheng K-K, Li J. Distribution and diversity of filamentous bacteria in wastewater treatment plants exhibiting foaming of Taihu Lake Basin, China. Environmental Pollution. 2020;267:115644.
273. Banti DC, Mitrakas M, Samaras P. Membrane Fouling Controlled by Adjustment of Biological Treatment Parameters in Step-Aerating MBR. Membranes. 2021;11(8).
274. Banti DC, Karayannakidis PD, Samaras P, Mitrakas MG. An innovative bioreactor set-up that reduces membrane fouling by adjusting the filamentous bacterial population. Journal of Membrane Science. 2017;542:430-8.
275. Banti DC, Tsali A, Mitrakas M, Samaras P. The Dissolved Oxygen Effect on the Controlled Growth of Filamentous Microorganisms in Membrane Bioreactors. Environmental Sciences Proceedings. 2020;2(1).
276. Shen Y, Huang D-M, Chen Y-P, Yan P, Gao X. New insight into filamentous sludge bulking during wastewater treatment: Surface characteristics and thermodynamics. Science of The Total Environment. 2020;712:135795.
277. Deng L, Guo W, Ngo HH, Zhang H, Wang J, Li J, et al. Biofouling and control approaches in membrane bioreactors. Bioresource Technology. 2016;221:656-65.
278. Cydzik-Kwiatkowska A, Rusanowska P, Zielińska M, Bernat K, Wojnowska-Baryła I. Microbial structure and nitrogen compound conversions in aerobic granular

sludge reactors with non-aeration phases and acetate pulse feeding. Environ Sci Pollut Res Int. 2016;23(24):24857-70.
279. Zhou Y, Lambrides CJ, Li J, Xu Q, Toh R, Tian S, et al. Nitrifying Microbes in the Rhizosphere of Perennial Grasses are Modified by Biological Nitrification Inhibition. Microorganisms. 2020;8(11):1687.
280. Brigmon RL, Furlong M, Whitman WB. Identification of Thiothrix unzii in two distinct ecosystems. Letters in Applied Microbiology. 2003;36(2):88-91.
281. Quintero EJ, Busch K, Weiner RM. Spatial and Temporal Deposition of Adhesive Extracellular Polysaccharide Capsule and Fimbriae by Hyphomonas Strain MHS-3. Applied and environmental microbiology. 1998;64(4):1246-55.
282. Marcondes de Souza JA, Carareto Alves LM, de Mello Varani A, de Macedo Lemos EG. The Family Bradyrhizobiaceae. In: Rosenberg E, DeLong EF, Lory S, Stackebrandt E, Thompson F, editors. The Prokaryotes: Alphaproteobacteria and Betaproteobacteria. Berlin, Heidelberg: Springer Berlin Heidelberg; 2014. p. 135-54.
283. Vuko M, Cania B, Vogel C, Kublik S, Schloter M, Schulz S. Shifts in reclamation management strategies shape the role of exopolysaccharide and lipopolysaccharide-producing bacteria during soil formation. Microb Biotechnol. 2020;13(2):584-98.
284. Vu B, Chen M, Crawford RJ, Ivanova EP. Bacterial extracellular polysaccharides involved in biofilm formation. Molecules. 2009;14(7):2535-54.
285. Dang H, Lovell CR. Microbial Surface Colonization and Biofilm Development in Marine Environments. Microbiol Mol Biol Rev. 2015;80(1):91-138.
286. Sun Y, Wang Y, Huang X. Relationship between sludge settleability and membrane fouling in a membrane bioreactor. Frontiers of Environmental Science & Engineering in China. 2007;1(2):221-5.
287. Donkin MJ. Bulking in aerobic biological systems treating dairy processing wastewaters. International Journal of Dairy Technology. 1997;50(2):67-72.
288. Guo J, Peng Y, Wang Z, Yuan Z, Yang X, Wang S. Control filamentous bulking caused by chlorine-resistant Type 021N bacteria through adding a biocide CTAB. Water Research. 2012;46(19):6531-42.
289. Nghiem LD, Nguyen LN, Phan HV, Ngo HH, Guo W, Hai F. 7 - Aerobic membrane bioreactors and micropollutant removal. In: Ng HY, Ng TCA, Ngo HH, Mannina G, Pandey A, editors. Current Developments in Biotechnology and Bioengineering: Elsevier; 2020. p. 147-62.
290. Xiaolei Zhang XC, Jiayao Reng, Xiao Ma, Qiang Liu, Ping Yao, Hao H. Ngo, and Long D. Nghiem. UV assisted backwashing for fouling control in membrane bioreactor operation. Journal of Membrane Science 2021;Accepted
291. Yeon K-M, Cheong W-S, Oh H-S, Lee W-N, Hwang B-K, Lee C-H, et al. Quorum Sensing: A New Biofouling Control Paradigm in a Membrane Bioreactor for Advanced Wastewater Treatment. Environmental Science & Technology. 2009;43(2):380-5.
292. Oh H-S, Lee C-H. Origin and evolution of quorum quenching technology for biofouling control in MBRs for wastewater treatment. Journal of Membrane Science. 2018;554:331-45.
293. Kim H-W, Oh H-S, Kim S-R, Lee K-B, Yeon K-M, Lee C-H, et al. Microbial population dynamics and proteomics in membrane bioreactors with enzymatic quorum quenching. Applied Microbiology and Biotechnology. 2013;97(10):4665-75.
294. Cui Y, Gao H, Yu R, Gao L, Zhan M. Biological-based control strategies for MBR membrane biofouling: a review. Water Science and Technology. 2021;83(11):2597-614.
295. Nguyen LN, Commault AS, Kahlke T, Ralph PJ, Semblante GU, Johir MAH, et al. Genome sequencing as a new window into the microbial community of membrane bioreactors – A critical review. Science of The Total Environment. 2020;704:135279.

296. Miura Y, Watanabe Y, Okabe S. Membrane Biofouling in Pilot-Scale Membrane Bioreactors (MBRs) Treating Municipal Wastewater: Impact of Biofilm Formation. Environmental Science & Technology. 2007;41(2):632-8.
297. Piasecka A, Souffreau C, Vandepitte K, Vanysacker L, Bilad RM, De Bie T, et al. Analysis of the microbial community structure in a membrane bioreactor during initial stages of filtration. Biofouling. 2012;28(2):225-38.
298. Luo J, Lv P, Zhang J, Fane AG, McDougald D, Rice SA. Succession of biofilm communities responsible for biofouling of membrane bio-reactors (MBRs). PloS one. 2017;12(7):e0179855-e.
299. Matar GK, Bagchi S, Zhang K, Oerther DB, Saikaly PE. Membrane biofilm communities in full-scale membrane bioreactors are not randomly assembled and consist of a core microbiome. Water Research. 2017;123:124-33.
300. Gao D-W, Wen Z-D, Li B, Liang H. Microbial community structure characteristics associated membrane fouling in A/O-MBR system. Bioresource Technology. 2014;154:87-93.
301. Inaba T, Hori T, Aizawa H, Ogata A, Habe H. Architecture, component, and microbiome of biofilm involved in the fouling of membrane bioreactors. NPJ biofilms and microbiomes. 2017;3:5-.
302. Ishizaki S, Fukushima T, Ishii S, Okabe S. Membrane fouling potentials and cellular properties of bacteria isolated from fouled membranes in a MBR treating municipal wastewater. Water Research. 2016;100:448-57.
303. Yao Y, Xu R, Zhou Z, Meng F. Linking dynamics in morphology, components, and microbial communities of biocakes to fouling evolution: A comparative study of anaerobic and aerobic membrane bioreactors. Chemical Engineering Journal. 2021;413:127483.
304. Hong P-N, Noguchi M, Matsuura N, Honda R. Mechanism of biofouling enhancement in a membrane bioreactor under constant trans-membrane pressure operation. Journal of Membrane Science. 2019;592:117391.
305. Xu Z, Qi C, Zhang L, Ma Y, Li G, Nghiem LD, et al. Regulating bacterial dynamics by lime addition to enhance kitchen waste composting. Bioresource Technology. 2021:125749.
306. Wijekoon KC, Hai FI, Kang J, Price WE, Guo W, Ngo HH, et al. A novel membrane distillation–thermophilic bioreactor system: Biological stability and trace organic compound removal. Bioresource Technology. 2014;159:334-41.
307. AD Eaton LC, EW Rice, AE Greenberg. Standard Methods for the Examination of Water and Wastewater. 21 ed. Washington DC, New York: APHA; 2005.
308. R.S. Hanson JAP. Chemical composition. In: Gerhardt P, editor. Manual of methods for general bacteriology. Washington, D.C: American Society for Microbiology; 1981. p. 328–64.
309. Comte S, Guibaud G, Baudu M. Relations between extraction protocols for activated sludge extracellular polymeric substances (EPS) and EPS complexation properties: Part I. Comparison of the efficiency of eight EPS extraction methods. Enzyme and Microbial Technology. 2006;38(1):237-45.
310. Dubois M, Gilles K, Hamilton JK, Rebers PA, Smith F. A Colorimetric Method for the Determination of Sugars. Nature. 1951;168(4265):167-.
311. Mandal S, Van Treuren W, White RA, Eggesbø M, Knight R, Peddada SD. Analysis of composition of microbiomes: a novel method for studying microbial composition. Microb Ecol Health Dis. 2015;26:27663-.
312. Deng Y, Jiang Y-H, Yang Y, He Z, Luo F, Zhou J. Molecular ecological network analyses. BMC Bioinformatics. 2012;13(1):113.

313. Shannon P, Markiel A, Ozier O, Baliga NS, Wang JT, Ramage D, et al. Cytoscape: a software environment for integrated models of biomolecular interaction networks. Genome Res. 2003;13(11):2498-504.
314. Di Martino P. Extracellular polymeric substances, a key element in understanding biofilm phenotype. AIMS Microbiol. 2018;4(2):274-88.
315. Du X, Shi Y, Jegatheesan V, Haq IU. A Review on the Mechanism, Impacts and Control Methods of Membrane Fouling in MBR System. Membranes. 2020;10(2):24.
316. Maddela Naga R, Zhou Z, Yu Z, Zhao S, Meng F, Liu S-J. Functional Determinants of Extracellular Polymeric Substances in Membrane Biofouling: Experimental Evidence from Pure-Cultured Sludge Bacteria. Applied and Environmental Microbiology. 2018;84(15):e00756-18.
317. Costa OYA, Raaijmakers JM, Kuramae EE. Microbial Extracellular Polymeric Substances: Ecological Function and Impact on Soil Aggregation. Frontiers in microbiology. 2018;9(1636).
318. Entcheva-Dimitrov P, Spormann Alfred M. Dynamics and Control of Biofilms of the Oligotrophic Bacterium Caulobacter crescentus. J Bacteriol. 2004;186(24):8254-66.
319. Wan Z, Brown PJB, Elliott EN, Brun YV. The adhesive and cohesive properties of a bacterial polysaccharide adhesin are modulated by a deacetylase. Molecular Microbiology. 2013;88(3):486-500.
320. Zhu Y, Zhang Y, Ren H-q, Geng J-j, Xu K, Huang H, et al. Physicochemical characteristics and microbial community evolution of biofilms during the start-up period in a moving bed biofilm reactor. Bioresource Technology. 2015;180:345-51.
321. Flemming H-C, Wingender J. The biofilm matrix. Nature Reviews Microbiology. 2010;8(9):623-33.
322. Iorhemen OT, Hamza RA, Tay JH. Membrane Bioreactor (MBR) Technology for Wastewater Treatment and Reclamation: Membrane Fouling. Membranes. 2016;6(2):33.
323. Ramesh A, Lee DJ, Lai JY. Membrane biofouling by extracellular polymeric substances or soluble microbial products from membrane bioreactor sludge. Applied Microbiology and Biotechnology. 2007;74(3):699-707.
324. Hao L, Liss SN, Liao BQ. Influence of COD:N ratio on sludge properties and their role in membrane fouling of a submerged membrane bioreactor. Water Research. 2016;89:132-41.
325. Ng TCA, Ng HY. Characterisation of initial fouling in aerobic submerged membrane bioreactors in relation to physico-chemical characteristics under different flux conditions. Water Research. 2010;44(7):2336-48.
326. Yao M, Zhang K, Cui L. Characterization of protein–polysaccharide ratios on membrane fouling. Desalination. 2010;259(1):11-6.
327. Lozupone C, Knight R. UniFrac: a new phylogenetic method for comparing microbial communities. Applied and environmental microbiology. 2005;71(12):8228-35.
328. Meng F, Liao B, Liang S, Yang F, Zhang H, Song L. Morphological visualization, componential characterization and microbiological identification of membrane fouling in membrane bioreactors (MBRs). Journal of Membrane Science. 2010;361(1):1-14.
329. Gao WJ, Lin HJ, Leung KT, Schraft H, Liao BQ. Structure of cake layer in a submerged anaerobic membrane bioreactor. Journal of Membrane Science. 2011;374(1):110-20.
330. Lin H, Peddada SD. Analysis of microbial compositions: a review of normalization and differential abundance analysis. npj Biofilms and Microbiomes. 2020;6(1):60.
331. Celiker H, Gore J. Cellular cooperation: insights from microbes. Trends in Cell Biology. 2013;23(1):9-15.

332. Ju F, Zhang T. Bacterial assembly and temporal dynamics in activated sludge of a full-scale municipal wastewater treatment plant. The ISME Journal. 2015;9(3):683-95.
333. Aqeel H, Weissbrodt DG, Cerruti M, Wolfaardt GM, Wilén B-M, Liss SN. Drivers of bioaggregation from flocs to biofilms and granular sludge. Environmental Science: Water Research & Technology. 2019;5(12):2072-89.
334. Ayyaru S, Choi J, Ahn Y-H. Biofouling reduction in a MBR by the application of a lytic phage on a modified nanocomposite membrane. Environmental Science: Water Research & Technology. 2018;4(10):1624-38.
335. Scarascia G, Yap SA, Kaksonen AH, Hong P-Y. Bacteriophage Infectivity Against Pseudomonas aeruginosa in Saline Conditions. Frontiers in microbiology. 2018;9:875.
336. Scarascia G, Yap SA, Kaksonen AH, Hong P-Y. Bacteriophage Infectivity Against Pseudomonas aeruginosa in Saline Conditions. Frontiers in Microbiology. 2018;9(875).
337. Goldman G, Starosvetsky J, Armon R. Inhibition of biofilm formation on UF membrane by use of specific bacteriophages. Journal of Membrane Science. 2009;342(1):145-52.
338. Ma W, Panecka M, Tufenkji N, Rahaman MS. Bacteriophage-based strategies for biofouling control in ultrafiltration: In situ biofouling mitigation, biocidal additives and biofilm cleanser. Journal of Colloid and Interface Science. 2018;523:254-65.
339. Nanda S, Azargohar R, Dalai AK, Kozinski JA. An assessment on the sustainability of lignocellulosic biomass for biorefining. Renewable and Sustainable Energy Reviews. 2015;50:925-41.
340. Sawatdeenarunat C, Surendra KC, Takara D, Oechsner H, Khanal SK. Anaerobic digestion of lignocellulosic biomass: Challenges and opportunities. Bioresource Technology. 2015;178:178-86.
341. Rouches E, Zhou S, Steyer JP, Carrere H. White-Rot Fungi pretreatment of lignocellulosic biomass for anaerobic digestion: Impact of glucose supplementation. Process Biochemistry. 2016;51(11):1784-92.
342. Zabed H, Sahu JN, Boyce AN, Faruq G. Fuel ethanol production from lignocellulosic biomass: An overview on feedstocks and technological approaches. Renewable and Sustainable Energy Reviews. 2016;66:751-74.
343. Wen F, Nair NU, Zhao H. Protein engineering in designing tailored enzymes and microorganisms for biofuels production. Current Opinion in Biotechnology. 2009;20(4):412-9.
344. Lazuka A, Auer L, O'Donohue M, Hernandez-Raquet G. Anaerobic lignocellulolytic microbial consortium derived from termite gut: enrichment, lignocellulose degradation and community dynamics. Biotechnology for Biofuels. 2018;11(1):284.
345. Nghiem LD, Koch K, Bolzonella D, Drewes JE. Full scale co-digestion of wastewater sludge and food waste: Bottlenecks and possibilities. Renewable and Sustainable Energy Reviews. 2017;72:354-62.
346. Yue Z-B, Li W-W, Yu H-Q. Application of rumen microorganisms for anaerobic bioconversion of lignocellulosic biomass. Bioresource Technology. 2013;128:738-44.
347. Nghiem LD, Nguyen TT, Manassa P, Fitzgerald SK, Dawson M, Vierboom S. Co-digestion of sewage sludge and crude glycerol for on-demand biogas production. International Biodeterioration & Biodegradation. 2014;95:160-6.
348. Duarte AC, Holman DB, Alexander TW, Kiri K, Breves G, Chaves AV. Incubation temperature, but not pequi oil supplementation, affects methane production,

and the ruminal microbiota in a rumen simulation technique (Rusitec) system. Frontiers in microbiology. 2017;8(1076).
349. Takahashi S, Tomita J, Nishioka K, Hisada T, Nishijima M. Development of a Prokaryotic Universal Primer for Simultaneous Analysis of Bacteria and Archaea Using Next-Generation Sequencing. PLOS ONE. 2014;9(8):e105592.
350. Caporaso JG, Kuczynski J, Stombaugh J, Bittinger K, Bushman FD, Costello EK, et al. QIIME allows analysis of high-throughput community sequencing data. Nature Methods. 2010;7:335.
351. McIlroy SJ, Kirkegaard RH, McIlroy B, Nierychlo M, Kristensen JM, Karst SM, et al. MiDAS 2.0: an ecosystem-specific taxonomy and online database for the organisms of wastewater treatment systems expanded for anaerobic digester groups. Database : the journal of biological databases and curation. 2017;2017(1):bax016.
352. Atasoy M, Owusu-Agyeman I, Plaza E, Cetecioglu Z. Bio-based volatile fatty acid production and recovery from waste streams: Current status and future challenges. Bioresource Technology. 2018.
353. Reddy MV, Hayashi S, Choi D, Cho H, Chang Y-C. Short chain and medium chain fatty acids production using food waste under non-augmented and bio-augmented conditions. Journal of Cleaner Production. 2018;176:645-53.
354. Tale VP, Maki JS, Struble CA, Zitomer DH. Methanogen community structure-activity relationship and bioaugmentation of overloaded anaerobic digesters. Water Research. 2011;45(16):5249-56.
355. Hao L, Bize A, Conteau D, Chapleur O, Courtois S, Kroff P, et al. New insights into the key microbial phylotypes of anaerobic sludge digesters under different operational conditions. Water Research. 2016;102:158-69.
356. Patra A, Park T, Kim M, Yu Z. Rumen methanogens and mitigation of methane emission by anti-methanogenic compounds and substances. Journal of Animal Science and Biotechnology. 2017;8(1):13.
357. Nguyen LN, Nguyen AQ, Nghiem LD. Microbial Community in Anaerobic Digestion System: Progression in Microbial Ecology. In: Bui X-T, Chiemchaisri C, Fujioka T, Varjani S, editors. Water and Wastewater Treatment Technologies. Singapore: Springer Singapore; 2019. p. 331-55.
358. Xie S, Wickham R, Nghiem LD. Synergistic effect from anaerobic co-digestion of sewage sludge and organic wastes. International Biodeterioration & Biodegradation. 2017;116:191-7.
359. Suen G, Weimer PJ, Stevenson DM, Aylward FO, Boyum J, Deneke J, et al. The complete genome sequence of *Fibrobacter succinogenes* S85 reveals a cellulolytic and metabolic specialist. PLOS ONE. 2011;6(4):e18814.
360. Devillard E, Bera-Maillet C, Flint HJ, Scott KP, Newbold CJ, Wallace RJ, et al. Characterization of XYN10B, a modular xylanase from the ruminal protozoan Polyplastron multivesiculatum, with a family 22 carbohydrate-binding module that binds to cellulose. The Biochemical journal. 2003;373(Pt 2):495-503.
361. Bayané A, Guiot SR. Animal digestive strategies versus anaerobic digestion bioprocesses for biogas production from lignocellulosic biomass. Reviews in Environmental Science and Bio/Technology. 2011;10(1):43-62.
362. Agematu H, Takahashi T, Hamano Y. Continuous volatile fatty acid production from lignocellulosic biomass by a novel rumen-mimetic bioprocess. Journal of Bioscience and Bioengineering. 2017;124(5):528-33.
363. Chen S, He Q. Persistence of Methanosaeta populations in anaerobic digestion during process instability. Journal of Industrial Microbiology & Biotechnology. 2015;42(8):1129-37.

364. Ozbayram EG, Akyol Ç, Ince B, Karakoç C, Ince O. Rumen bacteria at work: bioaugmentation strategies to enhance biogas production from cow manure. Journal of Applied Microbiology. 2018;124(2):491-502.
365. Balat M, Ayar G. Biomass Energy in the World, Use of Biomass and Potential Trends. Energy Sources. 2005;27(10):931-40.
366. Flint HJ, Bayer EA, Rincon MT, Lamed R, White BA. Polysaccharide utilization by gut bacteria: potential for new insights from genomic analysis. Nature Reviews Microbiology. 2008;6(2):121-31.
367. Christopherson MR, Dawson JA, Stevenson DM, Cunningham AC, Bramhacharya S, Weimer PJ, et al. Unique aspects of fiber degradation by the ruminal ethanologen Ruminococcus albus 7 revealed by physiological and transcriptomic analysis. BMC Genomics. 2014;15(1):1066-.
368. Nguyen LN, Nguyen AQ, Johir MAH, Guo W, Ngo HH, Chaves AV, et al. Application of rumen and anaerobic sludge microbes for bio harvesting from lignocellulosic biomass. Chemosphere. 2019;228:702-8.
369. Lueangwattanapong K, Ammam F, Mason PM, Whitehead C, McQueen-Mason SJ, Gomez LD, et al. Anaerobic digestion of Crassulacean Acid Metabolism plants: Exploring alternative feedstocks for semi-arid lands. Bioresource Technology. 2020;297:122262.
370. Lazuka A, Auer L, Bozonnet S, Morgavi DP, O'Donohue M, Hernandez-Raquet G. Efficient anaerobic transformation of raw wheat straw by a robust cow rumen-derived microbial consortium. Bioresource Technology. 2015;196:241-9.
371. Njokweni SG, Weimer PJ, Warburg L, Botes M, van Zyl WH. Valorisation of the invasive species, Prosopis juliflora, using the carboxylate platform to produce volatile fatty acids. Bioresource Technology. 2019;288.
372. Aydin S, Yesil H, Tugtas AE. Recovery of mixed volatile fatty acids from anaerobically fermented organic wastes by vapor permeation membrane contactors. Bioresource Technology. 2018;250:548-55.
373. Zacharof M-P, Mandale SJ, Williams PM, Lovitt RW. Nanofiltration of treated digested agricultural wastewater for recovery of carboxylic acids. Journal of Cleaner Production. 2016;112:4749-61.
374. Pan X-R, Li W-W, Huang L, Liu H-Q, Wang Y-K, Geng Y-K, et al. Recovery of high-concentration volatile fatty acids from wastewater using an acidogenesis-electrodialysis integrated system. Bioresource Technology. 2018;260:61-7.
375. Ramos AFO, Terry SA, Holman DB, Breves G, Pereira LGR, Silva AGM, et al. Tucumã Oil Shifted Ruminal Fermentation, Reducing Methane Production and Altering the Microbiome but Decreased Substrate Digestibility Within a RUSITEC Fed a Mixed Hay – Concentrate Diet. Frontiers in microbiology. 2018;9(1647).
376. Forwood DL, Hooker K, Caro E, Huo Y, Holman DB, Meale SJ, et al. Crop Sorghum Ensiled With Unsalable Vegetables Increases Silage Microbial Diversity. Frontiers in microbiology. 2019;10(2599).
377. Takahashi S, Tomita J, Nishioka K, Hisada T, Nishijima M. Development of a prokaryotic universal primer for simultaneous analysis of Bacteria and Archaea using next-generation sequencing. PloS one. 2014;9(8):e105592-e.
378. Duarte AC, Holman DB, Alexander TW, Kiri K, Breves G, Chaves AV. Incubation Temperature, But Not Pequi Oil Supplementation, Affects Methane Production, and the Ruminal Microbiota in a Rumen Simulation Technique (Rusitec) System. Front Microbiol. 2017;8:1076-.
379. Jin W, Xu X, Yang F. Application of Rumen Microorganisms for Enhancing Biogas Production of Corn Straw and Livestock Manure in a Pilot-Scale Anaerobic

Digestion System: Performance and Microbial Community Analysis. Energies. 2018;11(4).
380. Barnes SP, Keller J. Anaerobic rumen SBR for degradation of cellulosic material. Water Science and Technology. 2004;50(10):305-11.
381. Waszak M, Gryta M. The ultrafiltration ceramic membrane used for broth separation in membrane bioreactor. Chemical Engineering Journal. 2016;305:129-35.
382. Arslan D, Zhang Y, Steinbusch KJJ, Diels L, Hamelers HVM, Buisman CJN, et al. In-situ carboxylate recovery and simultaneous pH control with tailor-configured bipolar membrane electrodialysis during continuous mixed culture fermentation. Separation and Purification Technology. 2017;175:27-35.
383. Liu Q, Wang C, Guo G, Huo WJ, Zhang YL, Pei CX, et al. Effects of branched-chain volatile fatty acids supplementation on growth performance, ruminal fermentation, nutrient digestibility, hepatic lipid content and gene expression of dairy calves. Animal Feed Science and Technology. 2018;237:27-34.
384. Atasoy M, Owusu-Agyeman I, Plaza E, Cetecioglu Z. Bio-based volatile fatty acid production and recovery from waste streams: Current status and future challenges. Bioresource Technology. 2018;268:773-86.
385. MordorIntelligence. Acetic Acid Market - Segmented by End-user Industry, Application, and Geography – Growth, Trends, and Forecast (2019–2024). Hyderabad (India)2018 [Available from: https://www.mordorintelligence.com/industry-reports/acetic-acid-market.
386. Wang C, Hong F, Lu Y, Li X, Liu H. Improved biogas production and biodegradation of oilseed rape straw by using kitchen waste and duck droppings as co-substrates in two-phase anaerobic digestion. PLOS ONE. 2017;12(8):e0182361.
387. Kullavanijaya P, Chavalparit O. The production of volatile fatty acids from Napier grass via an anaerobic leach bed process: The influence of leachate dilution, inoculum, recirculation, and buffering agent addition. Journal of Environmental Chemical Engineering. 2019;7(6):103458.
388. Alexandri M, Schneider R, Venus J. Membrane Technologies for Lactic Acid Separation from Fermentation Broths Derived from Renewable Resources. Membranes. 2018;8(4):94.
389. Tessier L, Bouchard P, Rahni M. Separation and purification of benzylpenicillin produced by fermentation using coupled ultrafiltration and nanofiltration technologies. Journal of Biotechnology. 2005;116(1):79-89.
390. Krause DO, Denman SE, Mackie RI, Morrison M, Rae AL, Attwood GT, et al. Opportunities to improve fiber degradation in the rumen: microbiology, ecology, and genomics. FEMS Microbiology Reviews. 2003;27(5):663-93.
391. Palevich N, Kelly WJ, Leahy SC, Denman S, Altermann E, Rakonjac J, et al. Comparative Genomics of Rumen Butyrivibrio spp. Uncovers a Continuum of Polysaccharide-Degrading Capabilities. Applied and Environmental Microbiology. 2019;86(1):e01993-19.
392. Ransom-Jones E, Jones DL, McCarthy AJ, McDonald JE. The Fibrobacteres: an Important Phylum of Cellulose-Degrading Bacteria. Microbial Ecology. 2012;63(2):267-81.
393. Gagen EJ, Padmanabha J, Denman SE, McSweeney CS. Hydrogenotrophic culture enrichment reveals rumen Lachnospiraceae and Ruminococcaceae acetogens and hydrogen-responsive Bacteroidetes from pasture-fed cattle. FEMS microbiology letters. 2015;362(14).

394. Van Gylswyk NO. Succiniclasticum ruminis gen. nov., sp. nov., a Ruminal Bacterium Converting Succinate to Propionate as the Sole Energy-Yielding Mechanism. International Journal of Systematic and Evolutionary Microbiology. 1995;45(2):297-300.
395. Kraatz M, Wallace RJ, Svensson L. Olsenella umbonata sp. nov., a microaerotolerant anaerobic lactic acid bacterium from the sheep rumen and pig jejunum, and emended descriptions of Olsenella, Olsenella uli and Olsenella profusa. International Journal of Systematic and Evolutionary Microbiology. 2011;61(4):795-803.
396. Oliveira A, Oliveira LC, Aburjaile F, Benevides L, Tiwari S, Jamal SB, et al. Insight of Genus Corynebacterium: Ascertaining the Role of Pathogenic and Non-pathogenic Species. Frontiers in microbiology. 2017;8(1937).
397. Kishimoto A, Ushida K, Phillips GO, Ogasawara T, Sasaki Y. Identification of Intestinal Bacteria Responsible for Fermentation of Gum Arabic in Pig Model. Current Microbiology. 2006;53(3):173-7.
398. Le Van TD, Robinson JA, Ralph J, Greening RC, Smolenski WJ, Leedle JA, et al. Assessment of reductive acetogenesis with indigenous ruminal bacterium populations and Acetitomaculum ruminis. Applied and environmental microbiology. 1998;64(9):3429-36.
399. Janssen PH, Kirs M. Structure of the Archaeal Community of the Rumen. Applied and Environmental Microbiology. 2008;74(12):3619.
400. Henderson G, Cox F, Ganesh S, Jonker A, Young W, Abecia L, et al. Rumen microbial community composition varies with diet and host, but a core microbiome is found across a wide geographical range. Scientific Reports. 2015;5(1):14567.
401. Han Q, Jiang Y, Brandt BW, Yang J, Chen Y, Buijs MJ, et al. Regrowth of Microcosm Biofilms on Titanium Surfaces After Various Antimicrobial Treatments. Frontiers in microbiology. 2019;10(2693).
402. Cieplik F, Zaura E, Brandt BW, Buijs MJ, Buchalla W, Crielaard W, et al. Microcosm biofilms cultured from different oral niches in periodontitis patients. J Oral Microbiol. 2018;11(1):1551596-.
403. Stack RJ, Cotta MA. Effect of 3-Phenylpropanoic Acid on Growth of and Cellulose Utilization by Cellulolytic Ruminal Bacteria. Applied and Environmental Microbiology. 1986;52(1):209.
404. De Mulder T, Goossens K, Peiren N, Vandaele L, Haegeman A, De Tender C, et al. Exploring the methanogen and bacterial communities of rumen environments: solid adherent, fluid and epimural. FEMS microbiology ecology. 2016;93(3).
405. Schären M, Frahm J, Kersten S, Meyer U, Hummel J, Breves G, et al. Interrelations between the rumen microbiota and production, behavioral, rumen fermentation, metabolic, and immunological attributes of dairy cows. Journal of Dairy Science. 2018;101(5):4615-37.
406. McConathy J, Owens MJ. Stereochemistry in drug action. Primary Care Companion J Clin Phsychiatry. 2003;5(2):70-3.
407. Hashim NH, Shafie S, Khan SJ. Enantiomeric fraction as an indicator of pharmaceutical biotransformation during wastewater treatment and in the environment – a review. Environmental Technology. 2010;31(12):1349-70.
408. Stanley JK, Ramirez AJ, Chambliss CK, Brooks BW. Enantiospecific sublethal effects of the antidepressant fluoxetine to a model aquatic vertebrate and invertebrate. Chemosphere. 2007;69(1):9-16.
409. Stanley JK, Ramirez AJ, Mottaleb M, Chambliss CK, Brooks BW. Enantiospecific toxicity of the beta-blocker propranolol to Daphnia magna and Pimephales promelas. Environ Toxicol Chem. 2006;25(7):1780-6.

410. Arenas M, Martin J, Santos JL, Aparicio I, Alonso E. Enantioselective behavior of environmental chiral pollutants: A comprehensive review. Critical Reviews in Environmental Science and Technology.
411. Pérez S, Barceló D. Applications of LC-MS to quantitation and evaluation of the environmental fate of chiral drugs and their metabolites. Tr Anal Chem. 2008;27(10):836-46.
412. Langa I, Goncalves R, Tiritan ME, Ribeiro C. Wastewater analysis of psychoactive drugs: Non-enantioselective vs enantioselective methods for estimation of consumption. Forensic Science International. 2021;325.
413. Vane J. The mechanism of action of anti-inflammatory drugs. Int J Clin Prac 2003;Supplement 135:2.
414. Caldwell J, Hutt AJ, Fournel-Gigleux S. The metabolic chiral inversion and dispositional enantioselectivity of the 2-arylpropionic acids and their biological consequences. Biochem Pharmacol 1988;37(7):105-14.
415. Adams SS, Bresloff P, Mason GC. Pharmacological difference between the optical isomers of ibuprofen: evidence for metabolic inversion of the (-) isomer. J Pharmac Pharmacol. 1976;28:156-7.
416. Buser H-R, Poiger T, Müller MD. Occurrence and environmental behaviour of the chiral pharmaceutical drug ibuprofen in surface waters and in wastewater. Environ Sci Technol. 1999;33:2529-35.
417. Gasser G, Pankratov I, Elhanany S, Werner P, Gun J, Gelman F, et al. Field and laboratory studies of the fate and enantiomeric enrichment of venlafaxine and O-desmethylvenlafaxine under aerobic and anaerobic conditions. Chemosphere. 2012;88(1):98-105.
418. Kasprzyk-Hordern B, Baker DR. Enantiomeric profiling of chiral drugs in wastewater and receiving waters. Environmental Science & Technology. 2012;46(3):1681-91.
419. Fono LJ, Sedlak DL. Use of the chiral pharmaceutical propranolol to identify sewage discharges into surface waters. Environ Sci Technol. 2005;39(23):9244-52.
420. Wechter WJ. Drug chirality - On the mechanism of R-aryl propionic-acid class NSAIDs -Epimerization in humans and the clinical implications for the use of racemates. Journal of Clinical Pharmacology. 1994;34(11):1036-42.
421. Dogan A, Plotka-Wasylka J, Kempinska-Kupczyk D, Namiesnik J, Kot-Wasik A. Detection, identification and determination of chiral pharmaceutical residues in wastewater: Problems and challenges. Trac-Trends in Analytical Chemistry. 2020;122.
422. Hashim NH, Nghiem LD, Stuetz RM, Khan SJ. Enantiospecific fate of ibuprofen, ketoprofen and naproxen in a laboratory-scale membrane bioreactor. Water Research. 2011;45(18):6249-58.
423. Selke S, Scheurell M, Shah MR, Huhnerfuss H. Identification and enantioselective gas chromatographic mass-spectrometric separation of O-desmethylnaproxen, the main metabolite of the drug naproxen, as a new environmental contaminant. Journal of Chromatography A. 2010;1217(3):419-23.
424. Wijekoon KC, McDonald JA, Khan SJ, Hai FI, Price WE, Nghiem LD. Development of a predictive framework to assess the removal of trace organic chemicals by anaerobic membrane bioreactor. Bioresource Technology. 2015;189:391-8.
425. Tadkaew N, Hai FI, McDonald JA, Khan SJ, Nghiem LD. Removal of trace organics by MBR treatment: The role of molecular properties. Water Research. 2011;45(8):2439-51.
426. Liu Y, Han P, Li X-y, Shih K, Gu J-D. Enantioselective degradation and unidirectional chiral inversion of 2-phenylbutyric acid, an intermediate from linear

alkylbenzene, by Xanthobacter flavus PA1. Journal of Hazardous Materials. 2011;192(3):1633-40.
427. Simoni S, Klinke S, Zipper C, Angst W, Kohler HE. Enantioselective Metabolism of Chiral 3-Phenylbutyric Acid, an Intermediate of Linear Alkylbenzene Degradation, by Rhodococcus rhodochrous PB1. Applied and Environmental Microbiology. 1996;62(3):749.
428. Tambosi JL, de Sena RF, Favier M, Gebhardt W, José HJ, Schröder HF, et al. Removal of pharmaceutical compounds in membrane bioreactors (MBR) applying submerged membranes. Desalination. 2010;261(1):148-56.
429. Kim SD, Cho J, Kim IS, Vanderford BJ, Snyder SA. Occurrence and removal of pharmaceuticals and endocrine disruptors in South Korean surface, drinking, and waste waters. Water Research. 2007;41(5):1013-21.
430. Wang X-c, Shen J-m, Chen Z-l, Zhao X, Xu H. Removal of pharmaceuticals from synthetic wastewater in an aerobic granular sludge membrane bioreactor and determination of the bioreactor microbial diversity. Applied Microbiology and Biotechnology. 2016;100(18):8213-23.
431. Alturki AA, Tadkaew N, McDonald JA, Khan SJ, Price WE, Nghiem LD. Combining MBR and NF/RO membrane filtration for the removal of trace organics in indirect potable water reuse applications. Journal of Membrane Science. 2010;365(1):206-15.
432. Nguyen LN, Hai FI, McDonald JA, Khan SJ, Price WE, Nghiem LD. Continuous transformation of chiral pharmaceuticals in enzymatic membrane bioreactors for advanced wastewater treatment. Water Science and Technology. 2017;76(7):1816-26.
433. Górny D, Guzik U, Hupert-Kocurek K, Wojcieszyńska D. A new pathway for naproxen utilisation by Bacillus thuringiensis B1(2015b) and its decomposition in the presence of organic and inorganic contaminants. Journal of Environmental Management. 2019;239:1-7.
434. Marco-Urrea E, Pérez-Trujillo M, Cruz-Morató C, Caminal G, Vicent T. White-rot fungus-mediated degradation of the analgesic ketoprofen and identification of intermediates by HPLC–DAD–MS and NMR. Chemosphere. 2010;78(4):474-81.
435. González-Pérez DM, Pérez JI, Gómez MA. Behaviour of the main nonsteroidal anti-inflammatory drugs in a membrane bioreactor treating urban wastewater at high hydraulic- and sludge-retention time. Journal of Hazardous Materials. 2017;336:128-38.
436. Evans S, Bagnall J, Kasprzyk-Hordern B. Enantiomeric profiling of a chemically diverse mixture of chiral pharmaceuticals in urban water. Environmental Pollution. 2017;230:368-77.
437. Petrie B, Mrazova J, Kasprzyk-Hordern B, Yates K. Multi-residue analysis of chiral and achiral trace organic contaminants in soil by accelerated solvent extraction and enantioselective liquid chromatography tandem–mass spectrometry. Journal of Chromatography A. 2018;1572:62-71.
438. Hanlon GW, Kooloobandi A, Hutt AJ. Microbial metabolism of 2-arylpropionic acids: effect of environment on the metabolism of ibuprofen by Verticillium lecanii. Journal of Applied Bacteriology. 1994;76(5):442-7.
439. Hutt AJ, Kooloobandi A, Hanlon GW. Microbial metabolism of 2-arylpropionic acids: Chiral inversion of ibuprofen and 2-phenylpropionic acid. Chirality. 1993;5(8):596-601.
440. Rhys-Williams W, Thomason MJ, Hung YF, Hanlon GW, Lloyd AW. Extent of chiral inversion of the 2-arylpropionic acids by Cordyceps militaris. Chirality. 1998;10(6):528-34.

441. Hung YF, Thomason MJ, Rhys-Williams W, Lloyd AW, Hanlon GW. Chiral inversion of 2-phenylpropionic acid by Cordyceps militaris. Journal of Applied Bacteriology. 1996;81(3):242-50.
442. Thomason MJ, Rhys-Williams W, Lloyd AW, Hanlon GW. Optimization of the Chiral Inversion of 2-Phenylpropionic Acid by Verticillium lecanii. Journal of Pharmacy and Pharmacology. 1997;49(3):263-9.
443. Kato D-i, Mitsuda S, Ohta H. Microbial Deracemization of α-Substituted Carboxylic Acids: Substrate Specificity and Mechanistic Investigation. The Journal of Organic Chemistry. 2003;68(19):7234-42.
444. Thomason, Rhys W, Lloyd, Hanlon. The stereo inversion of 2-arylpropionic acid non-steroidal anti-inflammatory drugs and structurally related compounds by Verticillium lecanii. Journal of Applied Microbiology. 1998;85(1):155-63.
445. Thibaut R, Porte C. Effects of fibrates, anti-inflammatory drugs and antidepressants in the fish hepatoma cell line PLHC-1: Cytotoxicity and interactions with cytochrome P450 1A. Toxicology in Vitro. 2008;22(5):1128-35.
446. Bertin S, Yates K, Petrie B. Enantiospecific behaviour of chiral drugs in soil. Environmental Pollution. 2020;262:114364.
447. Sanganyado E, Lu Z, Fu Q, Schlenk D, Gan J. Chiral pharmaceuticals: A review on their environmental occurrence and fate processes. Water Research. 2017;124:527-42.
448. Suzuki T, Kosugi Y, Hosaka M, Nishimura T, Nakae D. Occurrence and behavior of the chiral anti-inflammatory drug naproxen in an aquatic environment. Environmental Toxicology and Chemistry. 2014;33(12):2671-8.
449. Wsol V, Skalova L, Szotakova B. Chiral Inversion of Drugs: Coincidence or Principle? Current Drug Metabolism. 2004;5(6):517-33.
450. Khan SJ. Biologically Mediated Chiral Inversion of Emerging Contaminants. Transformation Products of Emerging Contaminants in the Environment2014. p. 261-80.
451. Mechelke J, Rust D, Jaeger A, Hollender J. Enantiomeric Fractionation during Biotransformation of Chiral Pharmaceuticals in Recirculating Water-Sediment Test Flumes. Environmental Science & Technology. 2020;54(12):7291-301.
452. Zhang Q, Fu L, Cang T, Tang T, Guo M, Zhou B, et al. Toxicological Effect and Molecular Mechanism of the Chiral Neonicotinoid Dinotefuran in Honeybees. Environmental Science & Technology. 2022;56(2):1104-12.
453. Cui F, Zhu Y, Di S, Wang X, Zhang Y, Chai T. Toxicological Study on Chiral Fluoxetine Exposure to Adult Zebrafish (Danio rerio): Enantioselective and Sexual Mechanism on Disruption of the Brain Serotonergic System. Environmental Science & Technology. 2021;55(11):7479-90.
454. Adams SS, Bresloff P, Mason CG. Pharmacological differences between the optical isomers of ibuprofen: evidence for metabolic inversion of the (—)-isomer. Journal of Pharmacy and Pharmacology. 1976;28(3):256-7.
455. Guerra P, Kim M, Shah A, Alaee M, Smyth SA. Occurrence and fate of antibiotic, analgesic/anti-inflammatory, and antifungal compounds in five wastewater treatment processes. Science of The Total Environment. 2014;473-474:235-43.
456. Tiwari B, Sellamuthu B, Ouarda Y, Drogui P, Tyagi RD, Buelna G. Review on fate and mechanism of removal of pharmaceutical pollutants from wastewater using biological approach. Bioresource Technology. 2017;224:1-12.
457. Phan HV, Wickham R, Xie S, McDonald JA, Khan SJ, Ngo HH, et al. The fate of trace organic contaminants during anaerobic digestion of primary sludge: A pilot scale study. Bioresource Technology. 2018;256:384-90.

458. Gonzalez-Gil L, Papa M, Feretti D, Ceretti E, Mazzoleni G, Steimberg N, et al. Is anaerobic digestion effective for the removal of organic micropollutants and biological activities from sewage sludge? Water Research. 2016;102:211-20.
459. Hayball P. Chirality and Nonsteroidal Anti-Inflammatory Drugs. Drugs. 1996;52(5):47-58.
460. Langa I, Gonçalves R, Tiritan ME, Ribeiro C. Wastewater analysis of psychoactive drugs: Non-enantioselective vs enantioselective methods for estimation of consumption. Forensic Science International. 2021;325:110873.
461. Thomaidis NS, Gago-Ferrero P, Ort C, Maragou NC, Alygizakis NA, Borova VL, et al. Reflection of Socioeconomic Changes in Wastewater: Licit and Illicit Drug Use Patterns. Environmental Science & Technology. 2016;50(18):10065-72.
462. Iwakawa S, Spahn H, Benet LZ, Lin ET. Stereoselective disposition of carprofen, flunoxaprofen, and naproxen in rats. Drug Metabolism & Disposition. 1991;19(5):853-7.
463. Caldwell J, Hutt AJ, Fournel-Gigleux S. The metabolic chiral inversion and dispositional enantioselectivity of the 2-arylpropionic acids and their biological consequences. Biochemical Pharmacology. 1988;37(1):105-14.
464. Nguyen AQ, Nguyen LN, McDonald JA, Nghiem LD, Leusch FDL, Neale PA, et al. Chiral inversion of 2-arylpropionic acid (2-APA) enantiomers during simulated biological wastewater treatment. Water Research. 2021:117871.
465. Gerba CP, Pepper IL. Chapter 24 - Wastewater Treatment and Biosolids Reuse. In: Maier RM, Pepper IL, Gerba CP, editors. Environmental Microbiology (Second Edition). San Diego: Academic Press; 2009. p. 503-30.
466. Semblante GU, Hai FI, Huang X, Ball AS, Price WE, Nghiem LD. Trace organic contaminants in biosolids: Impact of conventional wastewater and sludge processing technologies and emerging alternatives. Journal of Hazardous Materials. 2015;300:1-17.
467. Pino MR, Val J, Mainar AM, Zuriaga E, Español C, Langa E. Acute toxicological effects on the earthworm Eisenia fetida of 18 common pharmaceuticals in artificial soil. Science of The Total Environment. 2015;518-519:225-37.
468. Han S, Choi K, Kim J, Ji K, Kim S, Ahn B, et al. Endocrine disruption and consequences of chronic exposure to ibuprofen in Japanese medaka (Oryzias latipes) and freshwater cladocerans Daphnia magna and Moina macrocopa. Aquatic Toxicology. 2010;98(3):256-64.
469. Thomason MJ, Rhys-Williams W, Hung YF, Baker JA, Hanlon GW, Lloyd AW. A mechanistic investigation of the microbial chiral inversion of 2-phenylpropionic acid by Verticillium lecanii. Chirality. 1997;9(3):254-60.
470. Sanz JL, Köchling T. Next-generation sequencing and waste/wastewater treatment: a comprehensive overview. Reviews in Environmental Science and Bio/Technology. 2019;18(4):635-80.
471. Douglas GM, Maffei VJ, Zaneveld JR, Yurgel SN, Brown JR, Taylor CM, et al. PICRUSt2 for prediction of metagenome functions. Nature Biotechnology. 2020;38(6):685-8.
472. Reichel C, Brugger R, Bang H, Geisslinger G, Brune K. Molecular Cloning and Expression of a 2-Arylpropionyl-Coenzyme A Epimerase: A Key Enzyme in the Inversion Metabolism of Ibuprofen. Molecular Pharmacology. 1997;51(4):576.
473. Selke S, Scheurell M, Shah MR, Hühnerfuss H. Identification and enantioselective gas chromatographic mass-spectrometric separation of O-desmethylnaproxen, the main metabolite of the drug naproxen, as a new environmental contaminant. Journal of Chromatography A. 2010;1217(3):419-23.

474. Mitsukura K, Yoshida T, Nagasawa T. Synthesis of (R)-2-phenylpropanoic acid from its racemate through an isomerase-involving reaction by Nocardia diaphanozonaria. Biotechnology Letters. 2002;24(19):1615-21.
475. Lievano R, Pérez HI, Manjarrez N, Solís A, Solís-Oba M. Hydrolysis of Ibuprofen Nitrile and Ibuprofen Amide and Deracemisation of Ibuprofen Using Nocardia corallina B-276. Molecules. 2012;17(3).
476. Ma K, Wang W, Liu Y, Bao L, Cui Y, Kang W, et al. Insight into the performance and microbial community profiles of magnetite-amended anaerobic digestion: Varying promotion effects at increased loads. Bioresource Technology. 2021;329:124928.
477. Li W-J, Xu P, Schumann P, Zhang Y-Q, Pukall R, Xu L-H, et al. Georgenia ruanii sp. nov., a novel actinobacterium isolated from forest soil in Yunnan (China), and emended description of the genus Georgenia. International Journal of Systematic and Evolutionary Microbiology. 2007;57(7):1424-8.
478. Ben Hania W, Fadhlaoui K, Brochier-Armanet C, Persillon C, Postec A, Hamdi M, et al. Draft genome sequence of Mesotoga strain PhosAC3, a mesophilic member of the bacterial order Thermotogales, isolated from a digestor treating phosphogypsum in Tunisia. Standards in Genomic Sciences. 2015;10(1):12.
479. Nguyen AQ, Wickham R, Nguyen LN, Phan HV, Galway B, Bustamante H, et al. Impact of anaerobic co-digestion between sewage sludge and carbon-rich organic waste on microbial community resilience. Environmental Science: Water Research & Technology. 2018;4(12):1956-65.
480. Sedano-Núñez VT, Boeren S, Stams AJM, Plugge CM. Comparative proteome analysis of propionate degradation by Syntrophobacter fumaroxidans in pure culture and in coculture with methanogens. Environmental microbiology. 2018;20(5):1842-56.
481. Wang P, Wang H, Qiu Y, Ren L, Jiang B. Microbial characteristics in anaerobic digestion process of food waste for methane production–A review. Bioresource Technology. 2018;248:29-36.
482. Zhu X, Campanaro S, Treu L, Seshadri R, Ivanova N, Kougias PG, et al. Metabolic dependencies govern microbial syntrophies during methanogenesis in an anaerobic digestion ecosystem. Microbiome. 2020;8(1):22.
483. Detman A, Mielecki D, Pleśniak Ł, Bucha M, Janiga M, Matyasik I, et al. Methane-yielding microbial communities processing lactate-rich substrates: a piece of the anaerobic digestion puzzle. Biotechnology for Biofuels. 2018;11(1):116.
484. Albertsen M, Hugenholtz P, Skarshewski A, Nielsen KL, Tyson GW, Nielsen PH. Genome sequences of rare, uncultured bacteria obtained by differential coverage binning of multiple metagenomes. Nature Biotechnology. 2013;31(6):533-8.
485. Yamada T, Imachi H, Ohashi A, Harada H, Hanada S, Kamagata Y, et al. Bellilinea caldifistulae gen. nov., sp. nov. and Longilinea arvoryzae gen. nov., sp. nov., strictly anaerobic, filamentous bacteria of the phylum Chloroflexi isolated from methanogenic propionate-degrading consortia. International Journal of Systematic and Evolutionary Microbiology. 2007;57(10):2299-306.
486. Ueki A, Akasaka H, Suzuki D, Ueki K. Paludibacter propionicigenes gen. nov., sp. nov., a novel strictly anaerobic, Gram-negative, propionate-producing bacterium isolated from plant residue in irrigated rice-field soil in Japan. International Journal of Systematic and Evolutionary Microbiology. 2006;56(1):39-44.
487. Pikuta EV, Menes RJ, Bruce AM, Lyu Z, Patel NB, Liu Y, et al. Raineyella antarctica gen. nov., sp. nov., a psychrotolerant, d-amino-acid-utilizing anaerobe isolated from two geographic locations of the Southern Hemisphere. International Journal of Systematic and Evolutionary Microbiology. 2016;66(12):5529-36.

488. Bae H-S, Moe WM, Yan J, Tiago I, da Costa MS, Rainey FA. Brooklawnia cerclae gen. nov., sp. nov., a propionate-forming bacterium isolated from chlorosolvent-contaminated groundwater. International Journal of Systematic and Evolutionary Microbiology. 2006;56(8):1977-83.
489. Mechichi T, Labat M, Woo THS, Thomas P, Garcia J-L, Patel BKC. Eubacterium aggreganssp. nov., a New Homoacetogenic Bacterium from Olive Mill Wastewater Treatment Digestor. Anaerobe. 1998;4(6):283-91.
490. Patil Y, Müller N, Schink B, Whitman WB, Huntemann M, Clum A, et al. High-quality-draft genome sequence of the fermenting bacterium Anaerobium acetethylicum type strain GluBS11T (DSM 29698). Standards in Genomic Sciences. 2017;12(1):24.
491. Su X-L, Tian Q, Zhang J, Yuan X-Z, Shi X-S, Guo R-B, et al. Acetobacteroides hydrogenigenes gen. nov., sp. nov., an anaerobic hydrogen-producing bacterium in the family Rikenellaceae isolated from a reed swamp. International Journal of Systematic and Evolutionary Microbiology. 2014;64(Pt_9):2986-91.
492. Zheng H, Dietrich C, Radek R, Brune A. Endomicrobium proavitum, the first isolate of Endomicrobia class. nov. (phylum Elusimicrobia) – an ultramicrobacterium with an unusual cell cycle that fixes nitrogen with a Group IV nitrogenase. Environmental microbiology. 2016;18(1):191-204.
493. Zheng H, Dietrich C, Brune A, Drake Harold L. Genome Analysis of Endomicrobium proavitum Suggests Loss and Gain of Relevant Functions during the Evolution of Intracellular Symbionts. Applied and Environmental Microbiology. 2017;83(17):e00656-17.
494. Allison SD, Martiny JBH. Resistance, resilience, and redundancy in microbial communities. Proceedings of the National Academy of Sciences. 2008;105(Supplement 1):11512.
495. Grostern A, Duhamel M, Dworatzek S, Edwards EA. Chloroform respiration to dichloromethane by a Dehalobacter population. Environmental microbiology. 2010;12(4):1053-60.
496. Smith BJ, Boothe MA, Fiddler BA, Lozano TM, Rahi RK, Krzmarzick MJ. Enumeration of Organohalide Respirers in Municipal Wastewater Anaerobic Digesters. Microbiol Insights. 2015;8(Suppl 2):9-14.
497. Justicia-Leon SD, Ritalahti KM, Mack EE, Löffler FE. Dichloromethane fermentation by a Dehalobacter sp. in an enrichment culture derived from pristine river sediment. Applied and Environmental Microbiology. 2012;78(4):1288-91.
498. Savolainen K, Bhaumik P, Schmitz W, Kotti TJ, Conzelmann E, Wierenga RK, et al. α-Methylacyl-CoA Racemase from from *Mycobacterium tuberculosis*: Mutational and structural characterization of the active site and the fold. Journal of Biological Chemistry. 2005;280(13):12611-20.
499. Bhaumik P, Schmitz W, Hassinen A, Hiltunen JK, Conzelmann E, Wierenga RK. The Catalysis of the 1,1-Proton Transfer by α-Methyl-acyl-CoA Racemase Is Coupled to a Movement of the Fatty Acyl Moiety Over a Hydrophobic, Methionine-rich Surface. Journal of Molecular Biology. 2007;367(4):1145-61.
500. Ouazia D, Bearne SL. A continuous assay for α-methylacyl-coenzyme A racemase using circular dichroism. Analytical Biochemistry. 2010;398(1):45-51.
501. Busch H, Hagedoorn P-L, Hanefeld U. Rhodococcus as A Versatile Biocatalyst in Organic Synthesis. Int J Mol Sci. 2019;20(19):4787.
502. Bewick DW, inventorProcess for producing optically active aryloxypropionic acids and derivatives thereof useful as herbicides. U.S1986.

503. Fan J, Jia Y, Xu D, Ye Z, Zhou J, Huang J, et al. Anaerobic condition induces a viable but nonculturable state of the PCB-degrading Bacteria Rhodococcus biphenylivorans TG9. Science of The Total Environment. 2021;764:142849.